University of Bath

PHD

Robust control of a hydraulically actuated friction damper for vehicle applications

Guglielmino, Emanuele

Award date:
2001

Awarding institution:
University of Bath

Link to publication

General rights
Copyright and moral rights for the publications made accessible in the public portal are retained by the authors and/or other copyright owners and it is a condition of accessing publications that users recognise and abide by the legal requirements associated with these rights.

- Users may download and print one copy of any publication from the public portal for the purpose of private study or research.
- You may not further distribute the material or use it for any profit-making activity or commercial gain
- You may freely distribute the URL identifying the publication in the public portal ?

Take down policy
If you believe that this document breaches copyright please contact us providing details, and we will remove access to the work immediately and investigate your claim.

Download date: 22. May. 2019

ROBUST CONTROL OF A HYDRAULICALLY ACTUATED FRICTION DAMPER FOR VEHICLE APPLICATIONS

submitted by

Emanuele Guglielmino

for the degree of

Ph.D.

of the University of Bath

2001

COPYRIGHT

Attention is drawn to the fact that copyright of this thesis rests with its author. This copy of the thesis has been supplied on condition that anyone who consults it is understood to recognise that its copyright rests with its author and that no quotation from the thesis and no information derived from it may be published without the prior written consent of the author.

This thesis may be made available for consultation within the University Library and may be photocopied or lent to other libraries for the purposes of consultation.

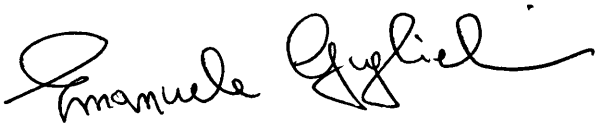

UMI Number: U601610

All rights reserved

INFORMATION TO ALL USERS
The quality of this reproduction is dependent upon the quality of the copy submitted.

In the unlikely event that the author did not send a complete manuscript
and there are missing pages, these will be noted. Also, if material had to be removed,
a note will indicate the deletion.

UMI U601610
Published by ProQuest LLC 2013. Copyright in the Dissertation held by the Author.
Microform Edition © ProQuest LLC.
All rights reserved. This work is protected against
unauthorized copying under Title 17, United States Code.

ProQuest LLC
789 East Eisenhower Parkway
P.O. Box 1346
Ann Arbor, MI 48106-1346

Considerate la vostra semenza :
fatti non foste a viver come bruti
ma per seguir virtute e conoscenza

***Dante**, Inf. XXVI, 118-120*

SUMMARY

The thesis is concerned with an investigation, both theoretical and experimental, on the feasibility of using a servo-driven dry-friction damper in vibration control. The thrust of the investigation is an automotive application to a controlled semi-active suspension. However applications potentially exist in other fields (e.g. structural engineering).

In a motor vehicle suspension, the friction damper device comprises, in essence, a friction pad fixed to the wheel which acts on a plate attached to the chassis of the car. The normal force between the pad and the plate, and hence the friction force is controlled by a hydraulic drive which modulates pressure. Various design options have been investigated for the drive. The final design entailed the use of a proportional underlapped control valve used in pressure control mode (exploiting the pressure gain characteristics). Because of the force-control scheme employed, the energy consumption of this system is relatively low.

A model of the hydraulic drive and of the vehicle has been developed and validated experimentally. A robust control strategy has been employed to tackle the problem of the inherent parameter uncertainties of the plant (particularly the friction coefficient), hence Variable Structure Control schemes have been investigated, namely sliding mode control and switched state feedback.

The controller performs a spring force tracking control, thereby reducing the total force experienced by the chassis. Additional pseudo-viscous damping can also be added. A Lyapounov-based method has been employed for the synthesis of the criterion which defines the change in the system structure.

Extensive simulations have been performed. Experimental work has been undertaken, initially on a pilot rig; subsequently a novel prototype of a friction damper has been designed and installed on a Ford Orion car and tested on the car itself. A preliminary numerical investigation of the problem of controlling independently four dampers, constituting a full car suspension, has been also carried out.

The model developed has predicted sufficiently accurately the actual system behaviour, particularly as far as the hydraulic drive is concerned. The variable structure controller

has achieved the targets of providing both the desired robustness and producing an overall improvement of vehicle ride, particularly in terms of RMS chassis acceleration reduction.

ACKNOWLEDGEMENTS

I would like to take this opportunity to express my most sincere thanks to my supervisor Prof Kevin Edge for his brilliant guidance and his continuous advice throughout all the work.

I would like to thank all the people from the Department of Mechanical Engineering who helped me in the course of these years, particularly Steve Dolan for his invaluable everyday help and his friendship, and the co-residents of the office, in particular Marcelle, Tom and Edmund.

And now I must mention here all those people who contributed, extremely successfully, to chill out my mind and make my life in Bath enjoyable when I was not busy in "stretching the boundary of science". First of all my legendary first-year flatmates, Patrick, Salva and Fred and all my friends over these years, particularly Angeliki, Aquiles, Beatriz, Bernd, Chiara, Daniele, Edwige, Gaia, Giulio, Juan, Nicolas, Pablo, Theo, the Quarry Erasmus group, the Spanish connection and the Greek connection.

Finally a special thanks to my parents.

CONTENTS

NOTATION

A	Actuator area	[m^2]
A, B, C, D	Canonical companion form matrices	
a	CG distance from front axle	[m]
a_i	Generic n^{th} order model coefficient	
a_{ij}	Position feedback gain matrix in the multivariable case	[N]
b	CG distance from rear axle (chapter 3)	[m]
b	Feedback gain in the quarter car case (chapter 5)	[-]
b_{ij}	Velocity feedback gain matrix in the multivariable case	[N]
B	Bulk modulus	[bar]
$\mathbf{B_1}$, $\mathbf{B_2}$	Matrix **B** partition matrices	
C	Road roughness coefficient	[-]
C, $\mathbf{C_0}$	Damping matrices	[N/ms^{-1}]
C_q	Valve discharge coefficient	[-]
c_i	Generic sliding surface coefficient	
c_o	Tyre damping coefficient in the 7 DOF model	[N/ms^{-1}]
c_1 , c_2	Front and rear damping coefficients in the 7 DOF model	[N/ms^{-1}]
D	Valve bore diameter	[m]
E	Rear suspension axle length	[m]
f	Frequency	[Hz]
f	Viscous coefficient in the cylinder	[N/ms^{-1}]
F_d	Frictional damping force	[N]

$\mathbf{F_d}$	Frictional force vector	[N]
F_{ext}	Force applied by the actuator load	[N]
$F_{friction}$	Friction force in the cylinder	[N]
F_{ij}	Generic sliding mode gain matrix	
F_n	Normal force applied to the plate	[N]
$\mathbf{F_n}$	Normal force matrix	[N]
F_s	Friction force at the breakaway	[N]
$F_{s,a}$	Breakaway friction force at the end of the previous sliding period	[N]
$F_{s,\infty}$	Friction force at the breakaway after a long time at rest	[N]
g	Acceleration due to gravity	[m/s^2]
g_{ij}	Velocity feedback gain matrix in the multivariable case	[N]
G	Generic transfer function	
H(·)	Heavyside step function	
i	Valve solenoid driving current	[A]
J	Performance index	
J_α	Pitch moment of inertia	[kgm^2]
J_β	Roll moment of inertia	[kgm^2]
$J_{\beta''}$	Axle roll moment of inertia	[kgm^2]
$\mathbf{K}$, $\mathbf{K_0}$	Stiffness matrices	[N/m]
k_c	Load-actuator compliance spring stiffness	[N/m]
k_c , k_{c1} , k_{c3}	Differential pressure-flow valve coefficients	[m^3s^{-1}/bar]
k_q , k_{q1} , k_{q3}	Spool displacement-flow valve coefficients	[m^3s^{-1}/m]
k_o	Tyre stiffness in the 7 DOF model	[N/m]

k_s	Quarter car suspension stiffness	[N/m]
k_t	Quarter car tyre stiffness	[N/m]
k_{tang}	Tangential stiffness in the static friction model	[N/m]
k_v	Viscous coefficient in Stribeck friction model	[N/ms^{-1}]
k_z	Spool displacement-current gain	[m/A]
k_1 , k_2	Front and rear spring rates in the 7 DOF model	[N/m]
k_{1s}	Valve leakage coefficient	[-]
L	Lipschitz constant (chapter 2)	[-]
L	Cylinder leakage coefficient (chapter 4)	[m^{3}s^{-1}/bar]
M	Mass matrix	
M_A	Actuator mass	[kg]
M_1	Quarter car sprung mass	[kg]
M_2	Quarter car unsprung mass	[kg]
m	Sprung mass in the 7 DOF model	[kg]
m_1	Wheel mass in the 7 DOF model	[kg]
m_2	Axle mass in the 7 DOF model	[kg]
P	Car geometry matrix	
P_A	Actuator pressure	[bar]
P_{Amax}	Max actuator pressure	[bar]
P_B	Actuator rod-end pressure	[bar]
P_c	Relief valve cracking pressure	[bar]
P_S	Supply pressure	[bar]
P_T	Tank pressure	[bar]

p_i	Linearised pressures	[bar]
$\mathbf{q}$	Lagrangian co-ordinate vector	
Q_c	Compressibility flow in the supply line	[m^3/s]
Q_p	Pump flow	[m^3/s]
Q_{rv}	Flow past the relief valve	[m^3/s]
Q_1, Q_3	Flow past the control valve	[m^3/s]
Q_2	Compressibility flow in the actuator	[m^3/s]
q_i	Linearised flows	[m^3/s]
$\Re$	Magnet reluctance	[H^{-1}]
T_L	Frictional memory	[s]
t	Time	[s]
t_2	Dwell time in friction model	[s]
S_α	Sensitivity to the variation of the parameter α	
s	Laplace complex variable	
sgn(·)	Sign function	
U	Generic friction force max value	[N]
u	Generic sliding mode controller (chapter 2)	
u	Valve lap (chapter 4)	[m]
$\mathbf{u_e}$	Equivalent control	
$\mathbf{u_1}$	Disturbance vector	
$\mathbf{u_2}$	Control vector	[N]
V	Car forward speed (chapter 3)	[km/h]
V	Lyapounov function (chapter 4)	

V_{hose}	Supply line volume	$[m^3]$
V_t	Actuator volume	$[m^3]$
v_s	Stribeck velocity	[m/s]
W	Mechanical power	[W]
x	Quarter car working space	[m]
$\mathbf{x}$	State vector	
$\mathbf{x_{ws}}$	Woking space vector	[m]
x_{act}	Actuator displacement	[m]
x_{act0}	Plate-pad initial distance	[m]
x_1	Quarter car sprung mass displacement	[m]
x_2	Quarter car unsprung mass displacement	[m]
Y_{in}, Y_{out}	Generic input and output spectral densities	
$\mathbf{y}$	Output vector	
z	Valve spool displacement	[m]
$\mathbf{z}$	Vertical displacement vector	[m]
z_0	Quarter car road input	[m]
$\mathbf{z_0}$	Road input vector	[m]
z_1 , z_2	Velocity feedback gains in the quarter car case	[-]

SYMBOLS

α	Max value of a generic sliding mode controller (chapter 2)	
α	Pitch angle (chapter 3)	[deg]

β	Min value of a generic sliding mode controller (chapter 2)	
β	Roll angle (chapter 3)	[deg]
β''	Axle roll angle	[deg]
γ	Temporal parameter of the rising static friction	[-]
δ	Exponent in Stribeck friction model	[-]
η	Efficiency	[-]
λ	Road wavelength	[m]
μ	Friction coefficient	[-]
ξ	Quarter car damping ratio	[-]
ξ_v	Valve damping ratio	[-]
ρ	Hydraulic oil density	[kg/m^3]
σ	Sliding surface	
ω_n	Valve natural angular frequency	[rad/s]
ω_1	Quarter car sprung mass angular frequency	[rad/s]
Ω	Spatial frequency	[m^{-1}]

ABBREVIATIONS

A/D	Analogue to Digital
CG	Centre of gravity
D/A	Digital to analogue
DC	Direct current
DMA	Direct memory access

DOF	Degree of freedom
DSP	Digital signal processor
ER	Electrorheological
FEM	Finite element method
LQG	Linear quadratic gaussian
LVDT	Linear voltage displacement transformer
MR	Magnetorheological
PID	Proportional-integral-derivative
PWM	Pulse-width modulation
RMS	Root mean square
SMC	Sliding mode control
VD	Vibration dose value
VSC	Variable structure control

1 INTRODUCTION

1.1 INTRODUCTION

The problem of vibration control is generally tackled by placing between the source of vibration and the structure to be protected, suspension systems composed of spring-type elements in parallel with dissipative elements. Isolation from the force transmitted from the ground or from a rotating load is the fundamental task of any suspension system. The static and dynamic characteristics of the elements of the suspension are chosen according to the system specifications. Suspensions are employed in mobile applications, such as terrain vehicles, or in static applications, such as vibrating machinery or structures.

In a vehicle application the suspension is designed according to both comfort and road holding criteria; depending upon the model of car, either the former or the latter criterion is emphasised. In a static application the comfort criterion is not usually an issue, but other specifications exist, such as on the maximum or minimum value of some quantities (displacements, velocities etc).

Passive suspensions have intrinsic limitations due to the design trade-off in the choice of the spring rate and damping, in order to have an acceptable behaviour both close to the resonance and at higher frequencies (Rao (1995)).

The necessity of compromising between these conflicting requirements has motivated the investigation of controlled suspension systems, where the spring and the damping characteristics are controlled in closed-loop. These controlled suspension systems will be called hereinafter (using an automotive terminology) semi-active and active suspensions.

A *semi-active suspension* is (Lizell (1988)) a device which allows a more or less rapid rate of spring or damping modulation, by using strictly dissipating elements (such as viscous, friction, electrorheological or magnetorheological dampers) or conserving elements (such as adjustable air springs). Therefore a semi-active system cannot add

any energy into the system. This makes a semi-active suspension different from an *active suspension* which can also introduce energy into the system at the price of a generally more complicated design, and a higher energy consumption and cost. In an active suspension the spring and the damper are partially or completely replaced by an actuator which can be either hydraulic, pneumatic or electromagnetic.

In a suspension, the damper element is typically of the viscous-type. In such a device the damping action is obtained by throttling a viscous fluid through orifices; depending on the viscosity of the fluid and the shape of the orifices, different force vs. velocity characteristics can be obtained. This technology is very reliable and has been used since the beginning of the last century (Bastow (1993)).

However in principle it is possible to achieve a damping effect by other means. A recent technology is based on the use of electrorheological (ER) or magnetorheological (MR) fluids. In the next section this technology will be illustrated. Another alternative is frictional damping, which is the scope of this investigation.

A friction damper is a device which is schematically composed of a plate fixed to a moving mass and a pad pressing against it. A schematic showing the physical principle of a friction device is depicted in figure 1.1. An external normal force F_n is applied to a mass by the pad and consequently, because of the relative motion between the pad and the plate and of the presence of friction (which can be represented by a friction coefficient μ or a more elaborated model), a damping force F_d is produced. This device is similar in its physical principle to a brake, even if the aim for which it is used in this work is different. In a brake the aim is to prevent skid and slip so as to minimise the braking distance, whereas in a friction damper the interest is in minimising displacements, velocities and accelerations so as to improve, for example, vehicle ride and handling. The choice of using dry friction as a mean of achieving a damping effect is non-conventional. In most servomechanisms a considerable amount of effort has been invested in order to identify and compensate friction (Åstrom (1998)), which is one of the principal causes of performance deterioration of control systems (e.g. steady-state errors, limit cycles). Here instead frictional force is the actual control force in the closed loop control system.

The pure dry (or lubricated) friction characteristic is of no practical use because of its harshness, but a controlled friction damper can potentially replace a conventional viscous damper with the purpose of reducing vibrations.

Applications of frictional damping can be envisaged in various fields of engineering practice, from automotive applications (controlled brakes and suspensions) to reduction of machinery transmitted loads to supporting structures, up to the active control of buildings.

The thrust of this investigation is an automotive application. This thesis is focussed on the semi-active control of a friction damper system, for a motor vehicle suspension application via an electrohydraulic drive.

Practical applications of friction dampers are present on the market. They are employed in the suspensions of some freight trains. The French company Lenoir is manufacturing friction dampers for this kind of application (Sebesan and Hanganu (1993)). In these devices the friction force produced is proportional to the weight of the train. The cooling is provided by forced convection of air during the train motion.

Most of the work on friction dampers are centred on structural applications, particularly for earthquake protection and in general for vibration damping in smart structures. The Canadian company Pall Dynamics Ltd (Pall Dynamics, www (1999)) is manufacturing friction dampers for building applications. Active control of structures by means of friction devices is extensively used in Japan, for high-cost buildings such as skyscrapers. Nishitani et al (1999) for example suggested the use of a controlled friction damper for earthquake protection. Stammers and Sireteanu (1997) studied the problem of vibration reduction in machines with friction dampers.

Friction dampers have been proposed also for blade vibration control (Sanliturk et al (1995)). The damping of turbine blades has been investigated by Ferri and Heck (1998). Applications to vehicle drive shaft vibration reduction has been also considered (Wang et al (1996)).

A major application where controlled frictional force is exploited is controlled braking. Anti-blocking and anti-skid systems have been largely studied. Two representative works are referred to here among the vast literature on the topic. In the automotive field Chin et al (1992) applied sliding mode control to the control of a vehicle anti-blocking

system (ABS). An aircraft application can be found in the work of Tunay et al (1998) who designed a robust aircraft anti-skid system by means of feedback linearisation.

It is also worthwhile remarking that historically early cars were equipped with friction dampers before the advent of the technology of viscous dampers (Bastow (1993)). Leaf spring suspensions too, exploit the damping properties of friction arising from the sliding motion among leaves when they are bent.

It is appropriate to note that most of the works on the field of controlled damping are concerned with controlled viscous dampers rather than with friction dampers which have been always left aside, particularly in automotive suspension applications, for the harshness of their characteristic and the difficulty in their design and control. The challenge of this work is the control of the friction force so as to obtain an appropriate damping characteristic for an automotive application.

1.2 FRICTIONAL DAMPING

A controlled semi-active friction damper is potentially advantageous in some applications. If this device is properly controlled, it can emulate viscous and spring-type characteristics or any combination of the two and it is possible to create any other type of damping (e.g. proportional to acceleration). It is also worth noting that, if opportunely driven, this device can produce a high damping at low velocity, differently from a passive viscous damper (where at zero velocity the damping is zero) and can "clamp" a mass if contingencies require it.

The main disadvantages of a friction damper are related to the nonlinearity and inherent uncertainty of the friction characteristic which makes the design of the control system a more arduous task.

A great deal of work has been done on the control of friction dampers. A detailed study on application of semi-active control to friction dampers was due to Lane et al (1992). Dupont et al (1997) proposed a group of algorithms oriented to maximise the energy dissipation in the damper and they investigated how different friction models affect the performance of the controllers.They compared the performance of a static friction model and of a model including also velocity dynamics and they found out that in

applications where the amplitude of vibration is large, both models perform equally well, whereas with in applications with small amplitude vibration a model which includes velocity dynamics achieves better performance.

A robust control design approach is a possible way to tackle these problems. Hence *Variable Structure Control* (VSC) has been considered in this study, because, for its robustness properties (Itkis (1976)), it can guarantee a fairly reasonable performance for a certain range of variations of the parameters. Among all the possible VSC algorithms, attention has been focussed on a particular class: *Sliding Mode Control* (SMC), both in the relay-type implementation and using a switched state feedback controller.

However, some of the problems related to controlling a friction damper can be solved at the design stage, rather than by using very complicated control algorithms (e.g. adaptive schemes). For instance the static characteristic can be "smoothed" by minimising stiction force. This can make the control algorithm simpler because it has not to take into account the effect of the stiction force. Stiction can be reduced with an appropriate choice of friction lubricant materials (Wills (1980)). This is also helpful to dissipate heat.

The friction damper is force-controlled and hence consumes lower energy compared to a controlled viscous damper. In an electrohydraulically-actuated scheme this translates to pressure control and hence the flow in the hydraulic circuit is negligible (virtually nil), since the actuator load (the pad) does not move. The flow required in order to set up the working pressure is very small.

A possible design of the whole system is depicted in figure 1.2; it is essentially composed of the mechanical plant and the hydraulic drive. The mechanical plant, representing a car suspension is excited by the external forces induced by the road profile. The hydraulic actuator, connected to the friction pad, acts on the plate fixed to the body of the car (sprung mass) and a friction force is produced as an effect of the relative movement between the pad connected to the wheel (unsprung mass) and the plate.

The force produced by the friction damper is oriented in the same direction as spring, viscous damping and inertial forces and it is modulated by controlling in closed-loop the pressure in the actuator via the control valve. Because the valve works in pressure

control mode the pressure versus spool displacement characteristic (*pressure gain*) can be exploited for controlling the normal force.

The circuit configuration of figure 1.2, which uses an underlapped proportional valve has been employed in the simulation studies which will be discussed in a subsequent chapter; however alternative configurations exist that allow to control pressure as the circuit of figure 1.2. Two other possible solutions are depicted in figures 1.3 and 1.4.

Figure 1.3 shows a circuit composed of a pump and an electrohydraulic pressure relief valve mounted in parallel. The pressure is modulated by the relief valve which is driven by an external electrical current signal.

A third solution is depicted in figure 1.4. An underlapped proportional valve is employed, as in the circuit of figure 1.2, but in this case a service port is blocked and an additional orifice provides a return flow path. An additional orifice is necessary also if a 2-way valve is used.

From the point of view of providing a circuit which modulates pressure, all three configurations are equivalent. The typical responses of the different valves are listed in table 1.1

Table 1.1: Typical bandwidths

TYPE OF VALVE	BANDWIDTH [Hz]
Three-way proportional valve	40
Pressure control valve	80
Four-way servo valve	100

however the first and the third configurations can be advantageous in cases where is necessary to control more dampers at the same time (as it is the case of a car suspension). Using the circuit of figure 1.3, in fact it would be necessary to install as many pumps and valves as the number of controlled dampers, while with the first and the third circuit it is possible to use only one pump which supplies a main line and to derive the valves in parallel (figure 1.5).

The working pressure required for this application is not very large (10-15 bar), and it can be further reduced by making the friction pad contact area larger. Therefore also a pneumatic system (which typically does not work at a very high pressure) can be potentially used. All the configurations described above can be used in principle with pneumatic, rather than hydraulic, actuation.

An electromechanical actuation is another possibility. However some thoughts about the problem has made it clear that a hydraulic solution is preferred.

A torque controlled electrical drive is required in order to control the pressure; power electronic devices controlling the motor can provide the necessary switching logic. A possible drive can be constituted by a motor, which directly acts on the hydraulic actuator, controlling the pressure in the actuator chamber. In this way an electrical motor can substitute both the pump and the valve. Direct control of the pump speed is not advisable in this application because it could be too slow: the main limitations that can be envisaged are mainly related to the greater total inertia. A high stall motor torque is necessary: from this angle a series-connected DC motor, current driven through a PWM-modulated chopper seems to be a good and economical solution, even if for this motor the torque vs. current relationship is nonlinear (quadratic). A valid alternative is a separately excited DC motor, in which the current-torque characteristic is linear and moreover the dynamics are faster because the total inductance of the motor is smaller (the inductance of the field excitation is not present). This motor is however slightly more expensive than the series-connected motor. The torque has to be then converted in a force by a mechanical system, such as a crank and connecting rod mechanism. However both solutions are not feasible in practice, because in this application the rotor of the motor is blocked while a large current circulates in order to produce the required torque. This would cause a fast overheating and the motor would eventually burn out. Therefore a rotating machine is not appropriate.

The alternative to a rotating machine is an electrical linear actuator driven by a solenoid. The problem is that a solenoid with a huge magnetic core would be necessary in order to create the field necessary to produce a force of the order of magnitude required in this application (about 200 N). The force produced by the solenoid, in fact, is proportional to the magnetic induction field, the current and the geometry of the magnet.

In order to achieve a damping force of 200 N, a normal force F_n about twice larger (depending upon the value friction coefficient) is required. The force produced by the solenoid can be expressed by the relationship:

$$F_n = \frac{1}{2}\left(\frac{NI}{\Re}\right)^2 \frac{d\Re}{dx} \tag{1.1}$$

where $\Re$ is the reluctance of the magnetic circuit, I the current, N the number of turns and x the air gap. The reluctance for a standard C-shaped magnet is:

$$\Re = \frac{x}{\mu_0 A} \tag{1.2}$$

A being the cross-sectional area of the magnet and μ_0 the vacuum magnetic permeability. Hence solving equations (1.1) and (1.2) as a function of the magnet area A and using realistic values for ampere-turns and the air gap, the resulting area is of the order of 10^{-1} m^2 which is excessively large.

Because of size constraints electromechanical actuation has been left aside and efforts have been directed towards the hydraulic solution.

1.3 MAGNETORHEOLOGICAL DAMPERS

A magnetorheological damper is another effective alternative to a pure passive viscous damper. It is based on the properties of magnetorheological (MR) fluids. A MR fluid consists of magnetically soft particles in suspension in a viscous fluid. If a current is applied to a coil inside the damper, the particles line up into fibrous structures. In this situation the fluid passes from a Newtonian to a Bingham behaviour. The yield stress is controlled by the applied magnetic field. This creates a controllable damping action, without taking recourse to valves. A very similar device is the electrorheological (ER) damper which uses an ER fluid. MR fluids are similar to ER fluids, but MR fluids are 20-50 times stronger and they are far less sensitive to contaminants and extremes in temperature (Lord Corporation, www (2001)). Temperature dependency is a second order effect; oil and silicone oil based fluids can typically operate from –40 °C to 150 °C. Water based fluids are rated from 0 °C to 70 °C.

Delphi has developed and produced a MR damper, commercially known as MagneRide installed on the Cadillac Imaj (Anon (2000)).

A great amount of research work is carried out at present on MR dampers. As far as their control is concerned, several strategies have been investigated. An interesting work is that due to Dyke and Spencer (1997), who compared several control strategies for MR dampers. Ramallo et al (1999) investigated an H_2/LQG control for a semi-active MR damper to be employed in the control of structures under seismic excitation. Specifically in the automotive field, Peel et al (1996) developed a model of an ER damper for vehicle applications. Choi et al (2000) proposed sliding mode for controlling an ER damper-based suspension and they found that the switching control was causing a jerk phenomenon, leading to an uncomfortable ride although road holding was generally improved.

1.4 ACTIVE SUSPENSIONS

Controlled suspensions (both active and semi-active) have appealed to automotive engineers for many years. At present on the European market 70 vehicles offer some kind of controlled suspensions. They are mainly saloon cars (Anon, www (2001)).

There is a large amount of work on controlled suspension systems in the literature. The first paper dealing with active suspensions dates back to the nineteen fifties (Federspiel-Labrosse (1954)). A review of the state-of-the-art of controlled suspensions was carried out by Hedrick and Wormely (1975). A more up-to-date review was produced in 1983 by Goodall and Kortüm who surveyed the active suspension technology. A few years later, Sharp and Crolla (1987) and Crolla and Aboul Nour (1988b) produced comparative reviews of advantages and drawbacks of various types of suspensions. Another historical review and also an attempt to present some design criteria was given by Crolla (1995). Hillebrecht et al (1992) from BMW discussed the trade-off between customer benefit and technological challenge from the angle of a car manufacturer.

Active suspension's first development was in the world of Formula 1 cars: Lotus was the first car to be equipped with an active system in 1983 (Baker (1984), Milliken (1987)). Besides racing cars, active systems have been studied and developed for a long

time also for road vehicles (typically saloon cars). Citroën worked on active suspensions for many years (Curtis (1991)): its BX model was fitted with a low bandwidth leveller system and the Xantia Activa is equipped with active anti-roll bars. Mercedes worked for over 20 years on active suspensions. The Mercedes CL Coupe (Cross (1999)) is equipped with a fully integrated suspension and traction control, commercially known as ABC (Active Body Control). Toyota worked on controlled suspension, for example in the Toyota Celica (Yokoya et al (1990)) and also Volvo investigated the feasibility of active suspensions (Tiliback and Brood (1989)).

Active suspensions have been investigated and developed also for off-road vehicles (Crolla et al (1987)), such as the Land Rover Discovery. Stayner (1988) proposed an active suspension for agricultural vehicles. Active devices have been investigated also for rail applications as reported by Goodall et al (1981).

A first choice in the design of a fully active suspension is the type of actuation. The force actuator can be either hydraulic or pneumatic or electromagnetic; hybrid systems are also possible. Williams et al (1996) designed an oleo-pneumatic actuator, Martins et al (1999) proposed an alternative hybrid electromagnetic controlled suspension. An active suspension employing a hydraulic actuator, pressure controlled rather than flow controlled has been proposed by Satoh et al (1990).

Active suspensions are a challenging field for control engineers. All the major control techniques developed in the past 30 years have been applied to the problem of controlling vehicle suspensions. An overview of this research now follows.

At the outset it must be stressed that one of the main problems in the design of control algorithms is the identification of the vehicle and suspension parameters. Errors in their knowledge can spoil the performance of the most sophisticated controllers, designed with very refined mathematical techniques. Majjad (1997) and Tan and Bradshaw (1997) addressed the problem of the identification of car parameters.

The necessity of trading-off among the conflicting requirements of the suspensions in term of comfort and road holding led to the use of optimisation techniques. Thompson (1976) studied a quarter car model and employed optimal linear state feedback for designing a controlled suspension; Chalasani (1987) optimised active ride perfomance,

using a full car model. An H_∞ algorithm for active suspensions was proposed by Sammier et al (2000).

The driving conditions in a car change very much depending upon the roads and the speed. This suggests the necessity of some form of adaptive control. Hac (1987) implemented this kind of scheme. Other types of adaptive controls were proposed over the years. Ramsbottom et al (1999) and Chantranuwathana and Peng (1999) studied an adaptive robust control schemes for active suspensions.

Robust control, the opposite control philosophy for dealing with uncertain systems, has been investigated by many authors as well. Mohan and Phadke (1996) studied a VSC controller for a quarter car. Park and Kim (1998) extended this study to a full 7 DOF ride model. Sliding mode control was investigated by Yagtz et al (1997) and by Kim and Ro (1998). A mixed sliding mode-fuzzy controller was proposed by Al-Houlu et al (1999).

A control scheme known as "skyhook damping" based on the measurement of the absolute vertical velocity of the body of the car was proposed in the nineteen seventies and is still employed in a number of variations (Alleyne et al (1993)). Yi and Song (1999) proposed an adaptive version of the skyhook control. Some authors (Chang and Wu (1997)), in order to improve comfort, designed a suspension based on a biological, neuromuscular-like control system.

1.5 SEMI-ACTIVE SUSPENSIONS

Semi-active suspensions were firstly introduced in the nineteen seventies (Crosby and Karnopp (1973), Karnopp et al (1974)) as an alternative to the costly, highly complicated and power demanding active systems. A comparative study with passive systems was carried out by Margolis (1982) and by Ahmadian and Marjoram (1989).

As far as the applications of semi-active suspensions are concerned, they have been envisaged not only for saloon cars but also for other types of vehicles. Besinger et al (1991) proposed an application of semi-active dampers on lorries.

In a study of GEC-Alstom and Metro-Cammell, O'Neill and Wale (1994) pointed out how, in order to reach higher speed and have better comfort, in rail transport, semi-active systems can be a relatively lower-cost solution than improving the quality of tracks. A skyhook algorithm for train applications was proposed by Ogawa et al (1999). Miller and Nobes (1988) designed a semi-active suspension for military tanks.

As with active systems, a variety of control schemes have been proposed for semi-active suspensions: adaptive schemes (Bellizzi and Bouc (1989)), optimal control (Tseng and Hedrick (1994)); LQG schemes (Barak and Hrovat (1988)) as well as robust algorithms (Titli et al (1993)). Crolla and Abdel Hady (1988a) proposed a multivariable controller for a full vehicle model.

Many designs are based on more or less sophisticated car models, but the actuator dynamics have not always been modelled adequately. This problem has been addressed by various authors. Miller (1988) for example analysed the effects of the hardware limitation. Decker et al (1988) focussed their work on the transducer performances.

A novel solution has been proposed by Groenewald and Gouws (1996) who suggested improving ride and handling by controlling in closed-loop the tyre pressure. Such a technique is only applicable to certain off-road vehicles, such as those used in military, agricultural, forestry or construction applications. By controlling tyre pressure it is possible to control wheel-hop resonance and therefore improving the so-called secondary ride, i.e. the behaviour close to the wheel-hop resonance (Shaw (1999)) as well as improving the lifespan of tyres and reducing fuel consumption.

This survey on active and semi-active suspension systems has pointed out the main design problems that exist and how they have been tackled. Some vehicles equipped with controlled suspension are also listed. The survey shows that a great deal of research work has been and it is still being carried out on designing a cheap and reliable controlled suspension system. The work of this thesis is a contribution in the field of controlled suspension. The semi-active friction damper based suspension can provide an improvement in ride without excessive power dissipation and costs.

1.6 OPTIMISED PASSIVE SUSPENSIONS

Some car manufacturers instead decided to direct the efforts towards optimising passive suspensions rather than developing active or semi-active systems. The optimisation of the suspensions is achieved not only via an appropriate design of springs and dampers, but also by improving the design of the other components (rubber bushes, mountings), so as to better exploit their damping properties for obtaining an overall ride improvement, and through an appropriate design of the suspension geometry (links, arms, levers).

A great deal of research has been carried out on the optimisation of passive suspensions. The following references point out some of the efforts in this area over the past decades. Thompson (1973) calculated the optimal damping for a passive suspension using optimal control theory; Jolly (1983) and Karadayi and Hasada (1986) investigated ride improvement using nonlinear models of the suspension. Genta and Campanile (1989) proposed an approximate approach to study the nonlinear behaviour of a passive suspension.

1.7 AIMS OF THE RESEARCH

The aims of this research are:

1) To design an energy-efficient (i.e. with small power consumption) electrohydraulic drive for a friction damper, which constitutes a part of a vehicle suspension unit. In order to reduce capital costs, the drive must be designed employing the least number of components.

2) To develop a model of the electrohydraulically-actuated friction damper, utilised as a part of a motor vehicle suspension. The model has to be sufficiently accurate for control design studies.

3) To design a robust controller, capable to deal with the inherent uncertainties of the plant and to improve the vehicle ride.

4) To develop a working prototype of a friction damper.

5) To investigate experimentally its performance on a vehicle.

6) To preliminary investigate the problem of controlling independently four dampers, constituting a full car suspension.

1.8 STRUCTURE OF THE THESIS

Subsequent chapters are organised in the following manner.

Chapter 2 presents an overview on the state-of-the-art control techniques employed in the control of uncertain systems: PID, adaptive and robust schemes with particular reference to the third ones (VSC, SMC). The general principles are outlined and a literature survey presented. The second part of the chapter is centred on systems with friction. A literature survey on friction models is presented and particular emphasis is placed on friction models for control design.

Chapter 3 describes the passive system modelling and the experimentation on the passively-damped vehicle. This piece of work is necessary in order to define the benchmark system against which the semi-active system can be compared.

Chapter 4 describes the mathematical model of the electrohydraulic-actuated friction damper. Subsequently the design and simulation of the sliding mode controller is outlined.

Chapter 5 describes the switched state feedback controller design and simulation. In the second part the initial experimentation on a pilot rig and tests of the friction damper for the vehicle are described.

Chapter 6 describes the experimental work and the validation against the experimental data of the hydraulic circuit and of the semi-active damper installed on the car.

Chapter 7 describes the extension to a multivariable case where up to four friction dampers, constituting a full car suspension, are controlled independently.

Chapter 8 presents the conclusions and gives some proposals for further work.

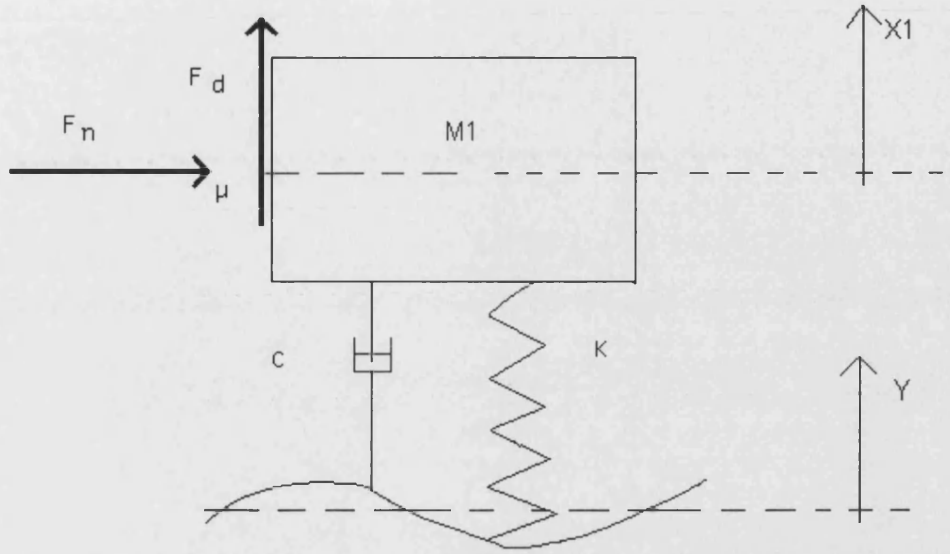

Figure 1.1 Principle of a friction damper.

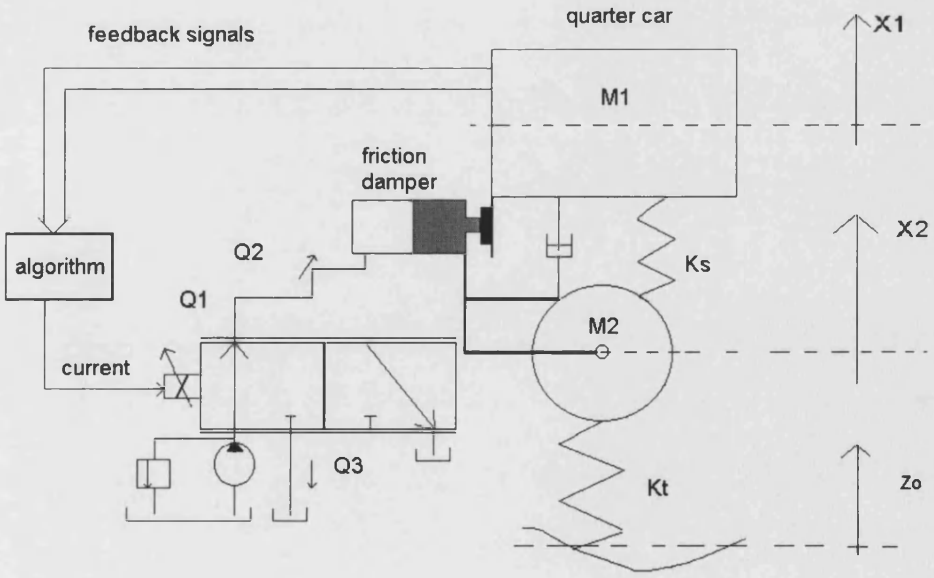

Figure 1.2 Hydraulic drive using an underlapped 3-way proportional valve.

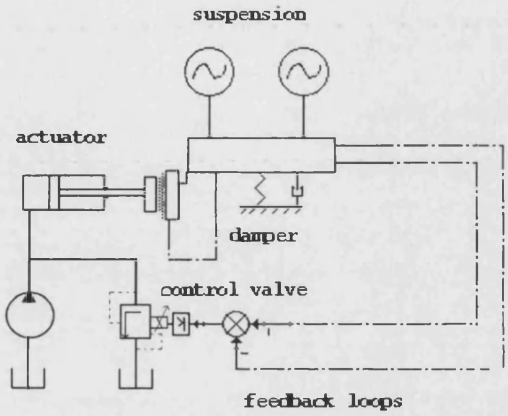

Figure 1.3 Hydraulic circuit using a proportional pressure relief valve.

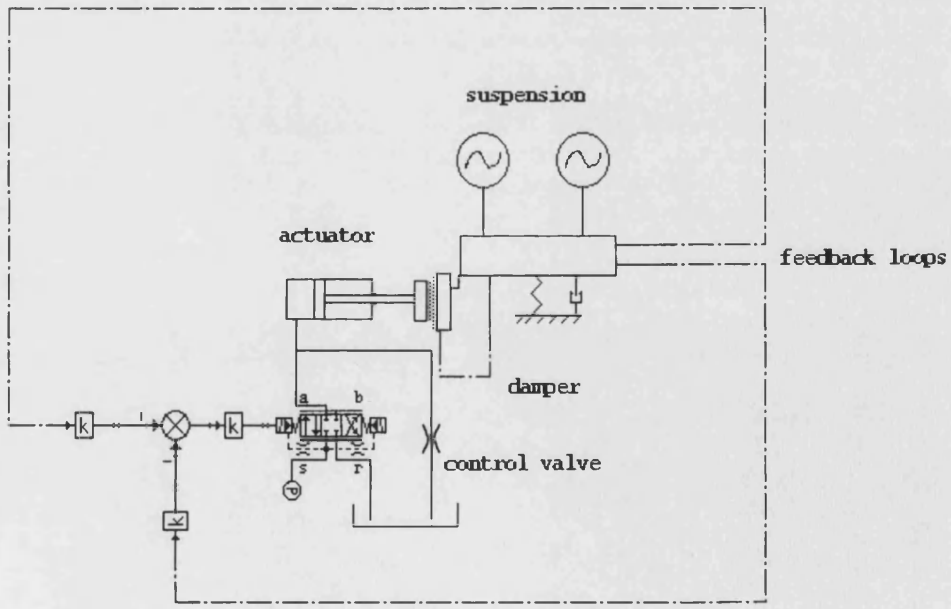

Figure 1.4 Hydraulic circuit using a 3-way 4-position valve with a port blanked-off and an additional orifice to dump flow.

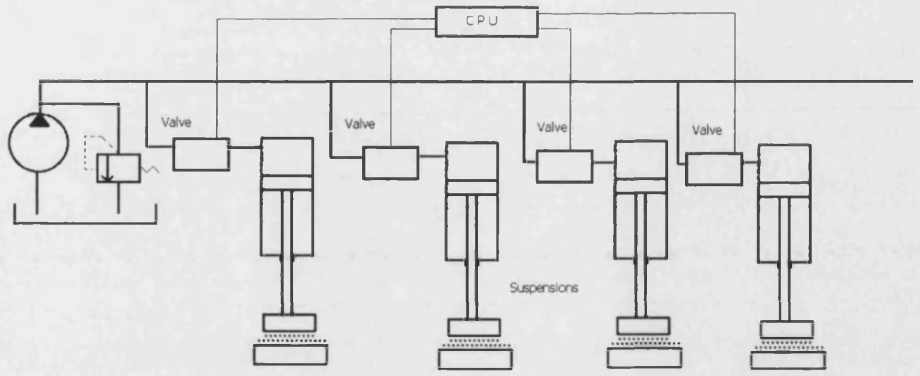

Figure 1.5 Hydraulic schematic for the independent control of the four suspensions.

2 CONTROL OF UNCERTAIN SYSTEMS WITH FRICTION

2.1 INTRODUCTION

A suspension based on a semi-active electrohydraulically-actuated friction damper can, from a control point of view, be classified as a system with parametric uncertainty and affected by external disturbances. The friction characteristic is a major source of uncertainty, although not the only one. Parameter uncertainties and unmodelled dynamics in the hydraulic drive and in the vehicle models are always present. The principal sources of disturbance are the road profile and the steering input (when handling dynamics are also considered).

A number of control strategies can be employed to cope with this class of systems. They can be grouped into three families:

- PID controllers
- Adaptive algorithms
- Robust algorithms

Robust control is the approach used throughout this work. However the other types of controllers could have been utilised as well. This chapter provides an overview of all of them.

A friction damper based suspension can be thought of, to a rough approximation (taking the hydraulic dynamics to be instantaneous and referring for ease to a scalar case), as a nonlinear forced oscillator described by a second order spring-mass-damper model:

$$M_1 \ddot{x}_1 + c(\dot{x}_1 - \dot{y}) + k(x_1 - y) + \mu F_n(x_1 - y,\ \dot{x}_1 - \dot{y},\ \ddot{x}_1, t)\,sgn(\dot{x}_1 - \dot{y}) = 0 \qquad (2.1)$$

Figure 1.1 depicts the system described by this equation: k and c are respectively the elastic and viscous coefficients, M_1 is the sprung mass, y and $\dot{y}$ represent the external

inputs, x_1 the mass displacement, $\dot{x}_1$ its velocity and $\ddot{x}_1$ its acceleration. The function $F_n(\cdot)$ is the control action; friction force $F_d(\cdot)$ is given by:

$$F_d(\cdot) = -\mu F_n(\cdot) sgn(\dot{x}_1 - \dot{y}) \tag{2.2}$$

From a pure mathematical viewpoint the control problem can be regarded as finding a piecewise function $F_n(x_1 - y,\ \dot{x}_1 - \dot{y}, \ddot{x}_1, t)$ that forces the solution of the equation (chassis position) and its derivatives (i.e. velocity and acceleration) to behave in a predefined manner, according to a set of specifications.

The function $F_n(\cdot)$ is physically an external control force that attempts to compensate spring and viscous damping forces present in the system. The specification of this function (in terms of ride and road holding) is the target of the control (see chapter 3, section 3.4) .

2.2 PID CONTROLLERS

PID controllers were and are still largely used in a wide range of applications. These controllers are frequently designed in the frequency domain, and hence on the hypothesis of linearity. Therefore they work well if this hypothesis is fairly close to the actual behaviour of the system. If this is not the case, performance is likely to worsen. A linear system is defined in the frequency domain by its transfer function $G(j\omega)$. The transfer function is often the result of a linearisation of a mathematical model and it gives a more or less accurate representation of the actual physical system. The major sources of uncertainty are due to parameter changes, unmodelled dynamics and time delays, changes in the operating point, sensor noise and unpredicted disturbance inputs. Although a PID scheme is not supposed to perform well in conditions different from those for which it has been designed, its performance can be optimised using a robust design approach or by including an additional adaptive loop (see next section). In this way, it can be made to exhibit the desired performance over a larger range.

A controller is said to be *robust* (Dorf and Bishop (1995)) if it has low sensitivities and it is stable and continues to meet its nominal specifications over a typical range of

parameter variations. A measure of the robustness to small parameter variations is the sensitivity, defined as:

$$S_\alpha = \frac{\partial G / G}{\partial \alpha / \alpha} \tag{2.3}$$

with α being a parameter of the system. The design of a PID controller entails the choice of the type of transfer function of the controller (its static gain, the poles and the zeros). The main features of robust design are:

1) Largest possible bandwidth.

2) Largest possible loop gain, attained primarily in the controller and in the forward path transfer functions (in this way the disturbance rejection is increased).

Several design and tuning methods have been developed over the years for PID controllers. The most common classical tuning method involves the so-called Ziegler and Nichols rules (Ziegler and Nichols (1942)); they permit to tune the PID parameters, based on the partial knowledge of the transfer function, which can be obtained by simple tests on the system; another classical method is based on the Cohen and Coon rules (Cohen and Coon (1953)); in this method the PID parameters are tuned by fixing a damping ratio of 0.25 in response to a disturbance input. In the subsequent years other methods have been developed, such as the Smith Predictor (Smith (1957)), the Haalman method (Haalman (1965)) and the Dahlin Regulator (Dahlin (1968)). It is worthwhole noting that all these techniques are linear. Other methods exist that minimise a performance index of the error (ISE, IAE etc). A review of all these and other methods can be found in Åström et al (1993) which enters into the details of the analytical calculation of the controller parameters.

In the friction damper control problem, a linear approach cannot be taken because the friction force characteristic, in the forward path of the loop, is the core of control and cannot be linearised.

As opposed to linear frequency domain based methods, in the past 40 years nonlinear control methods, specifically adaptive and robust algorithms (Slotine and Li (1992)), have been developed, in the time domain, as a consequence of the development between

the nineteen sixties and the nineteen seventies of various nonlinear methods (e.g. state space and phase plane methods, Lyapounov stability theory etc).

2.3 ADAPTIVE CONTROL

A possible approach which can be employed to deal with uncertain systems is adaptive control. The philosophy of this control is opposite to robust control. Although this work is focussed on the use of the latter type of control, it is worthwhile describing in the context of this chapter the basic principles of adaptive control, which in principle can potentially be used to tackle the problem of the control of a friction damper.

An adaptive control can be thought as a control with *on-line estimation of uncertain parameters* (Slotine (1984)). The parameters, estimated on the basis of the measured plant signals, are then used in the control action. Systems with constant or slowly-varying uncertain parameters are the most likely to have an improvement in their responses with this type of control. In such systems the on-line estimation requires a minor amount of computational power and therefore the controller "learns" more quickly (the more the adaption goes on, the more an adaptive controller improves its performance). The target of the adaptive control is to try and keep consistent performance in systems with unknown variations in its parameters. A controller with fixed parameters (such as a PID) can become innacurate or even unstable for large parameter variations; however an adaptive loop can be added to a PID controller, enhancing its performance.

Typical applications of adaptive algorithms are in robotics (where the payload can vary), power systems (where the energy demand varies slowly in the course of the day) or process control (chemical or metallurgical processes, etc). There are two main approaches to design adaptive controllers. With *model-reference adaptive control* a reference model is used to set the ideal response of the system, with the error between the ideal and the actual response being the input to the adaptation law. The second approach is *self-tuning control* where the estimation of the parameters is obtained by measuring the inputs and the outputs to the plant. These are then used for the on-line design of the controller, which is continually updated as parameters change with operating conditions.

2.4 ROBUST CONTROL

A robust controller is meant to provide a reasonable level of performance in systems with uncertain parameters, no matter how fast they vary, but it usually requires the knowledge (or an estimate) of the uncertain parameter bounds. The typical structure of a robust control law is composed of a nominal part (such as a state feedback or an inverse model control law), plus a term which deals with model uncertainty.

A certain degree of robustness can be achieved with PID controllers; however robust control is typically associated with *Variable Structure Control.* Variable structure controllers are a very large class of robust controllers (Hung et al (1993)). The distinctive feature of VSC is that the structure of the system is intentionally changed according to an assigned law. This can be obtained by switching on or cutting off a primary feedback, a local feedback, derivative connections and so forth (Itkis (1976)). By using VSC, it is possible to take the best out of several different systems (or better structures), switching between them with an appropriate law. The control law defines various regions in the phase space and the controller switches between a structure and another at the boundary between two different regions according to the control law. Therefore the designer is no longer forced to pursue trade-offs between the classical control requirements (static and dynamic accuracy). It is possible to synthesise a wide range of trajectories by switching between two or more systems according to a predefined law, improving therefore the transient and steady-state responses of the new system with respect to the responses of the original systems.

In principle the laws governing the change in the structure can be very different; however the law that is given greatest attention is that producing the so-called sliding regime. The reason why it has been so widely studied lies in the fact that when the sliding motion occurs, the system becomes insensitive (*invariant*) to parametric and external disturbances of the plant. This particular type of VSC is known as *Sliding Mode Control.* It must be stressed that VSC system can be devised without a sliding mode, but in this general case the robustness properties are not guaranteed.

The principles of adaptive and robust control have been now outlined. The designer must make a decision on which control is more suitable to a particular type of plant to be controlled. There is no general rule; however some rules of thumb can be given.

In general adaptive control performs better with constant or slowly-varying parameters. An adaptive controller improves its performance as adaptation proceeds, whereas a robust controller only attempts to keep good performance. Robust control however can cope better with fast-varying parameters and unmodelled dynamics. Some advanced controllers exist which combine adaptive and robust features. They are known as robust adaptive controllers. Furthermore the implementation of an adaptive controller requires more computational effort to perform the on-line identification and this frequently requires a more sophisticated control board (such as a DSP). Robust control algorithms are usually simple from a computational viewpoint and they can be implemented readily on cheap boards.

For the system investigated a robust control strategy has been chosen. In the friction damper system the most critical parameter is the friction coefficient. This parameter cannot be measured directly but it must be inferred by measuring inertial, viscous and elastic forces. Its identification requires a certain amount of computational load and the learning of the adaptive controller can be slow. Furthermore in an automotive application, low-cost is a major issue and, from this angle, robust control is advantageous in the sense it can be implemented with cheap electronics and possibly with a low number of transducers.

2.5 SLIDING MODE CONTROL

The basic idea of sliding mode control is to force the system to join and to stay on a predefined surface, the *sliding surface* (or hypersurface) in the phase space. During the motion of the system state towards the surface, the system structure changes according to a predefined switching law. When the state begins to move onto the hypersurface switching between the two original systems occurs, ideally, at infinite frequency and in such conditions the system becomes formally equivalent to an autonomous system of lower order.

On the sliding surface the controller is bang-bang type and the closer to an ideal on-off controller the higher the frequency of switching and the more its trajectory tracks attentively the sliding surface. The actual behaviour in a real system (with a real switching controller) is called *quasi-sliding motion* and the trajectories are said (using a

fluid dynamic analogy) to stay within a *boundary layer* of the switching surface. As a consequence of this, a ripple phenomenon, known as *chattering*, is produced on the highest derivative of the original system. This kind of motion is what actually can be physically achieved. Under ideal conditions there is no chattering. In practice, chattering can be a serious problem; it may be an undesired side-effect because (since it is usually at high frequency) it may excite unmodelled higher order dynamics. A great deal of work has been done to tackle this problem. Some insights on the chattering problem are given in subsection 2.5.6.

In order to implement SMC a switching element is necessary. Typically, this can be a power electronic device (such as a BJT or a MOSFET) or, if the required level of power is not very high an operational amplifier working in open-loop (in fact op-amps constitute the firing circuits of the power electronic devices). Other possible sliding mode actuators are electromechanical relays and on-off valves or any other device capable to toggle swiftly between an on- and an off-state.

The design of a sliding mode controller is articulated in two steps. The first one entails the choice of the switching surface. The second concerns the specification of the discontinuous control functions and the determination of the switching logic associated with the surface. The first step can be completed, in principle, without any assumption on the form of the control functions, while the second step involves the selection of the control which ensures that the specified sliding mode is attained.

The following subsections outline the basic concepts of SMC assuming an ideal switching element. A second order system is initially utilised for illustration purposes. A more formal approach is then employed to generalise the concepts and describe the main features of SMC. Subsequently the problem of chattering in the actual sliding motion is considered. Finally some examples of applications of SMC are given.

2.5.1 SMC of a second order system

The results hereby presented follows the approach by Itkis (1976). Consider a second order system; in controllable canonical form as described by the following equations[1]:

$$\dot{x}_1 = x_2$$

$$\dot{x}_2 = -a_2 x_2 - a_1 x_1 - u \tag{2.4}$$

a sliding surface is defined by:

$$\sigma = x_2 + c_1 x_1 = 0 \tag{2.5}$$

A control is chosen in the form of:

$$u = V x_1 \tag{2.6}$$

where

$$V(x, t) = \begin{cases} \alpha \\ \beta \end{cases} \qquad \text{if } x_1 \sigma > 0 \text{ or } < 0 \tag{2.7}$$

The derivative of σ is:

$$\frac{d\sigma}{dt} = \frac{d(x_2 + c_1 x_1)}{dt} = -(a_2 - c_1) x_2 - a_1 x_1 - u \tag{2.8}$$

On the sliding surface $\sigma = 0$ then $x_2 = -c_1 x_1$.

Hence when the state is moving on the surface the dynamics of the system become first order and they are described by the following equation:

---

[1] Most of the symbols used in this chapter are listed in the notation section. Some of them used only once in some mathematical developments, are defined only in the course of the chapter.

$$\dot{x}_1 = -c_1 x_1 \tag{2.9}$$

From equation (2.9) it follows that the dynamics of the system now are independent from the parameters of the plant and they only depend upon the coefficient c_1 that unequivocally identifies the sliding surface. In such an ideal situation the system is said to be *invariant* (more than just robust) to modelling error and disturbances. The invariance property requires that certain *matching conditions* are satisfied (Drazenovic (1969)). The matching conditions are a constraint on the upper and lower bound of the disturbance and uncertainty.

The trajectory is depicted in figure 2.1 (highlighted line). The dynamics of a system in the sliding mode regime can be divided in two parts: an initial transient during which the state of the system joins the required surface in the phase space (*reaching phase*) and a regime, occurring after hitting the sliding surface, where the state moves onto it (*sliding phase*). This new phase is characterised by high frequency switching (theoretically infinite), small (ideally zero) steady-state error and disturbance rejection.

It is interesting to remark that the actual switching function is a quadratic form $x_1 \sigma$ and the controller is a switched feedback gain. This was the approach followed by the first developments of VSC. More general forms for the switching surfaces and the controllers have been developed in the further stages of the research on VSC.

This example has given some initial insights into SMC. In the following subsections a more formal approach will be followed.

2.5.2 Statement of the SMC problem

Many physical systems are described by ordinary differential equations whose right-hand sides feature discontinuities with respect to the independent variable. These systems are described by the general equation (bold letters denote matrices and vectors):

$$\dot{\boldsymbol{x}} = \boldsymbol{f}(\boldsymbol{x},\boldsymbol{u},t) \tag{2.10}$$

where the state vector $\boldsymbol{x} \in \Re^n$, the input vector $\boldsymbol{u} \in \Re^m$ and t is the independent variable time; $\boldsymbol{f}(\boldsymbol{x},\boldsymbol{u},t)$ is discontinuous on a set of surfaces $\sigma_i(x,t)$ ($i = 1,\ldots, m;\ m<n$), in vector form $\sigma(\boldsymbol{x},t)$.

Without excessively losing generality the system is supposed to be linear with the control (if it is not, it can be put in this form by a non-singular transformation). Hence:

$$\dot{x} = A(x,t) + B(x,t)u \tag{2.11}$$

A SMC is defined as:

$$u(x,t) = u(x,t)^{+} \quad \text{if} \quad \sigma(x,t) > 0 \tag{2.12a}$$

$$u(x,t) = u(x,t)^{-} \quad \text{if} \quad \sigma(x,t) < 0 \tag{2.12b}$$

such that the state reaches $\sigma(x,t)=0$ in finite time.

2.5.3 Mathematical background

Non-continuous control functions are the object of the investigation. The theoretical foundation of SMC is the theory of a differential equation with discontinuous right-hand side (Filippov (1988)).

The concept is that on the sliding surface the differential equation is not defined, because its right-hand side is not analytic. In these regions, existence and uniqueness of the solution are not guaranteed. The Cauchy-Lipschitz theorem on existence and uniqueness of the solution states that the solution of an ordinary differential equation exists and it is unique if and only if a Lipschitz constant may be found so that for any x_1 and x_2 :

$$|f(x_1, t) - f(x_2, t)| \leq L |x_1 - x_2| \tag{2.13}$$

In the sliding mode, the theorem is violated in the neighbourhood of the sliding surface. Hence from a knowledge of the equation (2.10) it is not possible to obtain information on the behaviour on the sliding surface. An *auxiliary equation,* which models the switching on the sliding surface must be added to completely describe the behaviour of the system.

The unavailability of a well-established theory has brought about the rise of different approaches to the problem. Most of these studies were carried out in the former Soviet

Union, starting from the nineteen sixties. Utkin (1992) reports these early developments of the theory. In parallel with the development of the general theory of VSC, a more practical approach was undertaken by practising control engineers working with relay control systems which sometimes showed an unpredicted (and undesired) sliding mode behaviour which caused wear and damage of the relay contacts.

An overview of the main methods proposed to describe sliding motion are now reported.

A first method (that employed in the previous example) is due to Wonham and Johnson (1963). They propose the virtual substitution of the "infinitely fast" oscillations of the state about the switching surface by the slow average component of the motion on the surface itself. This means that the state simply moves onto the surface $\sigma=0$ and never leaves it. This is mathematically described by the vanishing of the function $\sigma=0$ and its derivative $\dot{\sigma}$.

In more quantitative terms, consider a generic n^{th} order linear system that is sliding mode controlled:

$$\begin{aligned} \dot{x}_i &= x_{i+1} \qquad (i=1\ldots n-1) \\ \dot{x}_n &= -\sum_{i=1}^{n} a_i x_i - u \end{aligned} \tag{2.14}$$

and the sliding surface:

$$\sigma = \sum_{i=1}^{n} c_i x_i \qquad (i=1\ldots n-1) \tag{2.15}$$

By placing $\sigma = 0$ and $\dot{\sigma} = 0$, it is possible to eliminate, by substitution, one equation from system (2.14), thus lowering the order of the system by one. If the sliding mode is achieved the dynamics of the original n^{th} order system are described by a system of (n-1) linear differential equations, whose controllable canonical form is:

$$\dot{x}_i = x_{i+1} \qquad (i = 1 \ldots n-2)$$
$$\dot{x}_{n-1} = -\sum_{i=1}^{n-1} c_i x_i \tag{2.16}$$

This method is extremely practical from an operational point of view.

Another method is the *equivalent control* method proposed by Utkin (1972). In this scheme the switching control law is replaced by a continuous law $\boldsymbol{u_e(x,t)}$ which maintains the state onto the sliding surface. When $\boldsymbol{u_e(x,t)}$ is known the dynamics in sliding mode can be obtained by substituting $\boldsymbol{u_e(x,t)}$ in (2.10).

A more analytical method is due to Filippov (1960). He proposed to describe the sliding motion by taking the average of the state vectors of the two structures on the sliding surface. The resulting vector can be proved to be tangent to the sliding surface.

Other methods for describing the sliding motion are based on co-ordinate transformations (Utkin and Young (1978)) and on the theory of differential equations with the right-hand side being a set-mapping function (Roxin (1965)).

2.5.4 Reaching conditions

It has been previously stated in subsection 2.5.1 that the dynamics of a sliding mode controlled system are divided into two parts: a reaching phase and a sliding phase. The focus is now on the former. It is useful to obtain necessary (and possibly sufficient) conditions that guarantee the existence of a sliding mode regime. In physical terms, this means establishing the minimum value of the controller gain to drive and keep the state vector $\boldsymbol{x}$ of the system on the sliding surface.

Conditions expressed in several different forms have been obtained. The most classical approach (Itkis (1976), Utkin (1992)) is based on the knowledge of the sliding function itself. The *necessary and sufficient* condition for the *existence* of a sliding mode regime is that:

$$\sigma_i \dot{\sigma}_i \leq 0 \qquad (i=1 \ldots m) \tag{2.17}$$

This condition results from some mathematical manipulations of the governing equations of the system. Consider the system:

$$\dot{x}_i = f_i(x_1, \ldots x_n, t) \qquad (i=1 \ldots n) \tag{2.18}$$

and suppose that the right-hand members are discontinuous on the surface:

$$\sigma(x_1, \ldots x_n, t) = 0 \tag{2.19}$$

Hence the right- and left- hand limits of the function are:

$$\lim_{\sigma \to 0-} f_i(x_1, \ldots x_n, t) = f_i^- (x_1, \ldots x_n, t) \tag{2.20}$$

$$\lim_{\sigma \to 0+} f_i(x_1, \ldots x_n, t) = f_i^+ (x_1, \ldots x_n, t) \tag{2.21}$$

The derivative of (2.19) along the trajectories is:

$$\dot{\sigma} = \sum_{i=1}^{n} \frac{\partial \sigma}{\partial x_i} \dot{x}_i = \sum_{i=1}^{n} \frac{\partial \sigma}{\partial x_i} f_i = (\boldsymbol{f} \cdot \nabla \sigma) = \left[\sum_{i=1}^{n} \left(\frac{\partial \sigma}{\partial x_i} \right)^2 \right]^{1/2} (\boldsymbol{N} \cdot \boldsymbol{f}) \tag{2.22}$$

where $\boldsymbol{f}$ is the vector with components $f_1, \ldots f_n$ and $\boldsymbol{N}$ is the normal to the surface σ:

Taking the limits:

$$\lim_{\sigma \to 0-} \dot{\sigma} = (\boldsymbol{f}^- \cdot \nabla \sigma) \tag{2.23a}$$

$$\lim_{\sigma \to 0+} \dot{\sigma} = (\boldsymbol{f}^+ \cdot \nabla \sigma) \tag{2.23b}$$

The sign of these two limits can be greater, less or equal to zero, but the sliding mode will be achieved if and only if:

$$\lim_{\sigma \to 0+} \dot{\sigma} \leq 0 \leq \lim_{\sigma \to 0-} \dot{\sigma} \tag{2.24}$$

or equivalently:

$$\lim_{\sigma \to 0} \sigma \dot{\sigma} \leq 0 \tag{2.25}$$

This is the *necessary and sufficient* condition for the *existence* of a sliding mode regime.

As an illustrative example, consider the system defined by (2.14):

$$\begin{aligned} \dot{x}_i &= x_{i+1} \qquad (i = 1 \ldots n-1) \\ \dot{x}_n &= -\sum_{i=1}^{n} a_i x_i - u \end{aligned} \tag{2.14}$$

with the sliding surface:

$$\sigma = \sum_{i=1}^{n} c_i x_i \qquad (i=1 \ldots n-1) \tag{2.15}$$

If a control law is chosen of the form:

$$U = Z(x,t)\, x_1 \tag{2.26}$$

with

$$Z(x,t) = \begin{cases} \alpha \\ \beta \end{cases} \quad \text{if } x_1 \sigma > 0 \text{ or } < 0 \tag{2.27}$$

then applying (2.17) yields:

$$\frac{c_{i-1} - a_i}{c_i} = c_{n-1} - a_n \qquad (i=2 \ldots n) \tag{2.28}$$

and

$$\alpha \geq (a_n c_1 - c_1 c_{n-1} - a_1) \tag{2.29a}$$

$$\beta \leq (a_n c_1 - c_1 c_{n-1} - a_1) \tag{2.29b}$$

These are the minimum values of the switched gains of the controller (2.27) in order to promote SMC.

For the particular case of the second order system defined by (2.4), yields:

$$\alpha \geq (a_2 c_1 - c_1^2 - a_1) \tag{2.30a}$$

$$\beta \leq (a_2 c_1 - c_1^2 - a_1) \tag{2.30b}$$

Condition (2.17) can be also obtained with a *Lyapounov approach* (Itkis (1976)). In order to apply Lyapounov stability theory it is necessary to define a Lyapounov function. Such a function can be physically thought as an energy function in the general case of non-conservative systems. Lyapounov theory is based on the assertion that if the total energy of a system is continuously dissipated, the system evolves towards a state of equilibrium. There are no established rules to choose a Lyapounov function; the only constraint lies in the fact that it must be a continuous and definite positive function of the system states, with a continuous first derivative in its domain. One of the main results of Lyapounov theory (Hagedorn (1988)) is that a system is stable (weakly or asymptotically) if the first derivative of the Lyapounov function is semidefinite negative.

After this premise consider (2.25). If it is written as:

$$\lim_{\sigma \to 0} \frac{d(\sigma^2)}{dt} \leq 0 \tag{2.31}$$

it can be thought that there exists a Lyapounov function of the form:

$$V(x_1, \ldots x_n, t) = \sigma^2 (x_1, \ldots x_n, t) \tag{2.32}$$

or in vector form:

$$V(\mathbf{x},t) = \sigma^T \sigma \tag{2.33}$$

Then a global reaching condition is given by $\dot{V}(\mathbf{x},t) \leq 0$ i.e. by (2.31).

Inequality (2.31) states that the system is stable relative to the surface $\sigma = \mathbf{0}$.

In more rigorous terms the existence condition for a sliding mode regime is a sufficient condition for the system (2.18) to be stable with respect to the manifold $\sigma=0$.

Consider what would happen if condition (2.17) was not satisfied. In this case (see again figure 2.1), the state trajectory after hitting the sliding surface may continue in the region $\sigma<0$ on an unspecified trajectory, yielding generic bang-bang control. Other control logic, different from SMC, can result in a bang-bang control action, such as the minimum time optimal control, where the switching logic is obtained as a result of the application of Pontryagin Maximum Principle (Pontryagin et al (1962)). Under these circumstances the disturbance rejection property does not hold. Conversely when condition (2.17) is respected, the state moves onto a first order surface (a straight line) heading towards the origin.

A third approach is known as the *reaching law method* (Gao and Hung (1993)). This method not only establishes the reaching condition, but also specifies the dynamic characteristics of the system during the reaching phase. Such an approach directly defines the sliding function dynamics via a differential equation's right-hand side:

$$\dot{\sigma} = -\boldsymbol{Q}sgn(\sigma) - \boldsymbol{K}f(\sigma) \tag{2.34}$$

where gains $\boldsymbol{Q}$ and $\boldsymbol{K}$ are diagonal matrices with positive elements. In this way the reaching law defines both the reaching conditions and the dynamics during the reaching phase. Two important subcases of this general law are the constant rate reaching law:

$$\dot{\sigma} = -\boldsymbol{Q}sgn(\sigma) \tag{2.35}$$

and the constant plus proportional rate reaching law:

$$\dot{\sigma} = -\boldsymbol{Q}sgn(\sigma) - \boldsymbol{K}\sigma \tag{2.36}$$

2.5.5 SMC laws

The control law can be either pre-assigned *a priori* and then the correct values of the controller gains can be calculated using any of the reaching conditions described above.

Alternatively, the control law can be obtained analytically starting from the above conditions.

The "natural" SMC controller is a *relay* control:

$$u_i(\boldsymbol{x}) = V_i^+ \quad \text{if} \quad \sigma_i(\boldsymbol{x}) > 0 \tag{2.37a}$$

$$u_i(\boldsymbol{x}) = V_i^- \quad \text{if} \quad \sigma_i(\boldsymbol{x}) < 0 \quad (i=1...m) \tag{2.37b}$$

Another very common SMC law is *linear state feedback with switched gains.* The general form is:

$$\boldsymbol{u}(\boldsymbol{x}) = \boldsymbol{F}(\boldsymbol{x})\,\boldsymbol{x} \tag{2.38}$$

$\boldsymbol{F} \in \Re^{mxn}$ being a matrix of state-dependent gains.

A typical form for $\boldsymbol{F}$ for is:

$$F_{ij}(\boldsymbol{x}) = \alpha_{ij} \quad \text{if} \quad \sigma_i(\boldsymbol{x})\, x_j > 0 \tag{2.39a}$$

$$F_{ij}(\boldsymbol{x}) = \beta_{ij} \quad \text{if} \quad \sigma_i(\boldsymbol{x})\, x_j < 0 \quad (i=1...m;\ j=1...n) \tag{2.39b}$$

Applications of this control law can be found in Zinober (1990).

De Carlo et al (1988) proposed a control law consisting of two terms: an equivalent continuous term obtained from the equivalent control method plus a switching term in order to satisfy the reaching condition.

In the friction damper control, two classes of SMC law have been investigated (described in chapters 4 and 5). A first class of schemes is relay-type. This has been implemented taking advantage of the pressure gain-saturation shaped characteristic of the hydraulic control valve, which results in a relay-like sliding mode controller with boundary layer. The second class of controllers investigated belongs to the family of the state feedback with switched gain controllers. From now onwards this control scheme will be called more simply *switched state feedback.* These latter SMC laws have been synthesised by switching between different proportional feedback controllers according

to a predefined switching condition. The linear range of the pressure gain characteristic of the valve has been exploited to implement them.

2.5.6 Disturbance rejection and chattering

The ideal SMC is invariant to uncertainties and disturbances. The dynamics are dictated only by the parameters of the sliding surface. This is because of a particular property of the sliding mode controller. It can be proved (Tsypkin (1974)) that during the sliding motion the gain of the controller, in this ideal situation, is *infinite*. This justifies the complete rejection to disturbances.

Consider the ideal switching element defined by the following (normalised) equation:

$$V=sgn(\sigma) \tag{2.40}$$

with σ being the input. The gain of this relay is:

$$K=\frac{sgn(\sigma)}{\sigma}=\frac{1}{|\sigma|} \tag{2.41}$$

So in the limit of $\sigma \to 0$:

$$\lim_{\sigma \to 0} K=\infty \tag{2.42}$$

This infinite gain ensures a complete disturbance rejection. This property of the sliding motion is peculiar among all the possible motions with a generic VSC.

In reality an ideal sliding mode controller does not exist. Hence chattering will be always present. The second cause of chattering is all the unmodelled dynamics in cascade with the plant. These produce chattering even in the absence of non-ideal switching. In practice both effects are present together.

A solution proposed to reduce chattering is to introduce a boundary layer. Its amplitude is dictated by the actual gain of the controller. If the physics of the controller allows it, the boundary layer can be tuned. By appropriate sizing of the boundary layer (Slotine (1984)) it is possible to control, up to a certain extent, the chattering (which is

proportional to the boundary layer size). In practice this means replacing the relay controller with a continuous control where the on-off characteristic is replaced by a saturation characteristic. In this situation the gain close to the sliding surface is no longer infinite but still very high. With this control, chattering is ideally eliminated but the sliding mode, in the sense described before, virtually does not exist. Using a saturation element with finite gain instead of a relay, the state trajectory is no longer forced to stay on the sliding surface. Therefore the state tends to the equilibrium position following a trajectory which only approximates the sliding surface. This also causes a loss of robustness.

Another possibility is using a relay with hysteresis. In this case a nonideal quasi-sliding mode occurs, which means chattering arises. Also in this case robustness is affected. If a saturation controller with hysteresis is employed, both the aforementioned problems are combined.

A large amount of work can be found in literature regarding the problem of chattering.

A comprehensive survey can be found in Young and Özgüner (1999).

2.5.7 Nonlinear and other types of SMC

Some of the results presented so far refer to linear systems. In a generic nonlinear case the underlying concepts are the same; however in a nonlinear case many requirements (especially necessary and sufficient reaching conditions) must be found from case to case, often by trial and error (Handroos and Liu (1998)). This is the case of the friction damper system where the control action is "semi-active" in the sense it cannot assume negative values.

The extension of SMC to discrete time is not straightforward (Sarpturk et al (1987)). In the discrete time implementation, the switching device is controlled by a digital computer and the control input is switching at discrete instants, in general different from the ones in which the state crosses the sliding surface in the continuous time case. The arising quasi-sliding regime is different from the one that appears in continuous time systems in the case of a non-ideal controller. The discrete time regime can make the system unstable. It can be proved that unlike the continuous time case where there is

only a bound on the amplitude of the control action, here the bound depends upon the sampling time and the system uncertainties.

2.6 APPLICATIONS OF ROBUST CONTROL

Many applications of SMC have been proposed over the years since this theory was developed between the nineteen sixties and the nineteen seventies (Utkin (1977)). Its more interesting feature, the robustness, together with the simplicity of its control laws has made this scheme the most widely used among all the possible VSC schemes. A field where SMC seems to be particularly convenient is power electronics and electrical drives. All converters work in switching mode (using techniques ranging from the simple square wave modulation up to various PWM techniques) and the trend in this technology is towards increasing the switching frequency by means of faster and faster devices (Mohan et al (1995)). In this framework a switching logic like SMC is appealing.

Much work has been done in the field of electrical drives and SMC has been applied to the control of different types of motors. Dote et al (1982) studied the SMC of a DC motor; Bose (1985) investigated the SMC of an induction motor, Hashimoto et al (1988) studied the control of a brushless servo motor; Gayed et al (1995) considered the permanent magnet synchronous motor. With regard to the control of the converters in itself (independently from the motor), Silva (1999) studied the sliding control of an IGBT inverter; other contributions are due to Lopez et al (1999) who studied the SMC of a buck-boost converter.

SMC has been successfully applied in contexts different from electrical engineering. Much work has been done in the control of hydraulic and pneumatic systems which show the robustness of the method in controlling highly nonlinear systems. Lantto et al (1993) studied the SMC of an electrohydraulic pump using a valve as the control element. Vaughan and Gamble (1991) investigated the SMC of a proportional solenoid valve, pointing out the robustness to flow reaction forces acting on the spool. Handroos and Liu (1998) studied the robustness of a SMC using different kinds of load for a hydraulic position servomechanism. Pandian et al (1998) developed a sliding mode controller for a pneumatic rotary actuator exemplifying its robustness to payload

variations. Uebing (1999) applied the SMC techniques to the control of a pneumatically actuated multi-axis system.

Many applications are present in structural engineering as well. The robustness of SMC with respect to parametric uncertainties has been verified by Yang et al (1993). Singh et al (1997) investigated the applicability of SMC to develop active and semi-active schemes in the control of structures under seismic excitation, focussing their attention on smoothing algorithms for chattering reduction.

2.7 SYSTEMS WITH FRICTION

Friction arises because of the dissipative microscopic phenomena occuring between the microscopical asperities of two nominally smooth surfaces. The type of contact between two surfaces can be conformal, such as a machine guide or a journal bearing, in this case the macroscopic contact area is proportional to the dimension of the object. The second type of contact is punctual, such as a gear tooth, where actual contact area is proportional to load and material strength (in the ideal punctual contact the contact area is zero since it degenerates in a point or in a line). The latter is usually referred as Hertzian contact (Hertz (1881)).

2.8 FRICTION MODELS

2.8.1 Static models

Many models have been developed over the years to describe the frictional interaction between two materials (Armstrong-Helouvry et al (1994)). Both static and dynamic models can be used to describe friction force. In a static model the common approach is to describe friction levels in terms of a velocity-dependent friction coefficient. Friction is mainly a function of velocity (although also depends on other factors, such as pressure, temperature, wear and so forth) because the physical process of shear at the junction changes with velocity. This is in general expressed through an expression of the type:

$$F_d(\dot{x}) = -\mu(\dot{x}) F_n \, sgn(\dot{x}) \tag{2.43}$$

F_d being the friction force and F_n the normal force and $\dot{x}$ the relative sliding velocity between the two surfaces.

Dynamic effects occur at the breakaway, in response to change in velocity and normal force.

The most classical Coulomb friction model was originally envisaged by Leonardo da Vinci (1519) and subsequently rediscovered by Coulomb (1785). In this model the function $\mu(\dot{x})$ is taken to be constant.

The Coulomb model is still largely used because it is easy to handle and in many situations it captures fairly decently the friction effect, even though it is very approximate. The stiction or zero-velocity friction was introduced by Morin (1833). Subsequently Reynolds (1886) took into account the viscous effect. Stribeck (1902) further improved the model, producing a fairly complete model usable in a variety of applications. The Stribeck model is described by:

$$F_d(\dot{x}) = -F_d sgn(\dot{x}) - (F_s - F_d) \, e^{(-\frac{\dot{x}}{v_s})^{\delta}} \, sgn(\dot{x}) - k_v \dot{x} \tag{2.44}$$

where F_s and F_d are the stiction and the frictional forces, k_v is a speed-dependent coefficient and v_s and δ are parameters; v_s is known as Stribeck velocity which corresponds to the minimum frictional force. The Stribeck model describes the friction regimes between two lubricated surfaces with grease or oil.

In general friction interaction between two lubricated surfaces as a function of velocity is described by four regimes: pre-sliding or static friction, boundary lubrication, partial fluid lubrication and full fluid lubrication.

Pre-sliding or static friction: in this regime the asperities of the two materials deform elastically producing pre-sliding micro displacement and plastically causing rising static friction (stiction). A junction in static friction behaves like a spring; therefore in this regime friction force is proportional to micro-slip (order of microns):

$$F_d(x) = -k_{tang} \, x \tag{2.45}$$

k_{tang} being the tangential stiffness of the contact, function of asperity, geometry, material elasticity and normal load (Johnson (1987)).

If tangential force is increasing there exists a breakaway force which causes the actual sliding to begin (hence passing from static to velocity friction). In this situation the undesired *stick-slip* effect may occur.

From a control point of view the pre-sliding can be important in position and pointing servos where leverage systems can amplify this micro-slip to an actual displacement of the order of the millimeter (Canudas de Wit et al (1993)), hence triggering the feedback loop. Some dynamic effects in the pre-sliding to actual sliding transition also occur, which are described in subsection 2.8.2.

Boundary lubrication: it is a regime arising at very low velocities, when velocity is not large enough to maintain a fluid film in-between the two materials. A high stiction occurs when lubricants which provide small boundary lubrication are employed. If lubricants made with low-stiction additives (Wills (1980)) are chosen, stick-slip can be reduced or even eliminated. Stick-slip can be also reduced by increasing the stiffness of the system.

Partial fluid lubrication: this is the most complicated regime to model (Sadeghi and Sui (1989)). In this regime a dynamic effect occurs in response to change of velocity in the form of a delay between a change of velocity and a change of friction force. This phenomenon is known as *frictional memory* (Rice and Ruina (1983)).

Full fluid lubrication: in this regime the fluid film between the two materials is fully developed and it dictates the trend of the friction characteristic in that region, which is of viscous type. The transition between partial and full fluid lubrication regime produces a negative slope in the friction characteristic (known as Stribeck effect), which controlwise produces a destabilising effect because in such conditions the system has a negative damping. Hence if the working velocity of the system is in that range, the system can become unstable and self-sustained oscillations can arise.

2.8.2 Dynamic models

Dynamic phenomena occur in the transition from static to Coulomb friction and in response to changes in velocity. These phenomena are known as *relaxation oscillations*

and were firstly investigated by Rabinowicz (1958). Further dynamics exist in response to change in the normal force.

The dynamics associated with the breakaway transition have been modelled by various authors using exponential (Kato et al (1972)) or linear (Armstrong-Helouvry (1990)) models. The "rising" time is known as *dwell time.*

The dynamic effect in response to changes in velocity is the so-called *frictional memory*: it produces a lag between a change in velocity and the change in friction force to a new steady value: this delay can range from milliseconds to seconds depending upon the materials and appears to be independent of the input frequency (Hess and Soom (1990))

From a control point of view frictional memory can help reduce the destabilising effect of the negative slope of the Stribeck effect. Rabinowicz (1965) verified that if the time constants of the system are short compared to the frictional memory (i.e. if the system is stiff), the limit cycle is unstable.

Dynamics associated with changes in the normal force also exist. Anderson and Ferri (1990) studied this effect. However Dupont and co-workers (1997) verified that friction dynamics associated with variations in normal force are fast in comparison with dynamics associated with relaxation oscillations. Therefore for usual hydromechanical control applications this effect is negligible.

2.8.3 Seven parameter friction model

Taking into account both static and dynamic effects a very sophisticated model known as *seven parameter friction model* has been proposed (Armstrong-Helouvry et al (1994)). This model is summed up by the following set of equations:

Pre-sliding displacement:

$$F_d(x) = -k_{tang}\, x \tag{2.45}$$

Sliding (Coulomb, viscous, Stribeck effects and frictional memory):

$$F_d(\dot{x},t) = -[F_d + k_v|\dot{x}| - F_s(\gamma,t_2)\frac{1}{1+(\frac{\dot{x}(t-T_L)}{\dot{x}_s})^2}]\ sgn(\dot{x}) \tag{2.46}$$

Rising static friction (friction levels at breakaway):

$$F_s(\gamma,t_2) = F_{s,a} + (F_{s,\infty} - F_{s,a})\frac{t_2}{t_2+\gamma} \tag{2.47}$$

Parameters are defined in the notation section. In this model a polynomial model has replaced the exponential model used to represent the Stribeck effect.

Other friction models exist which include both static and dynamic effects, such as Dahl's model (Dahl (1968)) and Bliman-Sorine's model (1991).

This survey on friction models has outlined the main phenomena occuring in the sliding friction between two surfaces and their modelling. Depending upon the application the designer can adopt a more or less advanced friction model. The major problem however is the identification of the correct numerical values for the coefficients of the models. An effective method is carrying out experimental tests on the materials in the working conditions of the system. This approach has been undertaken in the course of the work in order to identify the most suitable friction model in the damper.

2.9 CONCLUDING REMARKS

An overview on the most suitable control techniques employed to tackle uncertain systems has been presented. Particular attention has been given to robust control schemes, particularly VSC, which will be employed throughout this work.

In the second part of the chapter, an overview on friction has been presented, since friction force is the core of the system. Particular emphasis has been given to the modelling and control aspects of friction, pointing out, in subsections 2.8.1 and 2.8.2, the extent to what the various models are suitable for control design.

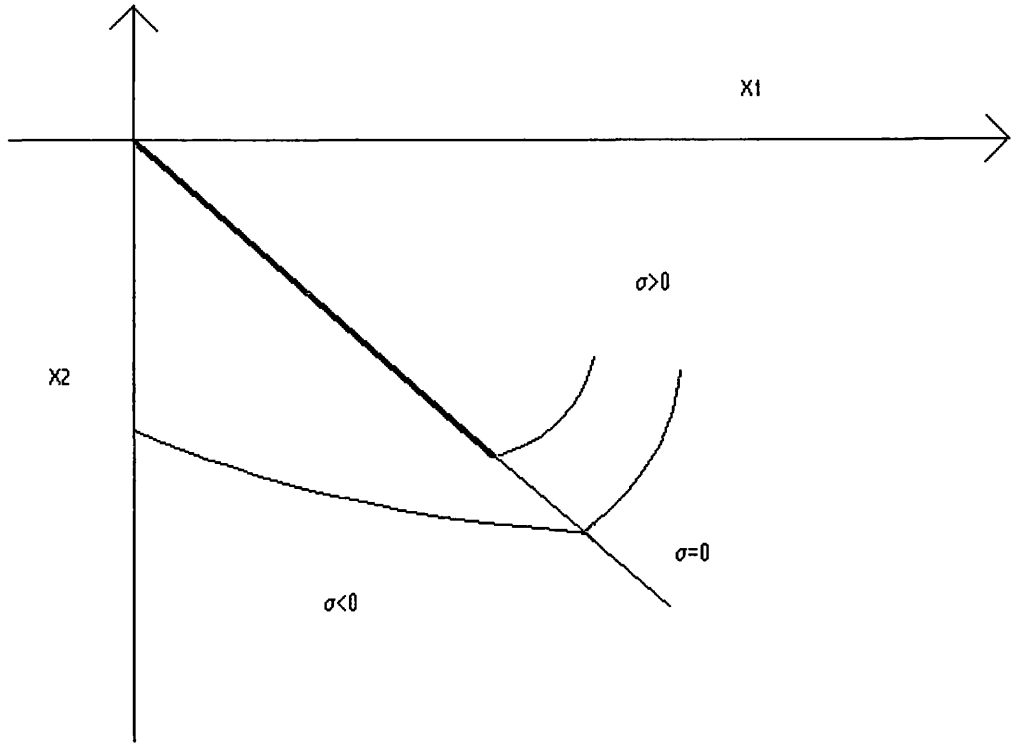

Figure 2.1 Sliding mode control trajectory (highlighted) versus generic bang-bang control trajectory.

3 PASSIVELY-DAMPED VEHICLE BENCHMARK

3.1 INTRODUCTION

This chapter describes the modelling, testing and validation of a passenger car equipped with its original suspension system. The car employed in this work is a Ford Orion.

The chapter is organised as follows. Section 3.2 and 3.3 describe the mathematical models of the car and of the road; section 3.4 outlines suspension requirements in terms of ride and road holding; section 3.5 is focussed on comfort assessment; section 3.6 and 3.7 describe the car test and the experimental validation of the model.

3.2 VEHICLE MODEL

3.2.1 Introduction

Many car models with increasing degree of complexity have been developed over the years by automotive engineers to meet the demand of having a reliable, low-cost, computer-aided tool for automotive design.

In very general terms, vehicle models can be broadly divided into two categories: distributed or lumped parameter models. The former are of interest mainly to car component design (stress analysis etc); FEM techniques are required to handle them. Codes, such as ANSYS, are widely used for this purpose. For car dynamic and control studies, lumped parameter models are employed. They aim to model either ride or handling dynamics or both.

A car can be thought as composed of two rigid parts: the sprung mass (chassis) and the unsprung masses (wheels, rigid axles and linkages), connected via a number of elastic

and dissipative elements (suspensions, tyres etc) and subjected to inputs and disturbances coming from the road profile, the steering and wind gust.

The motions of a vehicle with the nonholonomic constraint of the road has 6 DOF, classified as follows:

-longitudinal translation (forward and backward motion)

-lateral translation (side slip)

-vertical translation (bounce)

-rotation around a longitudinal axis (roll)

-rotation around a transversal axis (pitch)

-rotation around a vertical axis (yaw)

Ride is concerned with the car vertical dynamics (bounce, pitch, roll, wheel vertical motion) whereas handling with the lateral dynamics (side slip, yaw, roll). This study is concerned with the ride properties, therefore handling inputs are not considered. Ride models can be represented by spring-mass-damper systems (also including nonlinear elements). The most trivial representation has 1 DOF, where the chassis is represented by a mass and the suspension by a spring and a damper: tyre mass and stiffness are neglected as well as any cross-coupling dynamics.

A slightly more accurate model is with 2 DOF; it is usually known as quarter car. This model was very popular in the automotive engineers community, especially before the widespread use of computer simulation. The quarter car model, in fact, despite its simplicity, features the main variables of interest for control: body acceleration, dynamic tyre force, suspension working space (Sharp and Hassan (1987)), and it permits the focus of attention of the designer on the controller, in the sense that the effects of modifications in control parameters can be more straightforwardly evaluated, because higher-order dynamics and cross-coupling terms due to the other suspensions are not taken into account. A good design should produce both improvement of both vehicle road holding and passenger comfort (or possibly improvement of one without degradation of the other).

A 2 DOF model (having a rotational state variable) can be also used to describe bounce and pitch motions (bicycle model) or bounce and roll motions, although a 4 DOF model, including also tyre masses and elasticity is more pertinent. However the 4 DOF model cannot take into account all the cross-coupling between front and rear or right- and left-hand side of the car. These interactions can be taken into account using a 7 DOF model (sometimes referred as "full" car model). This model will be utilised for validation purposes and in the development of the multivariable controller.

Higher order ride models can be obtained including further degrees of freedom, such as seat and engine mounting elasticity. Analogously handling models with different degree of complexity can be developed. The equivalent handling model of the quarter car is a linear single track model which describes lateral and yaw dynamic responses to handling manoeuvres (ignoring the effect of sprung and unsprung masses). More refined models make use of the concept of roll centre to describe separately the right- and left-hand side of the vehicle.

Models including both ride and handling dynamics exist and are used either to study the limit of handling characteristics or elements such as anti-roll bars (Ross-Martin (1994)), where there is a need to accurately investigate the interaction between ride and handling (during a turning manoeuvre the vehicle body rolls). As far as the computer simulation of these models is concerned, most packages available are based on multibody techniques (such as ADAMS, DADS and EASY 5). By using these packages, extremely complicated models with many DOF have been developed such the one described by Zeid and Chang (1991) with 64 DOF. Such involved models, however, despite their sophistication, suffer from two main drawbacks: parameter uncertainty and long simulation running time. For these reasons sometimes they are not the best choice for control design. Especially in the initial stages of the design, a less complicated model is preferable, reserving the use of higher order models for further refinements and optimisation. Furthermore, some of the car simulation packages do not readily permit the introduction of elements such as switchable dampers (Hickson (1996)).

In this work two codes have been employed. Initially Bath*fp* was used. This is a fluid power simulation package, developed at the Centre for Power Transmission and Motion Control, at the University of Bath (UK). The code adopts a multi-step, type-insensitive integrator (Petzold (1983), Richards et al (1990), Richards (1993)). Subsequently,

Simulink, the dynamical system graphical simulation environment of MATLAB (The MathWorks Inc. (1992)) was used. A variety of integrators are available within this package.

At the outset a few general remarks are necessary relating to the numerical techniques employed to tackle the discontinuous and stiff[1] equations arising. The system is modelled as lumped and therefore its simulation requires an ordinary differential equation integrator. The two codes used in the course of the work, Bath*fp* and Simulink, both have powerful integrators; their capabilities and limitations in relation to the numerical difficulties arising in the numerical integration of the system equations are briefly discussed.

The multi-step type-insensitive Bath*fp* integrator presents some adaptive features i.e. it is able to choose automatically the most suitable numerical method according to the numerical stiffness of equations to be solved and to switch to another method if necessary (e.g. if equations change because of a modification in the structure of the plant). Adams methods of orders 1 to 12 are used as non-stiff algorithms, while Gear's method with backward differentiation fitting of orders 1 to 5 is used to cope with stiff equations. As far as discontinuities are concerned, they are handled by means of a routine able to restart the integrator in correspondence of each discontinuity encountered.

A crucial feature when discontinuities (such as that introduced by the friction damper) are present is the capability of the integrator to toggle the zero-crossing detection routine. Such a routine (necessary if nonlinear equations must be solved) is usually present within the Jacobian matrix calculation algorithm (Chapra and Canale (1988)). Disabling it, means in some cases, a significant reduction of the simulation run-time, at the price of a slightly smaller accuracy in the neighbourhood of the zeros of the solution. Bath*fp* does not allow the user to choose whether this feature is enabled or

---

[1] A system of ordinary differential equations $\dot{x} = f(x,t)$ is said to be stiff (according to Lambert (1973)) if the eigenvalues λ_i of the Jacobian matrix $J=\frac{\partial f}{\partial x}$ satisfy $Re(\lambda_i)<1$ and $\frac{Max[-Re(\lambda_i)]}{min[-Re(\lambda_i)]} << 1$. In more operative terms (Richards et al (1990)) the stiffness can be measured via the dimensionless quantity $\frac{Integration\ range}{Smallest\ time\ constant}$.

disabled. Simulink presents a wide choice of algorithms for both stiff and non-stiff problems, belonging either to the Runge-Kutta or Gear-Adams family, but it does not include an adaptation routine able to swap among different numerical methods or orders in the course of a simulation. Simulink instead allows the zero-crossing detection routine in the algorithm to be toggled. It was found necessary to disable this routine in order to speed-up the simulation, otherwise for a set tolerance the integrator would take too small step sizes in correspondence of the discontinuities, virtually blocking the simulation. In neither of the codes it is easily possible to fix the minimum step size (although such a feature would be useful in discontinuous systems).

3.2.2 Quarter car model

Consider initially the quarter car model. This model together with the friction damper, is described by the following system of second-order nonlinear ordinary differential equations (figure 3.1):

$$M_1 \ddot{x}_1 = -\mu F_n sgn(\dot{x}_1 - \dot{x}_2) - 2\xi\omega_1 M_1(\dot{x}_1 - \dot{x}_2) - k_s(x_1 - x_2) \tag{3.1a}$$

$$M_2 \ddot{x}_2 = \mu F_n sgn(\dot{x}_1 - \dot{x}_2) + 2\xi\omega_1 M_1(\dot{x}_1 - \dot{x}_2) + k_s(x_1 - x_2) - k_t(x_2 - z_0) \tag{3.1b}$$

neglecting tyre damping.

If relative displacement is defined as $x = x_1 - x_2$ (see figure 3.1 for axis notation), equation (3.1) can be rewritten in a more compact form:

$$M_1 \ddot{x}_1 = -\mu F_n sgn(\dot{x}) - 2\xi\omega_1 M_1 \dot{x} - k_s x \tag{3.2a}$$

$$M_2 \ddot{x}_2 = \mu F_n sgn(\dot{x}) + 2\xi\omega_1 M_1 \dot{x} + k_s x - k_t(x_2 - z_0) \tag{3.2b}$$

3.2.3 Full 7 DOF ride model

In order to design the multivariable suspension controller (see chapter 7) a 7 DOF car model has been developed; it is a car ride model (Wong (1993)) and it allows 3 DOF (bounce, roll and pitch) for the sprung mass and 4 DOF for the unsprung mass. It is

shown in figure 3.2. The front suspensions are independent and rear suspensions are dependent (connected via a rigid axle).

The governing equation expressed in matrix form is the following:

$$\boldsymbol{M\ddot{q} + P^T CP\dot{q} + P^T KPq + F_d = -P^T K_0 z_0 - P^T C_0 \dot{z}_0} \tag{3.3}$$

The analysis leading to equation (3.3) is reported in appendix A.

$\boldsymbol{q} \in \Re^7$ is the generalised (Lagrangian) co-ordinate vector; $\boldsymbol{z_0} \in \Re^4$ the road input vector and $\boldsymbol{F_d} \in \Re^7$ the frictional force and moment vector. $\boldsymbol{M} \in \Re^{7x7}$ is the mass matrix, $\boldsymbol{K} \in \Re^{8x8}$ and $\boldsymbol{C} \in \Re^{8x8}$ the stiffness and viscous damping matrices; $\boldsymbol{K_0} \in \Re^{8x4}$ and $\boldsymbol{C_0} \in \Re^{8x4}$ the unsprung mass stiffness and damping matrices and $\boldsymbol{P} \in \Re^{8x7}$ is a matrix related to the system geometry.

The generalised co-ordinate vector is:

$$\boldsymbol{q} = [q_1, q_2, q_3, q_4, q_5, q_6, q_7]^T \tag{3.4}$$

the road input vector:

$$\boldsymbol{z_0} = [z_{01}, z_{02}, z_{03}, z_{04}]^T \tag{3.5}$$

The vertical displacement vector $\boldsymbol{z} \in \Re^8$ is defined as:

$$\boldsymbol{z} = [z_1, z_2, z_3, z_4, z_5, z_6, z_7, z_8]^T \tag{3.6}$$

$\boldsymbol{z}$ and $\boldsymbol{q}$ being related by the matrix $\boldsymbol{P}$:

$$\boldsymbol{z = Pq} \tag{3.7}$$

The following choice of free co-ordinates is made:

$$q_1 = z\ ;\ q_2 = z_5\ ;\ q_3 = z_6\ ;\ q_4 = z''\ ;\ q_5 = \alpha\ ;\ q_6 = \beta\ ;\ q_7 = \beta'' \tag{3.8}$$

Equation (3.3) can be placed in canonical companion form:

$$\dot{x} = Ax + Bu$$
$$y = Cx + Du \tag{3.9}$$

with $A \in \Re^{14x14}$, $B \in \Re^{14x12}$, $C \in \Re^{24x14}$, $D \in \Re^{24x12}$, $x \in \Re^{14}$, $y \in \Re^{24}$ and $u \in \Re^{12}$. The state vector x is defined as:

$$x = [z, z_5, z_6, z'', \alpha, \beta, \beta'', \dot{z}, \dot{z}_5, \dot{z}_6, \dot{z}'', \dot{\alpha}, \dot{\beta}, \dot{\beta}'']^T \tag{3.10}$$

the input vector u is:

$$u = [z_{01}, z_{02}, z_{03}, z_{04}, \dot{z}_{01}, \dot{z}_{02}, \dot{z}_{03}, \dot{z}_{04}, F_{d1}, F_{d2}, F_{d3}, F_{d4}]^T \tag{3.11}$$

and the output vector y:

$$y = [z, \alpha, \beta, z_5, z_6, z_7, z_8, z_1 - z_5, z_2 - z_6, z_3 - z_7, z_4 - z_8, \dot{z}_1 - \dot{z}_5, \dot{z}_2 - \dot{z}_6, \dot{z}_3 - \dot{z}_7, \dot{z}_4 - \dot{z}_8,$$
$$\ddot{z}, \dot{z}_1, \dot{z}_2, \dot{z}_3, \dot{z}_4, \dot{z}_5, \dot{z}_6, \dot{z}_7, \dot{z}_8]^T \tag{3.12}$$

Equation (3.9) can be decomposed, separating the effects of the disturbance and of the control:

$$\dot{x} = Ax + B_1 u_1 + B_2 u_2$$
$$y = Cx + Du \tag{3.13}$$

with $B_1 \in \Re^{14x8}$ and $B_2 \in \Re^{14x4}$; $u_1 \in \Re^8$ is the disturbance vector and $u_2 \in \Re^4$ the control vector, respectively defined as:

$$u_1 = [z_{01}, z_{02}, z_{03}, z_{04}, \dot{z}_{01}, \dot{z}_{02}, \dot{z}_{03}, \dot{z}_{04}]^T \tag{3.14}$$

and

$$u_2 = [F_{d1}, F_{d2}, F_{d3}, F_{d4}]^T \tag{3.15}$$

For the particular case of a Ford Orion the values of relevant vehicle parameters have been obtained by direct measurement, calculations, vehicle manuals or from the Ford Motor Company. Table 3.1 lists the values:

Table 3.1: Ford Orion parameters

PARAMETER	VALUE	SOURCE
Sprung mass (m)	1020 [kg]	Haynes manual
Wheel mass (m_1)	14.17 [kg]	Measured
Axle mass (m_2)	50 [kg]	Calculated
Pitch moment of inertia (J_α)	1859 [kgm^2]	Ford Motor Company
Roll moment of inertia (J_β)	471 [kgm^2]	Ford Motor Company
Axle moment of inertia ($J_{\beta''}$)	5.343 [kgm^2]	Calculated
Front spring rate (k_1)	22000 [N/m]	Ford Motor Company
Rear spring rate (k_2)	19000 [N/m]	Ford Motor Company & Measured
Tyre stiffness (k_0)	148000 [N/m]	Measured
Viscous damper coefficients (c)	400 [N/ms^{-1}]	Ford Motor Company
Tyre damping (c_0)	20 [N/ms^{-1}]	Genta's textbook
Centre of gravity (CG) distance from the front of the car (a)	1.025 [m]	Ford Motor Company
CG distance from rear axle (b)	3.204 [m]	Ford Motor Company
Axle length (E)	1.462 [m]	Haynes manual

3.3 THE ROAD MODEL

The road vertical profile, identified by the co-ordinates z_{0i}, is the source of disturbance. The road vertical elevation produces the same effect as an external force applied to the plant. Road disturbances can be classified as being of three types: random-type inputs (but with fairly specific power density spectra, decreasing in an inversely proportional fashion), deterministic inputs (periodic and almost-periodic) and discrete events, such as bumps and potholes.

A stochastic input gives a fairly realistic representation of a road profile. An input often used in literature (Mastinu (1988)), Wong (1993)) is an ergodic process with spectral density expressed by:

$$S(f)=(\frac{C}{V^{-n}})f^{-n} \tag{3.16}$$

where V is the forward speed of the car, C is a coefficient dependent on the road roughness, f the frequency in Hz and n is a rational exponent. This approach involves an analysis in terms of power spectral densities of the quantities of interest. For a linear system the input and output spectral densities $Y_{in}(f)$ and $Y_{out}(f)$ are related through the transfer function of the system $G(f)$, from the equation:

$$Y_{out}(f)=|G(f)|^2 Y_{in}(f) \tag{3.17}$$

This frequency domain property only applies to linear systems. In this way the output spectral density can be readily calculated if the plant transfer function and the input spectral density are known. For a nonlinear system this property does not hold; therefore the analysis must be carried out firstly in the time domain, computing numerically the random process output and its autocorrelation function; eventually the latter must be Fourier-transformed in order to have the output spectral density. Furthermore the analysis of the results requires the use of probabilistic techniques (although RMS values around a centre frequency can be calculated by integrating the spectral density over a frequency interval i.e. a third-octave band) and the physical interpretation of the results may be not as straightforward as in the case of a deterministic input.

As far as the deterministic inputs are concerned, to a first approximation the disturbance can be assumed to be a sinusoidal waveform. Although not realistic, it is useful in a preliminary study because it readily permits a comparison of the performance of different designs in both the time domain and frequency domain. A multiharmonic input is closer to the actual road profile. A possible choice which approximates fairly well a real road profile is a so-called pseudo-random input which results from summing several non-commensurately related sine waves (i.e. the ratio of all possible pairs of frequencies is not a rational number) of decreasing amplitude, so as to provide a discrete approximation of the continuous spectrum of a random input. The trend can be proved to be non-periodic (often referred as almost-periodic) in spite of being a sum of periodic waveforms (Bendat and Piersol (1971)). Another choice consists in making the ratio between frequencies constant and decreasing with amplitude, but using a random phase

shift. In this case the resulting waveform is periodical. The latter approach has been used in the simulation.

Discrete events such as bumps or potholes must be considered apart.

3.4 SUSPENSION REQUIREMENTS

The typical specifications of a suspension system are now briefly described, before entering into the details of the various controllers. A suspension system should be able to minimise chassis acceleration as well as dynamic tyre force within the constraint of a working space that should be not too large.

Chassis acceleration is related to ride and comfort, whereas tyre force to road holding and handling.

Dynamic tyre force reduction results in better handling of the vehicle, for the cornering force, tractive and braking efforts developed by the tyre are related to normal load. Road holding and handling performance can be quantified precisely by the consideration of the forces and moments applied to the chassis and to the tyres.

Comfort is a more difficult to quantify and although standards exist, it is still not well established how to assess it, because it is an inherent subjective matter.

In the following section a survey on comfort and assessment criteria is presented to try and shed light on this problem.

3.5 COMFORT IN A VEHICLE

Ride quality is concerned with passenger comfort in a moving vehicle subject to vibrations. Vibrations transmitted to passengers originate from a host of causes, some of the most important being: road uneveness, aerodynamic forces and engine and powertrain induced vibrations. Road irregularities are however the major source of vibrations and the only ones considered here. In a "comfortable" vehicle, vibrations

must stay within some boundaries. In order to establish these boundaries, it is firstly necessary to quantify and assess human body response to vibrations.

3.5.1 Survey on comfort criteria

There is no generally accepted method to assess human sensitivity to vibrations; human response is quite subjective and dependent on several factors. First of all it must be noted that road disturbances applied at the tyre are asymmetrical. In the occurrence of a bump, vertical upward acceleration can reach several g while if a pothole is encountered, the vertical downward acceleration cannot be larger than 1 g. This is why hydraulic dampers are designed with different viscous coefficients for the bound and rebound stroke.

The human body presents asymmetric reactions to vibrations as well: the body reacts differently if the same vertical acceleration is applied upward or downward (Lucifredi (1978)). People can better withstand an increase rather than a decrease in the gravitational force (as can be experienced in a fast elevator, for instance). Furthermore motions with low roll centre (e.g. pitching of a ship) are more troublesome than those with a high roll centre (e.g. a wing). From these considerations it follows that comfort tests carried out with sinusoidal inputs are not sufficient, but only useful for comparison purposes. Even if a multiharmonic input is applied, it is difficult to weight the various frequencies to which the body is more, or less, sensitive.

Early studies associated the feeling of comfort with the frequency of vibration of the walking pace. A review of these early works is provided by Demic (1984). Thus early car suspensions were designed according to this criterion. Further studies (Dieckmann (1958)) proved that different frequency bands are uncomfortable for different organs. Frequencies lower than 1 Hz are related to symptoms like motion sickness; frequencies in the range 5-6 Hz are troublesome for the stomach, while frequencies around 20 Hz are pernicious for head and neck.

Several criteria have been proposed over the past 30 years to assess comfort based on some hypotheses on the nature of the vibrations. Some of them are general purpose, others are employed in specialist fields like off-road and military vehicles (Pollock and Craighead (1986)); it is worthwhile mentioning the latter applications, for a friction

damper is inherently a harsh suspension, hence potentially more appropriate for off-road vehicles.

One first criterion, relevant to the automotive field, is the *Janeway's comfort criterion* (SAE (1965)). It relates the comfort to vertical vibration amplitude: for each frequency the largest allowed chassis displacement can be found. In essence it states that the maximum allowable amplitude is the one that produces a peak jerk value, of not more than 12.6 m/s^3, within the range 1 to 6 Hz. In other words, if X is the max allowed displacement amplitude and ω the angular frequency, Janeway's criterion states that $X\omega^3 = 12.6$.

At higher frequencies the criterion refers not to jerk but to acceleration and velocity. It affirms that in the range 6-20 Hz, acceleration peak value should not exceed 0.33 m/s^2, whilst between 20 and 60 Hz the max velocity should stay below 2.7 mm/s.

The major limitation of SAE criterion is that it refers only to vertical sinusoidal disturbances and it does not give any indication for the case for multiharmonic inputs.

Steffens (1966) proposed an empirical formula to determine the amplitude of vibration causing discomfort: $X[cm]=7.62\cdot10^{-3}(1+125/f^2)$, where again vertical displacement (rather than acceleration) is used to assess comfort.

The most general criterion is the Standard *ISO 2631* (1978); it is a general standard applicable not only to vehicles but to all the vibrating environments. It defines the exposure limits for body vibration in the range 1-80 Hz, defining limits for reduced comfort, for decreased proficiency and for preservation of health. A subsequent addendum to the norm also takes into consideration the frequencies in the particular range 0.1 to 1 Hz. It relates discomfort to RMS acceleration as a function of frequency for different exposure times. If vibrations are applied in all three directions (foot-to-head, side-to-side, back-to-chest), the corresponding boundaries apply for each component.

Another criterion proposed is the *vibration dose value* (Griffin (1984)); it is an integral criterion which gives an indication based on the integral of the fourth power of the frequency weighted acceleration. The vibration dose value is calculated as:

$$VD = \int_0^t a^4 dt \tag{3.18}$$

If the acceleration has components along two or three axes, the total dose value is the algebraic sum of the values for each axis. A value above 15 m^4/s^7 is considered cause of discomfort. This criterion is independent of the type of waveform; besides the fourth power of weighted acceleration emphases peak values (that together with RMS values are the most important parameters of a waveform to assess comfort).

Some studies have been concerned with the energy absorbed by the body in a vibrating environment. An initial study by Zeller (1949) relates the comfort to the max specific kinetic energy absorbed by the body over a period for a sinusoidal input, establishing some boundaries for the max allowed energy absorbable. The energy is calculated as $E=0.5v^2_{max}/T=a^2_{max}/8\pi^2f^2$. The disturbance considered here is again sinusoidal and T is the period.

A further integral criterion is known as *absorbed power method* (Lee and Pradko (1969)); it calculates the power absorbed by the body when it experiences vibrations. It has been used by army to test human tolerance in military vehicles. The criterion is expressed by:

$$Power = \int_0^f (A^2 w) df \tag{3.19}$$

the parameter A being the acceleration spectrum along an axis and w a frequency weighting function. The tolerance limit is taken to be 6 W.

A criterion known as *DISC rating* value (Leatherwood, Dempsey et al (1980)) assesses the discomfort with the formula:

$$DISC = -0.44 + 1.65(DVERT^2 + DLAT^2) \tag{3.20}$$

where

$$DVERT = -1.75 + 0.857CFV - 0.102CFV^2 + 0.00346CFV^3 + 33.4GV$$

CFV being the centre frequency of vertical axis applied vibration band and *GV* the peak acceleration within this band (*DLAT* is defined by an analogous expression).

This survey has shown that the problem of assessing comfort is in some way quantifiable, but the problem is the choice of the most suitable comfort criteria for a particular application.

It must be recalled that if the friction damper is not employed as a part of a vehicle suspension but for a different application (i.e. reduction of machine vibrations or semi-active structural damping, for example) the comfort is not an issue and the major parameter of interest usually becomes the actual RMS reduction (which in any case is comfort related). Also the minimisation of displacement and acceleration peak values could be an issue: for example in a multi-storey structure the maximum inter-storey displacement must not exceed certain limits; furthermore high peak values could excite unwanted higher order structural dynamics, or they may reduce the fatigue life of machines.

3.5.2 Comfort assessment

From the previous survey it is clear that comfort assessment is an "ill-posed" problem from an engineering standpoint. In this work a choice has been made on how to assess it. For the purpose of this investigation the assessment will be based on RMS, peak and jerk values for sinusoidal input; a pseudo-random input response; a bump response and on the spectral characteristics of the nonlinear acceleration response.

At first the sinusoidal input will be considered. In terms of sinusoidal input, the simplest method to compare passive and semi-active suspension responses (in terms of ride quality) is through peak value chassis accelerations. In a linear case it is straightforward: for an output displacement expressed by $x(t)=X\sin(2\pi ft)$, the peak values of the higher order derivatives are:

$$\dot{x}_{MAX} = 2\pi fX$$

$$\ddot{x}_{MAX} = 4\pi^2 f^2 X$$

$$\dddot{x}_{MAX} = 8\pi^3 f^3 X$$

An assessment based on jerk peak value is another possibility (Hrovat and Hubbard (1987)). Another possible approach to estimating comfort is in the frequency domain, carrying out an analysis of the chassis acceleration amplitude spectrum. Actually a Fourier analysis is more appropriate to assess the degree of nonlinearity in terms of harmonic distortion. However, as a rule of thumb, a large harmonic content may possibly indicate higher peak acceleration and jerk amplitude (even if strictly speaking the analysis of the phase spectrum would be necessary) although there is no precise relationship between spectrum and comfort.

As far as the bump input is concerned now the relevant quantities to minimise, comfortwise, are the peak value acceleration and the number of oscillations after the bump.

3.6 BENCHMARK TEST ON THE PASSIVELY-DAMPED CAR

3.6.1 Introduction

The prime objective of the experimental work was to provide data to validate the mathematical models developed. In other words to verify that the order of complexity of the model and the precision in the knowledge of the system parameters and inputs is sufficient to give a reasonable accurate representation of the physical reality of the system over the range of the operating conditions. Backed by the validation process, if simulation is sufficiently accurate over the working range, further work can be solely made via simulation.

From an opposite viewpoint, experimental tests on single components of the plant also permit the identification of system parameters otherwise hard to select with sufficient precision (for instance, friction characteristics). Within this context, these experimental results can be logically seen as an *a priori* stage providing reliable input to the simulation (not as a validation tool). The friction and tyre characteristics employed in the simulation were estimated experimentally.

Preliminary tests on the car equipped with its original viscous damper were initially performed in order to have a set of data as a benchmark for the performance of the car

with the controlled friction damper. In addition tests on the suspension spring and on the tyre were performed in order to furnish experimental values for the spring rate and the tyre stiffness. In the following subsections it is reported how the measurements have been carried out and the main results obtained.

3.6.2 The behaviour of the car

It was said that the car unilaterally constrained by the road has 6 degrees of freedom, 3 rotational (forward and backward motion, side slip and bounce) and 3 translational (roll, pitch and yaw).

From the viewpoint of assessing the performance of a suspension system, bounce, roll and pitch motions are the most pertinent. Side slip, which occurs only for a lack of adhesion and yaw are negligible compared with the others and are of interest mainly in handling studies. Road unevenness, steering and aerodynamic forces constitute the external inputs to a car.

At the outset it is necessary to specify the inputs which best excite car dynamic responses of interest and which best represent real conditions on the road.

Vehicle driving tests in controlled conditions would appear to be the most natural solution. However it is possible to emulate the road input with a road simulator. This allows measurements to be made in more controlled conditions; besides it permits tests to be carried out which are not feasible on a road (e.g. frequency response analysis or the excitation of single suspension units separately). Moreover on a road simulator the level of external disturbances is reduced compared to a driving test on a road (for instance, there is no wind gust and other aerodynamic effects). These reasons together with the constraint that the car available was no longer driveable played a major role in the choice of using a road simulator for all the measurement campaigns.

3.6.3 The experimental set-up

The car was placed on the University of Bath four-poster hydraulically actuated road simulator. This is essentially composed of four hydraulic actuators on which the vehicle under testing is placed (figure 3.3); its main features are briefly described to identify its potential and its limits. Each hydraulic actuator is position-controlled through a valve,

each of them equipped with a local microprocessor; a PID control algorithm is downloaded from a control PC every time the rig is initialised. The rig is operated via software that manages and supervises all the operations. It is possible to select elementary inputs (sine waves, half sine waves, square waves) in the 0 to 25 Hz frequency range and ±125 mm amplitude range. Since each actuator is controlled independently, the relative phase-shift among the actuators is not controllable. In order to overcome this problem it was arranged to drive the actuators with an external voltage input, and to control the phase-shift among the actuators by means of analogue circuitry. In this way pure bounce, roll and pitch inputs, as well as other inputs, can be generated. Furthermore, it is possible to create user-defined waveforms by composing elementary functions through a graphical editor.

The following tests were carried out on the car:

-sinusoidal input to a single wheel

-bounce, roll and pitch tests with sinusoidal input

-pseudo-random input

-bump test

This choice provides enough information to gain an understanding of the dynamic phenomena of interest and to provide a comprehensive set of data to assess suspension performance.

Sinusoidal waveforms do not represent any realistic road condition. However they are simple and well-known inputs and they allow the use of frequency domain methods for manipulating data (the passive car behaves approximately linearly). Sinusoidal tests give a first clue on the effectiveness of the suspensions: they permit an assessment of how controlled suspensions behave with respect to passive suspensions.

It must be specified that because of the inherent nonlinearities (e.g. friction in the actuators) of the 4-poster shaker, it is not possible to obtain a pure sinusoidal motion in spite of a sinusoidal driving input voltage to the shaker. A small harmonic content would be always present. In addition the passive car is linear only to a first approximation (the main non-linearity being the tyre characteristics and the damper characteristics, including mountings and rubber bushes). As a consequence of the whole

system being nonlinear, it is not possible to obtain a proper frequency response. For this reason it was decided to plot the RMS of the ratio of chassis acceleration and of the wheel versus the fundamental harmonic of the excitation frequency for a fixed amplitude. This experimental "frequency response" must be called more appropriately acceleration transmissibility ratio, because it includes the effect of all the harmonic content of the signals. However for ease the terminology frequency response will be used hereafter.

The passive system frequency responses are expected to be worse (i.e. with larger values) than the semi-active frequency responses in the working frequency range. Ideally the controlled variable frequency response trends should be upper bounded by the corresponding passive trends. This is a first crucial assessment in the frequency domain before further investigations in order to evaluate the properties of their responses in the time domain (harmonic content, peak values, higher derivative trends and peak values etc).

The instrumentation employed consisted (a more detailed description of the hardware and software used in the experimentation is given in appendix C) of four capacitive accelerometers (Access, AMD-CK/0-A10 ±10 g) and one displacement transducer (Graham & White Instruments, Series 1850).

Two accelerometers were mounted on each rear wheel, connected through small cylinders bolted on the wheels. It was necessary to make the connections as compact as possible in order to reduce stray vibrations which affect the measurement. The other two accelerometers were fixed through magnets on the chassis of the car, close to each rear suspension. Accelerometers have a principal axis of sensitivity, therefore they need to be mounted vertically because what is of interest is the vertical component of chassis and wheel acceleration. The calibration of these devices is based on gravity (by interpolating readings at +1 g, 0 and –1 g). Because of their sensitivity to acceleration due to gravity, it is necessary to compensate the offset of 1 g that they can introduce.

Signals from the transducers were manipulated in a conditioning unit. Conditioning circuitry is essentially composed of an amplification stage followed by a filtering stage. A stabilised power supply provided the required constant voltage; the grounding was done through an earth resistance on the metallic trolley carrying the equipment (the ground is unique to avoid earth loops). Pre-amplification was necessary to make the

signal more robust, and making it less electrical interference sensitive. The amplifier gain was chosen so that the accelerometer calibration factor was 1 g=10 V, as vertical accelerations in a car are within this order of magnitude.

The second stage of the conditioning chain is filtering. Acceleration is typically a noisy signal: stray effects due to the mounting, rubber bushes, friction etc are recorded by the transducer and therefore it is necessary to low-pass filter the signal. The break frequency of the filter must be chosen by trading-off among different conflicting requirements: if it is too low it introduces an undesired phase-lag and further it smoothes the waveforms by cutting-off the high frequency harmonic content. This only slightly affects integral parameters like the RMS (higher order harmonics have typically small amplitudes), however it can diminish the actual value of some time domain information like peak acceleration value or jerk content which are comfort related (SAE Standard (1965) and ISO Standard (1978)) and they need be quantified properly (particularly in a controlled suspension with a switching based control logic). On the other hand if the break frequency is too high, quite a lot of noise can be superimposed on the signal affecting not only the readability of the signal but also the evaluation the RMS. In addition, with reference to the control logic adopted, a high level of noise could introduce chattering if acceleration signals were used in a switching logic based on the zero-crossing detection of the signal (although valve dynamics would help filter it).

In order to choose an appropriate break frequency an analogue manually-adjustable filter (Kemo-filter, dual variable filter type VBF/14J, 1 Hz -100 kHz) was used. By trial and error a second order Butterworth filter with a break frequency of 40 Hz was chosen. With the final choice made the phase-lag introduced is only 10 degree at 5 Hz (about the highest frequency where the control is supposed to work in the semi-active suspension).

The position transducer was mounted in-between body and wheel for measuring the relative displacement. Initially an LVDT was employed; however it was found not to be appropriate: when the car was undergoing testing, tyre torsional modes were turning the wheels risking damaging the device. Mounting connections through plastic bolts and rose joints were not sufficient to provide protection. Therefore it was decided to use a wire potentiometer. This device is intrinsically safe, since the position is measured with a flexible rope, not a rigid rod. The potentiometer is made in hybrid conductive plastic;

this results in an essentially infinite resolution and in a very clean measured signal; no filtering was in fact necessary. In order to properly calibrate it, a stepper motor was employed; the calibration factor was chosen to be 1 V=1 cm.

With regard to the car, measurements were carried out with the car unladen and with tyres inflated at the rated pressure of 2.1 bar. Wheels were braked to minimise tyre torsional vibrations, which tended to turn the wheels.

3.6.4 Post-processing and measurement results

As far as sinusoidal tests are concerned the most meaningful data are the time responses and the ratio of chassis to wheel RMS acceleration. The ride model of car is supposed to be linear to a first approximation; this implies that the acceleration ratio is equal to the velocity and displacement ratios:

$$\frac{a_1}{a_2} = \frac{j\omega v_1}{j\omega v_2} = \frac{\omega^2 x_1}{\omega^2 x_2} \tag{3.21}$$

a_i, v_i, x_i being chassis and wheel acceleration, velocity and displacement (subscripts 1 and 2). Hence transmissibility curves can be readily obtained. In order to verify if the car behaves linearly, inputs with three different amplitudes were applied. The closer the three responses are to one another the more the system approximates linear behaviour. Figure 3.4 shows the response of the car when only one wheel is excited; the ratio of body over wheel RMS acceleration is plotted. The demanded input to the actuator is a sinusoidal waveform with a peak value of 3 mm in the range 1-22 Hz. Three resonances are evident; the first one is the chassis resonance at about 3 Hz; this is fairly high: typically this resonance occurs at about 1.5 Hz. This shift is essentially due to the small portion of sprung mass loading the suspension strut, since only the rear right corner of the car is shaken; the additional tyre stiffness caused by the braked wheel may contribute as well to this frequency shift. The second resonance is at about 8.5 Hz; this is due to cross coupling effects: around that frequency range a compound motion of bounce, roll and pitch is present; an engine mounting resonance is also possible.

Eventually the wheel-hop resonance occurs at 18 Hz. It is not readily recognisable on the graph of figure 3.4; however if wheel acceleration response is plotted (figure 3.5) it becomes clearer.

Figure 3.6 shows the same response as above when three different inputs (3 mm, 5 mm and 7 mm amplitude) are applied (for the purpose of testing the linearity). The differences among the three graphs are reasonably small; hence it is possible to state that the nonlinear effects are negligible and the hypothesis of linearity is realistic within the amplitude range of the signals. Nonlinear effects occur typically with large signals (although small signals can also excite nonlinear phenomena, e.g. dead zones).

Figures 3.7 and 3.8 depict two responses in the time domain: relative body-wheel displacement and body acceleration, in response to a 3-mm amplitude sinusoidal signal at a frequency of 3.3 Hz. The traces are nearly sinusoidal. This further confirms the issue of linearity.

For subsequent studies, the frequency range was limited to 6 Hz. Such a range is sufficient to show all the main dynamic phenomena associated with the chassis, in response to bounce, roll and pitch inputs; also the controlled suspensions are meant to work in such a frequency range.

Figure 3.9 shows the rear right and left corner responses of the car to a pure bounce input, applied to all four wheels. It must be specified that in this measurement, with all four actuators in operation, the quantity of noise increases, making it more difficult to take stable RMS readings on the oscilloscope.

Two resonances are evident from the figure: the first (around 2.3 Hz) is the bounce resonance while the second resonance (around 3.8 Hz) is due to the pitch-bounce coupled motion. In order to identify which was the dominant parasitic responsible for that spurious resonance motion (with respect to pure bounce), two more accelerometers were mounted on the front of the car above each suspension and the relative phase-shift was recorded. A phase-shift of about 180 deg is associated with roll motion, while a null phase-shift corresponds to pitch motion. At the spurious resonance of 3.8 Hz the measured phase-shift was about 40 deg, hence this resonance was mainly due to the induced pitch motion.

The right and left corner trends exhibit some differences; this mainly because the rear left damper of the car is not the original one: the former damper was used to manufacture the friction damper (as discussed in chapter 5) and was replaced by another one taken from a younger Ford Orion. The different thermophysical properties of the hydraulic oils in the two dampers as well as the differences in the wear (because of their different age) are co-causes in the difference between the two curves. Furthermore the centre of gravity of the car does not exactly pass through the vertical plane of symmetry. Both these factors are responsible for the difference in the right and left side response of the car.

Pitch response is presented in figure 3.10. Two resonances again are present as before, the pitch resonance at around 2.3 Hz, plus another one at around 3.8 Hz due to cross-coupling effects.

Figure 3.11 plots the roll response for three different inputs applied from an external voltage signal generator (2.74 mm, 4.11 mm, and 5.48 mm, the calibration factor being 1 V=13.7 mm). Two resonances are clear from the graph: the roll resonance at around 2.3 Hz and another spurious cross-coupling resonance at about 6 Hz. The closeness of the three responses confirms once again the hypothesis of linearity.

Figure 3.12 depicts the rear right relative displacement (body to wheel) response to a roll input. This is proportional to the rolling angle (relative to the wheel). Rolling angle is usually referred to the ground. However in the frequency range considered the wheel can be considered almost steady so that the rolling angle with respect to the ground is not expected to differ very much from the one measured with respect to the wheel. As expected the resonance occurs at the same frequency as that of figure 3.11 measured in terms of acceleration.

For the pseudo-random input test, a 25-Hz filtered white noise, produced with an external noise generator, was applied to the rear right wheel. The body acceleration time trend is plotted in figure 3.13; its RMS is 0.75 m/s^2.

Finally a bump test was performed. A sinusoidal bump with a slight offset (to emulate the deformation of the tyre when a bump is encountered) has been generated using the graphical editor available; the demanded input was filtered by actuator dynamics, resulting in a smoother signal (closer to reality). Bumps with three different periods

have been tested to emulate different speeds Figure 3.14 shows the response of the car to a bump applied at the rear right wheel. The most meaningful parameters in a bump test are peak acceleration and number of oscillations. In this case the max overshoot and undershoot are symmetrical with a value of ± 0.85 m/s^2 and the number of oscillations is 3, corresponding to an equivalent damping ratio of approximately 0.3.

3.6.5 Suspension spring and tyre tests

This subsection reports on the tests performed on the suspension spring and on the tyre in order to measure their stiffness and to establish linearity. These parameters measured experimentally are required for simulation work.

The spring was loaded vertically in a material testing machine with a periodic force applied quasi-statically. The force cycled between 0 N and 2 kN. The compression of the spring under the load was measured with an extensometer and the force applied with a strain gauge. The spring characteristic was linear in the measured range (up to a deflection of 200 mm). The deflection applied is far larger than the one experimented in a car under normal conditions. This validates the hypothesis of linearity and allows to use a linear model for the spring. Nonlinear effects would have been probably present only if the coils had been distorted. The static stiffness is 19 kN/m. No hysteresis was present because the coils are made in steel.

The same type of test was carried out on the tyre. On a tyre it is possible to define a radial stiffness, which is the one of interest in ride analysis as well as a lateral stiffness, more of interest in handling behaviour.

The experimental set-up was the same; however, in this case, it is important to specify how the load is applied, concentrated or distributed: depending upon load distribution, the stiffness measured is different; the tyre behaves as a loaded beam or a membrane and according to the type of loading, the stress distribution, from which the stiffness value depends, is different. A distributed load however better represents the forces transmitted from the road, hence this type of load was used.

The trend is slightly nonlinear with hysteresis present because rubber is a viscoelastic material. The equivalent linear value of stiffness measured as the slope of the line interpolating the points corresponding to null force and maximum force is 74 kN/m.

The effective stiffness is twice this value because the tyre can be thought as two springs placed in parallel (neglecting the elasticity of the wheel). If the measure had been carried out on the tyre without the metallic part of the wheel, the measured value would have been the total radial tyre stiffness.

3.7 PASSIVELY-DAMPED CAR VALIDATION

3.7.1 Background

This section outlines the validation of the mathematical model developed, using the experimental data. The validation process ought to be carried out over the whole set of the expected operating conditions of the system. However in practice a selection of relevant inputs must be made, extrapolating the model behaviour for all the other possible inputs.

The accuracy achieved by the model is assessed in two ways. In the time domain, the simulated trends ought to reproduce the behaviour of the measured quantities, trying to follow as closely as possible the trends of the measured variables. In the frequency domain a good match of the frequency response is expected in the frequency range of interest, which for the vehicle is in a sufficiently large neighbourhood of the chassis resonance (from 1 to 5 Hz).

3.7.2 Passively-damped car validation

As previously explained a 7 DOF model has been adopted. Figure 3.15 shows a comparison of measured and predicted rear-right body acceleration time history at a frequency of 2.5 Hz (the phase shift was negligible). The experimental trend is almost sinusoidal; this confirms the hypothesis that for sufficiently large amplitudes the behaviour of the car is approximately linear. In such conditions the simulation closely models the trend of the experimental response. The model ought to work in a range of input amplitudes of the order of magnitude of the centimetre; if the inputs are too large or too small they can excite unmodelled dynamics. For smaller amplitudes the nonlinear

effects provoked by dead zones and stiction, and for larger inputs, by saturations, would have been present and a nonlinear car model would have been required to handle them.

Passing to the frequency domain analysis, figure 3.16 depicts the predicted and experimental frequency response to a 7-mm input. Up to around 2.8 Hz the match is fairly good; also the value of the resonance frequency is correctly predicted. Between 2.8 Hz and 4 Hz simulation underestimates the acceleration while at higher frequencies, there is an overestimation. This is principally due to some unmodelled nonlinearities (rather than to neglected dynamics), in particular the viscous damper characteristics. The linear viscous characteristics employed in the model have been obtained by linearising their actual characteristics around the origin (i.e. at the zero velocity). The real characteristics are nonlinear, approximately piecewise and with different trends for bound and rebound strokes. At higher frequency (which means at higher velocity) the local slope of the actual viscous characteristics is smaller than that modelled, resulting in a lower damping. Furthermore in a real viscous damper some hysteresis is present, attributable partly to the rubber bushes and the parasitic friction but also to the dissipative internal forces within the oil. This explains the mismatch between experimental data and simulation after the chassis resonance frequency.

At 8.5 Hz a resonance is present, due to the engine mounting or to the induced yaw; such a resonance is not predicted by the model, which would need further degrees of freedom to include these dynamic phenomena. The tyre model is not sophisticated, however highly complicated tyre models are essential in handling studies where lateral forces play a major role and not in ride studies where the dynamics of interest are vertical. A small amount of hysteresis is present in the tyre characteristics, but this mainly affects the behaviour around the wheel-hop resonance.

Some sensitivity analysis has been performed, by changing the viscous coefficient in the range 350 N/ms^{-1} to 425 N/ms^{-1}. An acceptable value was found to be 400 N/ms^{-1}, as the analysis of figure 3.16 confirms.

In conclusion, the car model, despite being linear and not extremely sophisticated (compared to those employed for car design), grasps the main features of the response both in the time domain and in the frequency domain, up to the chassis resonance. For a more accurate modelling of the higher frequency range a more complicated model would be required.

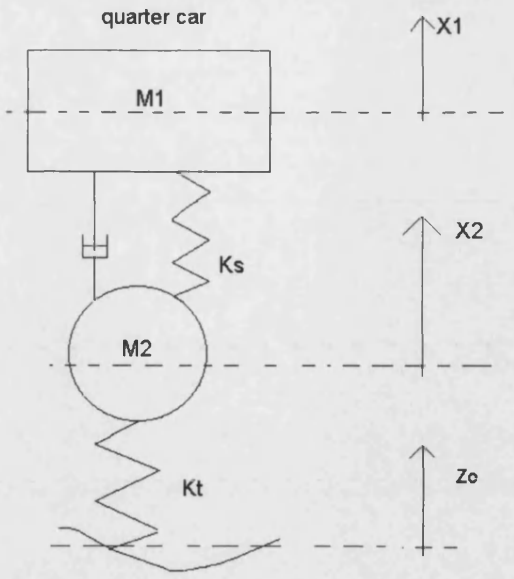

Figure 3.1 2 DOF quarter car model.

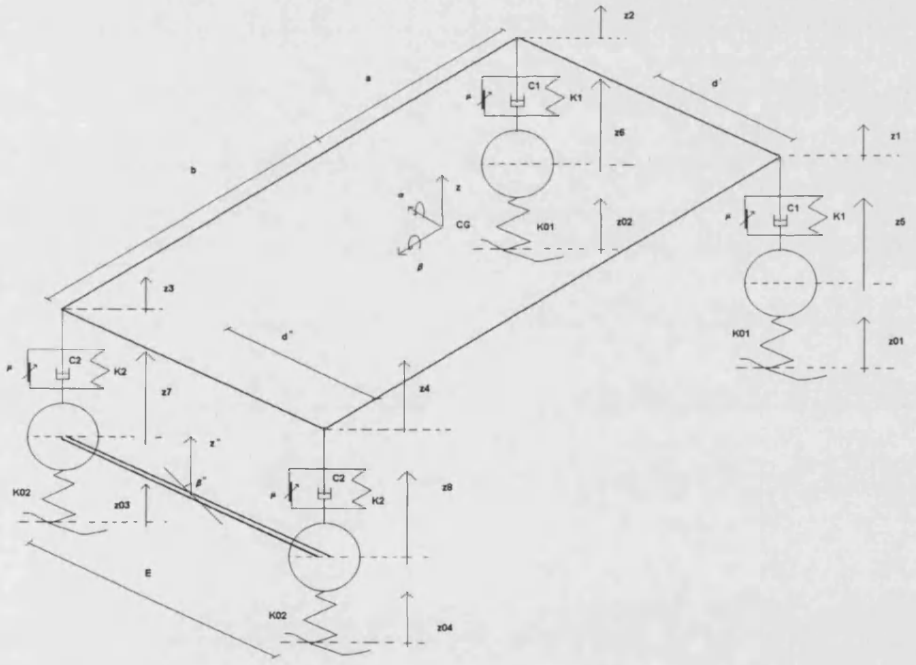

Figure 3.2 7 DOF full car model.

Figure 3.3 The Ford Orion on the four-poster road simulator.

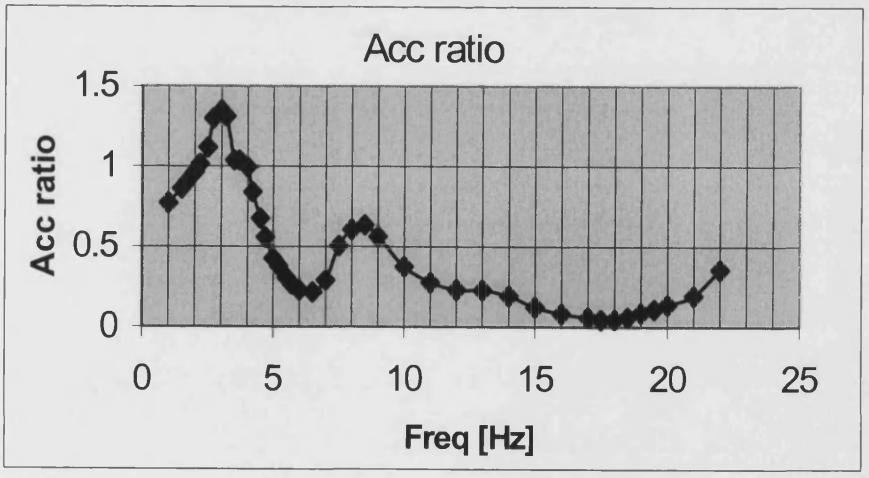

Figure 3.4 Body to wheel acceleration ratio of the rear-right corner of the car. Sinusoidal input to one wheel; amplitude: 3 mm.

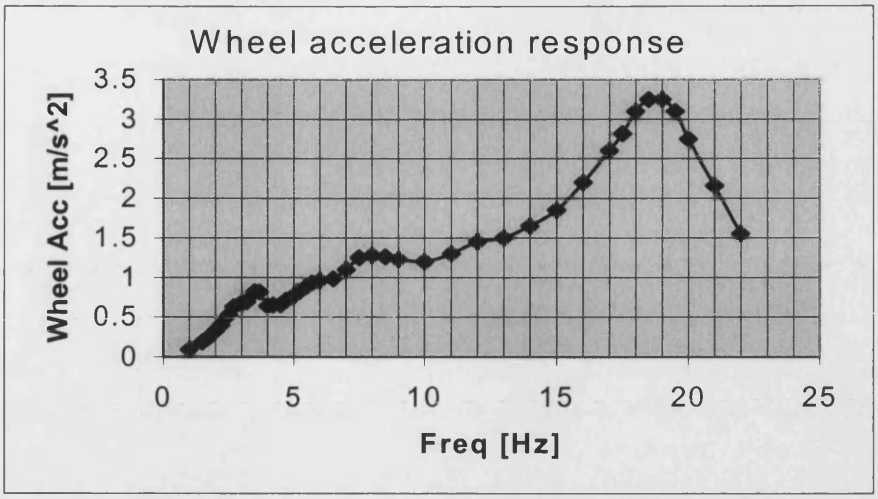

Figure 3.5 Rear-right wheel acceleration response. Sinusoidal input to one wheel; amplitude: 3 mm.

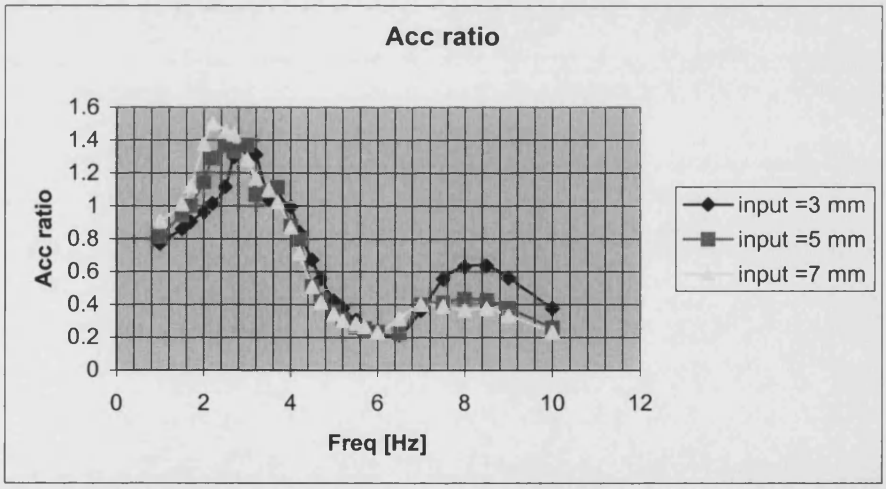

Figure 3.6 Body to wheel acceleration ratio of the rear right corner of the car. Sinusoidal input to one wheel; amplitudes: 3 mm, 5 mm, 7 mm.

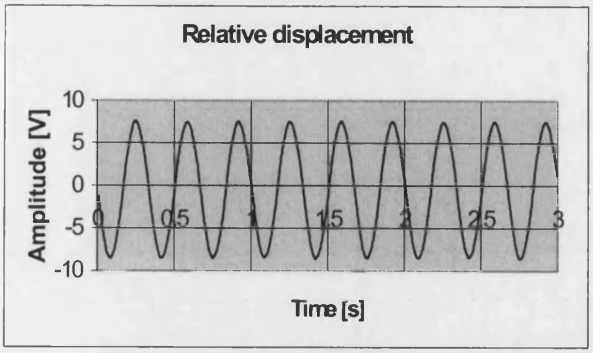

Figure 3.7 Relative displacement time trend. Sinusoidal input to one wheel; amplitude 3 mm, frequency 3.3 Hz.

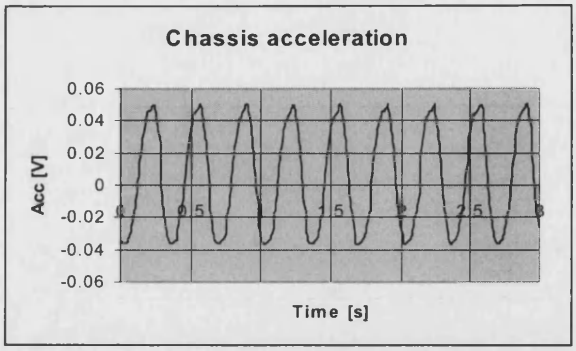

Figure 3.8 Chassis acceleration time trend. Sinusoidal input to one wheel; amplitude 3 mm, frequency 3.3 Hz.

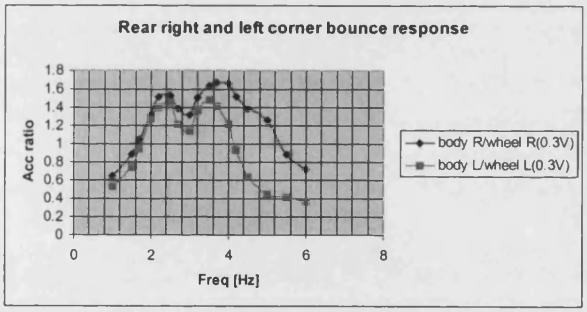

Figure 3.9 Body to wheel acceleration ratio of the rear of the car. Sinusoidal bounce input to all wheels; amplitude: 3 mm.

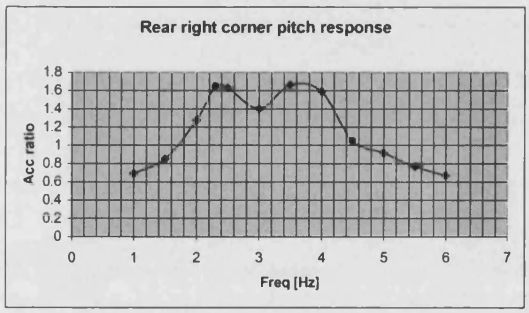

Figure 3.10 Body to wheel acceleration ratio of the rear-left corner of the car. Sinusoidal pitch input to all wheels; amplitude: 3 mm.

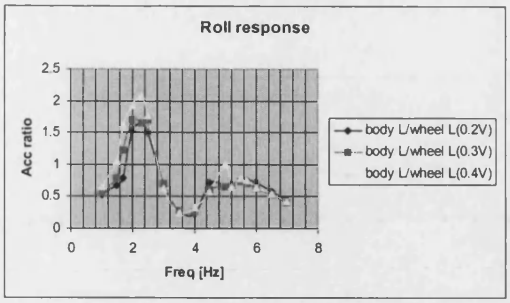

Figure 3.11 Body to wheel acceleration ratio of the rear-left corner of the car. Sinusoidal roll input to all wheels; amplitude: 0.2 V, 0.3 V, 0.4 V (1V=13.7 mm).

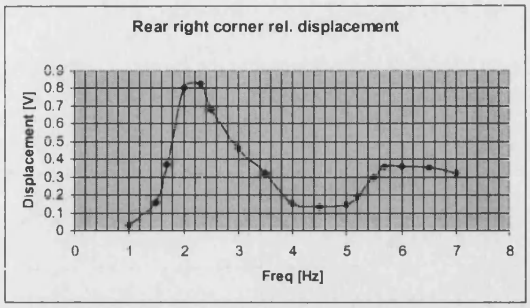

Figure 3.12 Relative displacement of the rear-right corner of the car. Sinusoidal roll input to all wheels; amplitude: 0.2 V, 0.3 V, 0.4 V (1V=13.7 mm).

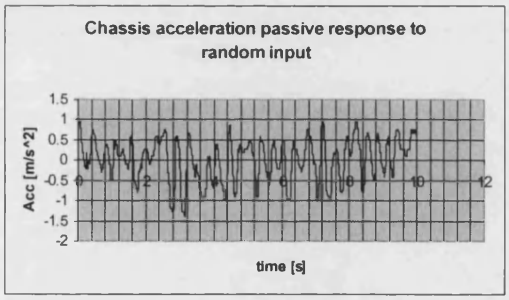

Figure 3.13 Chassis acceleration time trend. Random input: 25-Hz filtered white noise.

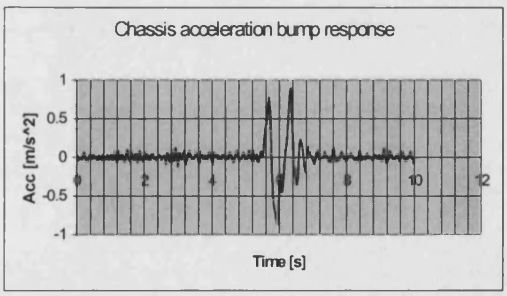

Figure 3.14 Chassis acceleration time trend. Sinusoidal bump input; amplitude 30 mm.

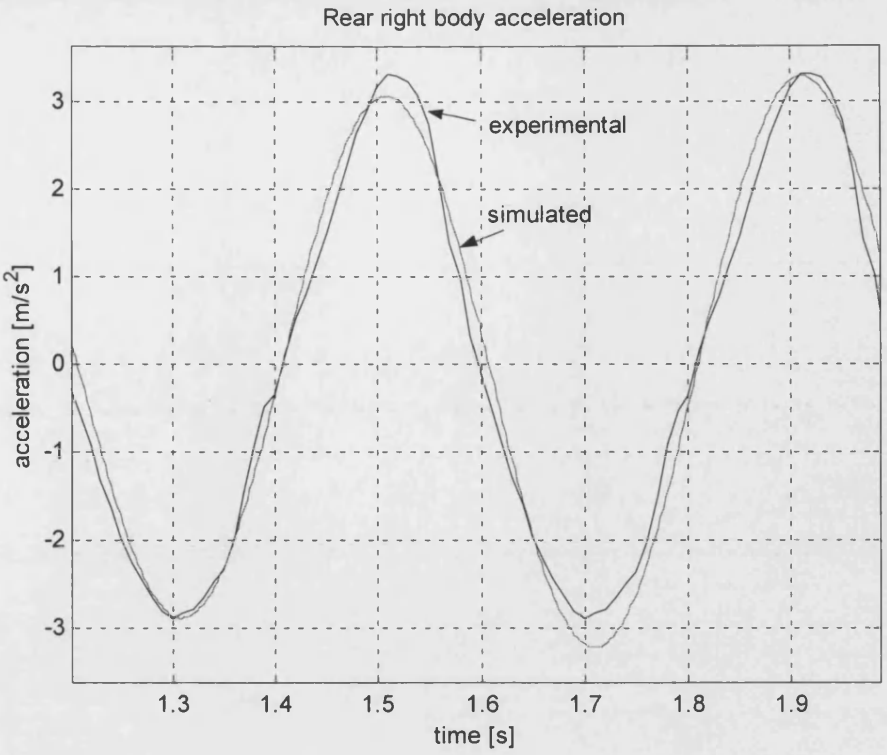

Figure 3.15 Rear-right passive acceleration; sinusoidal input to one wheel; amplitude: 7 mm; frequency 2.5 Hz.

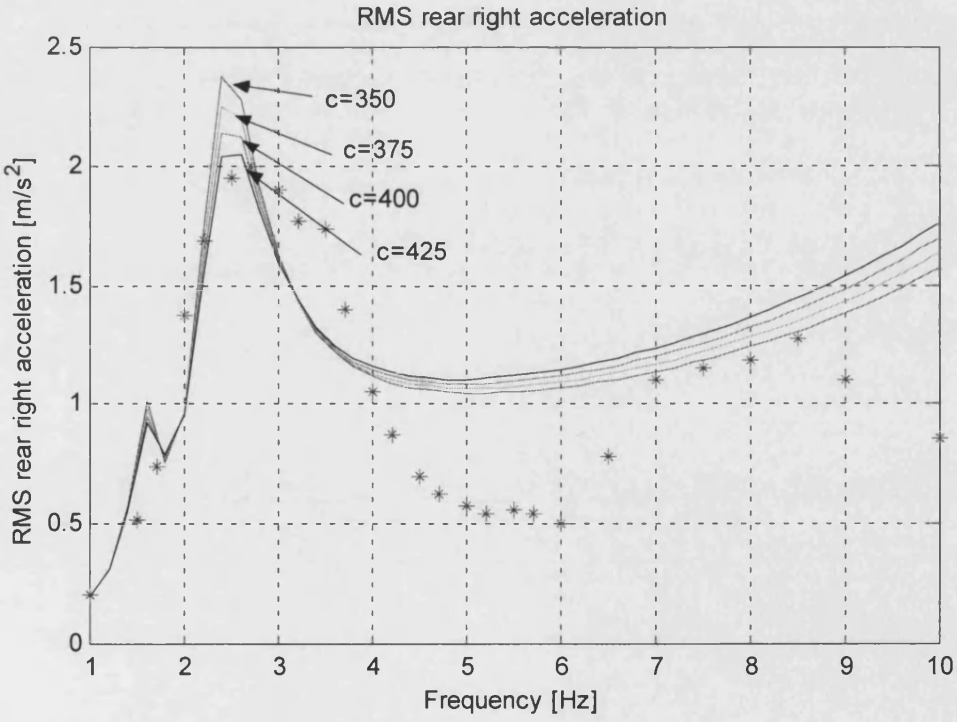

Figure 3.16 Rear-right passive acceleration "frequency response" (transmissibility); sinusoidal input to one wheel; amplitude: 7 mm.

4 FRICTION DAMPER MODEL AND SMC DESIGN AND SIMULATION

4.1 THE FRICTION DAMPER

This chapter outlines the modelling of the friction damper and of its electrohydraulic drive and the design and computer simulation of the sliding mode controller. A block diagram of the closed-loop control system is presented in figure 4.1.

The friction damper is the core of the system. Consider the quarter car model. The normal force F_n applied to the plate is expressed in general by:

$$F_n=F_n(x,\ \dot{x},\ \ddot{x}_1,\ P_A)H(P_A) \tag{4.1}$$

$H(\cdot)$ being the Heavyside step function and P_A the actuator pressure (either piston-side or differential pressure depending on the design of the hydraulic circuit). The introduction of the Heavyside function is necessary because if the differential pressure is negative, the friction pad and the plate are disengaged, hence $F_n=0$.

According to (2.43) the friction force F_d developed by the friction damper is:

$$F_d=-\mu(\dot{x})F_n\,sgn(\dot{x}) \tag{4.2}$$

It is worth remarking that friction force is a function of relative and not of the absolute velocity. This is because of the actual mounting of the friction device. In a real-life situation of a car, in fact, the hydraulic actuator with the pad is connected to the sprung mass, while the plate is fixed to the unsprung mass (or vice-versa). Hence, the actuator is not stationary but it follows the motion of the sprung mass while the plate is fixed to the unsprung mass, consequently the sign of the friction force depends on their relative velocity. Conversely, if the cylinder were ideally fixed to a stationary reference, the sign of the friction force would depend only upon the sign of sprung mass velocity. This could be the case, for instance of a friction damper used for vibration isolation of

rotating machines. To take into account the vertical motion of the cylinder, a mathematical model of a cylinder placed on a moving frame should be developed; however the problem has been more readily solved by considering the frictional force as a function of the relative velocity between the sprung and the unsprung mass, rather than of the absolute velocity of the body of the car. This has allowed the actuator to be modelled as a stationary entity with respect to the ground.

The friction model employed was identified based on the experimental measurement of the friction force on the friction damper itself (detailed in chapter 5) and expressed by:

$$F_d(t) = -\mu F_n(t-T_L)sgn(\dot{x}) \tag{4.3}$$

where the friction coefficient μ is velocity-independent and T_L is a delay due to the frictional memory effect. Stiction and the breakaway transition dynamics as well as Stribeck effect are not included in the model because they were found negligible (temperature effects have been not considered either in this analysis).

This model can be seen as a particular case of the more general seven parameter model described in chapter 2 where only Coulomb friction and the frictional memory effect are included (see chapter 2, subsection 2.8.2).

4.2 THE ELECTROHYDRAULIC DRIVE

4.2.1 The Bathfp model

The system was initially modelled in Bath*fp* as in figure 4.2, employing a 4-way 3-position proportional valve driving an actuator, whose load was the friction pad. Such a system had the advantage of completely disengaging the pad from the plate when demanded: for a negative pressure difference the two plates were not in contact, thus no residual friction force was present. However this model proved to be very difficult to integrate numerically (the practical feasibility problems of such a design were not considered at this stage), because the actuator virtually does not move. This has several modelling and numerical implications that are now discussed.

An equal area linear hydraulic actuator has been considered (the extension to an unequal area actuator is straightforward). The governing equation for the case of a horizontal cylinder is the following:

$$M_A\ddot{x}_{act} = (P_A - P_B)A - F_{ext} - f\,\dot{x}_{act} - F_{friction} \tag{4.4}$$

where P_A and P_B are the actuator piston end and rod end pressures, A is the cross-sectional annulus area, M_A is the total mass to be moved, x_{act} the actuator displacement, F_{ext} the external force applied to the rod, f is a speed-dependent friction coefficient and $F_{friction}$ is the term which represents cylinder Coulomb friction and stiction forces.

The compliance due to the connection between the actuating rod and the load (the pad) is modelled as a high stiffness spring located in-between. Forces applied to the actuator by the load are transmitted via the compliance spring. The force applied by the actuator to the load is given by:

$$F_n = -K_c(x_{act} - x_{act0}) \tag{4.5}$$

x_{act0} is the initial separation between the rod and the body of the car, K_c is the equivalent stiffness of the compliance spring (a damping term could be introduced when appropriate). The friction force is:

$$F_d = -\mu(\dot{x})F_n sgn(\dot{x}) \quad \text{if } x_{act} > x_{act0} \tag{4.6a}$$

$$F_d = 0 \quad \text{if } x_{act} < x_{act0} \tag{4.6b}$$

From a numerical point of view, this model presents two embedded discontinuities ($sgn(\dot{x})$ and $x_{act} > x_{act0}$). Furthermore equation (4.5) presents a product between the variable x_{act} (which assumes very low values since the motion of the actuator is tiny) and the high stiffness compliance spring. This product as well as the high frequency pole introduced by the spring, makes it numerically very stiff, although the dynamical effect of this additional spring on the overall dynamics of the system is negligible. In addition the SMC drives the valve with a switching input introducing other high frequency discontinuities.

The issue of the analytical relationship between pressure and spool displacement will be now tackled to understand how the model can present a critical behaviour under some circumstances.

Consider the control valve: by applying Bernoulli law, it is possible to write the following orifice equations; leakage flow past the spool between supply and return ports (modelled in Bath*fp* as laminar) are omitted in this description for brevity.

$$Q_1 = C_q \pi D(u+z)\sqrt{\frac{2(P_S - P_A)}{\rho}} - C_q \pi D(u-z)\sqrt{\frac{2(P_A - P_T)}{\rho}} \tag{4.7}$$

$$Q_2 = C_q \pi D(u+z)\sqrt{\frac{2(P_B - P_T)}{\rho}} - C_q \pi D(u-z)\sqrt{\frac{2(P_S - P_B)}{\rho}} \tag{4.8}$$

The spool dynamic behaviour is taken to be linear second order.

Linearising the previous equation and working on the assumption that $Q_1=Q_2$ (see figure 4.3), yields (lower case letters denote small variations):

$$q = k_q z - k_c p_m \tag{4.9}$$

with $p_m=p_A - p_B$. By combining the linearised equation of the flow in the valve (4.9) with the equation of the flow continuity and Newton's law for the actuator:

$$q = As x_{act} + \frac{V_t}{4B} s p_m + L p_m \tag{4.10}$$

$$A p_m = M_A s^2 x_{act} + f s x_{act} \tag{4.11}$$

where V_t is the total volume of the two chamber of the cylinder, L the leakage coefficient, and s the Laplace complex variable.

After some calculations, the following transfer function between differential pressure and spool displacement is obtained:

$$\frac{p_m}{z}(s) = \frac{K_q 4B(M_A s + f)}{M_A V_t s^2 + (K_c 4BM_A + 4BLM_A + V_t f)s + 4B(K_c f + A^2 + Lf)} \tag{4.12}$$

It was found that the discontinuities make this model extremely hard to simulate. To overcome this problem a new model was developed modifying slightly the design. The actuator governing equation was obtained not by applying Newton's second law, but adopting the flow continuity equation. In this way it is possible not to introduce the actuator displacement as a variable (which is a major source of numerical stiffness). In Bath*fp* this cannot be readily done. Therefore the model was implemented in Simulink.

4.2.2 The Simulink model

Because of the problems mentioned, the circuit was modified as in figure 4.4. The model was implemented in Simulink. This package presents some numerical features which are suitable for this kind of problem, such as the zero-crossing detection routine (see chapter 3, subsection 3.2.1). In this design an electrohydraulic proportional underlapped valve, supplied by a pump in parallel with a relief valve, drives a single-chamber actuator. The hydraulic circuit behaves as a potential divider. From consideration of figure 4.4:

$$Q_p = Q_l + Q_{rv} + Q_c \quad \text{for } P_s > P_c \tag{4.13}$$

P_c being the relief valve cracking pressure and Q_c the compressibility flow in the line connecting the outlet of the pump with the inlet of the relief valve and with the supply port of the control valve.

(also $Q_p = Q_l + Q_c$ for $P_s < P_c$. However in the model the pump is supposed to supply enough flow so as to keep the relief valve always open).

The governing equation of the relief valve is:

$$P_s = P_c + k_{rv}(Q_p - Q_l - Q_c) \tag{4.14}$$

Q_p is the rated flow of the pump. Relief valve dynamics have been not included because they are typically very fast (around 200 Hz). The compressibility flow in the connecting hose is:

$$Q_c = \frac{V_{hose}}{B} s P_s \tag{4.15}$$

Applying the continuity equation at the second node of the circuit of figure 4.5, yields:

$$Q_1 = Q_2 + Q_3 \tag{4.16}$$

An appropriate model of the valve must be developed. Because it works in pressure control mode and therefore around the central position, the leakage flows play an important role. Leakage flow could be considered to a first approximation as laminar and therefore expressed by a linear relationship between flow and pressure drop. However depending upon the length of the leakage flow path the regime can be either laminar or turbulent or transitional. The model proposed by Eryilmaz and Wilson (2000) uses a turbulent model and an empirical correlation to model the valve opening. The governing equations are (see figure 4.6):

$$Q_1 = C_q \pi D (u+z) \sqrt{\frac{2(P_S - P_A)}{\rho}} \qquad \text{if } z \geq 0 \tag{4.17a}$$

$$Q_1 = C_q \pi D \sqrt{\frac{2(P_S - P_A)}{\rho}} \frac{u^2}{(u - k_{1s} z)} \qquad \text{if } z < 0 \tag{4.17b}$$

$$Q_2 = \frac{V_t}{B} s P_A \tag{4.18}$$

$$Q_3 = C_q \pi D \sqrt{\frac{2(P_A - P_T)}{\rho}} \frac{u^2}{(u + k_{1s} z)} \qquad \text{if } z \geq 0 \tag{4.19a}$$

$$Q_3 = C_q \pi D (u-z) \sqrt{\frac{2(P_A - P_T)}{\rho}} \qquad \text{if } z < 0 \tag{4.19b}$$

with $-u \leq z \leq u$

where $k_{ls} = \frac{1}{2}\sqrt{\frac{P_S + P_A(u) - P_T}{P_S - P_A(u) - P_T}} - 1$ (4.20)

Spool-solenoid electromechanical dynamics can be expressed through a second-order linear model whose transfer function is:

$$\frac{z}{i}(s) = \frac{k_z}{\frac{s^2}{\omega_n^2} + 2\frac{\xi_v}{\omega_n}s + 1} \tag{4.21}$$

z being the spool displacement and i the solenoid current. The valve amplifier voltage-current dynamics are fast enough to be neglected (see chapter 6, section 6.2)

The transfer function relating pressure to current will be obtained solely to show which parameters (valve lap, volume, bulk modulus) affect the dynamic response of the drive. A linearised model cannot be used for detailed performance assessment because the pressure variations are too large to allow a linearisation.

Neglecting leakage flows past the valve, linearising (4.16) yields:

$$\frac{p_A}{z}(s) = \frac{\frac{k_{q1} - k_{q3}}{k_{c3} - k_{c1}}}{1 + \frac{V_t}{B(k_{c3} - k_{c1})}s} \tag{4.22}$$

Hence, the total transfer function between the solenoid current and pressure is third order:

$$\frac{p_A}{i}(s) = \frac{\frac{K_{q1} - K_{q3}}{K_{c3} - K_{c1}}}{1 + \frac{V_t}{B(K_{c3} - K_{c1})}s} \frac{k_z}{\frac{s^2}{\omega_n^2} + 2\frac{\xi_v}{\omega_n}s + 1} \tag{4.23}$$

where

$$k_{q1} = C_q \pi D \sqrt{\frac{2(P_S - P_A)}{\rho}} \tag{4.24}$$

$$k_{c1} = -\frac{C_q \pi D(u+z)}{\sqrt{2\rho(P_S - P_A)}} \tag{4.25}$$

$$k_{q3} = -C_q \pi D \sqrt{\frac{2(P_S - P_A)}{\rho}} \tag{4.26}$$

$$k_{c3} = \frac{C_q \pi D(u-z)}{\sqrt{2\rho(P_A - P_T)}} \tag{4.27}$$

The pressure-current transfer function points out that the dynamic response is dependent on the lap size and on the volume of the actuator chamber and connecting hose characteristics. A Simulink diagram of the whole system is depicted in figure 4.7.

4.2.3 The feedback chain

The friction force control system works in closed-loop. Relative displacement and velocity signals are fed back into the valve solenoid.

In principle, displacement transducer dynamics ought to be modelled (a first order lag would provide an accurate enough representation). However its bandwidth is extremely large, since it is a potentiometric device, to allow the high frequency pole (possibly due to either strain inductive or capacitive effects) to be neglected. Also the velocity signal is modelled as a pure algebraic block. In the experimental rig, velocity is actually obtained by performing the numerical differentiation of the measured position. However the operation is trivial and requires a negligible computer time. Theoretically velocity dynamics should be modelled as a first order lag (displacement transducer dynamics) and a pure delay (processor time to compute the derivative), but these dynamics are much faster compared to plant dynamics, that they can be assumed instantaneous. The delay in performing the derivative depends upon the computer sampling rate, if this is not fast enough, this delay cannot be negligible and it can have detrimental effects on the control, for example in SMC, Gamble (1992) found out that a delay in the highest state can introduce chattering. In this work the computer sampling rate was set to 100 Hz, which is far larger than the car dynamics considered (up to 5 Hz).

4.3 SLIDING MODE CONTROLLER DESIGN

The first control logic investigated was SMC in the switching-type implementation.

The pressure gain characteristics of an underlapped valve inherently constitutes a sliding mode controller with boundary layer proportional to valve lap (see figure 4.3): an ideal zero-lapped valve would behave as an on-off controller. Hysteresis, if present, only affects the motion inside the boundary layer and it can contribute to chattering reduction (Gerdes and Hedrick (1999)).

The expression of the pressure gain can be readily obtained. Under static conditions $Q_1=Q_3$ (compressibility flow is not present in static condition). If leakage flows are neglected, the following holds:

$$C_q \pi D(u+z)\sqrt{\frac{2(P_S - P_A)}{\rho}} = C_q \pi D(u-z)\sqrt{\frac{2(P_A - P_T)}{\rho}} \tag{4.28}$$

this yields (supposing for ease $P_T=0$):

$$(u+z)^2 (P_S - P_A)=(u-z)^2 P_A \tag{4.29}$$

Hence the analytical expression of the pressure gain as a function of spool displacement and underlap is:

$$P_A(z) = P_s \frac{z^2 + u^2 + 2uz}{2(u^2 + z^2)} \quad \text{with } -u \le z \le u \tag{4.30}$$

In the limit $u \to 0$ which gives an ideal on-off characteristics. Figure 4.8 shows a typical trend for the pressure gain.

If leakage flows (4.17b) and (4.19a) are included, it is still possible to obtain an analytical expression for the pressure gain but it is far more involved (Eryilmaz and Wilson (2000)).

For design purposes, the following developments are based on the simplifying hypotheses of an ideal zero-lapped valve. This allows to use the $sgn(\cdot)$ operator to describe the switching controller. This controller is not active, in the sense that it only

switches between zero (valve closed) and the positive upper bound (valve open), as opposed to an active controller, such as a switching amplifier, which switches between a fully positive and a fully negative value. This is the inherent limitation of the friction device, and this has a few consequences described below.

The first sliding surface investigated is:

$$\sigma = x + c_1 \dot{x} \tag{4.31}$$

Such a surface is meant to drive the system onto a straight line trajectory, therefore dictating first order dynamics and cancelling chassis acceleration. When the sliding regime is promoted, the demand voltage signal to the valve switches between $\pm V_{max}$, where V_{max} is the value of the voltage which saturates the pressure gain. Hence the normal control force applied to the plate is:

$$F_n = AP_{Amax} \qquad \text{if } \sigma > 0 \tag{4.32a}$$

$$F_n = 0 \qquad \text{if } \sigma < 0 \tag{4.32b}$$

This means that, differently from an active controller, the control force is null when $\sigma < 0$. In more compact form:

$$F_n = AP_{Amax} H(\sigma) = \frac{AP_{Amax}}{2} [1 + sgn(\sigma)] \tag{4.33}$$

The friction force applied to the plant is:

$$F_d = -\mu AP_{Amax} H(\sigma)\, sgn(\dot{x}) \tag{4.34}$$

which can be written as:

$$F_d = -\mu A P_{Amax} \frac{1 + sgn(x + c_1 \dot{x})}{2} sgn(\dot{x}) \tag{4.35}$$

and further rearranged as as [1]:

$$F_d = -\frac{\mu}{2} A\, P_{Amax}\, [sgn(\dot{x}) + sgn(x\dot{x} + c_1 \dot{x}^2)] \tag{4.36}$$

This shows the strong non linearity introduced by the friction device which appears in the expression (4.36) of the switching frictional force applied to the plant with the specified sliding surface (4.31)

It is necessary to provide a physical explanation to equation (4.36). This point is worth elaborating in some more detail, as it is one of the fundamental features of this system. In chapter 2 (subsection 2.5.4), necessary and sufficient conditions for obtaining a sliding mode regime were defined. Nevertheless, the application of the previously presented theory, in this case, is not straightforward, because those theorems are valid only in linear conditions, whilst this system is driven by a nonlinear element, the friction damper. In order to gain an understanding of the response, consider the open-loop response of the system and suppose that the valve spool is driven by a square wave signal of amplitude $\pm V_{max}$ and that it follows the same. If both spool and pressure dynamics are ideally taken to be instantaneous, the pressure applied to the plate will switch between the value of the supply pressure for $+V_{max}$ and zero (or strictly the residual back pressure value) for $-V_{max}$.

Analogous conclusions can be drawn for the initial design with the equal area actuator (the Bath*fp* model). In this case it must be related to the actuator differential pressure $P_m = P_A - P_B$. The normal force applied to the plate is different from zero only when $P_m > 0$ and it is set to zero when $P_m < 0$. This is the main peculiarity of a semi-active controller (a sort of hydraulic diode-bridge half-wave rectifier). The qualitative trend of the normal force transmitted to the plate is depicted in figure 4.9. It has the same mark-to-space ratio as the voltage demand. The trend of the frictional force, qualitatively portrayed in figure 4.10, is however different: the frictional force, in fact, is also a function of the sign of the relative vertical velocity. Therefore, the previous waveform

[1] Noting that $sgn(x)sgn(y) = sgn(xy) \quad \forall\, x, y \in \Re$.

of figure 4.9 is "modulated" from the velocity, consequently resulting in a three-state force applied at the plant level, despite the " two-state" square wave input.

In closed loop, with the sliding surface given by (4.34), the friction force applied to the plant is described by an equation of the type:

$F_d=-U$ if $\dot{x}>0$ & $(x+c_1\dot{x})>0;$ $c_1, U>0$ (4.37a)

$F_d=+U$ if $\dot{x}<0$ & $(x+c_1\dot{x})>0;$ (4.37b)

$F_d=0$ if $(x+c_1\dot{x})<0 \quad \forall \dot{x}$ (4.37c)

The phase plane portrait is depicted in figure 4.11. In fact, this means that the reaching phase is longer than that experienced with a more conventional switching device, because when $\sigma<0$ there is no control action and during this time the system is unforced.

Nevertheless, despite this inherent limitation, the sliding surface (4.31) can partially achieve its aim of controlling the transient response (or in other words, the complementary solution of the differential equation (3.1)). However, if the disturbance is sinusoidal or periodic (i.e. if the particular solution of (3.1) is considered), as in the case of a vehicle moving on a road, the sliding mode controller, as it is designed, would lead to the clamping of the chassis, because surface (4.31) is meant to cancel chassis acceleration. This is because the attainment of sliding mode regime in steady-state can be obtained only by increasing the supply pressure. Even if physically achievable, this leads to such a high value of the control force that the only result is the clamping of the mass. Therefore another control strategy must be sought in order to successfully cope with a bounded (typically periodical) disturbance. This can be achieved by developing a force tracking control with the purpose of reducing the total force experienced by the chassis. A sliding surface can be designed based on the tracking error between spring force F_s (assumed as the reference) and normal force F_n:

$$\sigma=F_s-\frac{F_n}{\mu}=k_s x-\frac{AP_A}{\mu} \tag{4.38}$$

therefore

$$F_n = AP_{Amax}\, H(\sigma) = AP_{Amax}\, H\left(k_s x - \frac{AP_A}{\mu}\right) \tag{4.39}$$

and

$$F_d = -\mu\, AP_{Amax} H\left(k_s x - \frac{AP_A}{\mu}\right) sgn(\dot{x}) \tag{4.40}$$

However there is no direct control on the sign of the friction force, which can only correctly track the spring force (so as to attempt to be equal and opposite) in some intervals within each period. Furthermore the scheme requires a pressure feedback.

An attempt to solve the problem was made by designing a sliding surface based on the tracking error between spring force and friction force, inferring the latter through a measurement of spring, viscous and inertial forces:

$$\sigma = F_s - F_d = -k_s x - (M_1 \ddot{x}_1 + 2\xi\omega_1 M_1 \dot{x} + k_s x) \tag{4.41}$$

However simulation showed that this control strategy was not successful (besides requiring an acceleration feedback). Also this surface was unable to provide a correct tracking (i.e. with the right sign) of the spring force.

Another possibility to improve steady-state periodical response (although not thoroughly investigated) can be the choice of a nonlinear bounded sliding surface, i.e. a closed curve, such as a circle or an ellipse, whose area is smaller than that enclosed by the steady-state passive trajectory. However also in this case a fully active controller would be necessary to keep the state on the trajectory.

It was eventually realised that it is not possible to always track the spring force with a friction force, but that spring force tracking can be only partially achieved with a semi-active friction device.

The sufficient condition that guarantees effective tracking was obtained from Lyapounov stability theory. In order to produce a control force which has the opposite sign to the spring force, the product of displacement and velocity must be negative:

$$x\dot{x} < 0 \tag{4.42}$$

This switching condition was obtained by considering a Lyapounov energy function:

$$V(x, \dot{x}) = \frac{1}{2}x^2 \tag{4.43}$$

Its derivative yields the sufficient condition for stability (4.42).

It is worth remarking that the controller defined by (4.31) and (4.37) does not fulfil this condition. With condition (4.42) the control must work only in the second and the fourth quadrant of the phase plane (see figure 4.12).

This condition can be incorporated in the previous tracking algorithm resulting in the following control law:

$$F_n = AP_{Amax}H(\sigma)\frac{1-sgn(x\dot{x})}{2} \tag{4.44}$$

and

$$F_d = -\frac{\mu}{2}AP_{Amax}[1-sgn(x\dot{x})+sgn(\sigma)-sgn(x\dot{x})sgn(\sigma)]sgn(\dot{x}) \tag{4.45}$$

This law provides a more attentive tracking. However in a car suspension every controller must assure not only a reduction of the transmitted forces but also smooth time trends for the controlled variables and in SMC a residual chattering is always present (although this can be reduced by an appropriate sizing of the boundary layer). The major limitations of this scheme has motivated the investigation of another type of VSC, described in chapter 5.

Next sections describe the simulation results for the SMC.

4.4 INITIAL SIMULATION AND ANALYSIS OF A 1 DOF SYSTEM

This section is concerned with the analysis of the response of a simple 1 DOF mass-spring-damper system sliding mode controlled. The purpose of this analysis is to solely point out the characteristics of the SMC for the simplest possible plant.

In the previous chapters the theory of SMC has been outlined and the whole system has been described. Now the results of the simulation performed in Simulink will be critically analysed, pointing out the extent to which the sliding mode behaviour has been achieved.

Consider the controller defined by sliding surface (4.31). Firstly note that in order to implement the SMC of the considered second order plant, relative, not absolute, displacement and velocity have been fed back, because the latter cannot be easily measured. This is not a problem and furthermore relative quantities are the ones of interest in this system, however in classical SMC the absolute quantities are used to implement the control (see chapter 2, subsection 2.5.1).

The natural response of the unforced system to non-zero initial conditions is initially analysed. The parameters employed are a mass of 165 kg, a spring rate of 12000 N/m and a damping ratio of 0.25. Consider the uncontrolled linear system. Figure 4.13 depicts its free response trajectory in the phase plane. This graph is presented in order to furnish a comparison with the trajectory of the same system when sliding mode controlled. The system has been excited with a non-zero initial condition $x(0)=0.2$, $\dot{x}(0)=0$ (point P in figure 4.13) and it evolves following second order underdamped dynamics, displaying the well-known logarithmic decay typical of a second order linear system.

Figures 4.14 to 4.17 refer to the controlled system. The parameters of the plant and the initial conditions are the same except the damping ratio now set to 0.1 (to represent the residual viscous damping likely to be inherent in the system). Figure 4.14 shows the trajectory of the controlled system. Figures 4.15, 4.16 and 4.17 respectively depict the time history of relative displacement, acceleration and the trend of spring and control forces.

In order to gain a better understanding of the behaviour of the controlled system and to properly interpret the trend of its trajectory, it is also useful to consider figure 4.17.

With reference to figure 4.14, the system starts its evolution from point A (corresponding to the initial conditions). The dotted straight line B-C, highlighted in the graph, represents the first order sliding surface (4.31). From A to B the evolution is second order, though non-linear, because of the constant frictional force applied by the

friction device (segment A-B in figure 4.17) is superimposed on the spring and residual viscous damping forces; at B (figure 4.14) the state reaches the sliding surface for the first time, however it does not start sliding onto it as expected. This is due to the inherent physical limitation of the semi-active friction device previously described: when the voltage demand assumes a negative value, the pressure is set to zero and there is no control force; hence the overall control action is not sufficient to allow the state to stay on the sliding surface after reaching it. The trajectory presents at B an angular point; in the corresponding time instant there is a commutation in the control force (segment B-B' in figure 4.17) and the structure of the system changes: the control force is set to zero (segment B'-C in figure 4.17) and the state evolves following a second order linear dynamics until point C, when it reaches again the sliding surface. The trajectory B-C is different from the corresponding arc of trajectory of the uncontrolled system of figure 4.13 because the initial conditions are now those corresponding to point B. At C the state reaches the sliding surface for the second time and subsequently starts sliding onto it, heading towards the origin O of the phase plane (the simulation has been stopped before the origin O was reached); from this moment the control force starts to chatter as expected in SMC (C-D in figure 4.17). Therefore, starting from point C in the phase plane the original second order system has been transformed into a first order system (whose trajectory is a straight line).

The simulation therefore has shown that the sliding mode is achieved in spite of the limitations of the friction device even if the reaching phase is longer compared to the one of an analogous plant controlled by a "conventional" sliding mode controller where the control action is applied for all the time and the state stays onto the sliding surface at the first intersection with it.

This result can be further confirmed by analysing the trend of displacement, and acceleration versus time. In figure 4.15 (displacement) it is possible to distinguish the reaching phase (A-C), characterised by a second order dynamics, and the sliding phase (C-D) which presents a first order dynamics; hence, starting from point C, the response has an exponential first order decay. 4.16 shows the trend of acceleration: the line A-B corresponds to the first part of the transient; at B there is a sudden discontinuity from B to B', corresponding to the first commutation of the control force, (corresponding in the phase plane, to the first intersection with the sliding surface). Subsequently the acceleration evolves following line B'-C. This part of the transient corresponds to the

time interval in-between the first and the second and definitive intersection with the sliding surface in the phase plane: from C onwards sliding mode is promoted and the acceleration begins to chatter (with a frequwency of around 100-150 Hz) with mean level decreasing exponentially, the decay being dependent on the sliding surface coefficient.

Consider now the forced response to a 1-Hz 3-cm sinusoidal input. The results are depicted from figure 4.18 to 4.20. As far as the 1 DOF uncontrolled linear system (that from now onwards will be termed the passive system) is concerned, its response is isofrequential with the input signal and with amplitudes and phases depending upon the value of the respective transfer functions at that frequency as known from linear system theory.

The trend of displacement is depicted in figure 4.18; it is quite smooth. It is worthwhile noting the presence of a negative offset of 0.01 m. This is due to the mean value different from null of the control force, as it can be seen from figure 4.20 reproducing the trend of spring and control forces. The acceleration (figure 4.19) instead does not present any offset. Its transient reveals an attempt of promoting sliding mode, occurring in the first second: the presence of a small chattering indicates in fact an attempt to slide. However the steady-state response does not present any sliding mode behaviour. The attainment of sliding mode regime would only be obtained with a higher control action, by increasing the supply pressure. However, this leads to such a high value of the control force that the only result is the clamping of the mass. This is due to the particular sliding surface employed. This is not what was expected: any control logic, in this kind of problem should compensate forces only partially so that the sprung mass is not clamped. Therefore a more appropriate surface must be chosen. Section 4.6 will deal with this approach.

At the end of this analysis, it is possible to draw some conclusions on this system. From a pure control theory point of view, the SMC in response to a non-zero initial condition is achieved, although it is not readily possible to calculate the minimum required pressure in order to promote it as happens in a linear case. In nonlinear systems (except for special classes) the minimum value of the gain which promotes a sliding regime can be found only via trial and error (Handroos and Liu (1998)). However the behaviour of the system with SMC is not really satisfactory. The free response in the actual reality of

a car on a road can only represent fairly approximately a bump (the forced response to a periodical input is more representative of a road disturbance). The first order displacement trend obtained is desired after a bump: a typical specification for a suspension is a trend with a small number of oscillations after a bump (Crolla (1995)) and this is obtainable, in a conventional suspension, only with a high damping ratio. The first order decay of the SMC, in fact, "resembles" an overdamped second order transient (in the sense that the response has no oscillation).

On the other side, the trend of acceleration is not satisfactory, both because of the chatter (which is something inherent to SMC) and also because of the sudden jump B-B' (figure 4.16).

As far as the forced response is concerned it was verified that SMC cannot be achieved without producing a clamping of the plant and the response in pre-sliding conditions is not satisfactory: the curve is less smooth than the corresponding one in the passive case because of the presence of spikes caused by the commutation of the control force. Figure 4.20 (spring and control forces) helps shed light on acceleration behaviour. By analysing it, it is evident that the control force has a square wave-like trend with the above-mentioned three-state characteristic: its effect is superimposed to the spring force. The sharp commutations of the control force cause the spikes in the trend of acceleration.

4.5 SMC SIMULATION WITH 2 DOF

This initial analysis of the behaviour of a 1 DOF system has clarified the peculiarity of SMC when controlling a friction damper employed for vibration control. The behaviour of a 2 DOF system is now presented. By using a 2 DOF model (see figure 3.1) it is possible to take into account the mass and the elasticity of the wheel (the unsprung mass).

At the outset it is necessary to specify a characteristic of the control. Only two states have been fed back also in the case of a 2 DOF model (theoretically four states would be required in a fourth order system): the relative displacement and velocity between the sprung and the unsprung mass. In practice this is not a serious limitation; in a car, it is

only possible to install a damper between sprung and unsprung mass. Such a solution works adequately, providing damping to both masses, as the distance between the resonance frequencies of sprung and unsprung masses is about a decade: the bounce resonance frequency for the chassis is typically in the range 1-2 Hz, while the one of the wheel is usually included between 10 and 20 Hz. Chassis movements are too slow to affect tyre motion and conversely tyre movements are too fast to affect chassis motion.

The system is excited with a non-zero initial condition for the displacement of the sprung mass. Figure 4.21 depicts the trajectory of the passive system; it can be divided into two parts: the first part of the trajectory (A-B) is governed by the high-frequency pole of the wheel-hop resonance (around 15 Hz); the state evolves making a "loop" in the phase plane. The second part is driven by the low-frequency pole of the chassis resonance (around 1 Hz); when the effect of the latter pole becomes dominant the trajectory starts to decay logarithmically.

Figure 4.22 displays the trajectory of the controlled system: the trajectory can be analysed by dividing it in various parts. Firstly note that the sliding surface is an imaginary straight line passing through B, C and D. The first part of the trajectory is included between A and B: at B the sliding surface is reached for the first time and there is the first attempt of the state to slide onto it, but as it happened in the 1 DOF system, the control action is not sufficient to promote sliding mode. It is worth noting that the loop in the trajectory present in the passive case between A and B is now degenerated into an angular point. From B to C the state evolves following linear dynamics: there is no frictional force superimposed to the system as it is evident from figure 4.27 which shows spring and control forces: the arc of trajectory B-C corresponds to the segment A B in figure 4.27. The reaching phase ends at C, when the sliding surface is reached for the second time and the sliding regime commences.

However now the sliding phase is less stable than the corresponding one in the 1 DOF system: the boundary layer is greater compared to the 1 DOF system, hence the chattering amplitude is greater and moreover between C and D the state abandons the sliding surface twice, making small "jumps".

This behaviour is due to the fact that a 2 DOF system is fourth order and it is controlled only by feeding back two states: relative position and velocity, while ideally it is

necessary to feed back all four states in order to implement SMC. The trend of the other quantities confirm this loss of robustness compared to the 1 DOF system.

The higher level of chattering is shown off in the time histories of body and wheel accelerations (figures 4.23 and 4.24). Body acceleration is tending to zero with an overdamped trend, while wheel acceleration is underdamped.

The trend of the suspension working space is reproduced in figure 4.25 and compared with the passive working space (figure 4.26). After point M the sliding phase starts; the lack of robustness due to the higher chattering present in the 2 DOF system affects the trend of the working space which is less smooth: the response is only approximately first order; the dynamics, occurring after sliding mode has been achieved, resembles in fact the one of a higher order system because of the presence of a ripple superimposed to the exponential tendency of the curve.

Figure 4.28 displays the trends of the dynamic tyre force. It is quite smooth even if it presents a large number of oscillations.

As far as the forced response of a 2 DOF system is concerned, analogous conclusions to the 1 DOF system can be drawn also for the 2 DOF case. The SMC with a sliding surface based on position and velocity feedback is not appropriate for controlling the forced motion of a 2 DOF system in the same way as happened for the 1 DOF system: if the control force is not large enough to achieve sliding mode there is no substantial improvement in the behaviour of the system; conversely if the sliding mode is promoted the mass is clamped.

4.6 SMC SIMULATION WITH 2 DOF AND OTHER CONTROL SURFACES

In order to prevent lockup which would result in the clamping of the chassis (since surface (4.31) is meant to cancel body acceleration), another control strategy had to be found in order to cope with bounded periodical disturbances such as those produced by the road profile. As illustrated before, this can be achieved by developing a force tracking control with the purpose of reducing the total force experienced by the chassis. Therefore a surface has been designed based on the tracking error between spring force

F_s (assumed as reference) and normal force F_n. The sliding surface is expressed by equation (4.38).

However with this surface there is no direct control on the sign of the friction force, which can track the spring force with the right sign only in some intervals within each period. Therefore surface (4.38) has been modified incorporating the tracking condition (4.42), resulting in the control law (4.44). The system has been excited with a 1-cm sinusoidal input. The resulting sliding motion now produces a more attentive tracking of the spring force from the normal force as depicted in figure 4.29 which represents the trajectory in the spring force-normal force plane. The control force is set to zero when it cannot physically track the spring force reference. Chattering however is fairly large and the inherent chattering of the control action results in a jerky acceleration time trend, as shown in figure 4.30.

4.7 CONCLUSIONS ON SMC

The simulation work on the feasibility of employing SMC showed that this switching logic is not appropriate to control a friction damper based suspension. The inherent limitation of the semi-active system makes the design of the controller harder and the consequent large chattering penalises ride comfort.

Therefore another technique has been sought, based on a switched proportional action rather than on a relay-type action.

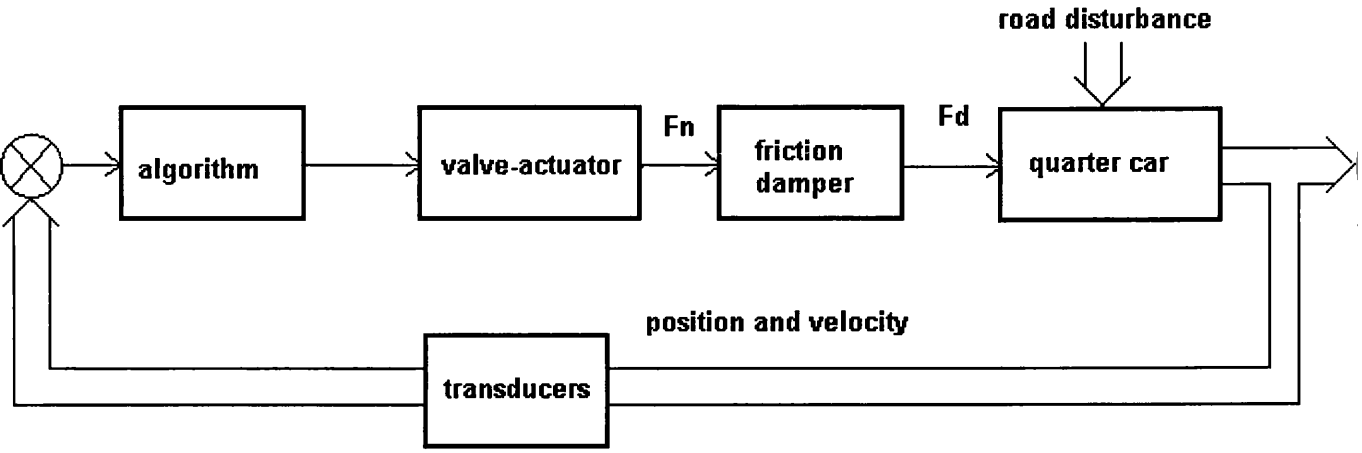

Figure 4.1 Block diagram of the friction damper based suspension unit.

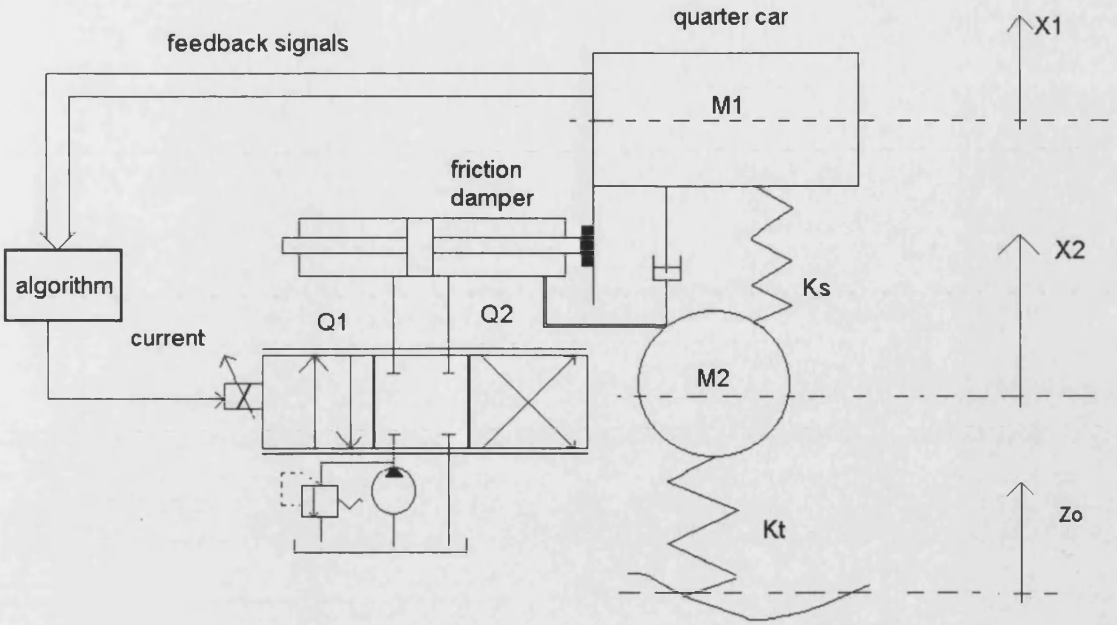

Figure 4.2 Schematic of the first hydraulic circuit design implemented in Bath*fp*.

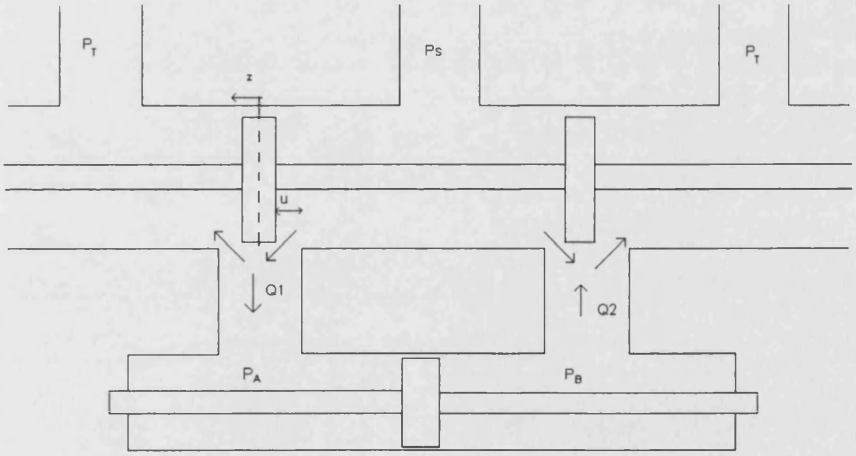

Figure 4.3 Schematic of the internal geometry of the valve.

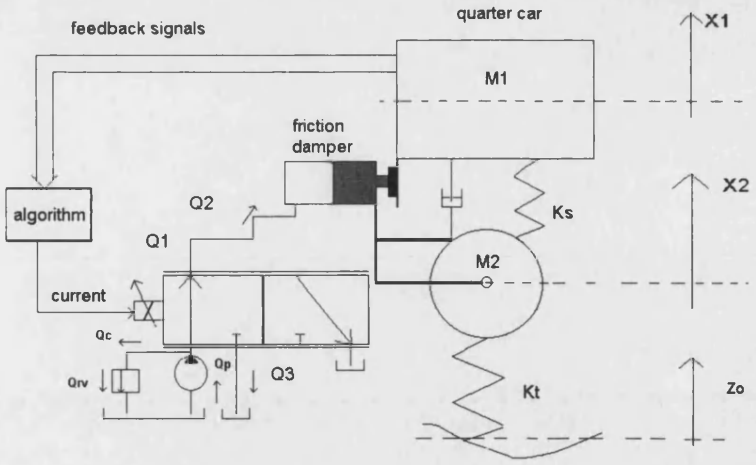

Figure 4.4 Schematic of the second hydraulic circuit design implemented in Simulink.

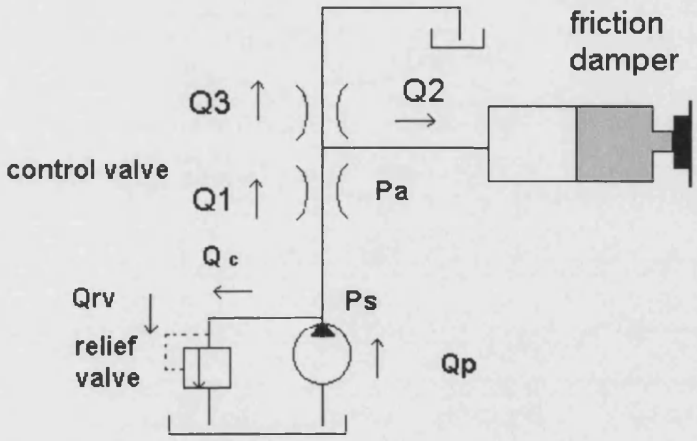

Figure 4.5 Equivalent hydraulic circuit.

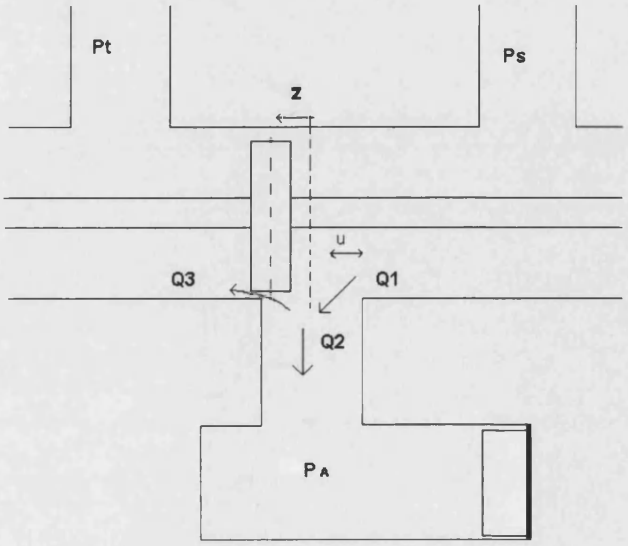

Figure 4.6 Schematic of the control valve.

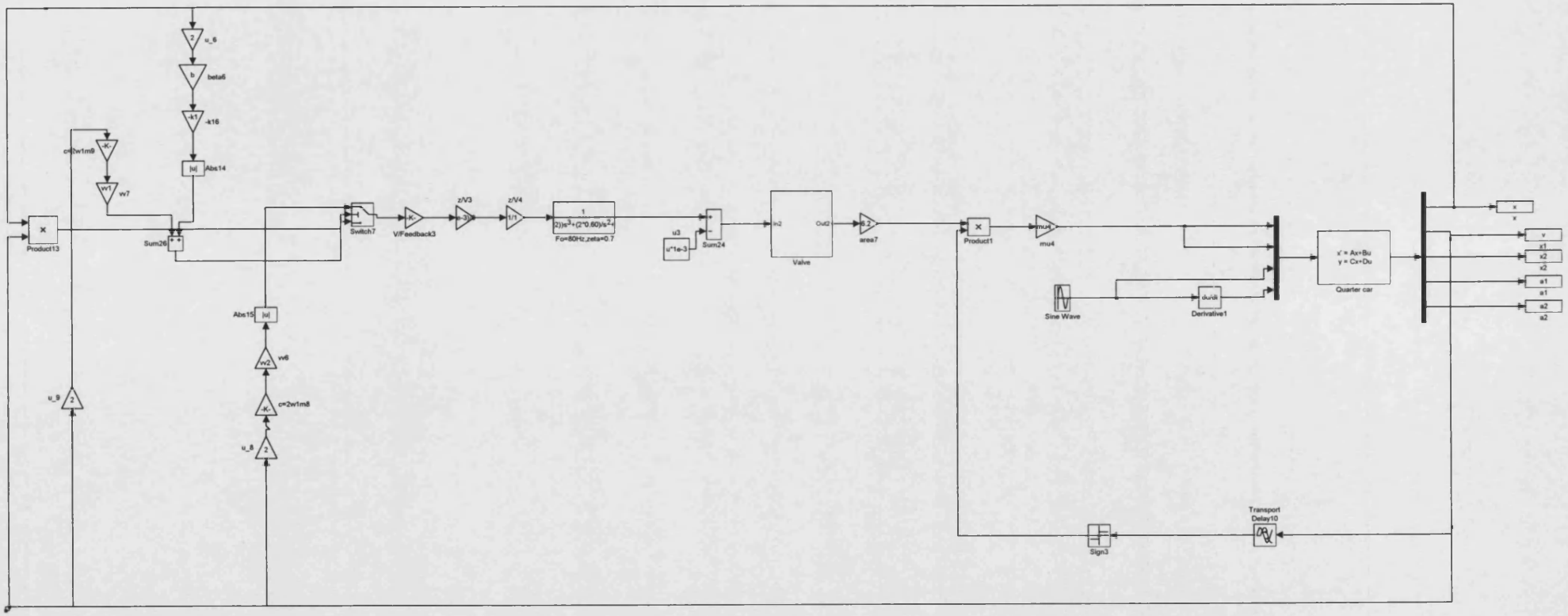
u_6
beta6
-k16
Abs14
c=2w1m9
vv7
Product13
Sum26
Switch7
V/Feedback3
z/V3
z/V4
Fo=80Hz,zeta=0.7
u3
Sum24
Valve
area7
Product1
mu4
Sine Wave
Derivative1
Quarter car
x' = Ax+Bu
y = Cx+Du
x
v
x1
x2
a1
a2
Abs15
vv6
c=2w1m8
u_8
u_9
Sign3
Transport
Delay10

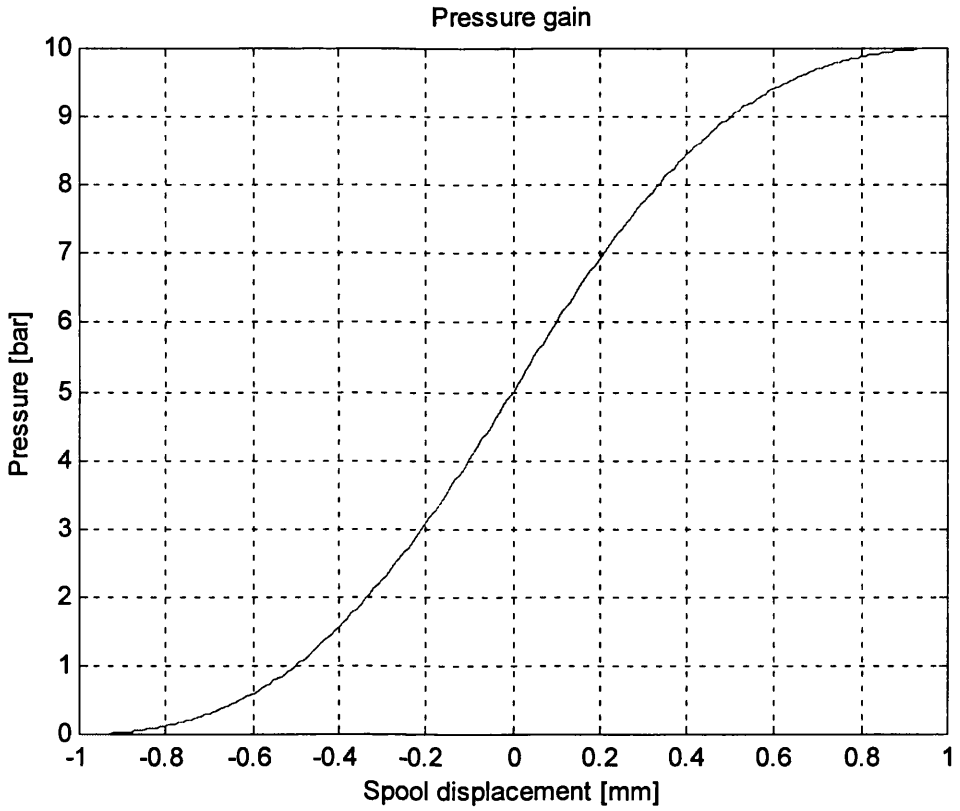

Figure 4.8 Trend of the pressure gain as defined by equation (4.30); supply pressure: 10 bar; valve underlap: 1 mm.

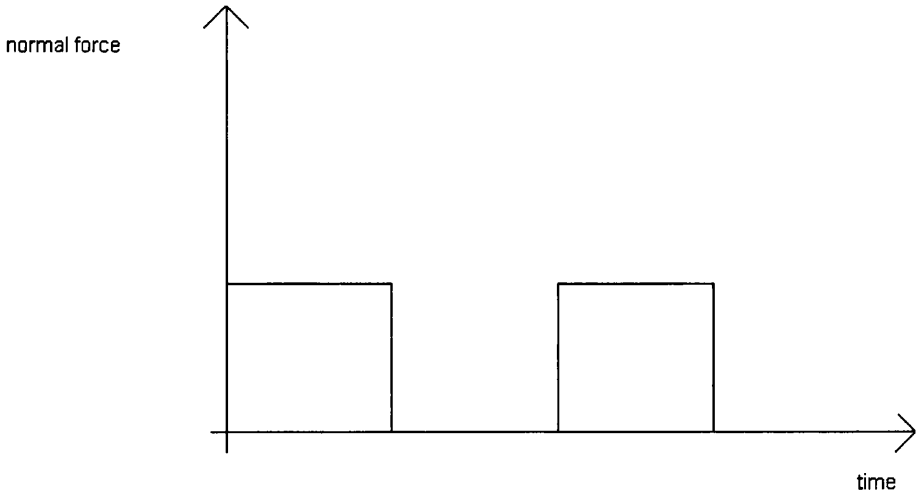

Figure 4.9 Qualitative trend of the normal force applied to the plate by the actuator.

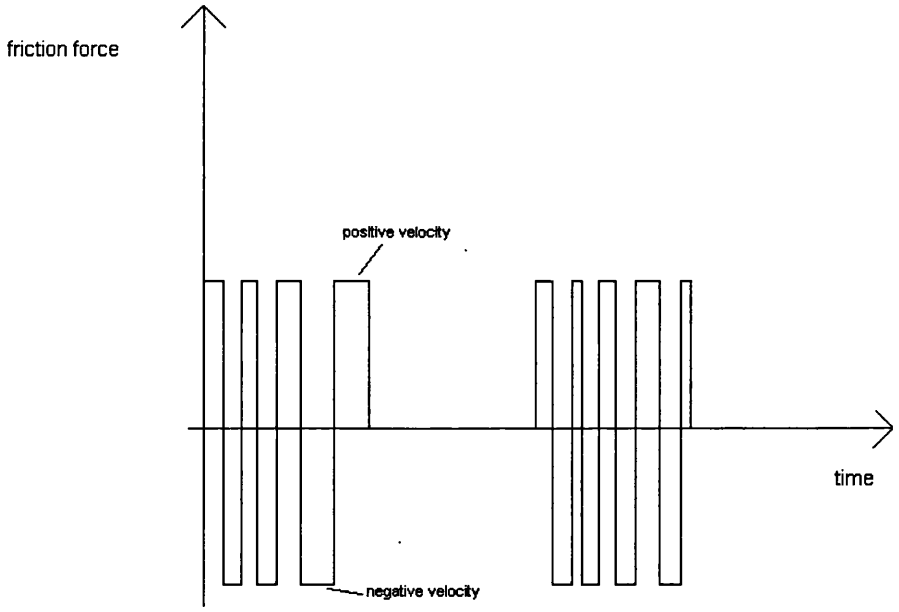

Figure 4.10 Qualitative trend of the frictional force applied to the car.

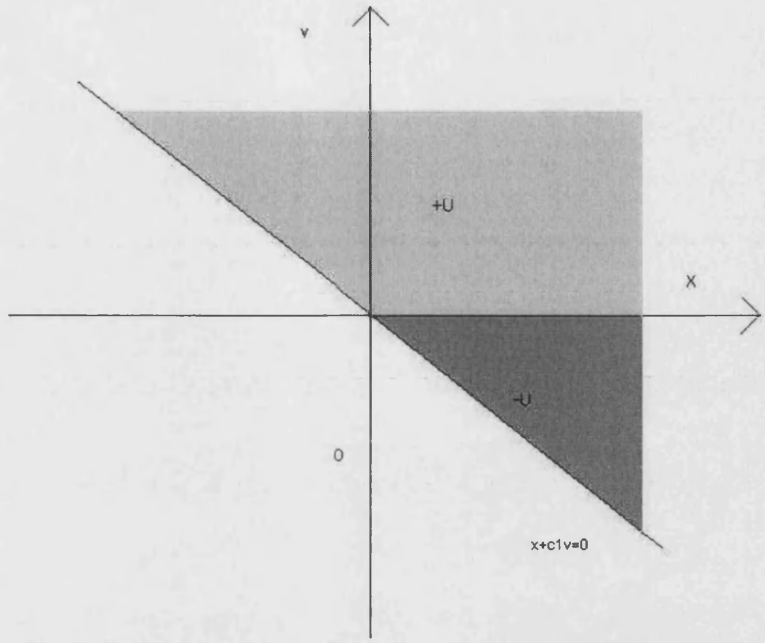

Figure 4.11 Phase plane portrait corresponding to the control action at the level of the plant using sliding mode controller (4.37).

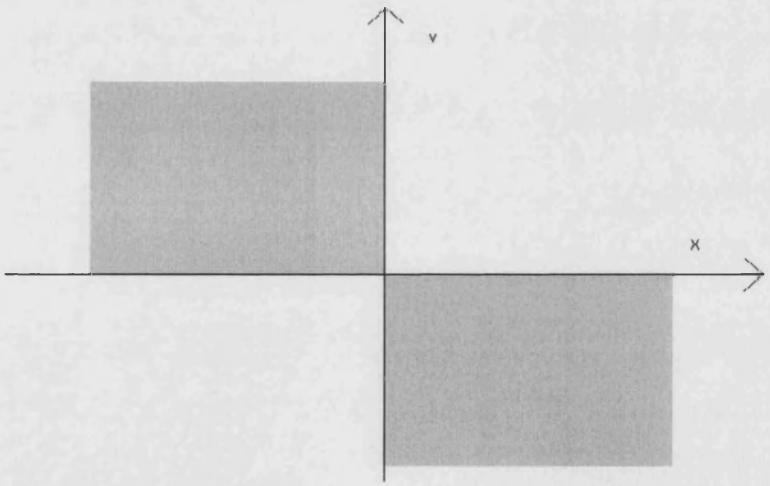

Figure 4.12 Phase plane portrait corresponding to the switching condition (4.42) which allows spring force cancellation.

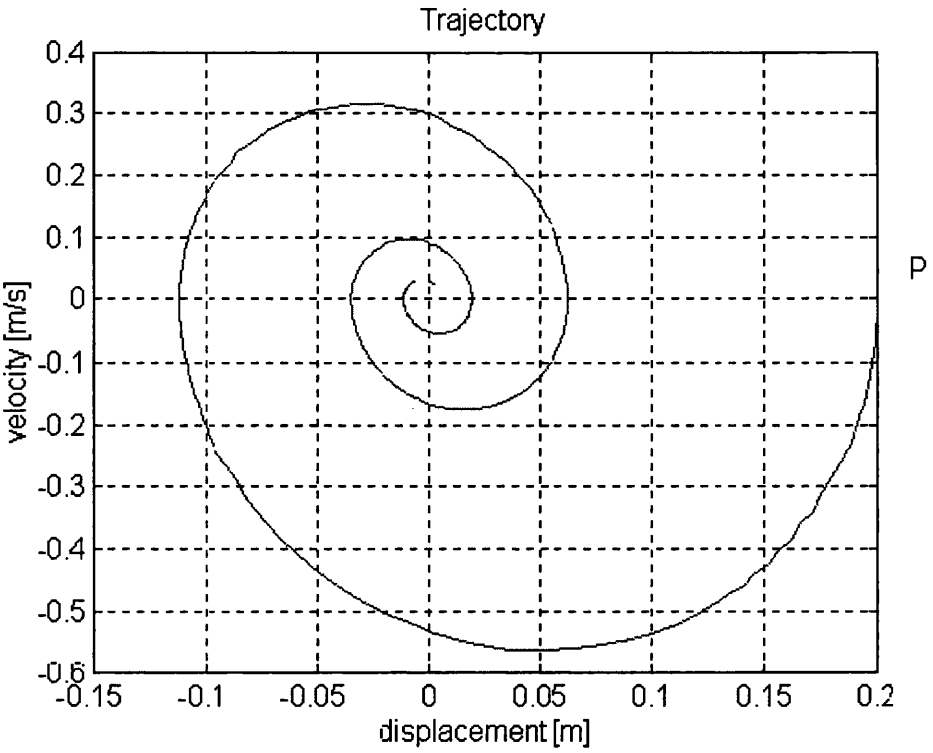

Figure 4.13 Trajectory of the free response of the uncontrolled 1 DOF system.

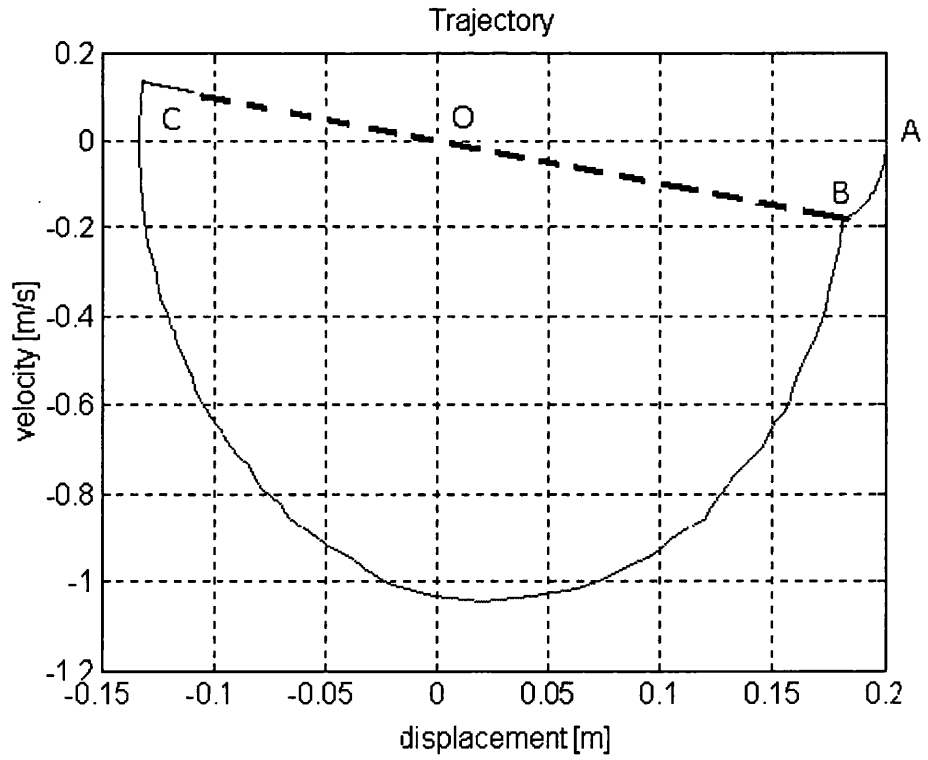

Figure 4.14 Trajectory of the free response of the controlled 1 DOF system.

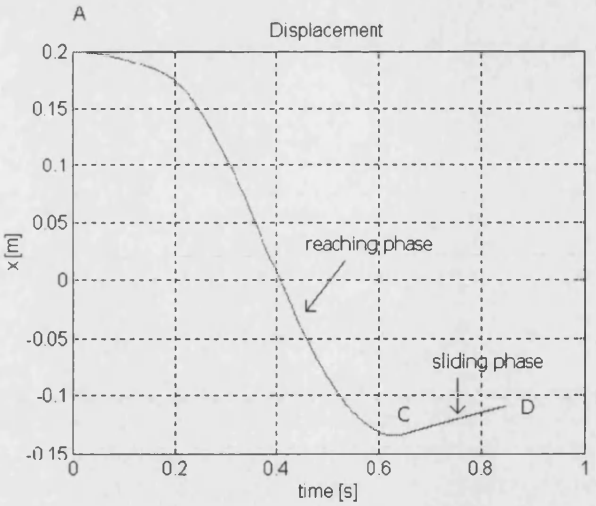

Figure 4.15 Trend of relative displacement for the controlled 1 DOF system.

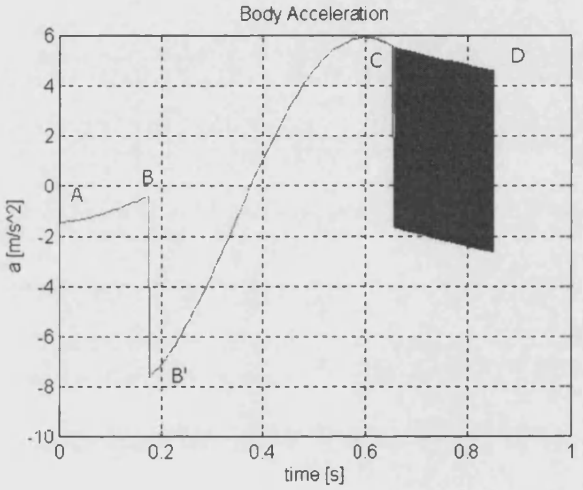

Figure 4.16 Trend of acceleration for the controlled 1 DOF system.

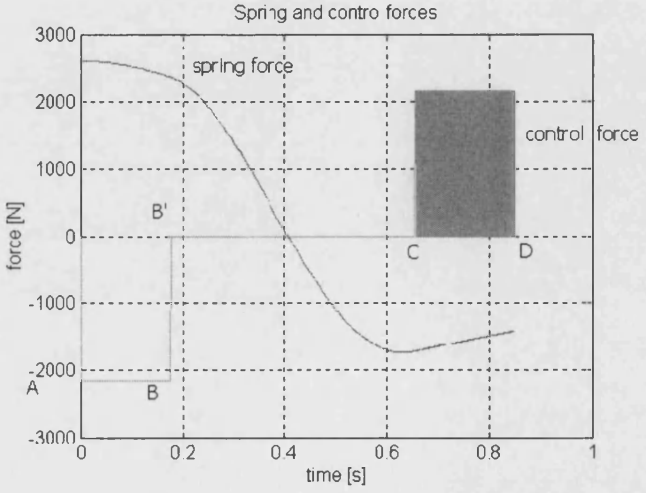

Figure 4.17 Trend of spring and control forces for the controlled 1 DOF system.

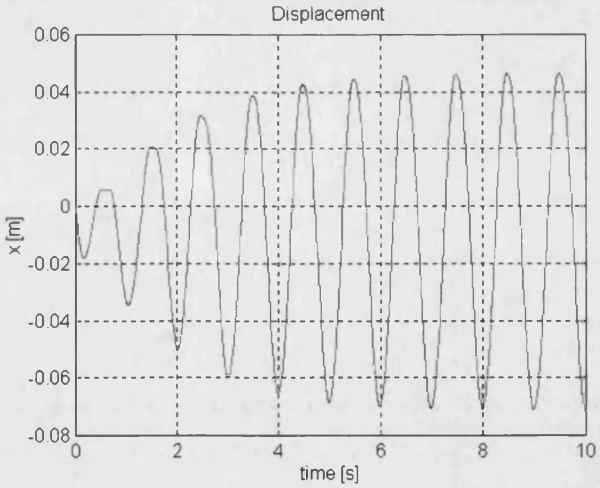

Figure 4.18 Trend of relative displacement in the controlled 1 DOF system with sinusoidal input.

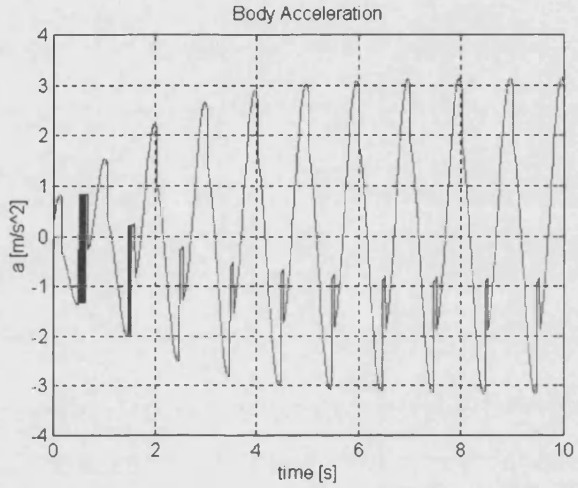

Figure 4.19 Trend of acceleration in the controlled 1 DOF system with sinusoidal input.

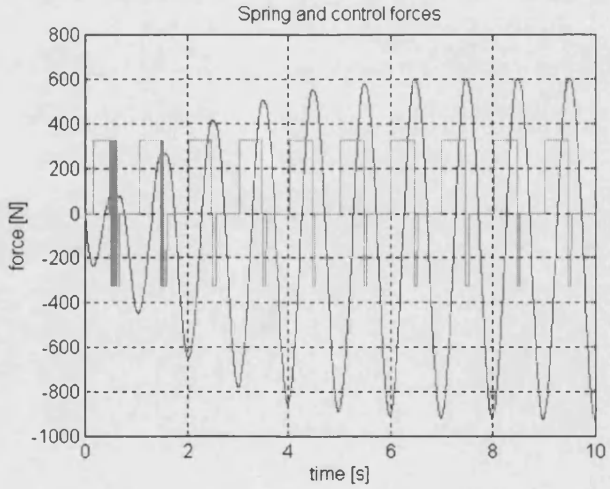

Figure 4.20 Trend of spring and control forces in the controlled 1 DOF system with sinusoidal input.

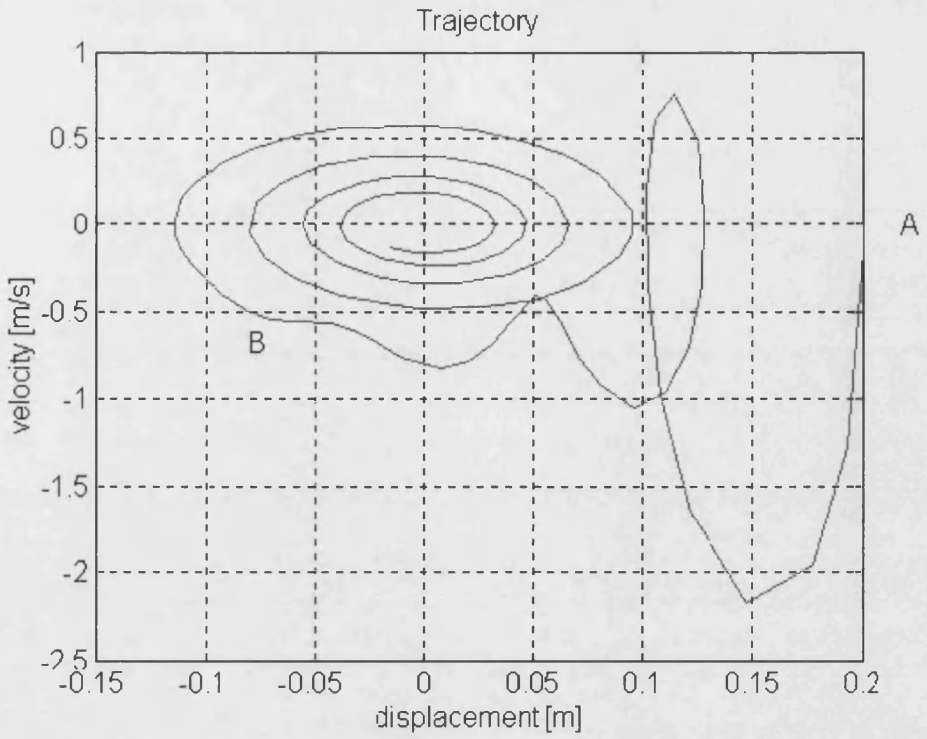

Figure 4.21 Trajectory of the free response of the uncontrolled 2 DOF system.

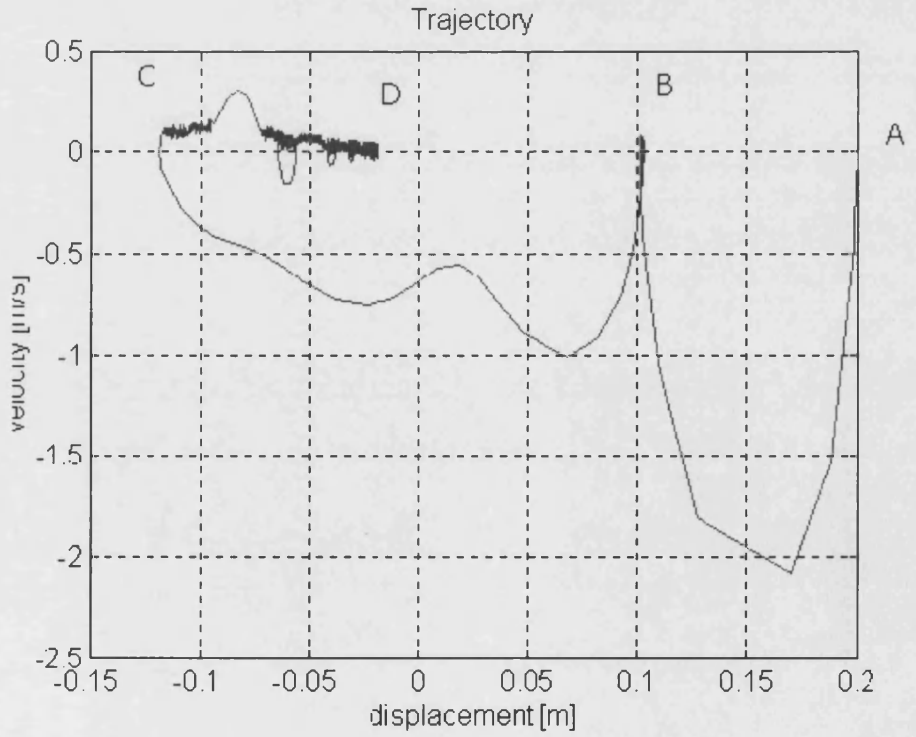

Figure 4.22 Trajectory of the free response of the controlled 2 DOF system.

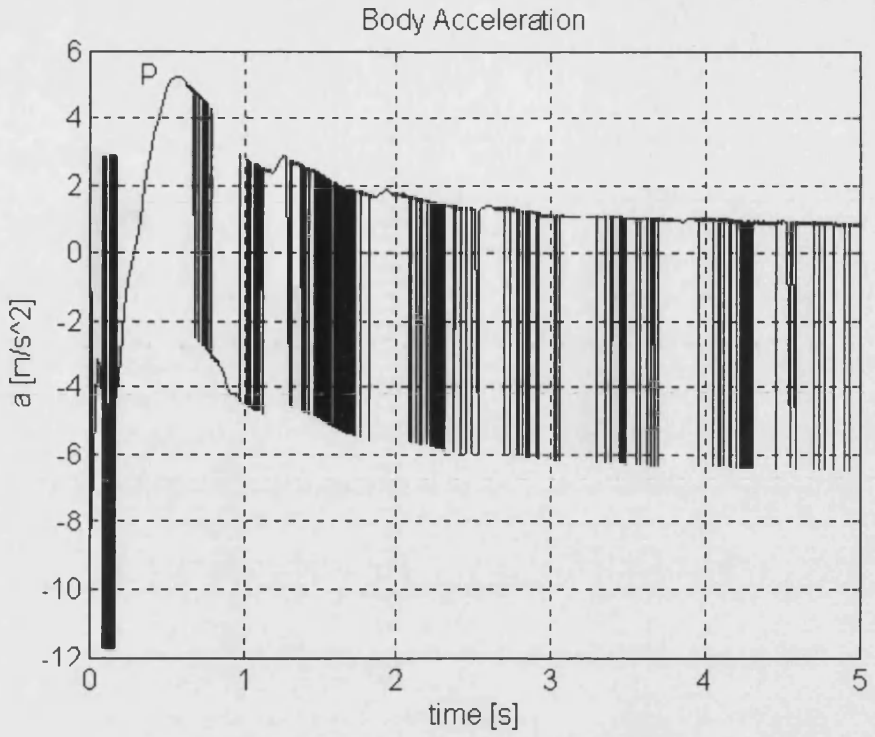

Figure 4.23 Trend of the free response of the body acceleration for the 2 DOF controlled system.

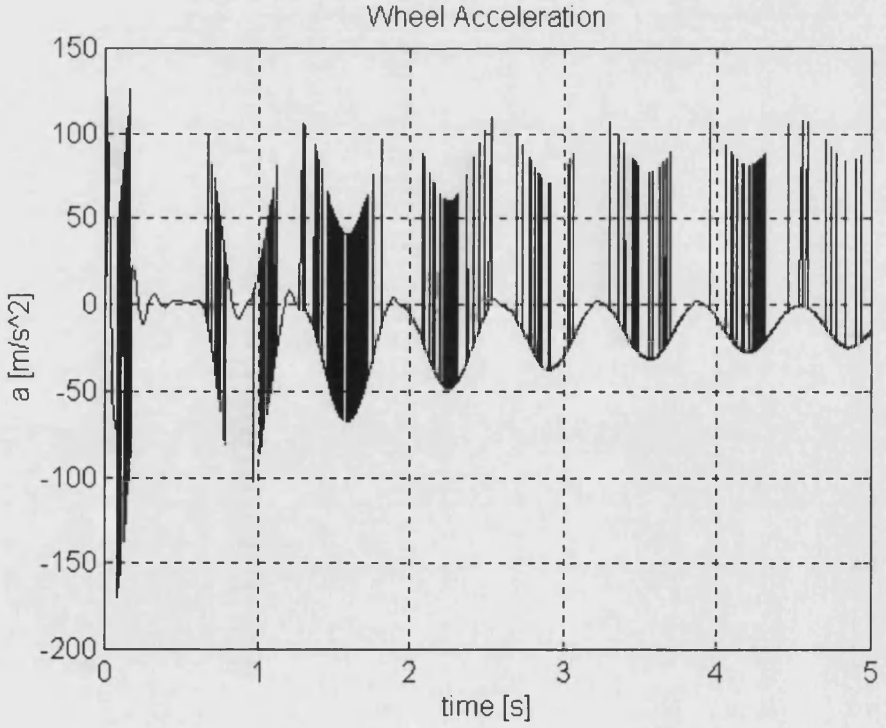

Figure 4.24 Trend of the free response of the wheel acceleration for the 2 DOF controlled system.

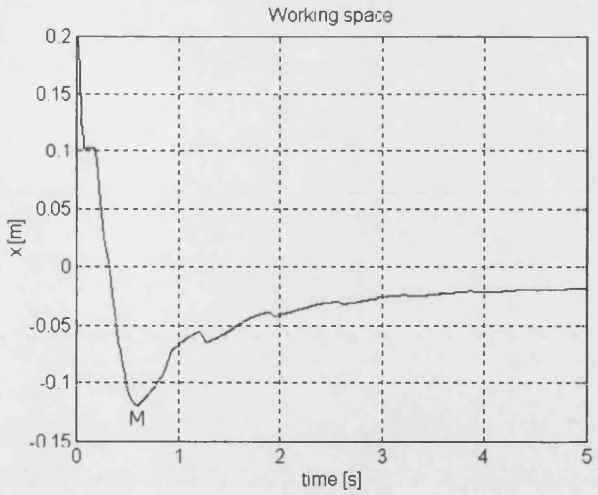

Figure 4.25 Trend of the free response of the suspension working space for the 2 DOF controlled system.

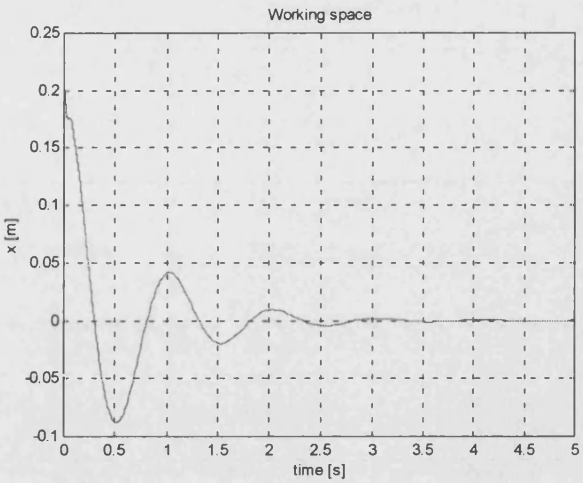

Figure 4.26 Trend of the free response of the suspension working space for the 2 DOF uncontrolled system.

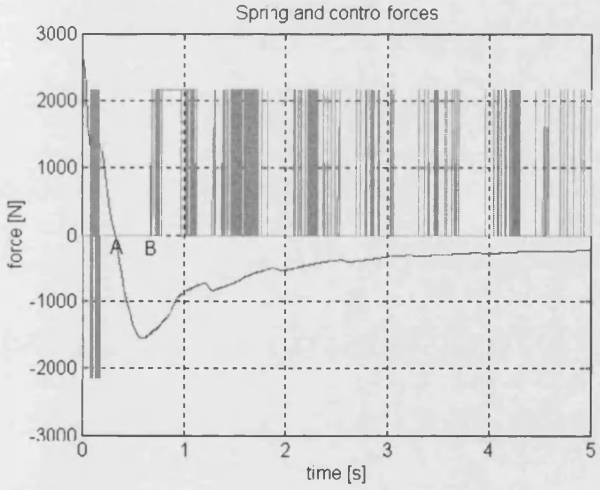

Figure 4.27 Trend of the free response of spring and control forces for the 2 DOF controlled system.

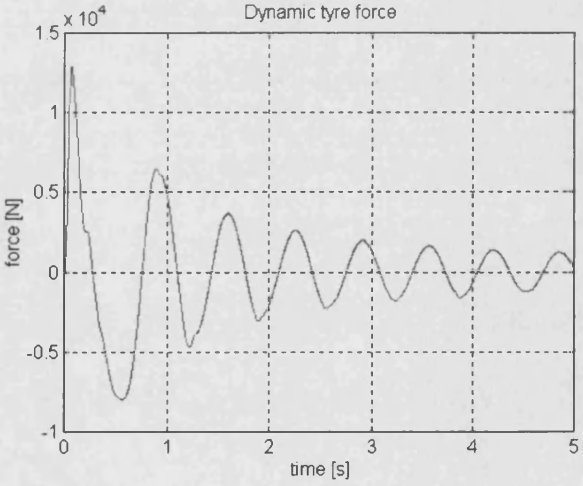

Figure 4.28 Trend of the free response of the dynamic tyre force for the 2 DOF controlled system.

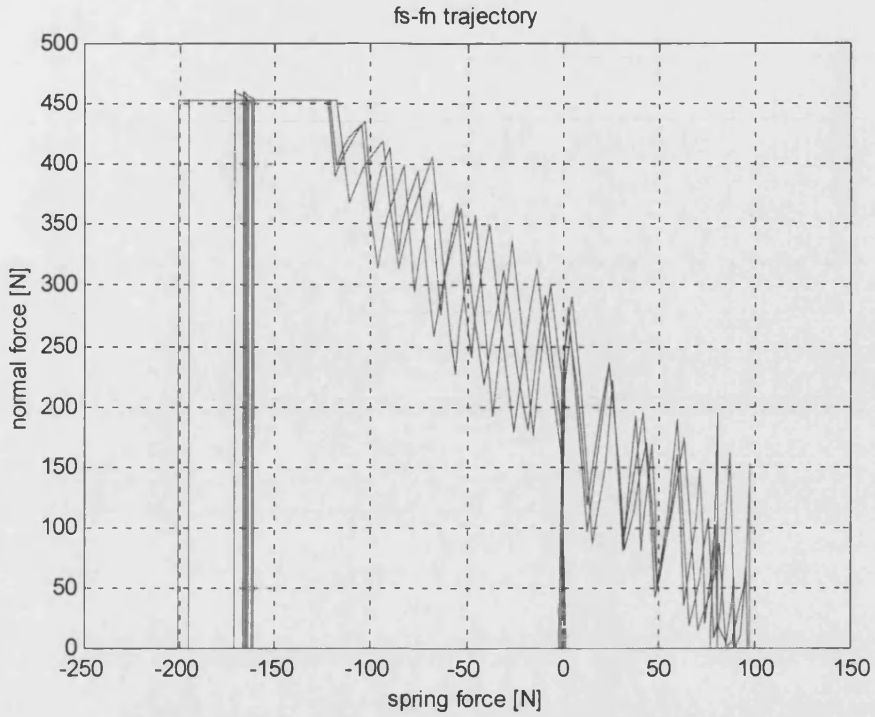

Figure 4.29 Normal force vs. spring force trajectory for the controller defined by equation (4.44).

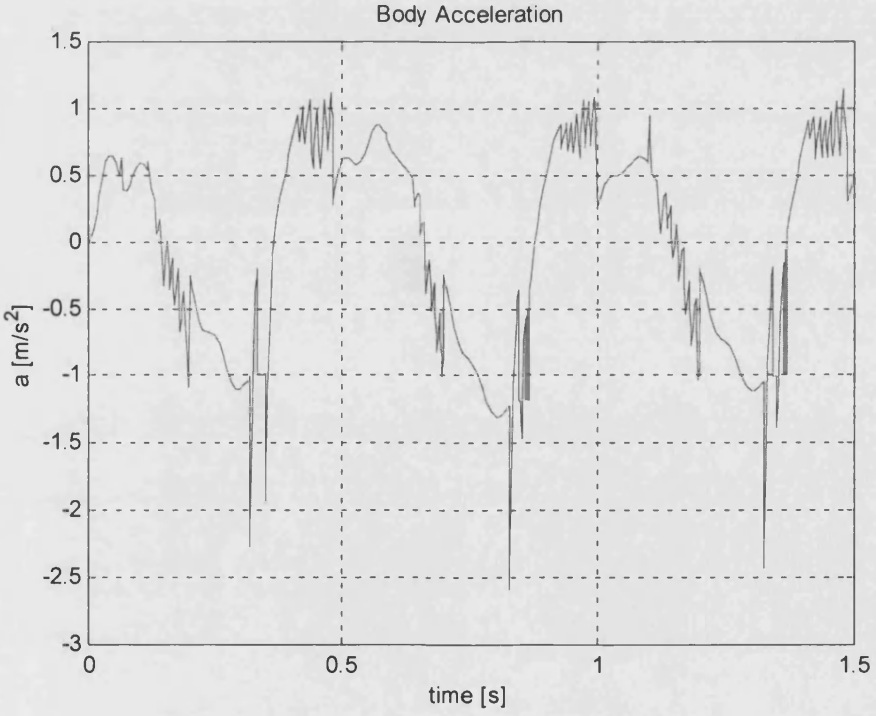

Figure 4.30 Chassis acceleration time trend for the controller defined by equation (4.44).

5. SWITCHED STATE FEEDBACK

5.1 SWITCHED STATE FEEDBACK CONTROLLER DESIGN

From the viewpoint of minimising chattering, a strategy based on a switching proportional controller could be of interest. Hence efforts were directed towards designing a proportional-type VSC, rather than a switching-type VSC.

It has previously been shown that because of the inherent physical limitation of the semi-active friction device, which can only oppose to the motion and not assist it, it is not possible to apply the control force continuously in order to obtain spring force cancellation, but only when condition (4.42) is fulfilled, otherwise the control force would have the same direction of the spring force.

The second step in the controller design, after the definition of the allowed regions of the phase plane via equation (4.42), is the definition the analytical expression of the control logic in these two regions. A physical consideration can aid this step: since it is necessary to track the spring force, the control action must be proportional to the elastic force. A solution is (Stammers and Sireteanu (1997)):

$$F_n = b\, k_s |x| \quad \text{if} \quad x\dot{x} \leq 0 \tag{5.1a}$$

$$F_n = 0 \quad \text{if} \quad x\dot{x} > 0 \tag{5.1b}$$

This is also called "*balance logic*" since it actually balances the spring force by attempting to produce an opposite control force which cancels it. Appendix B gives a proof of the stability of the controller and generalises it to a wider class of controllers. The coefficient b can be thought of as a gain defining the level of cancellation of the spring force, proportional to the reciprocal of the friction coefficient. Assuming that the friction coefficient is perfectly known (working on the assumption of pure Coulomb friction), then $b = \frac{1}{\mu}$. However there will be always a mismatch between the assumed

friction coefficient and the actual one. Hence it is more correct to say $b=\frac{1}{\mu_{assumed}}$ and the actual amount of spring cancellation is dictated by the ratio $\frac{\mu}{\mu_{assumed}}$.

Equation (5.1) can be written as:

$$F_n=\frac{bk_s}{2}|x|-\frac{bk_s}{2}|x|sgn(x\dot{x}) \tag{5.2}$$

Friction force is expressed by:

$$F_d=-\mu\frac{bk_s}{2}|x|sgn(\dot{x})+\mu\frac{bk_s}{2}|x|sgn(x\dot{x})sgn(\dot{x}) \tag{5.3}$$

A controller can be obtained composed of two terms: a state feedback controller and a switching term. The product $(x\dot{x})$ can be interpreted as a particular nonlinear sliding surface. With this strategy the valve mainly works in the linear zone of its characteristic, while in the previous scheme the saturation limits were exploited. The acceleration is less affected by chattering in this case, thus reducing the jerk. The jerk content due to valve commutations can be smoothed by the electrohydraulic and friction force dynamics.

Hence the overall logic can be regarded as nonlinear switched state feedback; it is actually a partial state feedback because only one state is used in the control action; the other state, the velocity, only dictates the switching condition. It is worth noting that this logic does not require a pressure feedback (and nor an acceleration feedback).

It is possible to design such a scheme taking into account also the friction force in the control loop, possibly increasing the robustness to friction coefficient variations. Considering that spring and friction forces depend upon displacement and velocity (with opposite sign), a switching condition based on the product of spring and friction force can be defined, yielding a control force defined by:

$$F_n=\frac{bk_s}{2}|x|-\frac{bk_s}{2}|x|sgn(F_sF_d) \tag{5.4}$$

where

$$F_s\ F_d = -k_s x(M_1 \ddot{x}_1 + 2\xi\omega_1 M_1 \dot{x} + k_s x) \tag{5.5}$$

In this case also acceleration feedback is required in order to infer friction force.

The actual friction force is:

$$F_d = -\mu \frac{bk_s}{2} |x| sgn(\dot{x}) + \mu \frac{bk_s}{2} |x| sgn[(-k_s x)(M_1 \ddot{x}_1 + 2\xi\omega_1 M_1 \dot{x} + k_s x)] sgn(\dot{x}) \tag{5.6}$$

The controller (5.2) or the one in the almost equivalent form (5.4) does not introduce any velocity feedback (or better, velocity needs be measured for implementing the switching condition, but the control signal is only a function of displacement). However a small amount of velocity feedback could be advantageous to help smooth further the transition between the on- and the off-state. For this reason, a more general controller has been considered whose general form is:

$$F_n = bk_s |x| + 2z_1\omega_1 M_1 |\dot{x}| \qquad \text{if} \quad x\dot{x} \le 0 \tag{5.7a}$$

$$F_n = 2z_2\omega_1 M_1 |\dot{x}| \qquad \text{if} \quad x\dot{x} > 0 \tag{5.7b}$$

with $b,\ z_1,\ z_2 \ge 0$.

In more compact form:

$$F_n = (bk_s |x| + 2z_1\omega_1 M_1 |\dot{x}|) \frac{1 - sgn(x\dot{x})}{2} + 2z_2\omega_1 M_1 |\dot{x}| \frac{1 + sgn(x\dot{x})}{2} \tag{5.8}$$

In the second and fourth quadrants of the phase plane it combines position damping (which results in a spring force reduction effect) blended with some pseudo-viscous damping; additional viscous damping is added in the first and third quadrants (there is no position damping in these quadrants because it would be in phase with the spring force). The latter not only introduces a viscous-like effect, but it also contributes to smooth the sudden transitions between the two structures defined by (5.1a) and (5.1b). By tuning the coefficients $b,\ z_1,\ z_2$, it is possible to emphasise the displacement or the viscous damping effect.

Control theory gives some tools to tune b, z_1, z_2. For example using the theory of optimal control the set $\{b, z_1, z_2\}$ could be chosen to minimise a performance index such as:

$$J(b, z_1, z_2) = \int_0^T \{[\alpha(x_2 - z_0)]^2 + [\beta(x_1 - x_2)]^4 + (\gamma\ddot{x}_1)^2\}dt \tag{5.9}$$

Such an index trades-off between the reduction of chassis acceleration and dynamic tyre force within the constraint of a set working space, for this reason emphasised by a power weighting (forth power in this example).

Formally speaking this is not an optimal control problem in strict sense, because the "optimal" function is assumed to be defined by (5.1). Therefore it is not necessary here to pass through a Hamiltonian system and a Riccati equation (particularly tricky to obtain since the functional is piecewise linear). It is only necessary to find the optimal value of its gains, by computing numerically the integral (5.8) and finding the minimum of the function $J=J(b, z_1, z_2)$ with the most suitable optimisation method (for instance a gradient method).

The main problem of this optimisation method is that the optimal set depends heavily on the type of disturbance (and also on the type of performance index), so in last instance on the type of road. Hence it would be necessary to adopt a further adaptive loop which chooses in real-time the most appropriate set of values (previously calculated for various road conditions and stored in a look-up table in the microcontroller memory) by the knowledge of the type of disturbance, inferred via some type of observer. This is complex and of questionable benefit. Hence a much simpler approach has been chosen based on using some reasonable physical values for b, z_1, z_2.

5.2 THE ISSUE OF POWER CONSUMPTION

One of the major benefits of a friction damper based suspension is the low power required compared to an active suspension employing controlled actuators. The hydraulic circuit described controls only pressure. Flow is negligible in the force control

schemes described, therefore the power required is smaller than that in a more conventional flow system.

It is possible to roughly estimate the power consumption. The pump is driven by an asynchronous motor with an electrical efficiency η_{el} of about 0.90. Said W_{el} the electrical power produced by the motor, the mechanical power W required is given by:

$$W=\eta_{el}W_{el} \tag{5.10}$$

where

$$W=\frac{P_S Q_P}{\eta} \tag{5.11}$$

P_S is the supply pressure, Q_p is the pump flow and η its overall efficiency, product of the volumetric and mechanical efficiencies. Assuming a pump volumetric efficiency of 0.90 and a mechanical efficiency of 0.95, with an operating pressure of 15 bar the power required is about 150 W per damper. The power dissipated is an increasing function of the underlap (see equation (4.30)).

5.3 SIMULATION OF THE SWITCHED STATE FEEDBACK CONTROLLER

This section is concerned with the analysis of the performance of the VSC, with a control based on state feedback. The performance of this family of controllers is analysed both in the frequency and time domains. The general expression of the controller (in terms of normal force) is given by equation (5.7).

Subsequent figures show transmissibility curves for body acceleration, working space and dynamic tyre force. These curves give an evaluation of the performance of the controller in terms of RMS signals. They are plotted in the frequency range 1 to 5 Hz, the main range of interest in a car suspension, for the purpose of controlling chassis resonance.

Figures 5.1, 5.2 and 5.3 have been plotted with Simulink for variations in the friction coefficient μ of ±20% around its nominal value (0.4). The scope of this sensitivity analysis is to assess how an uncertainty in the knowledge of the friction coefficient affects the results. Figure 5.1 shows that semi-active RMS acceleration is generally smaller than the passive. It is worth drawing an analogy in the behaviour of the semi-active response, when the friction coefficient varies, with the response of a linear system varying the viscous damping ratio: close to the resonance a high damped system (μ=0.5) performs better; conversely above the resonance frequency a low damped system (μ=0.3) behaves better and, analogously to a linear system, there exists a frequency where the three trends tend to cross one another and the behaviour is almost the same independently of the value of the friction coefficient.

The RMS semi-active working space (figure 5.2) is smaller than the corresponding passive one in the vicinity of the resonance; after the resonance, the controlled response tends asymptotically to the passive response. The reduction in RMS working space is somewhat related to the value of the friction coefficient.

The controlled RMS dynamic tyre force (figure 5.3) is reduced with respect to the passive case only in the neighbourhood of the resonance, but at higher frequencies the semi-active system, depending upon the value of the friction coefficient, can be better or worse than the passive.

Figures 5.4, 5.5 and 5.6 compare the performance of various types of controllers in terms of RMS frequency response. The benchmark controllers used in the following assessment are a pure position feedback controller (b=2.5, z_1=0, z_2=0) and other controllers where a certain amount of velocity feedback (equivalent to a damping ratio of 0.2) has been added (either in the second and fourth quadrants or in the first and third quadrants or in both). From consideration of figure 5.4 it is clear that the controller with b=2.5, z_1=0, z_2=0.2 achieves the best results in terms of acceleration reduction, particularly close to the resonance; however its performance is not as outstanding in terms of working space and tyre force (see figures 5.5 and 5.6). At the other extreme the controller with b=2.5, z_1=0.2, z_2=0 produces the least acceleration reduction among the four types of controllers investigated, but it better performs with respect to working space and tyre force. The other two controllers, the pure position feedback controller (b=2.5, z_1=0, z_2=0) and that with b=2.5, z_1=0.2, z_2=0.2 provide a reasonable trade-off

among the requirements of minimising acceleration and reducing working space and dynamic tyre force.

Figures 5.7 to 5.10 depict the time trends for spring and normal forces, in order to qualitatively assess how abrupt is the transition between the two structures for the four benchmark inputs above. Sharp transitions in the normal force are a first indirect and qualitative measure of the ride quality achievable with the different controllers. Abrupt transitions may result in spiky acceleration and jerk time histories.

The control force F_n in figure 5.7 results from the pure spring force cancellation controller (b=2.5, z_1=0, z_2=0); when the control is set to the off-state the transition is smoothed only by the hydraulic and frictional dynamics. Some viscous damping is helpful as figure 5.8 shows (case with b=2.5, z_1=0, z_2=0.2). The additional viscous action in the first and third quadrants smoothes the control force trend although it cannot compensate the sudden rise time when the controller is set to the on-state.

The controller with b=2.5, z_1=0.2, z_2=0 (figure 5.9) is probably the worst from a ride quality point of view. The additional viscous damping in the second and fourth quadrants sharpens both the on and off transitions. The controller of figure 5.10 (b=2.5, z_1=0.2, z_2=0.2) is fairly good instead, for the control force is never set to zero, the trend is relatively smooth.

A pseudo-random input is now considered. The road model is expressed by the following relationship (Horrocks et al (1997)):

$$z_0(t)=\sqrt{2}\sum_{i=1}^{45}\sqrt{\frac{\pi\Delta f V^{1.5}}{(\Delta f i)^{2.5}}}\,10^{-3}\sin[(2\pi\Delta f\, i)t+p(i)] \qquad (5.12)$$

the velocity V being in m/s.

This is a multiharmonic input where the amplitude is a decreasing function of the frequency (figures 5.11 and 5.12); the increment Δf is 0.25 Hz and the phase $p(i)$ is a random number between $-\pi$ and π. The signal is still periodic since the ratio of the frequencies of any pair of harmonics is a rational number; if this was not the case the resulting summation of periodic functions would have produced a nonperiodic function, (pseudo-random signal). However its spectrum constitutes a discrete approximation of

the continuous spectral density (equation 3.16). Lower harmonics are the most important; higher harmonics, although present, are mainly filtered by the tyre. Using this type of input in place of a filtered white noise permits the circumvention of the problems associated with the interpretation of the results in response to a stochastic input and at the same time it provides a fairly realistic input.

It must be stressed that, with the controlled system being nonlinear, the property of the response to this input cannot be inferred in any way by the properties of the response to sinusoidal inputs separately, i.e. the RMS and peak value percentage reductions (or increases) with respect to the passive system will be different, because the superposition principle does not hold.

Figures 5.13 to 5.16 show the working space and acceleration time responses to this input for the passive and the controlled systems with b=2.5, z_1=0, z_2=0. Simulations with various speeds have been carried out. These results correspond to a vehicle forward constant speed of 50 km/h.

The responses of the different state feedback controllers to this input can be more appropriately compared in terms of RMS and peak values rather than from their time histories. Tables 5.1 and 5.2 list RMS and peak values for acceleration and working spaces for the different controllers.

Table 5.1: RMS and peak acceleration for a pseudo-random input

CONTROLLER	RMS acceleration [m/s^2]	Max and min PEAK acceleration [m/s^2]
Passive	1.59	4.79/-4.24
b=2.5, z_1=0, z_2=0	1.66	4.51/-3.53
b=2.5, z_1=0.2, z_2=0	1.71	4.80/-3.35
b=2.5, z_1=0, z_2=0.2	1.41	4.46/-3.59
b=2.5, z_1=0.2, z_2=0.2	1.45	4.65/-3.44

Table 5.2: RMS and peak working space for a pseudo-random input

CONTROLLER	RMS working space [cm]	Max and min PEAK working space [cm]
Input	1.88	4.40/-5.10
Passive	1.67	3.57/-4.37
b=2.5, z_1=0, z_2=0	1.66	3.54/-4.54
b=2.5, z_1=0.2, z_2=0	1.77	3.45/-4.83
b=2.5, z_1=0, z_2=0.2	1.47	3.24/-4.09
b=2.5, z_1=0.2, z_2=0.2	1.53	3.20/-4.24

The pseudo-random test is a much more severe test than the sinusoidal one. The performance of the controlled system is somewhat less outstanding compared to that in response to the sinusoidal input and in some cases even worse: RMS acceleration is only slightly better in two cases out of the four benchmark controllers considered. RMS working space response is instead always slightly smaller than the corresponding passive one, all but in one case.

Last but not least, the response to a bump must be considered. This input, which represents a discrete event in a road profile must be analysed apart. The relevant quantities to minimise for this input are the peak value acceleration and the number of oscillations after the bump. Figures 5.17 and 5.18 show the chassis acceleration response in the two cases. The input is a 5 cm-high sinusoidal-shaped bump. The bump horizontal length is 0.5 m and the car is assumed to pass over it at a constant speed of 20 km/h. This is equivalent to say that the car is excited with half a sinusoid having a frequency of 11.11 Hz (for the frequency is equal to the car forward velocity divided by the bump span).

The controlled system acceleration overshoot and undershoot are much smaller albeit the number of oscillations is almost the same in both cases and in the controlled system some spikes are present because of the switching logic.

The values of the overshoot and of the undershoot for the different controllers are listed in table 5.3.

Table 5.3: Peak acceleration value for a bump input

CONTROLLER	Max and min PEAK acceleration [m/s^2]
Passive	13.77/-17.39
b=2.5, z_1=0, z_2=0	8.39/-8.58
b=2.5, z_1=0.2, z_2=0	8.39/-8.38
b=2.5, z_1=0, z_2=0.2	6.83/-8.18
b=2.5, z_1=0.2, z_2=0.2	6.83/-8.19

The controllers with b=2.5, z_1=0, z_2=0.2 and with b=2.5, z_1=0.2, z_2=0.2 provide the largest reduction of the peak values among the four types of controllers.

However some remarks must be made on the validity of the results of this test. A bump can be viewed as a sort of impulsive input which produces a high acceleration peak. When a tyre undergoes high accelerations, it should be modelled taking properly into account its dynamic characteristics. A tyre model which includes only wheel mass and the tyre static characteristic is no longer adequate (Genta (1993)). Furthermore during a bump the point of contact between the wheel and the road is not aligned with the vertical axis passing through the centre wheel, hence horizontal contact forces are generated that cannot be taken into account by the quarter car model (nor by the 7 DOF model). Therefore the results from this simulation must be considered carefully and taken only as a indication of the actual behaviour of the car.

5.4 THE INITIAL EXPERIMENTAL WORK ON THE PILOT RIG

In this section the first part of the experimental work is presented: the experimentation on a pilot rig. A description of the rig is given and the main results discussed. The aim of this initial piece of work was purely concept proving. The scope was to have an experimental verification in a very simple system, hence under carefully controlled conditions, that controlled dry friction can produce an effective damping effect and it can be advantageously exploited to reduce vibrations.

The rig was designed few years before, in the context of a related research project and it was employed as the starting point for the experimentation. The core of the rig is a mass suspended from a beam by springs. The mass is mounted on a frame moved by a hydraulically driven shaker, position controlled and it is constrained to move only vertically because of the presence of vertical rails. This prevents undesired longitudinal motion; moreover it reduces friction to a low level. A schematic diagram of the rig is shown in figure 5.19.

Such a design of the rig resembles in scale the sprung mass of a quarter car. The control force is produced by a friction pad, which is transmitting a force to a plate rigidly connected to the mass. The friction pad is mounted on a linear actuator, at a right angle to the block, driven by a proportional pressure relief valve. The valve is placed in parallel with a pump, driven by a 1-phase asynchronous motor, which is supplying a nominally constant flow. The rig is depicted in figure 5.20. The mass is 33 kg and the springs have a total equivalent stiffness of 2400 N/m, so that the natural frequency is 1.35 Hz, which is also a typical value for a car. The equivalent damping ratio, measured experimentally, is around 0.2.

The pressure relief valve is electrohydraulic, model EHST-3 produced by Vickers; the rated bandwidth is 120 Hz. The actuator is supplied only from the piston-end side; with this kind of design, the friction pad is always in contact with the mass, preventing damaging collisions.

The relative displacement between mass and shaking table is measured with a LVDT, while the relative velocity is measured with a velocity transducer (Schaevitz VT-Z series inductive transducer). Displacement and velocity signals are acquired from the control PC, which outputs a signal to the valve.

The "balance logic" algorithm was tested. The purpose of balance logic is the reduction of body acceleration by a partial cancellation of the spring force by tracking it. The normal control force is:

$$F_n = bk_s|x| \quad \text{if} \quad x\dot{x} \leq 0 \tag{5.13a}$$

$$F_n = 0 \quad \text{if} \quad x\dot{x} > 0 \tag{5.13b}$$

The algorithm has been proved in a range of frequencies up to 3.2 Hz, with a sinusoidal excitation of the shaker. This small range is sufficient to show all the major dynamic phenomena (the system is 1 DOF).

The hydraulic drive is slightly different from that used in simulation studies described in section 5.3, although both of them achieve in principle the same result of controlling the pressure proportionally to a valve driving signal. In the experimental apparatus a proportional pressure relief valve is employed, while the simulation circuit uses a 3-way 3-position valve to drive the cylinder. However, the main purpose of this rig is only to prove the concept. An experimental frequency response is shown in figure 5.21 which plots the RMS of the ratio of mass acceleration and of the shaker's versus the fundamental harmonic of the excitation frequency for a fixed amplitude.

The algorithm is effective in the neighbourhood of the resonance frequency where there is a reduction of the transmitted forces of about 35% with respect to the passive case. Far from the resonance frequency the behaviour is the same as in case without control. This is a good result, compared with a passive case, in which to achieve such a big reduction in the vicinity of the resonance frequency would have had as drawback larger amplitudes at higher frequencies.

Since at higher frequencies there is no actual improvement in the response compared to the one without control, it could be useful to low-pass filter the measured signals, choosing the cut-off frequency sufficiently distant from the resonance so that the phase-lag introduced by the filter does not affect the algorithm. This filtering action would reduce the number of commutations of the control force because some high-frequency noise would be removed without spoiling the effectiveness of the algorithm.

In the experimentation, however, in order to avoid unwanted commutations, due to noise and small perturbations around zero value, a dead-band of 3% was introduced in the algorithm: if position and/or velocity are smaller than a user-defined threshold there is no output to the valve. Actually the dead-band is not strictly critical for the practical implementation of the algorithm: the "undesired" chattering, filtered by the valve dynamics, would have acted as a sort of dither.

Figure 5.22 displays position and velocity controlled transient responses. The effect of control is evident from the asymmetry of the positive and negative overshoots: firstly

the control is off because position and velocity have the same sign, subsequently it is turned on; the variation in the system structure is evident from the fact that the positive overshoot is different from the negative one. When the product of position and velocity becomes positive again, the control is turned off for the second time. Therefore the structure of the system changes three times during this transient. When the values of position and velocity become small enough to enter the dead zone, the control remains switched off and the structure does not change any longer. Obviously the transition between on and off is not instantaneous, but depends upon the pump-valve-actuator dynamics.

Figure 5.23 plots on the same axis both passive and semi-active acceleration at the frequency of 1.5 Hz. The acceleration has been obtained by numerical differentiation because only velocity (and position) is acquired by the PC. The passive response is not exactly sinusoidal because of the actual non-sinusoidal motion of the shaker, of the parasitic friction effects in the rig (e.g. the rolling friction in the vertical rails) and because of the noise amplification as a consequence of the numerical differentiation. The acceleration at that frequency in the semi-active case is much reduced even if it has a bigger harmonic content due to the presence of the control action. It is worth remarking that the switching control has not provoked an extremely harsh trend. This is positive from the point of view of comfort.

By varying the coefficient b in equation (5.11), which defines the rate of control force applied (as said before it can be thought as related to the reciprocal of friction coefficient μ), it is possible to control the rate of cancellation and consequently vary the acceleration experienced by the mass. In order to check this feature, measurements have been carried out changing this parameter. The results are shown in figure 5.24. If b is increased the acceleration ratio at that frequency decreases tending to an asymptotic value of 2.3.

A difficulty in carrying out measurements arose due to the stiction force, especially in presence of a high control force. Such a phenomenon produced an undesired lockup of the mass from time to time; such a behaviour occurs when the stiction force is higher than inertial forces. Care had to be taken in choosing values of the control force not to lie extremely close to the maximum theoretical value that produces full cancellation. An attempt to reduce this problem was made by increasing the mass, from the original 20

kg to 33 kg (and increasing the spring stiffness as well, so that the natural frequency remained virtually unchanged). The improvement was minimal. The best way of addressing the problem of stiction would have been, during the design stage, the selection of a low-stiction material.

5.5 DESIGN OF THE FRICTION DAMPER

After the initial experimentation on the pilot rig a vehicle friction damper has been designed, manufactured and installed on a car (the Ford Orion). In this section its mechanical design is presented. The basic idea is to create a relative sliding movement between a part fixed to the chassis and one fixed to the wheel; the major problem is that in a car the motion of the sprung mass with respect to the unsprung mass is not a pure vertical translation: the composite motion of the car prevents a good contact between the two conjugated surfaces (the pad and the plate). In order to overcome this problem, different design solutions have been proposed and assessed.

The first idea was to manufacture a device mounted externally to the car. This was purely for experimental convenience, rather than as practical solution for real applications. In this scheme the hydraulic actuator would be fixed on the top of the suspension strut and would act on a vertical beam fixed to the wheel through a rose joint; a further spherical joint was also required between the cylinder and the friction pad. The two joints together would be able to accomplish the car motion, preventing therefore loss of contact between the two sliding surfaces. This solution, although feasible in principle, was rejected because it would have required a large amount of material and machining and would have created a permanent damage to the chassis of the car, since it was necessary to cut parts out of it.

A less clumsy solution involves trying to directly manufacture the friction device inside the existing shock absorber. An excellent solution would have been to install the cylinder, the friction pad and the supply pipe inside the original cylinder of the viscous damper (figure 5.25), leaving the external geometry unmodified but its cross-section was too small to allow it. It was therefore decided to enlarge the damper cross-section, retaining the spring in its original position. Placing the friction damper into the spring coils would have eliminated the risk of contact between the car body and the modified

damper, as the overall external dimensions of the original suspension were not modified.

The main manufacturing difficulty was to retain the maximum dimensions of the original damper in order to avoid difficulty in fixing it again into the car: the upper and the lower points could not be modified and moreover the room available in the car was limited, consequently putting an upper-bound to the maximum enlarged cross-section.

Initially it was thought to employ a square section, both for ease of manufacture and in order to have a better contact between the two conjugated surfaces. Inside the new strut, a pipe supplying the fluid and two actuator chambers was obtained and a piece of friction material was placed inside each chamber. This material would be the actual actuator piston and it was physically in contact with the external wall of the new square part. The oil, trapped into the pipe-actuator arrangement, would act on the friction material and by modulating the pressure, the frictional force would be controlled. Figures 5.26 and 5.27 show a section and the top view of this first design.

The second alternative was to adopt a circular cross-section (see figure 5.28); the upper part of the viscous damper would have been substituted with a cylinder of larger section. Inside the cylinder the pipe supplying the oil would have been mounted. The pipe would have been connected with two small horizontal actuators. The friction pads inside the actuator would act against the enlarged cylindrical wall. This was the final choice. The novel damper is portrayed in figure 5.29.

The cylinder wall thickness was sized using thin cylinder method, leading to a thickness of about 3 mm.

The last step was the choice of the friction material. A material the least susceptible to wear was searched for; it was necessary to find something with similar properties to the ones used in car brake pads. A material with this property was chosen and was provided by European Friction Industries. It is designated E 342 and its nominal friction coefficient is 0.40.

5.6 TEST OF THE FRICTION DAMPER

The purpose of this test was to identify the static and dynamic friction characteristics of the friction damper designed for the vehicle suspension.

The overall damping characteristic of the damper is not solely dependent on the friction damping effect; some nonlinear viscous damping is also present, because of the rubber bushes.

The damper test rig is depicted in figure 5.29. It is constituted by a frame where the damper under test is fitted. The vertical excitation is provided by a position-controlled actuator. The constant pressure necessary to produce the normal force is provided by an external hand-pump. The total damping force is measured by a load cell (RDP Sensotec, model 75) and the vertical displacement by an LVDT. Velocity was obtained by numerical differentiation within the data acquisition package (see appendix C).

Friction force versus velocity static characteristic is depicted in figure 5.30. The hysteresis is due both to the parasitic viscous effect and the frictional memory effect (i.e. the dynamic effect following a change in the sign of velocity).

The time history for a 1.2-Hz sinusoidal input, depicted in figure 5.31, reveals that stiction is negligible, only slightly bigger in the rebound stroke: this asymmetry in the friction characteristic was found also in pneumatic actuators (which have similar geometry and dry friction coupling) in a work by Brun et al (1998). The low stiction is due to the brake material employed, manufactured using some low-stiction additives (Wills (1980)). In response to changes in the sign of velocity, friction force lags by 40 ms. This delay is frequency independent. Figure 5.32 magnifies the first cycle, showing better the delay between friction force and velocity.

It was not readily possible to test the friction force dynamic response to a change in the normal force. However as said in chapter 2 Dupont et al (1997) verified that these friction dynamics are fast. Therefore this dynamic behaviour is negligible for the purpose of the work. It was instead possible to measure the static dependence of friction coefficient μ with pressure. In the pressure range of interest to the control (up to 20-25 bar at most), the variation were not very large (figure 5.33).

Also an 8-hour endurance test was carried out using a sinusoidal input and 5-bar pressure. The repeatability was good and wear negligible. Increase in temperature was minimal because of the good heat transfer properties of the steel wall. Besides in a car the heat dissipation would be aided also by the air forced convection when the vehicle is moving.

Therefore the friction force in the damper has the required characteristics for the application: negligible stiction and some dynamics in the desired range (not so fast to be negligible, but neither too slow to compromise the overall performance of the system). The pure delay from a dynamic viewpoint behaves approximately as a first order lag (Padè approximations) which can contribute together with the hydraulic dynamics to smooth the sharp transitions of the VSC.

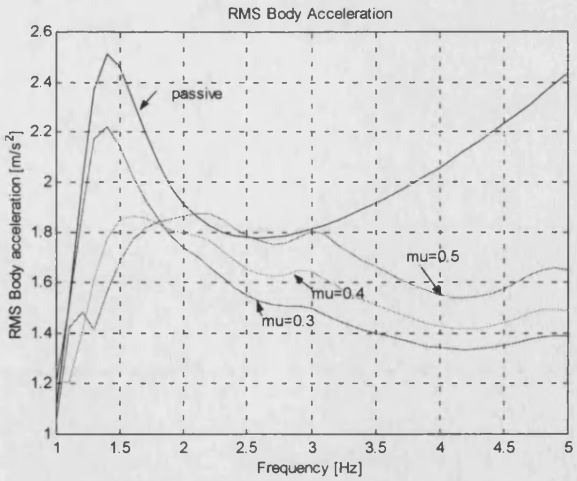

Figure 5.1 RMS chassis acceleration transmissibility curves varying friction coefficient (0.3, 0.4, 0.5). Controller with b=2.5, z_1=0, z_2=0.

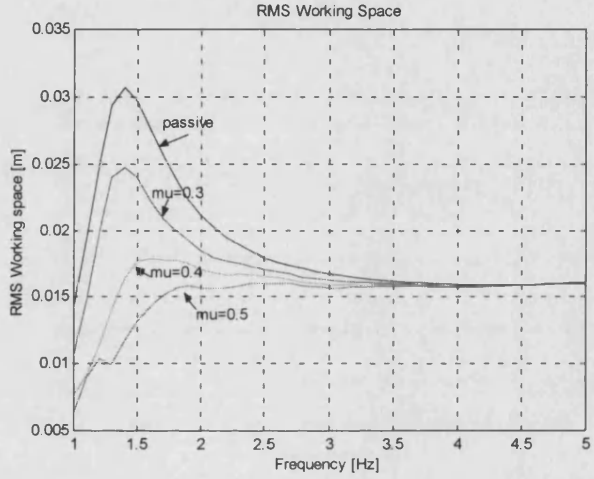

Figure 5.2 RMS working space transmissibility curves varying friction coefficient (0.3, 0.4, 0.5). Controller with b=2.5, z_1=0, z_2=0.

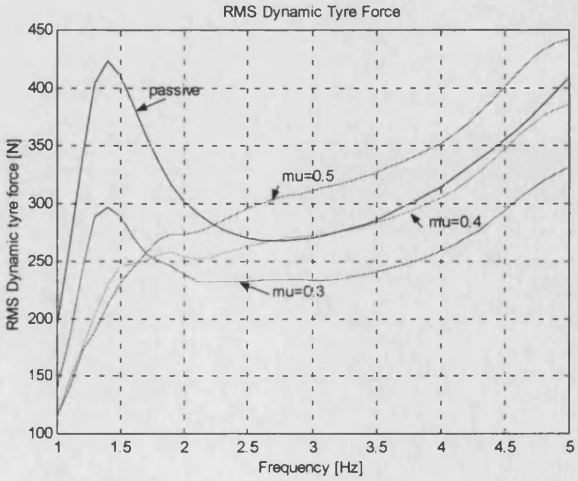

Figure 5.3 RMS dynamic tyre force transmissibility curves varying friction coefficient (0.3, 0.4, 0.5). Controller with b=2.5, z_1=0, z_2=0.

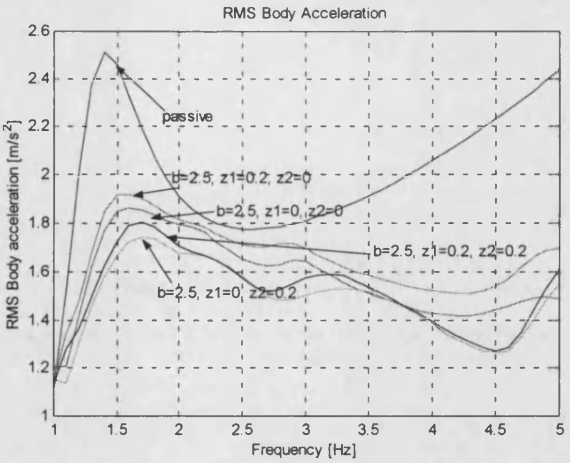

Figure 5.4 RMS chassis acceleration transmissibility curves for different controllers.

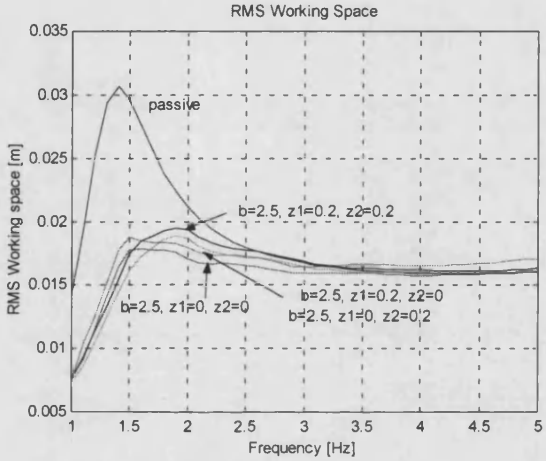

Figure 5.5 RMS working space transmissibility curves for different controllers.

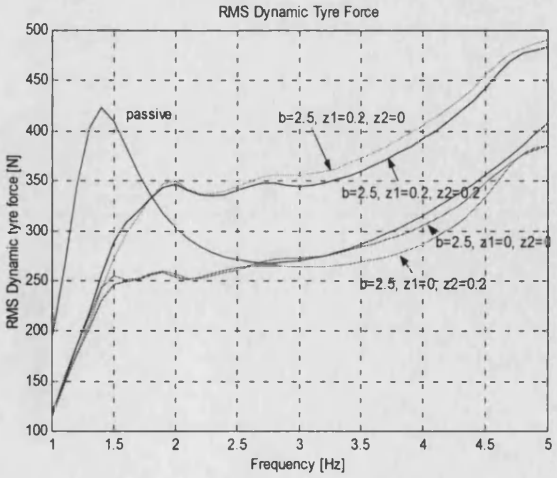

Figure 5.6 RMS dynamic tyre force transmissibility curves for different controllers.

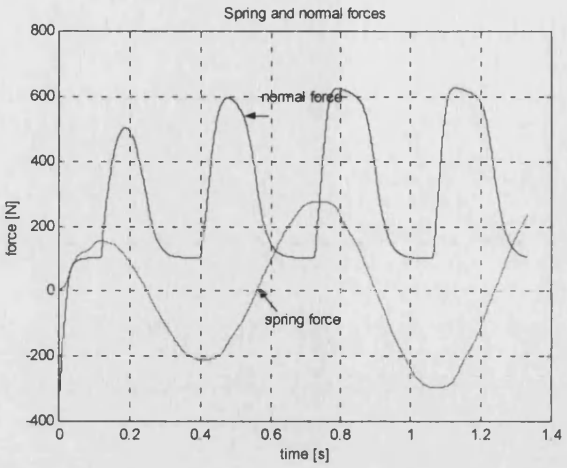

Figure 5.7 Spring and normal force time trends with a controller with b=2.5, z_1=0, z_2=0.

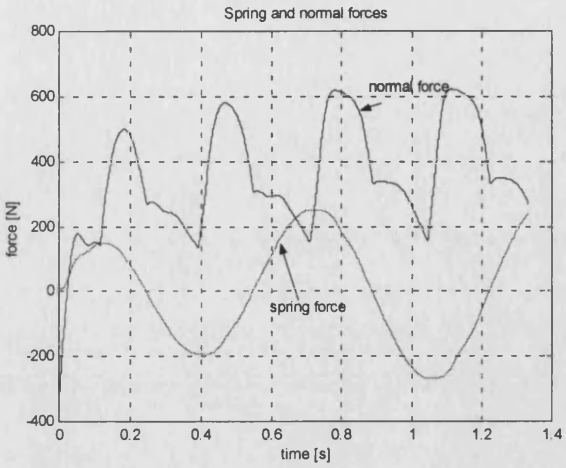

Figure 5.8 Spring and normal force time trends with a controller with b=2.5, z_1=0, z_2=0.2.

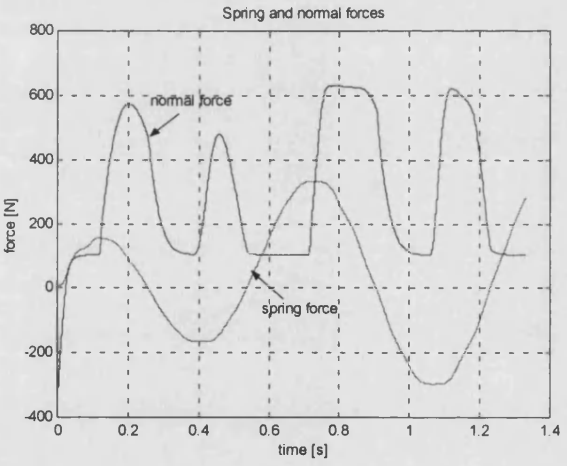

Figure 5.9 Spring and normal force time trends with a controller with b=2.5, z_1=0.2, z_2=0.

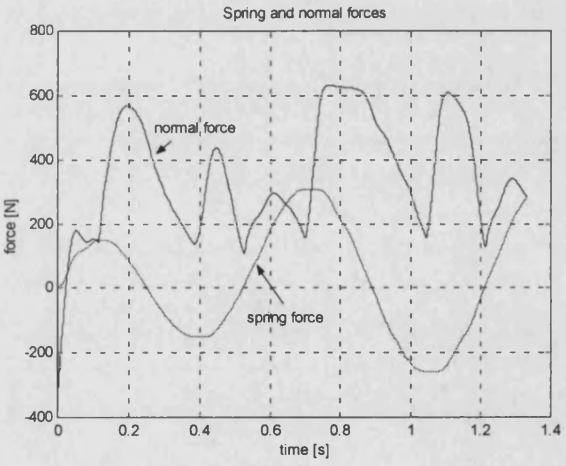

Figure 5.10 Spring and normal force time trends with a controller with b=2.5, z_1=0.2, z_2=0.2.

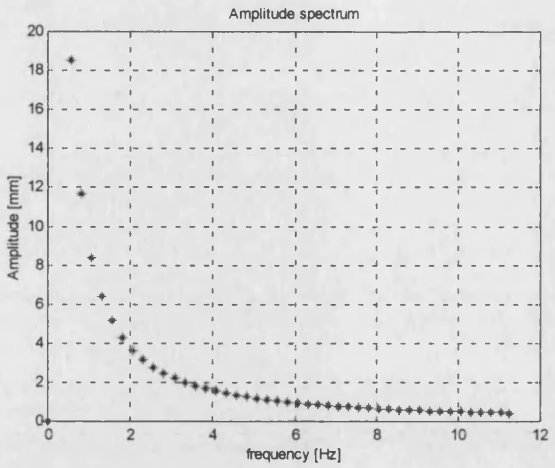

Figure 5.11 Amplitude spectrum of the road vertical profile.

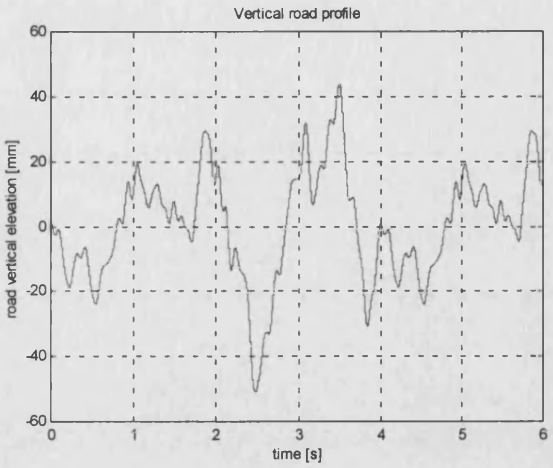

Figure 5.12 Road vertical profile time trace.

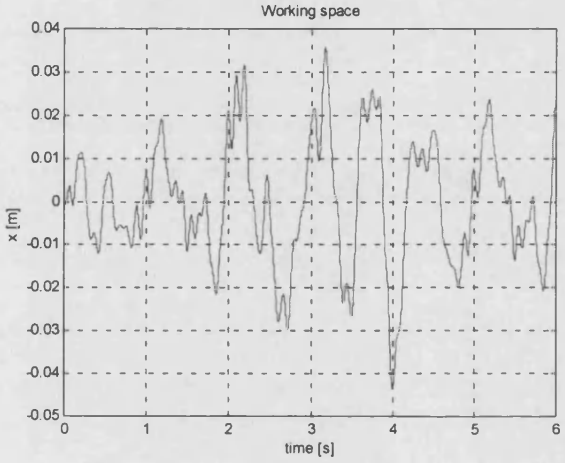

Figure 5.13 Working space time trace for the passive system. Speed: 50 km/h.

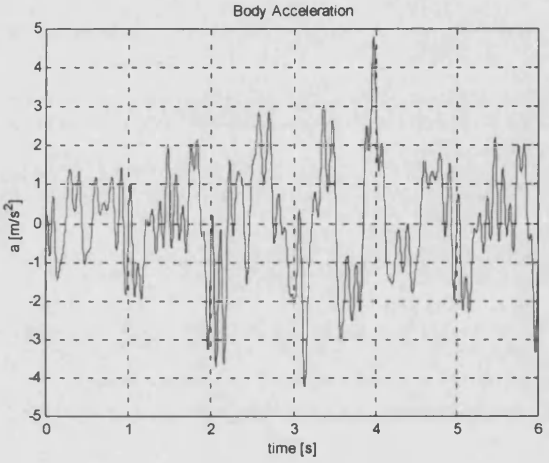

Figure 5.14 Chassis acceleration time trace for the passive system. Speed: 50 km/h.

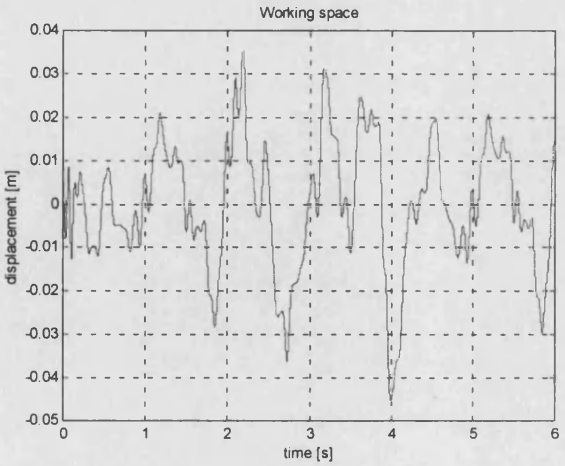

Figure 5.15 Working space time trace for the controlled system with b=2.5, z_1=0, z_2=0. Speed: 50 km/h.

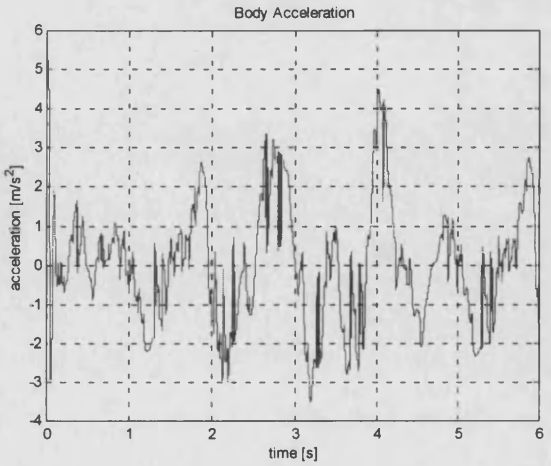

Figure 5.16 Chassis acceleration time trace for the controlled system with b=2.5, z_1=0, z_2=0. Speed: 50 km/h.

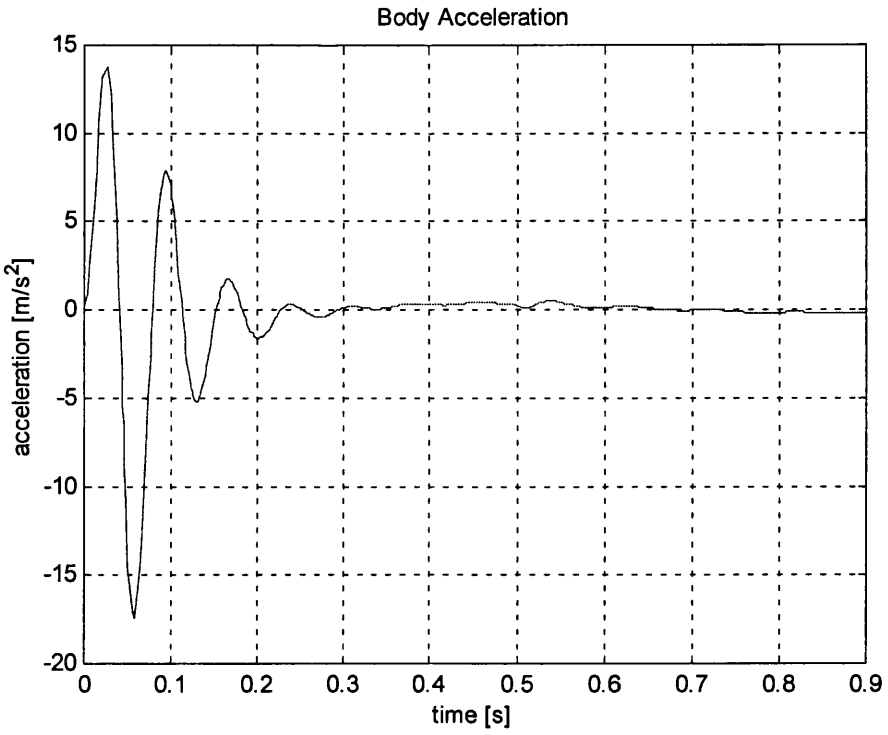

Figure 5.17 Bump response acceleration time trace for the passive system. Bump amplitude: 5 cm. Speed: 20 km/h.

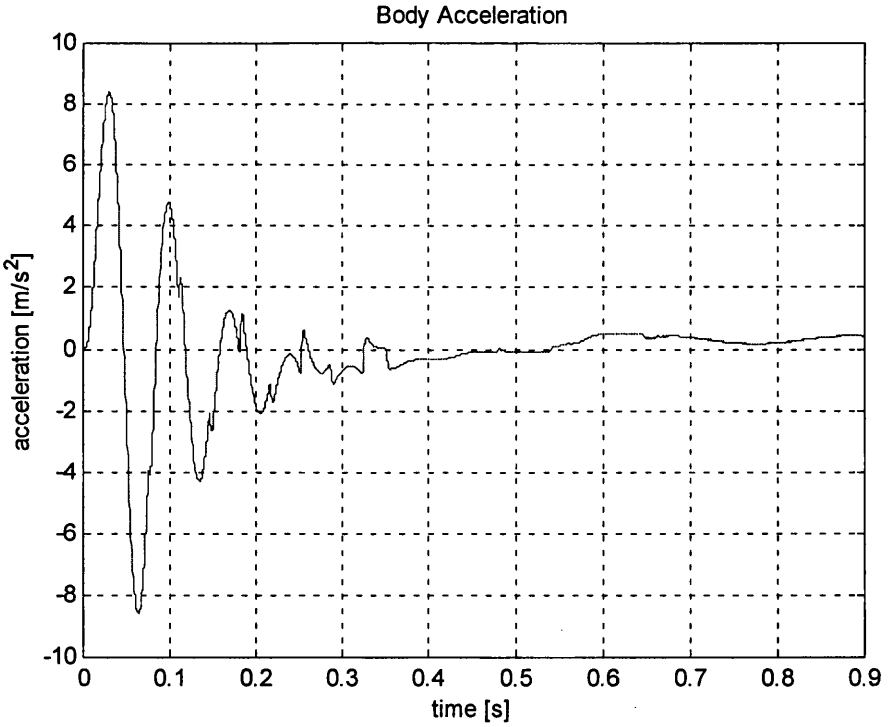

Figure 5.18 Bump response acceleration time trace for the controlled system. Bump amplitude: 5 cm. Speed: 20 km/h. Controller with $b=2.5$, $z_1=0$, $z_2=0$.

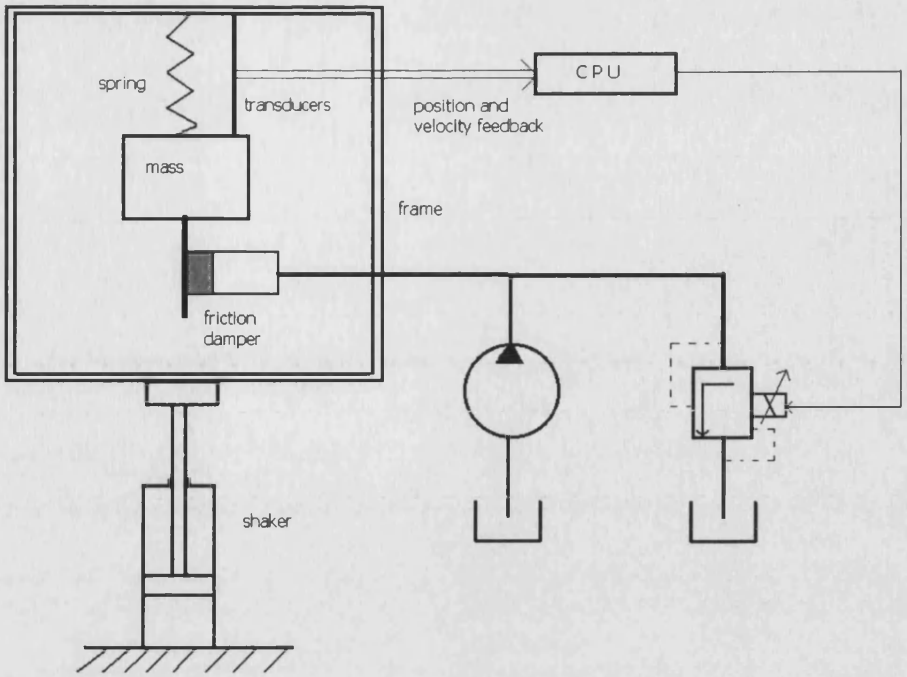

Figure 5.19 Schematic diagram of the pilot rig.

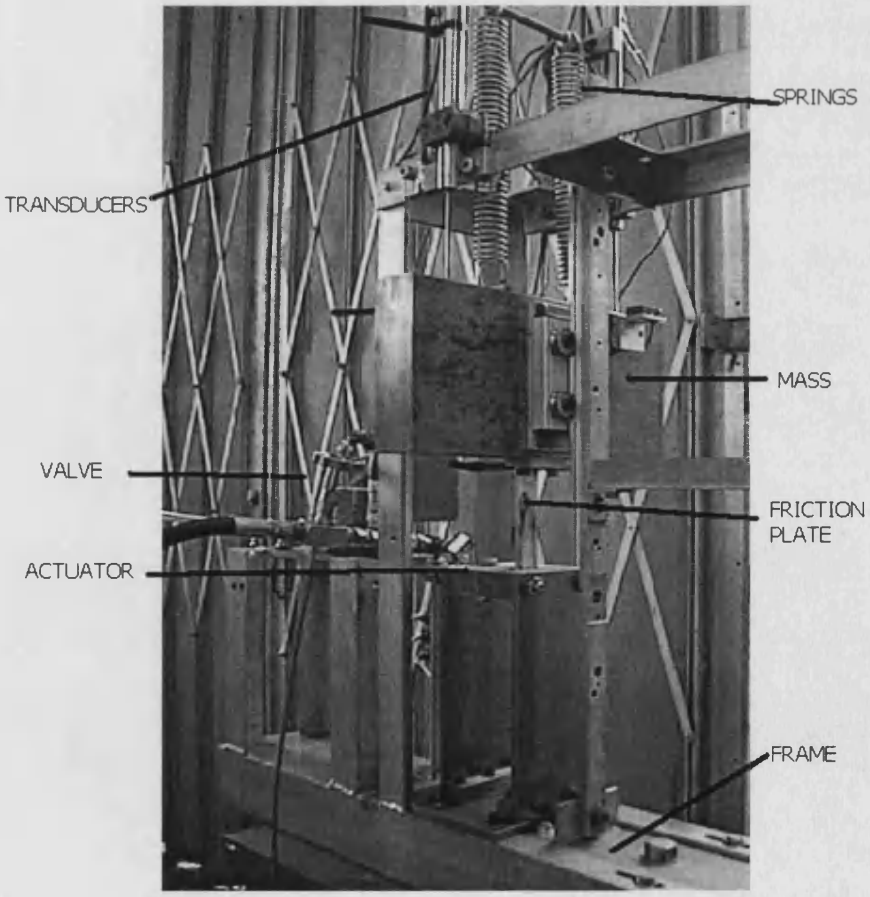

Figure 5.20 Photo of the pilot rig.

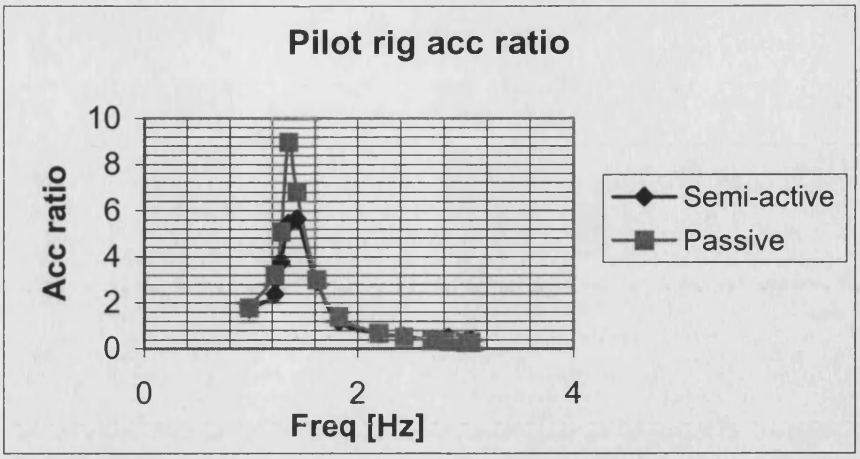

Figure 5.21 Pilot rig acceleration frequency response.

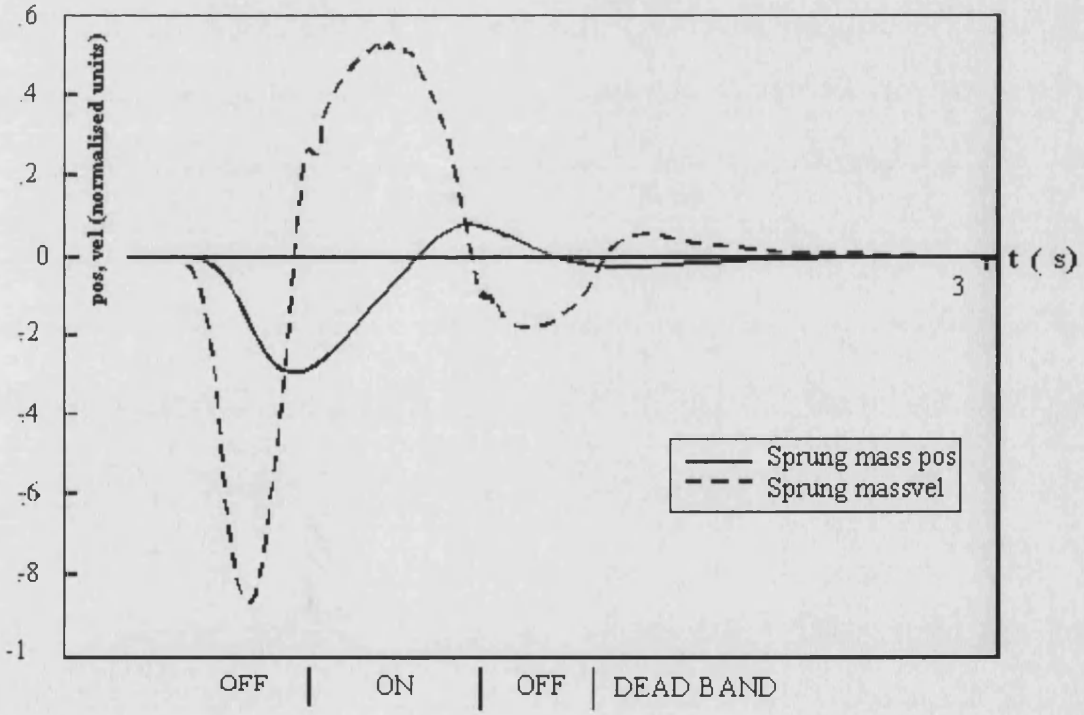

Figure 5.22 Pilot rig position and velocity transient response.

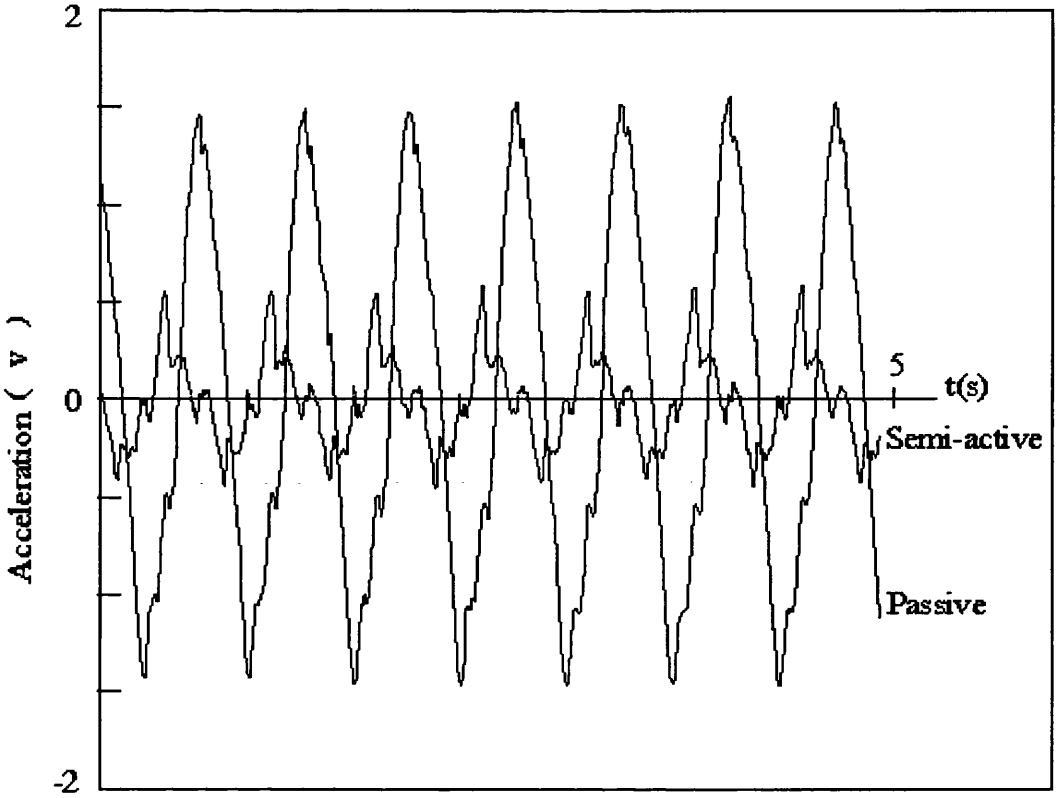

Figure 5.23 Pilot rig steady-state sinusoidal response.

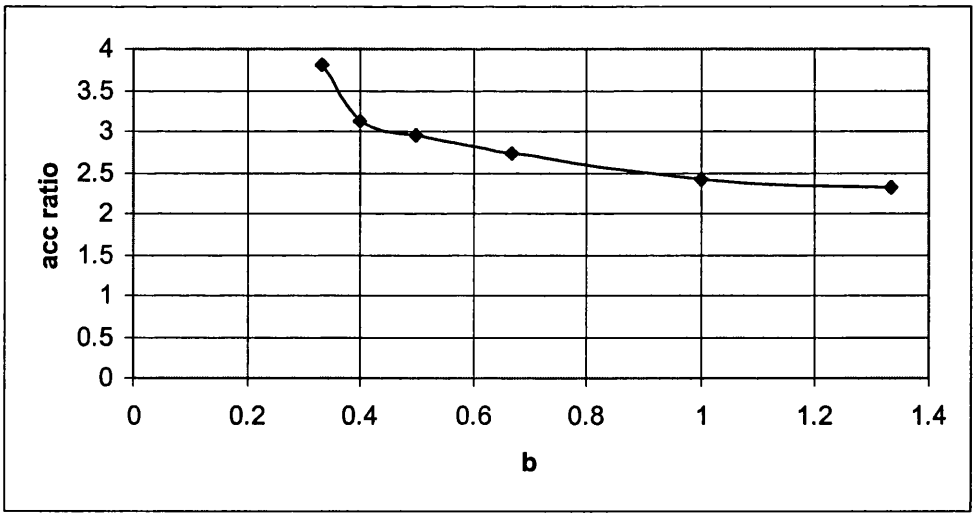

Figure 5.24 Pilot rig RMS acceleration versus "balance" gain *b*.

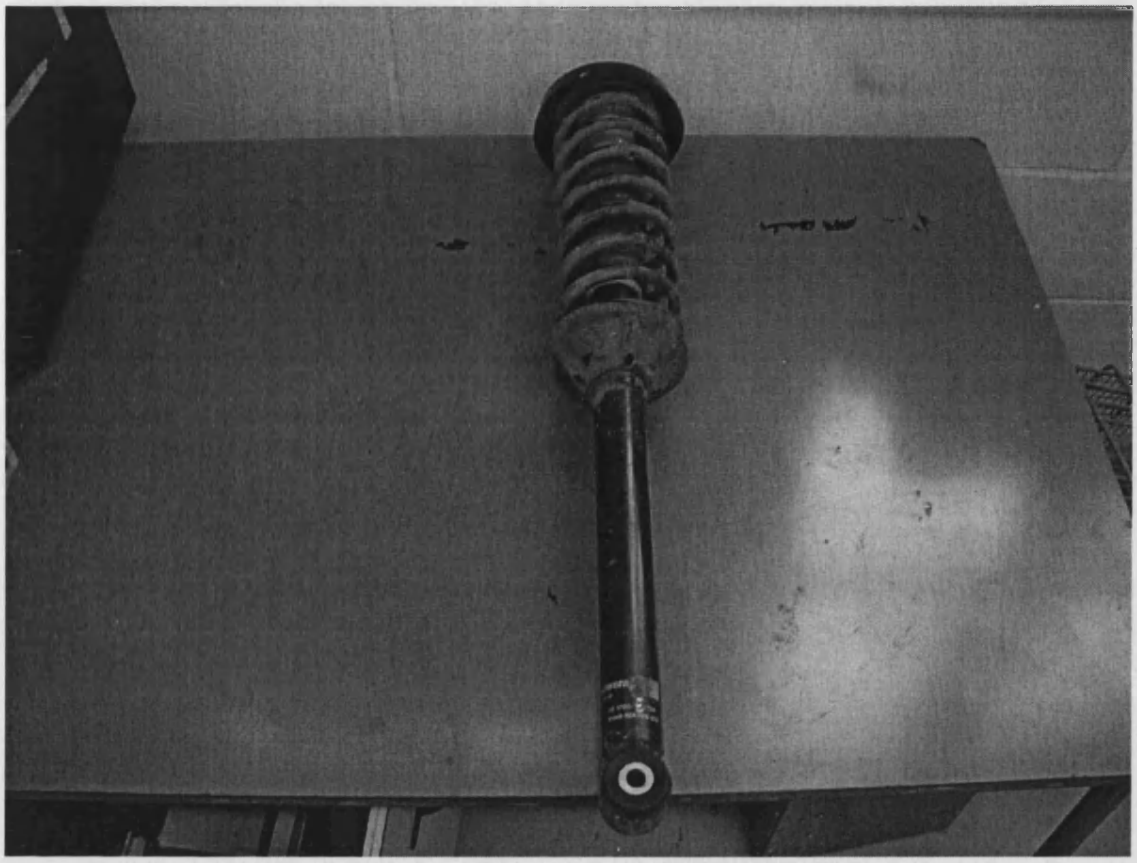

Figure 5.25 Original suspension unit: viscous damper and spring.

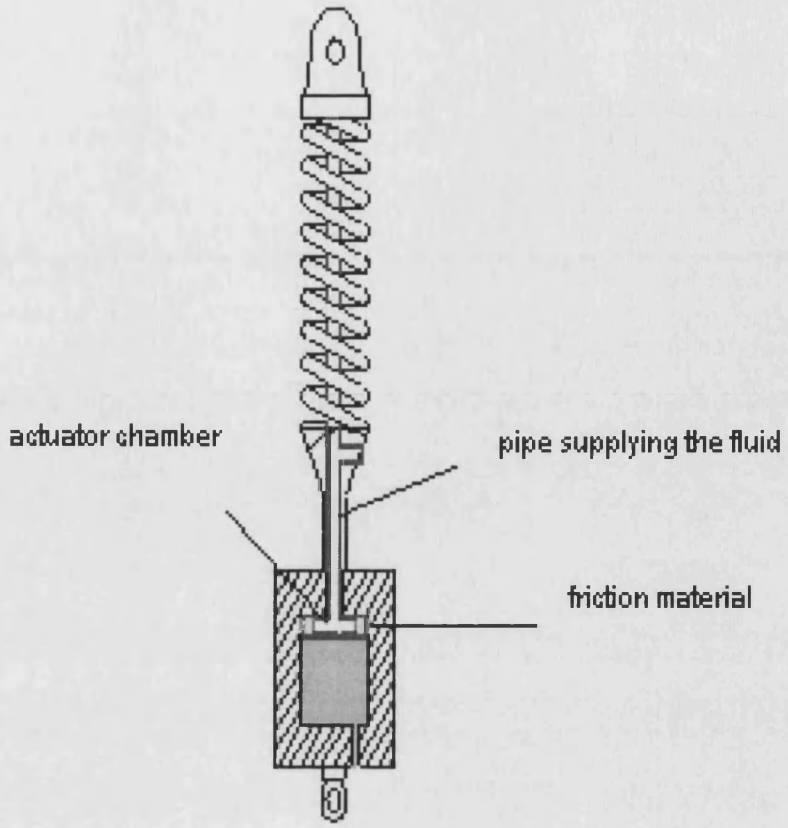

Figure 5.26 Vertical section of the friction damper; first design solution: square section.

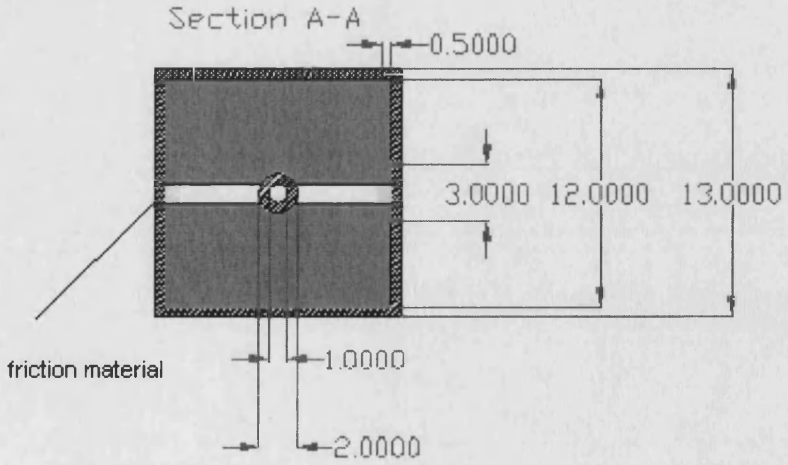

Figure 5.27 Top view of the square section.

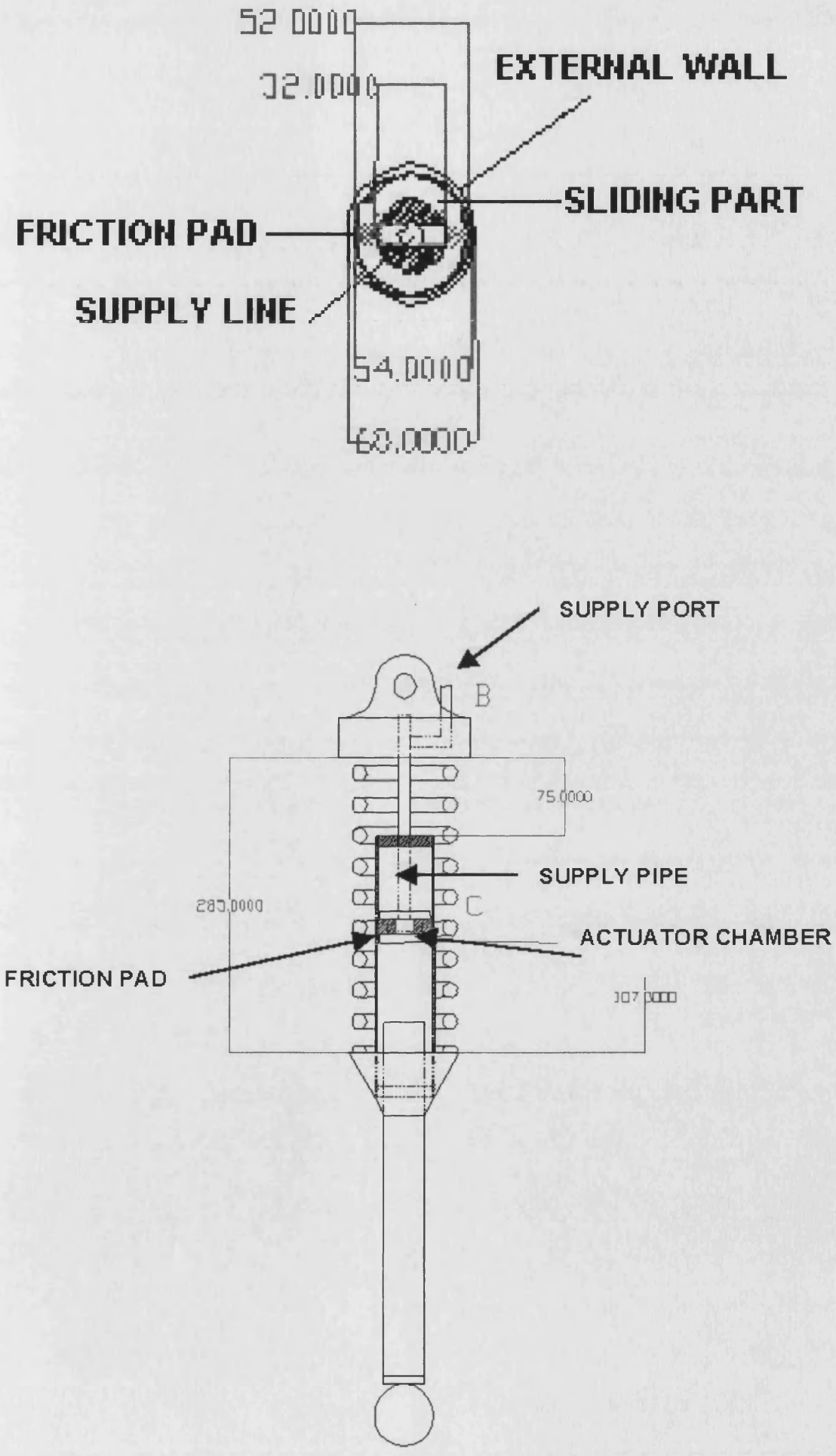

Figure 5.28 Drawing of the final design with enlarged circular cross-section.

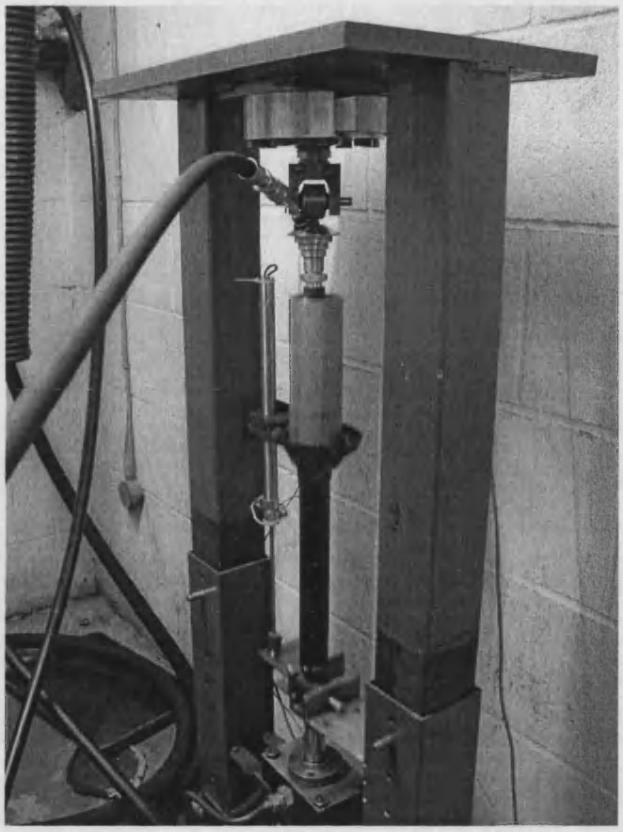

Figure 5.29 Photo of the friction damper (on the bench rig).

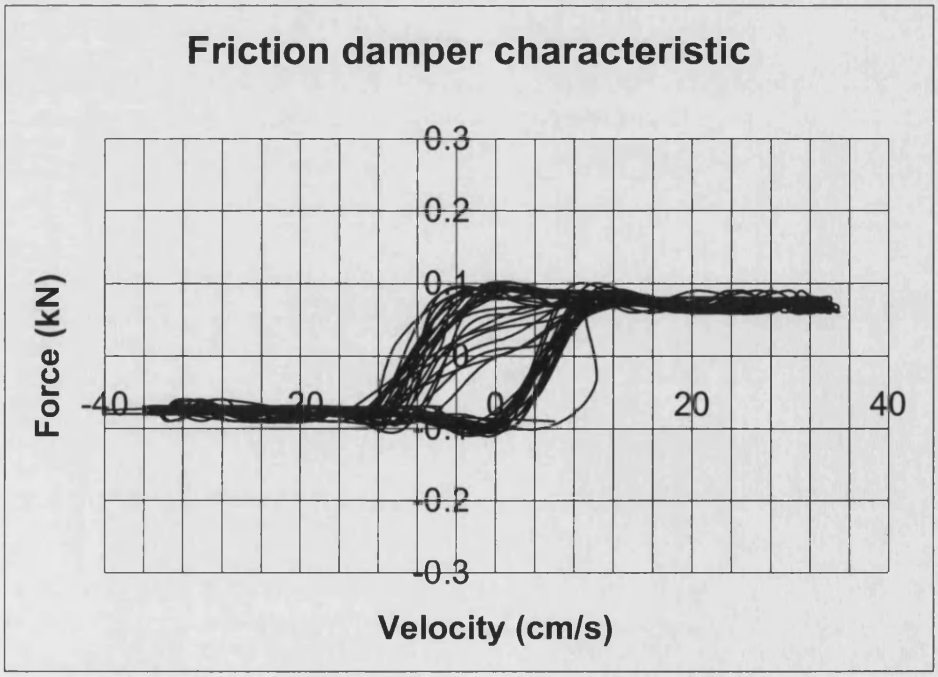

Figure 5.30 Friction damper static characteristics.

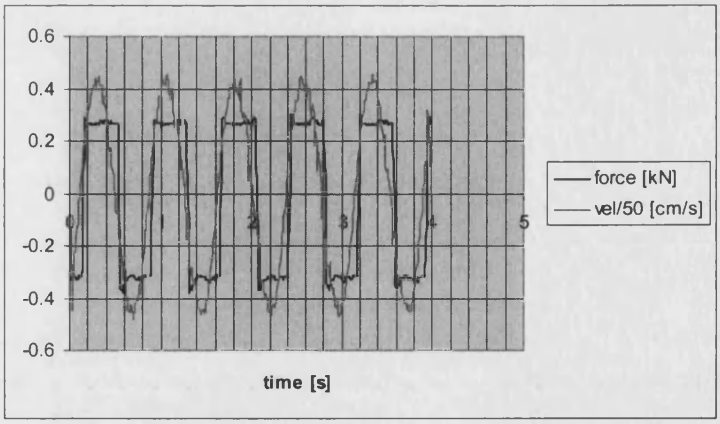

Figure 5.31 Friction force and velocity time trends.

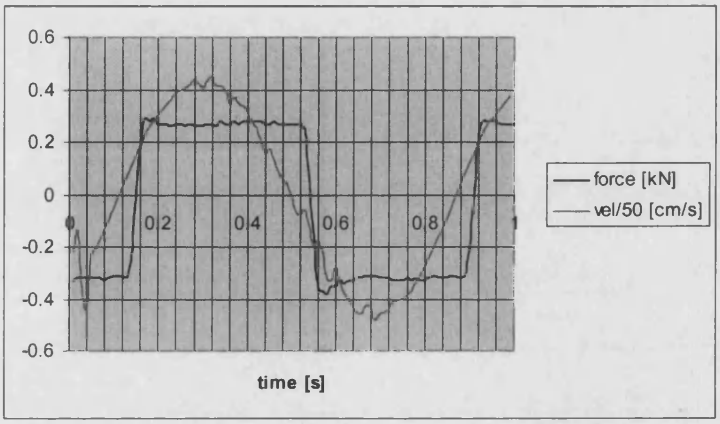

Figure 5.32 First period of friction force and velocity time trends.

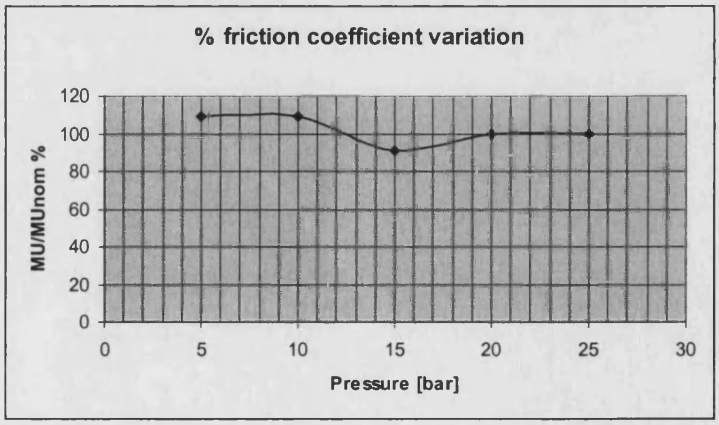

Figure 5.33 Friction coefficient pressure dependency.

6 THE ELECTROHYDRAULIC DRIVE

6.1 VALVE BENCH-TEST ASSESSMENT

6.1.1 Introduction

A major limiting factor in the dynamic performance of the controlled suspension is the pressure dynamic response of the valve. In order to establish the bandwidth of the valve as well as its pressure vs. driving signal static characteristic (pressure gain), a bench test assessment has been carried out on two different valves.

The first valve tested was a Sterling solenoid proportional valve (model HP02P 21). This is a low-cost valve (hence preferred for the automotive market) and the second a Vickers one-stage proportional directional valve with incorporated electronics (model KAFDG4V-3). This latter model is more costly.

6.1.2 Test on the Sterling valve

The Sterling valve is a 2-way proportional solenoid valve. The valve has been designed for flow control; hence its performance when it is used in pressure control mode was not known and not provided in the manufacturer's data-sheets. Therefore an experimental assessment is fundamental. For the control of the friction damper a 3-way valve is necessary; for this reason the hydraulic circuit needs to be completed with the connection of an additional orifice to the service port of the valve which allows the flow to tank to be damped. Thus the modified valve had a similar geometry to a 3-way valve. The restriction was easily created with an adjustable needle valve. A constant current amplifier was designed and built (figure 6.1) to provide a current driving signal. The whole arrangement was mounted on a flow bench.

The pressure gain of the valve was measured using the circuit drawn in figure 6.2. The valve was supplied at constant pressure by the laboratory main ring (around 60 bar) and the service port connected to tank through the orifice. Downstream pressure was

recorded by a variable reluctance pressure transducer (SE Labs, model 150 D). A sinusoidal voltage source provided the input to the amplifier. Since the valve is spring preloaded, the equilibrium position does not correspond to the null signal but to a biased constant value; for this purpose the amplifier was supplied with two non-symmetric voltages (10 V and 30 V).

Data were captured by the Hewlett-Packard DT-VEE data acquisition software. Other pressure gauges were installed to qualitatively control whether pressure was in the correct range.

The characteristic of interest is static, hence the measurement needed to be carried out in quasi-static conditions, driving the valve with a low frequency sinusoidal current otherwise the phase lag introduced at higher frequencies would have produced a distortion in the expected pressure vs. current trend. The expected pressure gain is saturation-shaped with some hysteresis depending upon the magnetic properties of the solenoid core and on the friction within the spool. The measured characteristic is plotted in figure 6.3; hysteresis is large. Such a hysteresis compromises its usage in applications where good tracking is crucial. However in the control of a suspension extremely good tracking is not strictly required. The slope is very high, meaning that the valve is almost critically lapped; this makes it more difficult to use it in a proportional fashion (it should be driven with low-amplitude signals).

Frequency response was measured using FRADOS, the frequency domain analysis software developed in-house. It extracts the first harmonic of the input and output signals and calculates modulus and phase of the resulting sinusoidal signals for each frequency.

Since the hysteresis introduces a strong nonlinear effect, frequency response was measured for three different amplitudes of the driving signal (0.4 V, 0.5 V, 0.55 V). Different input amplitudes produce frequency response traces which are not superimposable. This because for each input the valve works at a different point of its nonlinear pressure-flow characteristics.

Results are depicted in figure 6.4. At very low frequency results are not accurate because of the inherent limitation of the pressure transducer. The valve is very slow (the "average" bandwidth is less than 3 Hz).

Slightly better performance would have been obtained by restricting the cross-sectional area of the fixed orifice (the hydraulic time constant depends on the inverse of this area), but this would have had as a drawback a larger pressure drop and hence higher energy consumption at the pump.

The overall characteristics of this valve were too poor for the application: the static characteristic is too sharp and the bandwidth is not sufficient, thus the valve was rejected.

6.1.3 Test on the Vickers valve

This valve is, by far, more sophisticated but also more costly than the previous one. The amplifier is embedded inside the valve. The same tests described before were performed on this the valve. The major difference is that this valve is 4-way, therefore a service port must be blanked-off in order to obtain a 3-way type geometry.

The solenoid was supplied with a stabilised 10 V voltage supply (Weir 4000) and the valve was initially tested in the range 0-10 bar (the chosen operating pressure of the friction damper), 0.5-120 Hz. Pressure was recorded with the same variable reluctance pressure transducer.

The experimentation on this valve revealed an unexpected behaviour at low pressure. At first, initial tests revealed a large hysteresis, not expected for this type of valve. Hysteresis is due either too a poor magnetic material (not the case for a fairly costly valve) or to friction in the spool (measurements verified friction was negligible). It was thought that the inherent hysteresis of the variable reluctance pressure transducer was a co-cause, hence it was replaced with a semiconductive strain gauge transducer with very low hysteresis (Druck PDCR10), but without any progress. Subsequently the test was repeated superimposing a high frequency dither signal (square waves at 200 Hz, 300 Hz and 1 kHz) to the quasi-static signal. Dither reduces the amount of hysteresis; however also under these conditions there was no appreciable improvement. Finally, on advice of the manufacturer, the test was repeated at the extremely low frequency of 0.004 Hz. This test at such a low frequency was necessary because of the presence of a very slow integrator component in the electronics. In such conditions there was virtually no hysteresis, which was hence only apparent, due to a dynamic effect (the phase-lag

between driving signal and pressure). Figure 6.5 depicts the static characteristic at the supply pressure of 10 bar.

Likewise, dynamic performance was apparently extremely poor. Figure 6.6 depicts the frequency response for three different input voltages (0.1 V, 0.2 V, 0.3 V) and with the relief valve cracking pressure set at 10 bar. Bandwidth was enormously limited (around 4 Hz) despite the higher sophistication of the valve. Phase-lag was almost the same for all three inputs because hysteresis was negligible. The reasons of such a slow response were investigated thoroughly. A set of tests was designed to discover the cause of this unexpected behaviour.

It was finally discovered that the frequency response of the valve at low pressure (around 10 bar) is different from that at higher pressure (around 60 bar). The spool dynamic response, depicted in figure 6.7 (measured in presence of a flow, thus taking into account the effect of the flow forces), was quite fast (around 80 Hz) and was virtually independent from the supply pressure and from any measurement conditions, whereas the pressure bandwidth was dramatically limited at low pressure. Hence the problem did not depend on the valve itself but it was a fluid mechanic problem. A preliminary test was made to assess the dependency from the demand signal amplitude (the bandwidth usually decreases if the system is driven hard), but this dependency was found to be negligible.

The first hypothesis made was that at low pressure some air could have been trapped inside the valve: small quantities of air enormously reduces bulk modulus and therefore the response of the system since this one inversely depends on it, i.e. (reasoning in linear terms) the smaller the bulk modulus, the bigger the time constant.

In order to verify this hypothesis, the valve was mounted upright and oriented such that the unused port was physically in the highest point of the test circuit and beneath the load port (hence preventing air to stagnate close to the load port). The transducer was mounted horizontally for the same reason, then the valve was flushed through and immediately after the frequency response was measured (an additional test was even performed with a constant flow past the valve). However no appreciable change occurred and the bandwidth was still around 4 Hz). Figure 6.8 depicts the experimental frequency response under those test conditions.

A second hypothesis was made. It was thought that at low pressure the small pressure drop past the orifice did not locally produce enough velocity, so that the turbulent regime was not fully developed in the orifice. The low Reynolds number flow arising (in such a situation the flow-pressure correlation cannot be expressed correctly by the square-root law too) might be related to the small bandwidth. In order to verify this hypothesis the valve was driven with a biased signal so that the spool did not move symmetrically with respect to the centre of the land. This created a narrower flow path and hence a larger pressure drop, helping promote a turbulent flow regime. However, even in this situation the dynamic response did not show any improvement at all.

A third test was subsequently carried out on the relief valve to quantify the amount of dynamic variation in the supply pressure. If this had not been negligible and had been in phase opposition with the load pressure, it could have slowed the dynamic performance. However the measured pressure variation was negligible as depicted in figure 6.9. A relief valve dynamic effect (the second order spring-mass-damper dynamics of the relief valve spool) was excluded to be a co-cause, because relief valve dynamics are typically at much higher frequencies (around 200-300 Hz). Hence not even the relief valve was responsible of the poor pressure dynamic performance. This test, however, enabled it to be established that a single-stage relief valve, such as that employed, was sufficient for the application, without taking recourse to a more costly two-stage relief valve.

After the failure of all these tests it was decided to carry out a final test increasing the supply pressure (which required a different single-stage relief valve). Under these conditions the response was finally acceptably fast. It was found that the bandwidth was increasing with supply pressure. Figure 6.10 shows the frequency response measured with a relief valve cracking pressure of 60, 80 and 100 bar.

When pressure increases there is a much greater likelihood of any free air to be dissolved in the liquid: the greater the pressure, the higher the mole fraction of air passing in solution (Henry's law). Hence the reason of the slow dynamic response was to be sought in the presence of extremely small quantities of air that not even the initial flushing test had completely removed. This was a problem of the fluid at low pressure and hence independent of the valve itself. Spool dynamic performance were independent of the pressure condition. Therefore despite the required system pressure for the application being only 10 bar, it was necessary to pursue a trade-off between

higher power consumption and valve system bandwidth: all subsequent tests on the car with the friction damper were carried out with a supply pressure of 60 bar.

As far as the time domain response was concerned the step response (at 60 bar) had a trend similar to a first order linear response, which was what desired for the application. Figure 6.11 depicts the behaviour.

Previous tests were performed on the valve alone, without the presence of any additional volume. This was the most favourable condition. Any further volume increase produces a bandwidth reduction. In reality a certain amount of volume is present, the minimum being the internal pipe inside the damper plus the volume of the flexible hose connecting the valve to the damper. Hence further tests were performed in order to assess the influence of the volume on the dynamic response. They were carried out in three different situations, namely with the valve load port blanked off (the ideal situation), for an operating condition with the valve placed in the boot of the car and connected to the damper via a 50-cm hose and finally connecting the valve to the damper via a 2-metre long, 0.5-inch diameter hose. The results of figure 6.12 show how volume heavily affects the performance. Large volumes deteriorate valve response. Therefore in a final design the volume must be minimised, ideally mounting the valve on top of the damper.

Last but not least the problem of back-pressure must be mentioned. A 2-bar back-pressure is present as is evident from the measured pressure gain trend of figure 6.5. This creates a constant-amplitude friction force present also when the demand is set to zero. The larger the back-pressure the bigger the residual friction force. This can produce an undesired lockup of the damper. This puts a constraint on the final realisation of the friction damper: if the contact area were larger (for instance using four friction pads instead of two), this residual force would proportionally increase, (even if the operating pressure, and hence the power required is reduced). The back-pressure is due to the loss of head in the return line and to the leakage flow. This problem can however be addressed in the design phase, by mounting a pre-loaded spring in-between the friction pads. However from a dynamic viewpoint, this additional spring would introduce two further complex conjugated poles, that affect the overall system response. If these poles are of the order of magnitude of the valve bandwdith, they can slower the dynamic performance of the hydraulic drive.

6.2 ELECTROHYDRAULIC DRIVE PARAMETER ESTIMATION AND VALIDATION

The first characteristics to be assessed for the electrohydraulic drive is the pressure gain which establishes the closed-loop incremental gain and therefore the tracking ability of the controller. The local slope of the pressure gain depends upon the valve underlap u and the leakage coefficient k_{ls}. These two parameters cannot be readily measured, therefore they must be identified via a trial and error procedure, by performing a sensitivity analysis. The initial guess values chosen were a 0.6 mm underlap and a unit leakage coefficient (estimated with formula (4.20)).

Relief valve cracking pressure is 64 bar; the required pressure for the application is only 10-15 bar. With this increase in pressure the approximately proportional range is up to about 60 bar, therefore the control works only along the initial part of the pressure static characteristics (from the lower bound up to 10-15 bar); therefore it is imperative to have a good match in the lower region.

The dependence of the pressure gain upon valve lap is shown in figure 6.13. The latter assumes the values 0.1 mm, 1.1 mm and 2.1 mm. The upper bound region of the characteristics is affected more by a change in the underlap width than the lower bound region, which is the one of interest. The asymmetry in the behaviour is caused by the leakage term, the relief valve pressure override, the spool dynamics and from the compressibility flow. A symmetrical behaviour would have resulted if:

-the leakage had not been considered

-the supply pressure were perfectly constant

-the spool dynamics were neglected

-the simulation were perfectly static (not quasi-static)

In such an ideal situation, pressure gain is expressed as a function of the demand in a closed analytical form and the behaviour in the upper bound and lower bound region would be symmetrical. From the analysis of the figure, the best agreement is obtained when u is equal to 0.1 mm, although a larger value would not have affected the lower bound region.

Figure 6.14 depicts the dependence upon the leakage coefficient, varied between 0.5 and 2.5 (taking an underlap of 0.1 mm). From consideration of the figure, the best fit is obtained when k_{ls} assumes the value of 1.5.

The dynamic response of the valve is the other critical issue. Before passing on to the analysis of the results it is necessary to explain an approximation contained in them: the valve experimental response, recorded with a frequency response analysis software, is a "real" frequency response, obtained by extracting the first harmonic of input and output signals with a technique similar to the describing function. In the computer model the nonlinear valve dynamics have been simulated and the "frequency response" obtained by computing the actual RMS, including therefore the contribution of the higher harmonics. The approximation however is not that critical (and in any case comparable with that produced by a linearisation of the model) because the static characteristic of the valve is fairly linear and has negligible hysteresis. Hence it is inherently low-pass and therefore the overall contribution of the higher harmonics to the RMS is small.

The trends of the frequency responses are portrayed in figures 6.15 and 6.16.

Figure 6.15 shows the spool vs. voltage demand frequency response. The measured response is close to second order (from inspection of the figure): the simulation of a second order linear model with a natural frequency of 105 Hz and a damping ratio of 0.60 matches the results well. The suitability of a linear model confirms that friction of the spool within the valve sleeve is negligible.

Figure 6.16 shows the experimental phase diagram: as expected the phase varies between 0 and –180 deg, hence additional pure delays are not present. This also confirms the hypothesis made in chapter 4 (subsection 4.2.2) to neglect the voltage-current dynamics of the solenoid which are at a frequency higher than 100 Hz.

Figure 6.17 depicts the pressure response. The pressure vs. spool position frequency response is governed by a first order dynamics with a dominant pole at around 20 Hz (in cascade with the two complex conjugated poles of the spool response).

In the experimentation the bandwidth was substantially penalised by the presence of air bubbles formed in the oil because of the low system pressure. A simulation using standard value for the valve parameters and considering the actual volume formed by the valve with both load ports blanked-off results in an extremely large bandwidth,

absolutely unrealistic when compared to the experimental results. Such a pressure response would have been even faster than the spool dynamic response. In such a situation, the pressure response would have been close to second order with its dynamics dictated by the two complex poles of the spool mechanical response, which would become dominant. In order to match the simulation with the experimental results, it was necessary to include in the dynamical model the presence of air, whose effect is dynamically manifested through a drastic reduction in the bulk modulus. Hence this was reduced by two orders of magnitude with respect to its nominal value (1.6×10^4 bar). An exceptionally low bulk modulus of around 5×10^2 bar led to a reasonable agreement between the simulated and experimental responses. The actual value is probably higher. The volume (with both ports blanked-off) was assumed to be 2 cm^3: this is an underestimation. An error in the estimation of the volume would result in a bulk modulus few times higher. Such low values for the bulk modulus are physically possible in the presence of air (McCloy and Martin (1980)). Figure 6.18 shows how the presence of free air affects bulk modulus. The equivalent bulk modulus is expressed by the following equation:

$$\frac{1}{B_{eq}} = \frac{1}{B_{hose}} + \frac{\frac{V_{air}}{V_{tot}}}{B_{air}} + \frac{1}{B_{oil}} \qquad (6.1)$$

where V_{air} and V_{tot} are respectively the volume of the free air and the total volume. If $B_{hose}=8 \times 10^3$ bar $B_{oil}=16 \times 10^3$ bar and the ratio V_{air} over V_{tot} is equal to 2×10^{-2}, this yields an equivalent bulk modulus of around 5×10^2 bar.

In figure 6.19 the impact of an increase in volume, the other critical parameter, is investigated. The volume has been increased of an order of magnitude and this has produced a reduction of the bandwidth by about a decade. This is reasonable, recognising that in a linear approximation the hydraulic time constant is directly proportional to the volume.

6.3 TEST ON THE SEMI-ACTIVE SUSPENSION UNIT

After the experimental work on the valve and on the damper itself, the friction damper was installed on a car (figure 6.20) and has been tested. The system pressure defined by the relief valve was set to 60 bar.

The control valve placed in the boot of the car (figure 6.21) was connected to the friction damper, with a hose as short as possible, to reduce the volume. The instrumentation is the same employed in the tests on the passively-damped car. The results are presented in the following subsections. Firstly the frequency domain performance of the semi-active friction damper are discussed. In this domain it is possible to make an initial comparative assessment with the benchmark viscous damper response in terms of RMS values. Subsequently an analysis in the time domain is carried out. Particular care has been given to the issue of ride comfort assessment. This issue is critical in a suspension whose control is based on a switching logic: although a controlled suspension brings several benefits, time trends can be potentially nonsmooth and spiky, causing an uncomfortable ride.

6.3.1 Frequency domain analysis

The analysis in the frequency domain is based on RMS values. A comparative analysis of acceleration and working space transmissibility curves in the semi-active and passive case is presented.

Figures 6.22 shows the acceleration ratio transmissibility for an input of 7 mm in the range 1 to 5 Hz compared on the same graph with the passive system measurement taken in the same conditions. The controlled system is superior over most of frequency range considered. The passive system response is marginally better only up to 1.8 Hz. The controlled response presents three peaks: the first is the semi-active chassis resonance, at 1.7 Hz; its frequency is lower than the corresponding passive resonance and its amplitude is smaller; the shift of the chassis resonance at a lower frequency is advantageous in terms of comfort, although the actual passive response has a corresponding smaller value. The worse behaviour of the semi-active system at low frequency is due to the back-pressure, which causes a residual constant-amplitude friction force. The small amplitude of the disturbance at the lowest frequencies does not

produce very significant pressure variations: in that range the constant-amplitude friction force is not negligible. When the frequency increases, the feedback signal is larger and the friction damper works properly. Hence, the residual friction force deteriorates the performance of the damper if the disturbance is not large, i.e. on smooth roads and at low speed. This confirms that residual friction force compensation via a pre-loaded spring inside the damper is advisable. Two more peaks are evident in the semi-active trend. This is a nonlinear effect of the semi-active system, but in fact they do not create any problem, because they are far lower than the corresponding passive system values. In conclusion, this initial result proves that the semi-active device, despite the all the aforementioned problems is effective.

Figure 6.23 portrays working space responses in both cases. In the frequency range investigated the wheel can be assumed to be almost steady, hence working space is a good approximation to absolute chassis displacement. From the analysis of the figure, the passive response is generally better in particular close to the resonance. This because of the force tracking performed by the controller which inherently promotes higher displacements.

Figure 6.24 depicts the acceleration response with three different input amplitudes. Within reasonable approximations they are fairly similar. This means that the nonlinear effects are not very strong. Actually equation (2.1) with normal force specified by (5.1) is piecewise linear and for this particular class of equations the frequency response does not depend on the input amplitude as is the case in nonlinear systems[1].

Figures 6.25 to 6.8 show the effect of a change in the control law and in the friction properties. Figure 6.25 concerns the effect of changing the closed-loop "gain" b from 2 to 3.33; b is actually the reciprocal of a gain, in a strict control sense. It is the reciprocal of the friction coefficient μ, hence its increase from 2 to 3.33 is equivalent to a decrease of the friction coefficient from 0.5 to 0.3. The performance with the "lower" gain are overall slightly better over the frequency range: the lower the gain b, the higher the

[1] In a linear system the RMS and peak transmissibility ratios (e.g. body over wheel acceleration) are equal and independent on the amplitude of the input signal. In a piecewise linear system RMS and peak transmissibility ratios are not equal but still input amplitude independent. In a nonlinear system RMS and peak transmissibility ratios are not equal and input amplitude dependent.

assumed friction coefficient, the bigger the force cancellation, resulting in smaller acceleration.

Figure 6.26 and 6.27 relate to the effect of changing the control law. Figure 6.26 depicts RMS chassis acceleration and 6.27 wheel acceleration which is related to dynamic tyre force. The performance of three types of controllers are compared. These are:

-a pure position feedback (b=2.5, z_1=0, z_2=0) controller (X in the legend)

-a controller with position feedback in two quadrants and velocity feedback in the other two (b=2.5, z_1=0, z_2=0.1; XV in the legend)

-a controller with position plus velocity feedback in two quadrants and velocity feedback in the other two (b=2.5, z_1=0.1, z_2=0.1; XVV in the legend)

The pure position feedback control logic achieves the best results in terms of chassis acceleration reduction because it aims for pure spring force cancellation. It performs better in terms of wheel acceleration, compared to the other controllers, although the passive system is always superior. The reason why the controlled suspension produces an increase in wheel acceleration is to be sought in the absence of a wheel acceleration feedback in the loop.

The other controller (b=2.5, z_1=0, z_2=0.1) introduces a small viscous effect, thus it produces a slightly higher chassis acceleration. It is almost comparable with the previous controller in terms of wheel acceleration: over a part of frequency range is worse, but in other bands slightly better.

The final controller (b=2.5, z_1=0.1, z_2=0.1) produces the least chassis acceleration reduction among the three types of controllers investigated and also the worst wheel acceleration. Therefore the additional viscous damping in the first and third quadrants is not advantageous.

Hence, overall the best control logic is that with pure position feedback, which is also the easiest to implement.

It is of interest to evaluate how a change in the frictional characteristic would affect the performance of the control. The test of figure 6.28 was carried out in a situation of lubricated friction (that arose because of the failure of a seal). The response in dry

friction regime is here compared to that in lubricated friction regime. This test is important, because lubricated friction is a realistic alternative to pure dry friction: it helps reduce stiction and is potentially advantageous in terms of heat dissipation. At low frequencies dry friction system response is better than the lubricated friction system response although both worse than the passive response. In the central frequency band lubricated friction response is better, but at highest frequency the opposite. In both cases the performance of the controlled suspension are not worsened.

From the previous analysis the practical robustness of the schemes is verified. Particularly by changing the feedback gain and the control logic. However also by changing the friction properties the response is still fairly robust and in any case better than the passive response.

6.3.2 Time domain analysis

Time domain analysis typically permits an assessment of the transient behaviour. In this context it is mainly used to assess ride quality (see subsection 3.5.2).

Figures 6.29 and 6.30 show jerk trends in the passive and semi-active cases. The latter trend presents slightly higher peak values. From this angle the semi-active suspension system produce a slight worsening in ride comfort. This increas in jerk peak value is expected in a suspension controlled with a switching based logic.

Subsequently a Fourier analysis of the acceleration waveforms is presented. Although the spectrum is more appropriate to assess the degree of nonlinearity rather than comfort, it is possible to establish a qualitative correlation between a high harmonic content and comfort.

Figures 6.31 to 6.38 depict some experimental time traces and spectra for the passive and semi-active suspension. Figures 6.31 to 6.34 show measured acceleration time histories and spectra for the passive case at frequencies of 2.2 Hz and 4.5 Hz. At 2.2 Hz (figures 6.31 and 6.32) the behaviour is fairly linear (only a negligible third harmonic is present in the spectrum). The same is true at 4.5 Hz (figures 6.33 and 6.34). This furtherly validates the hypothesis of linearity of the passive system (ideally only the fundamental harmonic ought to be present in the case of linear behaviour): the Fourier transform of the passive system acceleration has a small harmonic content (and to a

greater extent the displacement, since acceleration is the noisiest signal). Figures 6.35 to 6.38 depict the same graphs for the controlled system. The harmonic content is not very large at 2.2 Hz, but is certainly larger at 4.5 Hz and actually the acceleration time trend is fairly spiky. This spectral analysis of the output signal has hence verified the qualitative correlation between jerky time trends and richer higher harmonic content.

Figure 6.39 shows the semi-active random response, the RMS is 0.58 m/s^2, which is smaller than the passive one (0.75 m/s^2).

Figure 6.40 shows the semi-active bump response. The bump input is the same as in the passive case. The acceleration overshoot and undershoot for the controlled system are 1.1 m/s^2 and -0.9 m/s^2 whereas for the controlled system (in the case b=2.5, z_1=0, z_2=0) are ±0.85 m/s^2. The number of oscillations is the same for both. Thus the controlled system is slightly worse in response to a bump. The explanation again depends upon the slow response of the valve. A bump can be thought has a high frequency half-wave input (the higher the velocity, the higher the frequency) and above a certain frequency the valve response is not fast enough.

6.4 SEMI-ACTIVE SYSTEM VALIDATION

The last step, after validating separately the electrohydraulic drive and the passive car, is the validation of the whole system. Figure 6.41 shows the steady-state sinusoidal response. Globally the simulation follows the overall trend of the measured acceleration well. It does not track all the spikes, but most of them can be attributed to the noise of all sorts present in the measurements. This good agreement permits ride assessments to be made on the basis of the simulated acceleration trends.

Consider now the frequency domain. A sensitivity analysis was carried out to identify the most suitable values for the critical parameters. Figure 6.42 represents the frequency response varying friction coefficient μ between 0.1 and 0.3. At low frequency the trend is virtually independent of the friction coefficient but after the resonance the dependency gets stronger. A smaller friction coefficient produces a larger resonance peak but it tracks the experimental response at higher frequency better; and vice-versa for a larger coefficient. Therefore, a trade-off value of 0.15 has been chosen. The

mismatch occurring for frequencies higher than 3.8 Hz is due to the limitations in car model rather than to the hydraulics. The actual value of the nominal friction coefficient of the material was 0.4. The mismatch between simulation and experiments is due to a reduction of the friction coefficient of the material occurred because of the wear of a seal during the experimental tests which created a lubricated friction regime. The controller demand signal was referred to the rated friction coefficient; as a consequence the ratio $\frac{\mu}{\mu_{assumed}}$ changed (see section 5.1).

Figure 6.43 portrays the frequency response varying the delay between velocity and friction force created by the "frictional memory" (see chapter 2, subsection 2.8.2) effect. A change of ±50% does not produce any remarkable effect, except at the lowest frequencies.

In figure 6.44 the impact of a change in the actuator and connecting pipe volume is considered. A change of an order of magnitude in the volume produces a noticeable effect in the frequency response, starting from frequencies higher than 2.5 Hz. The impact on the car of a reduction of the valve-actuator bandwidth, following an increase in volume, is a higher acceleration. Physically this is because the valve-actuator system cannot catch up with the higher frequency disturbance; therefore the effect of the residual constant friction force plays the dominant role.

In figure 6.45 the effect of the back-pressure is investigated, which introduces a constant friction force. Higher frequencies are slightly more sensitive to larger back-pressure, however its effect is not that crucial and it is not as critical as the presence of a larger volume.

Hence it can be stated that simulation works properly up to almost 4 Hz, subsequently it overpredicts acceleration. The reasons for this behaviour must be attributed to the car model rather than to the valve model.

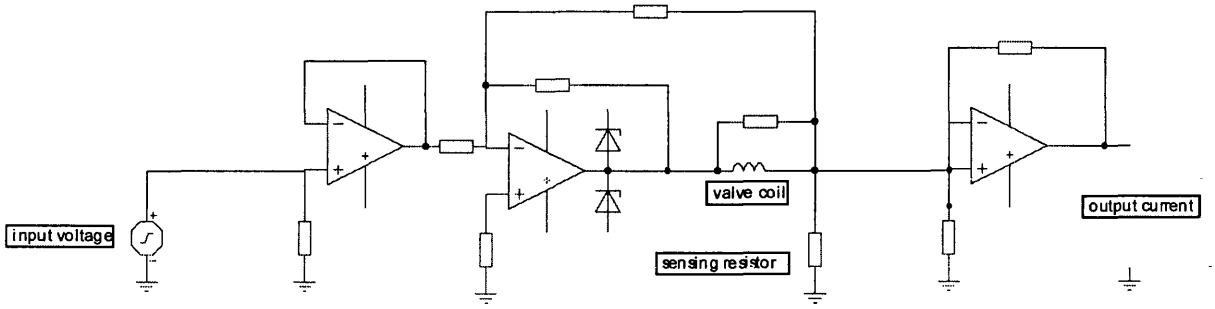

Figure 6.1 Electrical scheme of the Sterling valve current amplifier designed.

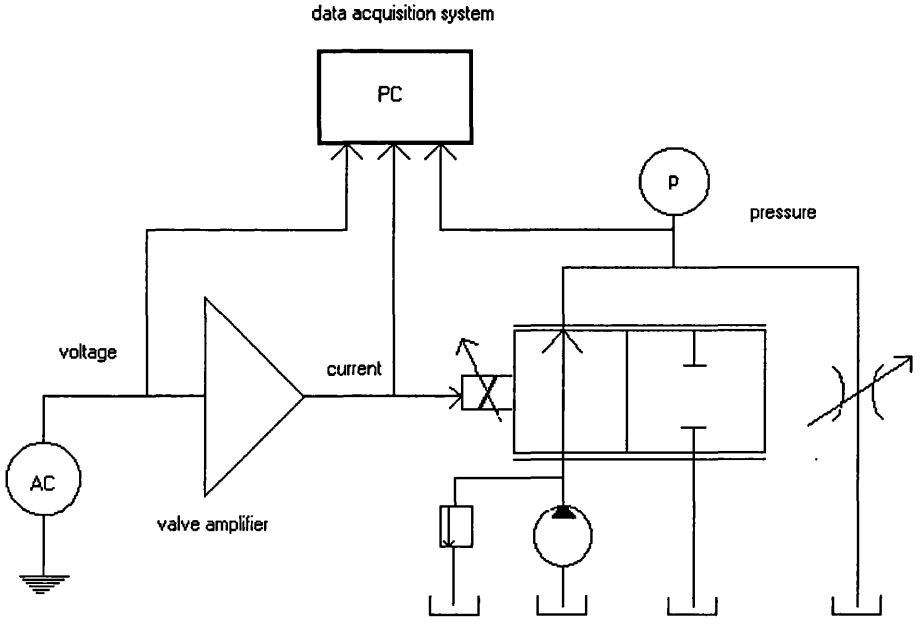

Figure 6.2 Schematic of the measurement circuit for the Sterling valve.

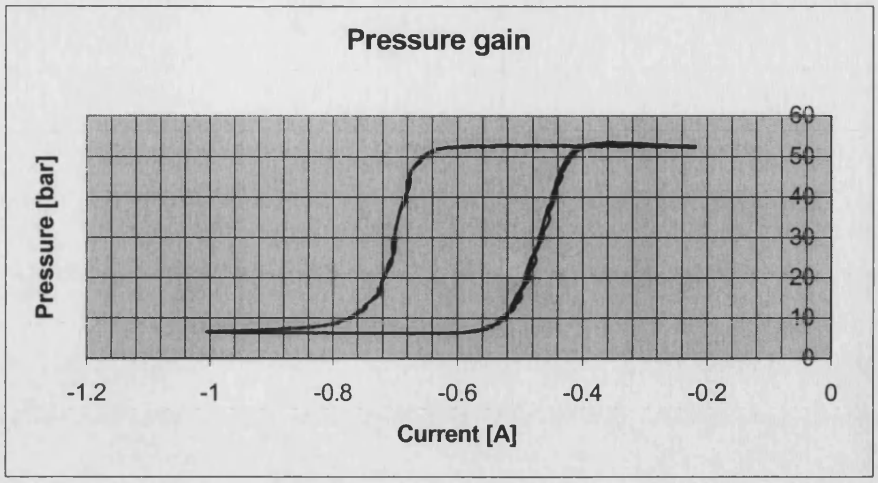

Figure 6.3 Pressure vs. current static characteristic of the Sterling valve.

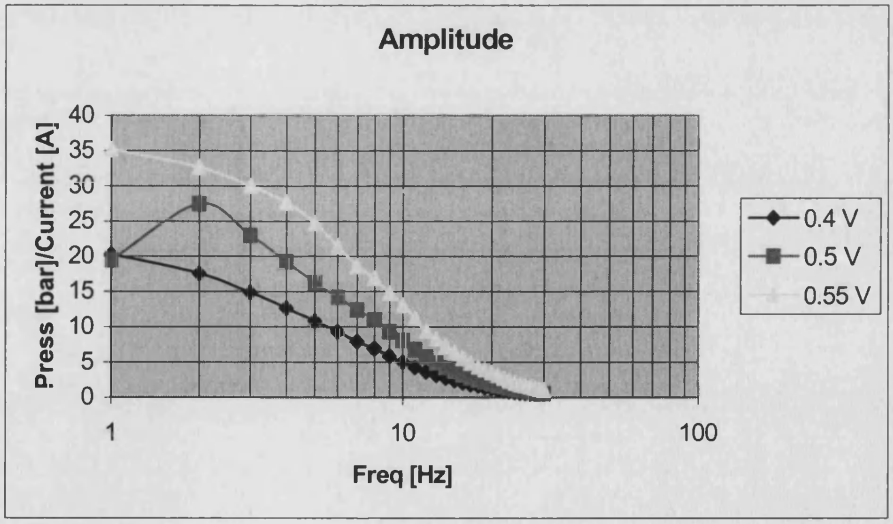

Figure 6.4 Modulus Bode diagram of the pressure vs. current transfer function of the Sterling valve.

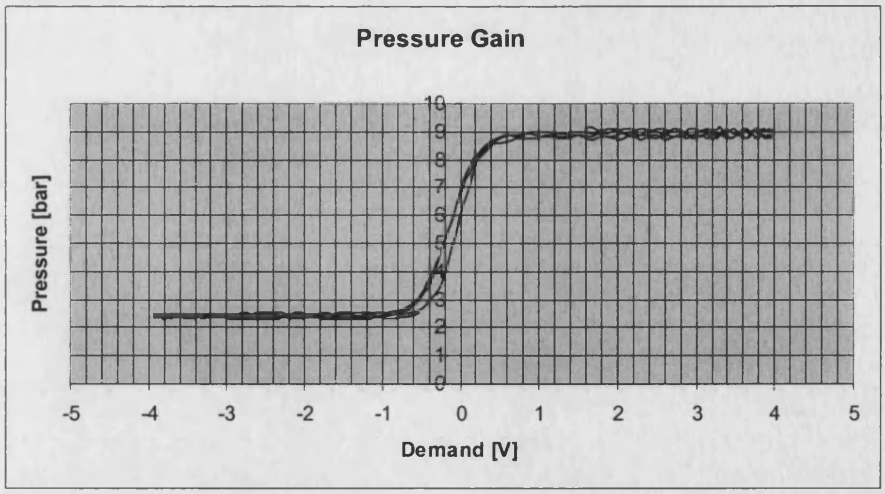

Figure 6.5 Vickers valve pressure gain.

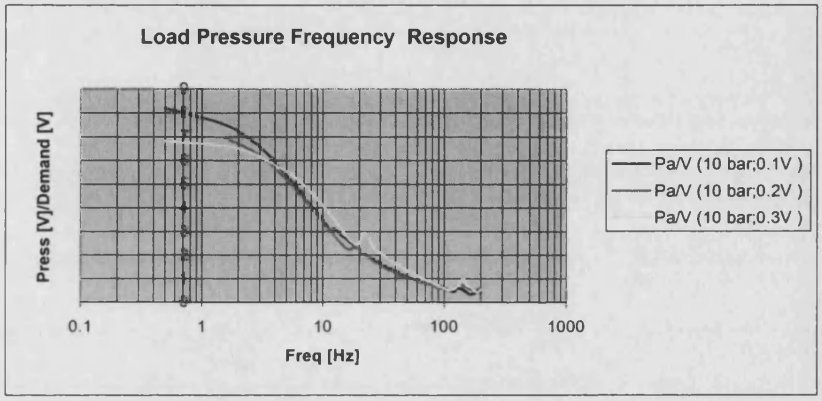

Figure 6.6 Modulus Bode diagram of the pressure vs. voltage transfer function of the Vickers valve.

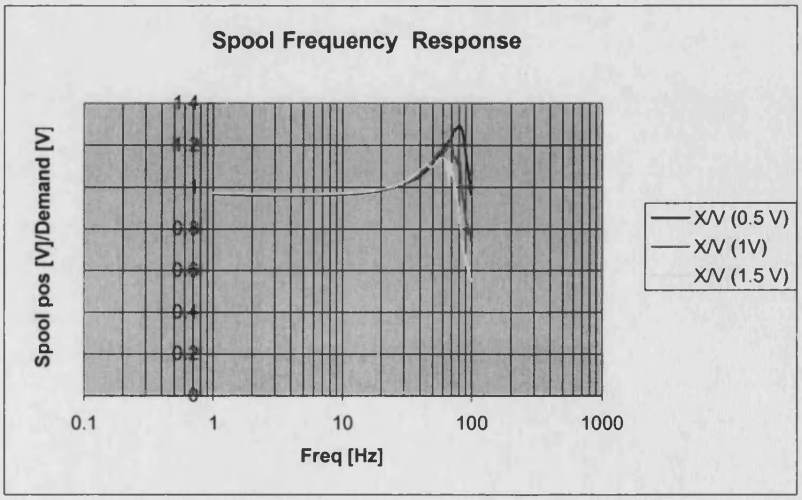

Figure 6.7 Modulus Bode diagram of the spool position vs. voltage transfer function of the Vickers valve.

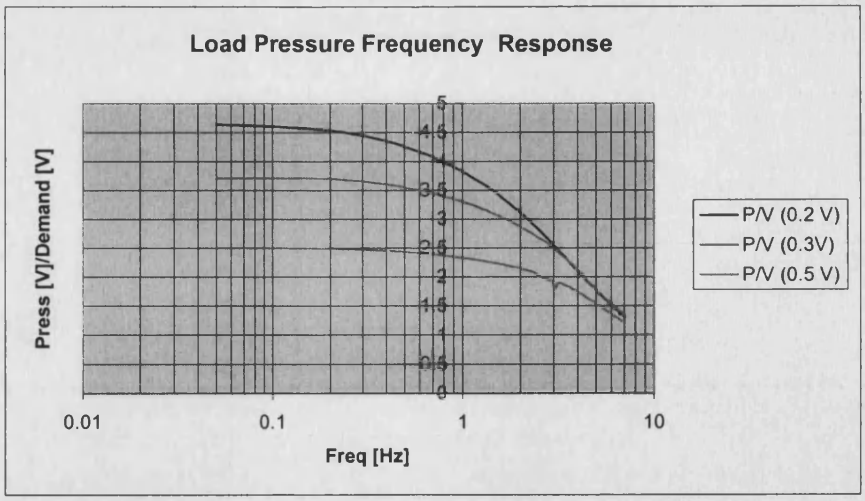

Figure 6.8 Modulus Bode diagram of the pressure vs. voltage transfer function of the Vickers valve measured in the air bubble test.

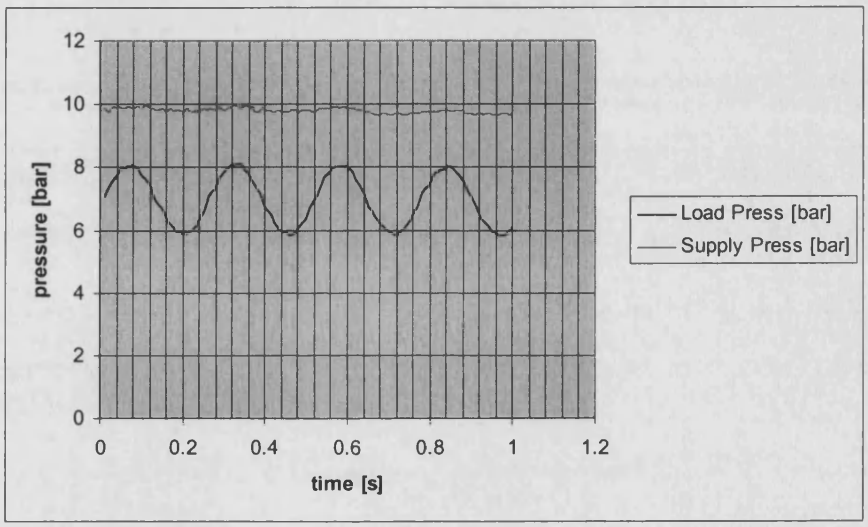

Figure 6.9 Supply pressure dynamic variation.

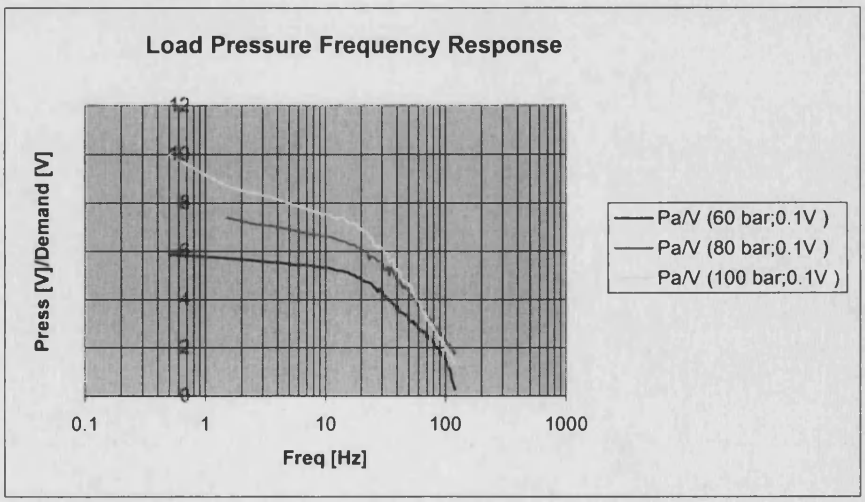

Figure 6.10 Modulus Bode diagram of the pressure vs. voltage transfer function of the Vickers valve at 60, 80, 100 bar.

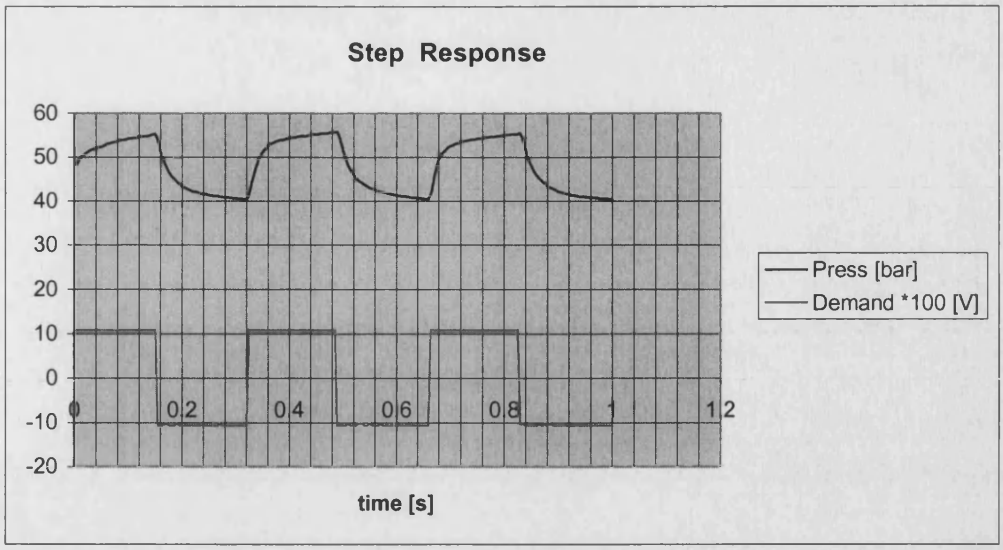

Figure 6.11 Vickers valve step response at 60 bar.

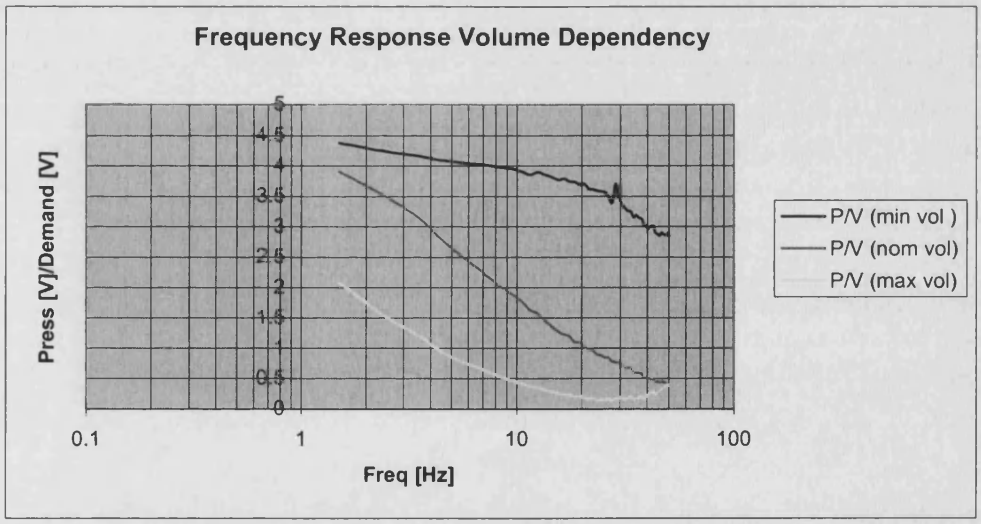

Figure 6.12 Modulus Bode diagram of the pressure vs. voltage transfer function of the Vickers valve varying volume.

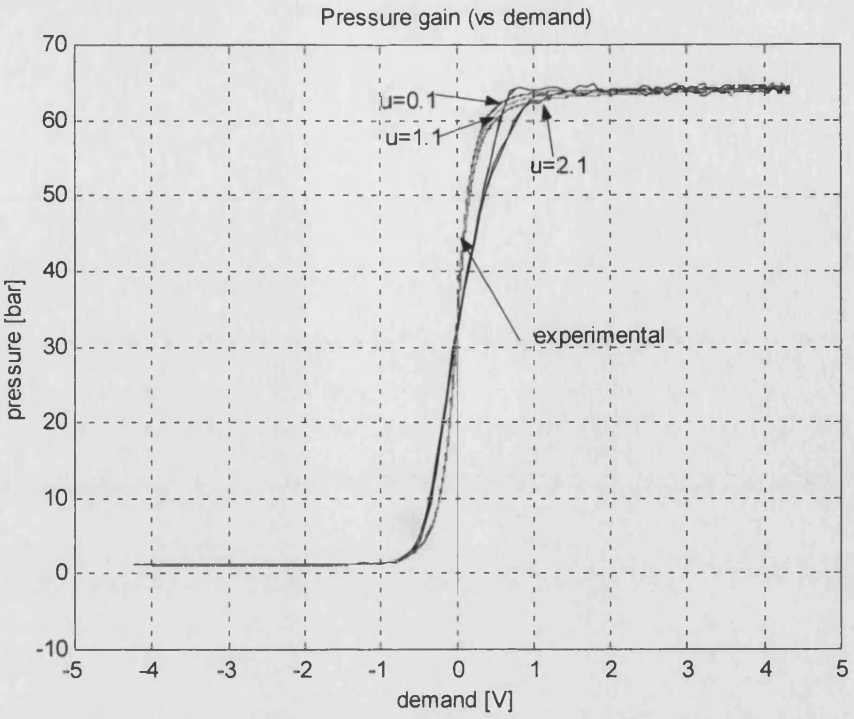

Figure 6.13 Comparison of experimental and predicted control valve pressure gain, varying the underlap from 0.1 mm to 2.1 mm.

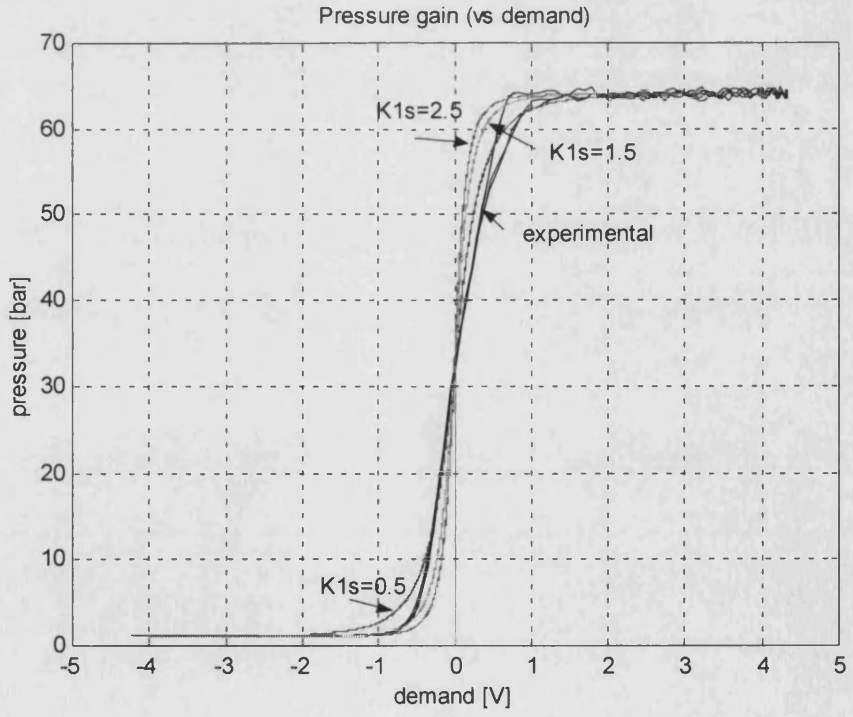

Figure 6.14 Comparison of experimental and predicted control valve pressure gain, varying the leakage coefficient from 0.5 to 2.5.

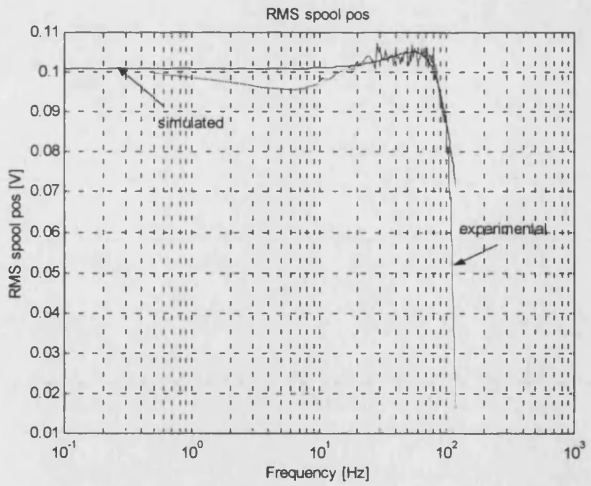

Figure 6.15 Comparison of experimental and predicted spool position vs. demand frequency response.

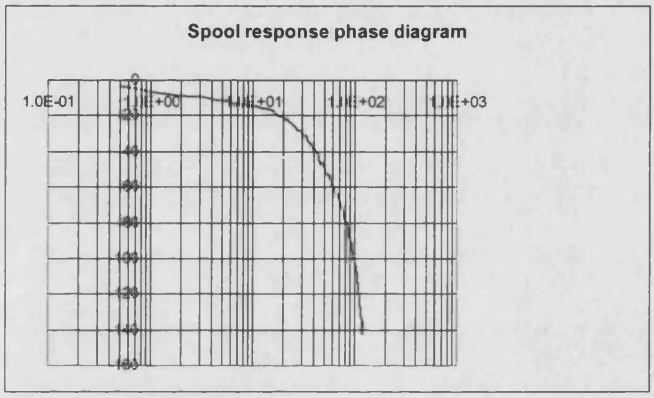

Figure 6.16 Spool position vs. demand experimental phase diagram.

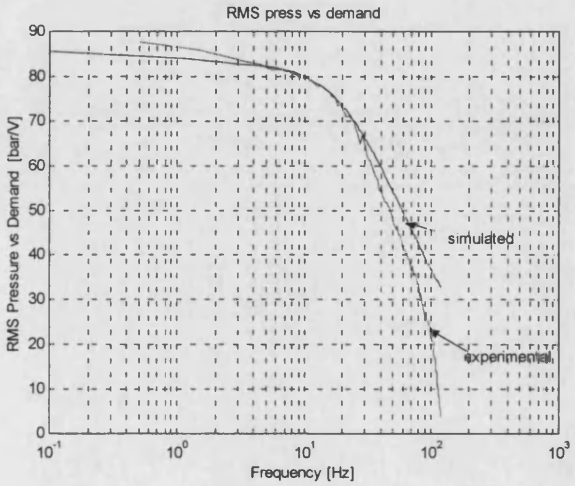

Figure 6.17 Comparison of experimental and predicted pressure vs. demand frequency response.

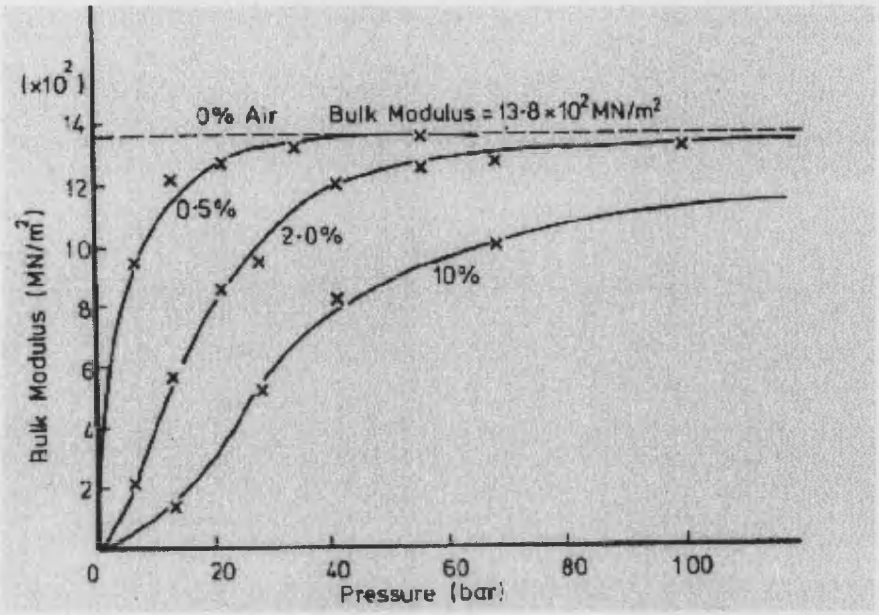

Figure 6.18 Bulk modulus variation with air for a typical hydraulic oil.

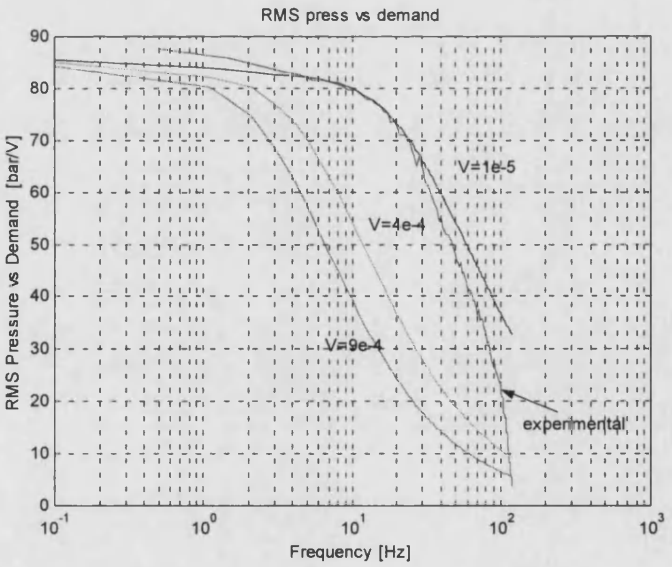

Figure 6.19 Comparison of experimental and predicted pressure vs. demand frequency response varying volume.

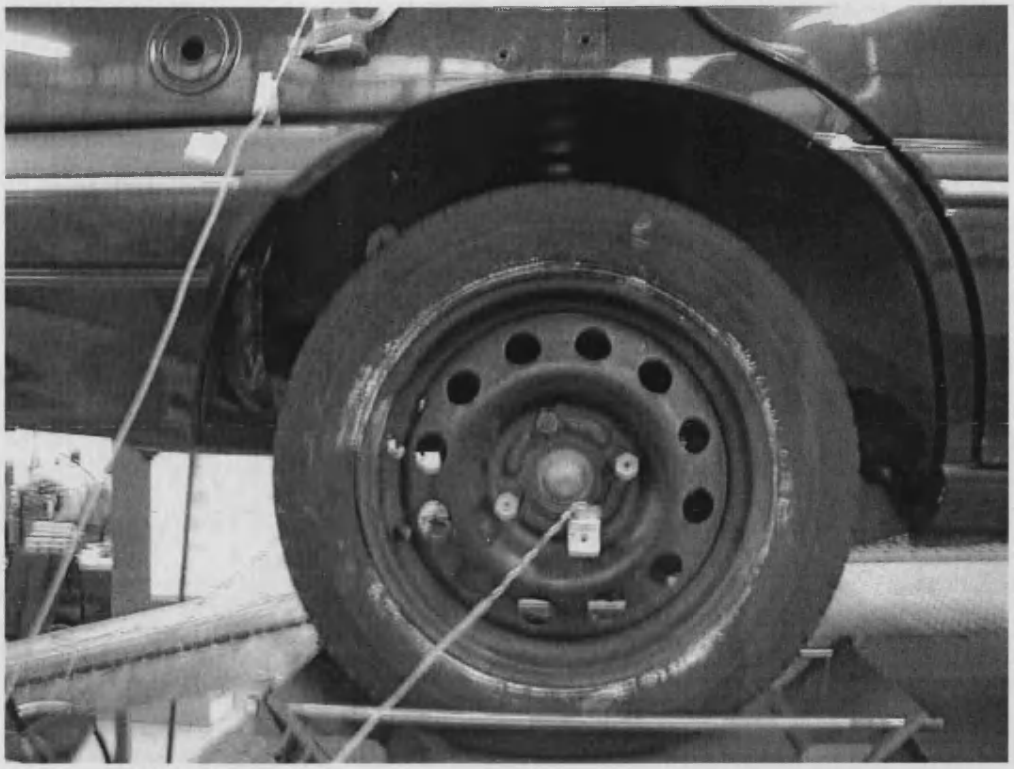

Figure 6.20 Friction damper installed on the car.

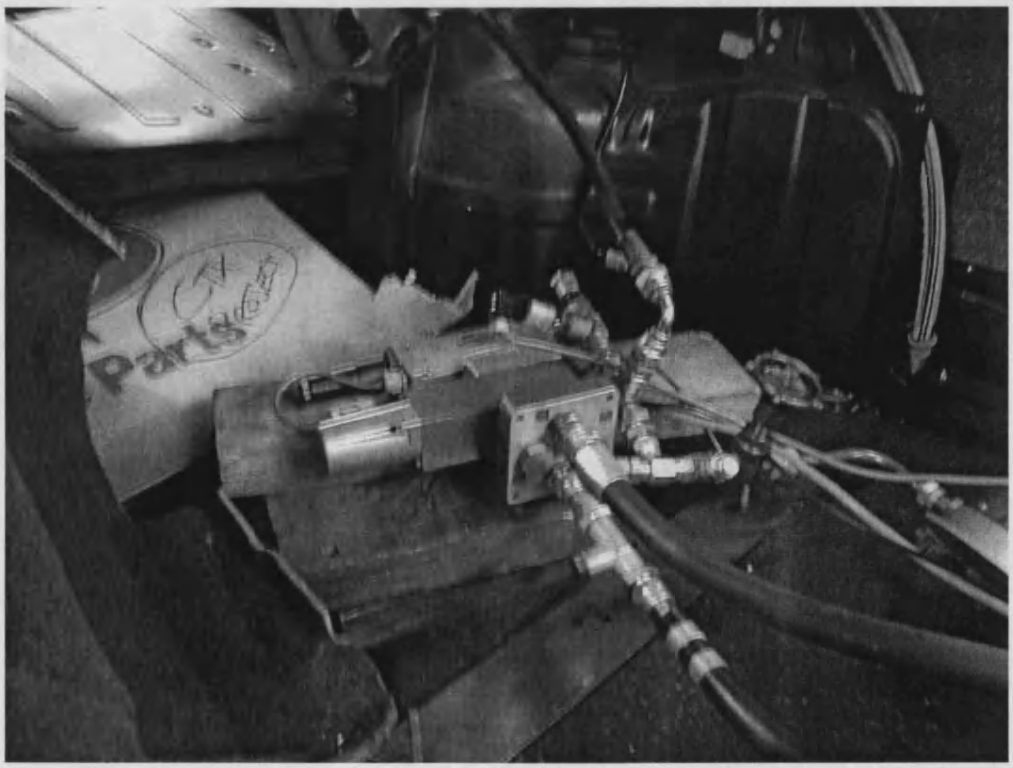

Figure 6.21 Control valve arrangement inside the boot.

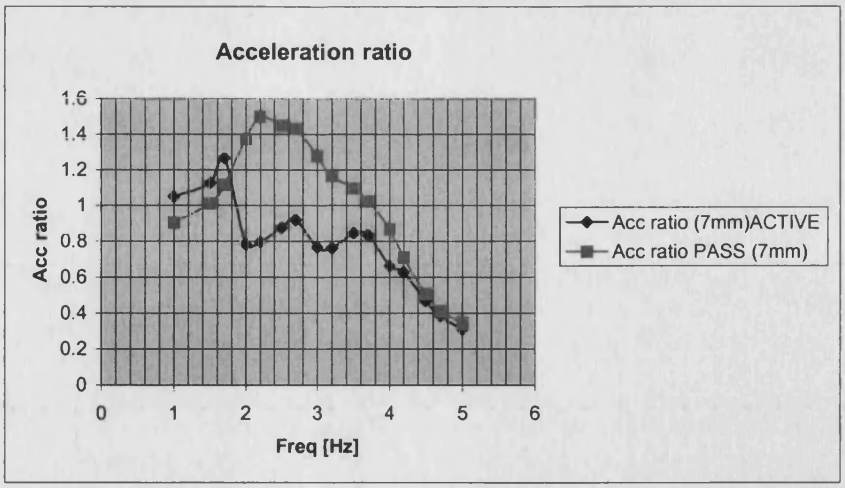

Figure 6.22 Acceleration ratio transmissibility for passive and semi-active systems. Sinusoidal input to one wheel; amplitude: 7 mm.

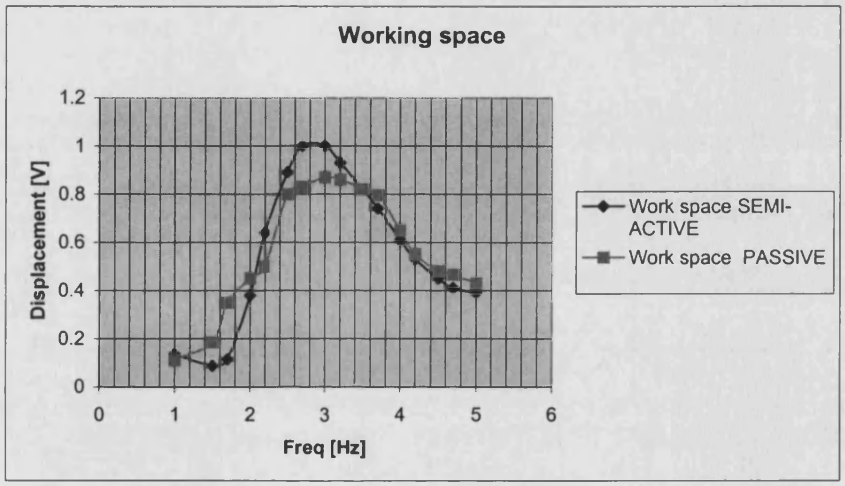

Figure 6.23 Working space for passive and semi-active systems. Sinusoidal input to one wheel; amplitude: 7 mm.

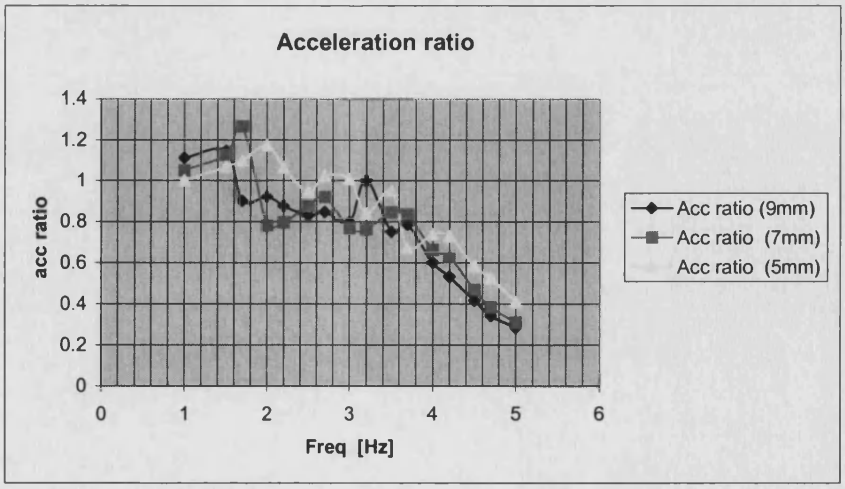

Figure 6.24 Acceleration ratio transmissibility for semi-active system. Sinusoidal input to one wheel; amplitude: 5 mm, 7 mm, 9 mm.

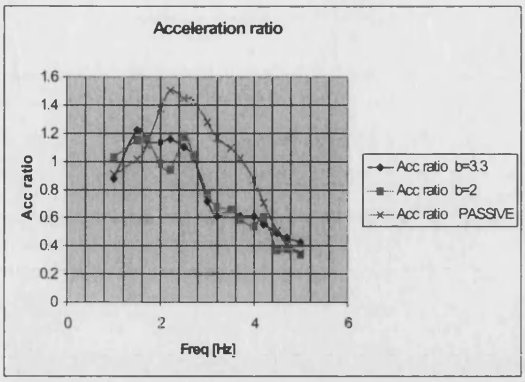

Figure 6.25 Acceleration ratio transmissibility for passive and semi-active systems; sinusoidal input to one wheel; amplitude: 7 mm.

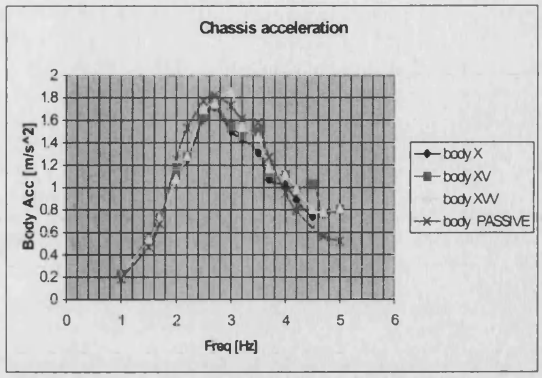

Figure 6.26 Chassis acceleration transmissibility for passive and semi-active systems; sinusoidal input to one wheel; amplitude: 7 mm.

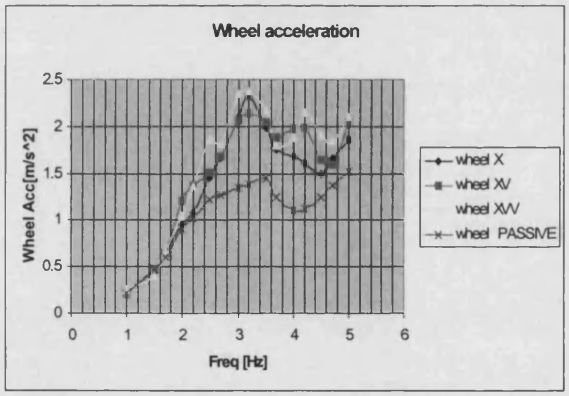

Figure 6.27 Wheel acceleration transmissibility for passive and semi-active systems; sinusoidal input to one wheel; amplitude: 7 mm.

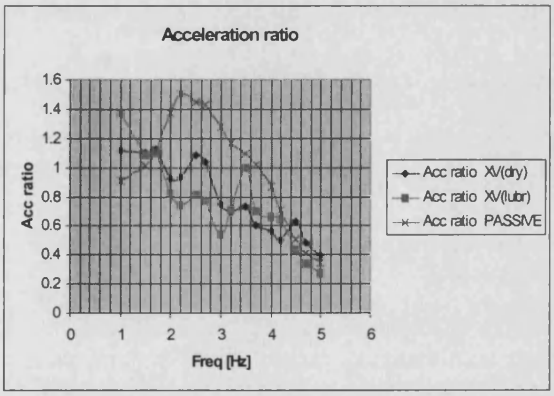

Figure 6.28 Acceleration ratio transmissibility with dry and lubricated friction; sinusoidal input to one wheel; amplitude: 7 mm.

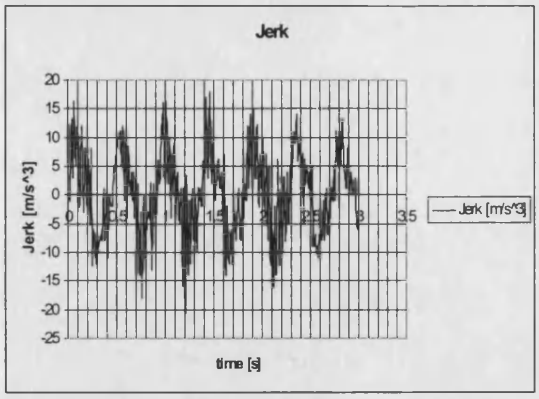

Figure 6.29 Experimental jerk (obtained numerically) for the passive system; sinusoidal input; amplitude 3 mm, frequency 2.2 Hz.

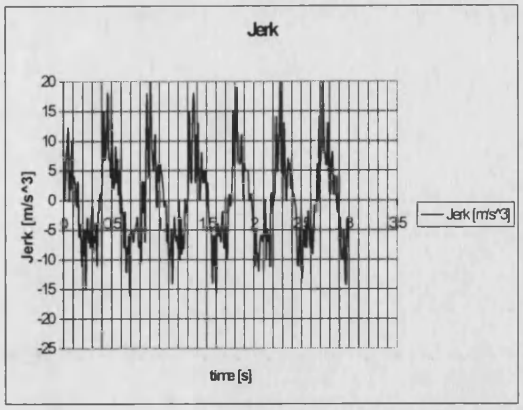

Figure 6.30 Experimental jerk (obtained numerically) for the controlled system; sinusoidal input; amplitude 3 mm, frequency 2.2 Hz.

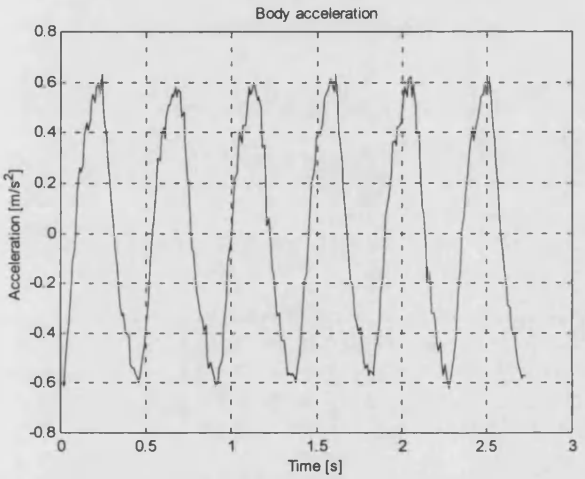

Figure 6.31 Experimental acceleration time trace for the passive system sinusoidal input: amplitude 3 mm, frequency 2.2 Hz.

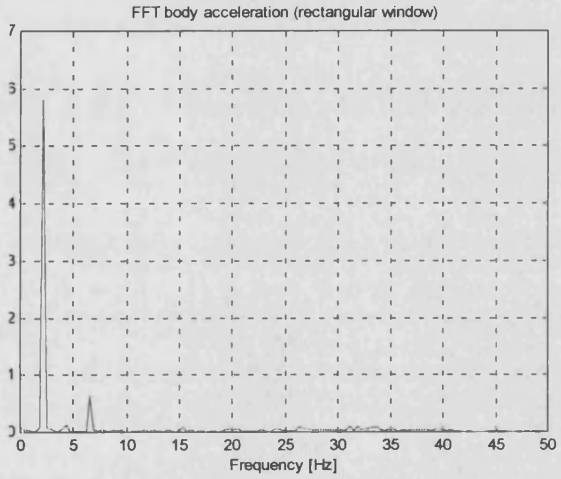

Figure 6.32 Experimental acceleration FFT for the passive system; sinusoidal input: amplitude 3 mm, frequency 2.2 Hz.

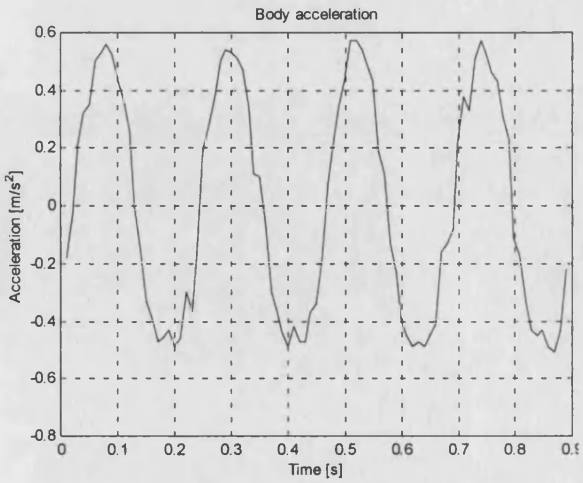

Figure 6.33 Experimental acceleration time trace for the passive system; sinusoidal input: amplitude 3 mm, frequency 4.5 Hz.

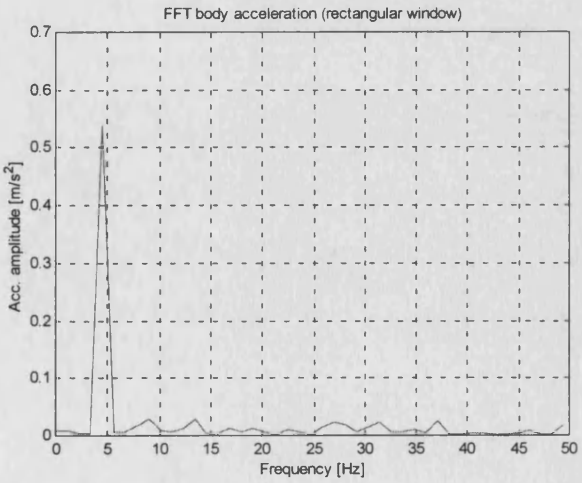

Figure 6.34 Experimental acceleration FFT for the passive system; sinusoidal input: amplitude 3 mm, frequency 4.5 Hz.

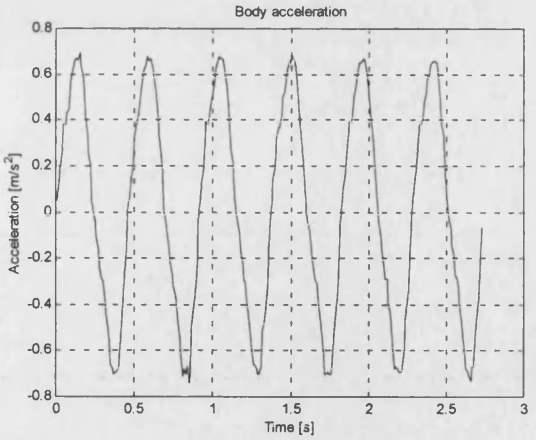

Figure 6.35 Experimental acceleration time trace for the controlled system; sinusoidal input; amplitude 3 mm, frequency 2.2 Hz.

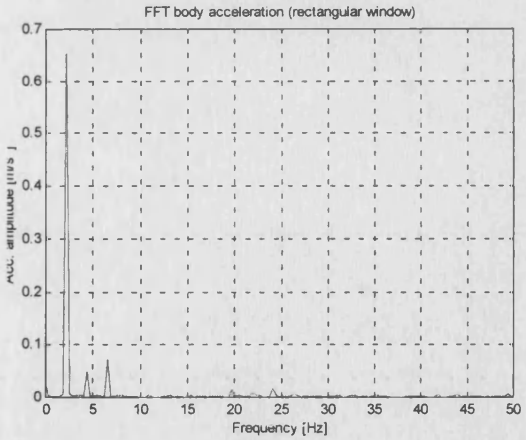

Figure 6.36 Experimental acceleration FFT for the controlled system; sinusoidal input; amplitude 3 mm, frequency 2.2 Hz.

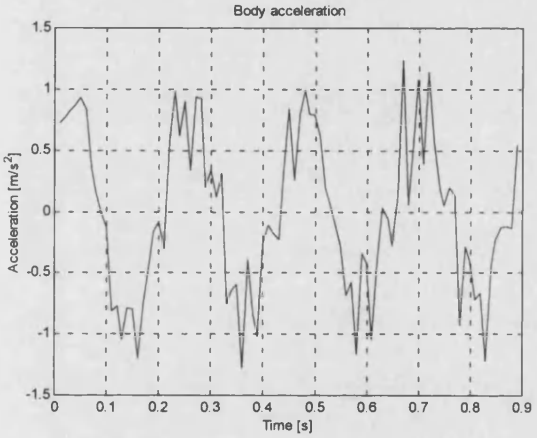

Figure 6.37 Experimental acceleration time trace for the controlled system; sinusoidal input; amplitude 3 mm, frequency 4.5 Hz.

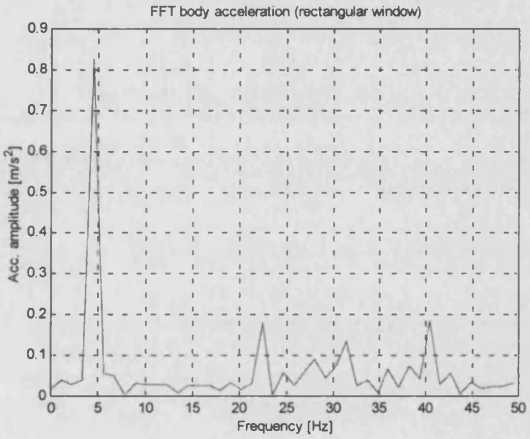

Figure 6.38 Experimental acceleration FFT for the controlled system; sinusoidal input; amplitude 3 mm, frequency 4.5 Hz.

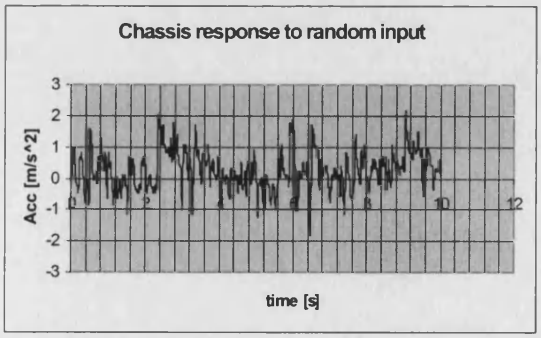

Figure 6.39 Semi- active chassis acceleration time trend; random input: 25-Hz filtered white noise.

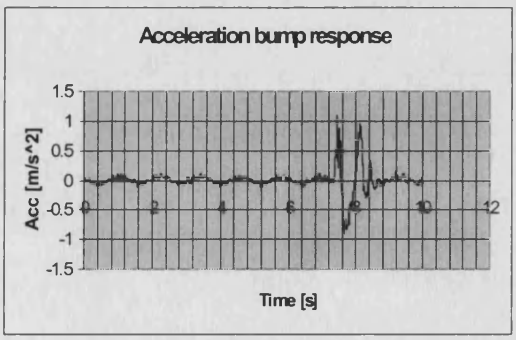

Figure 6.40 Bump response acceleration time trace for the controlled system.

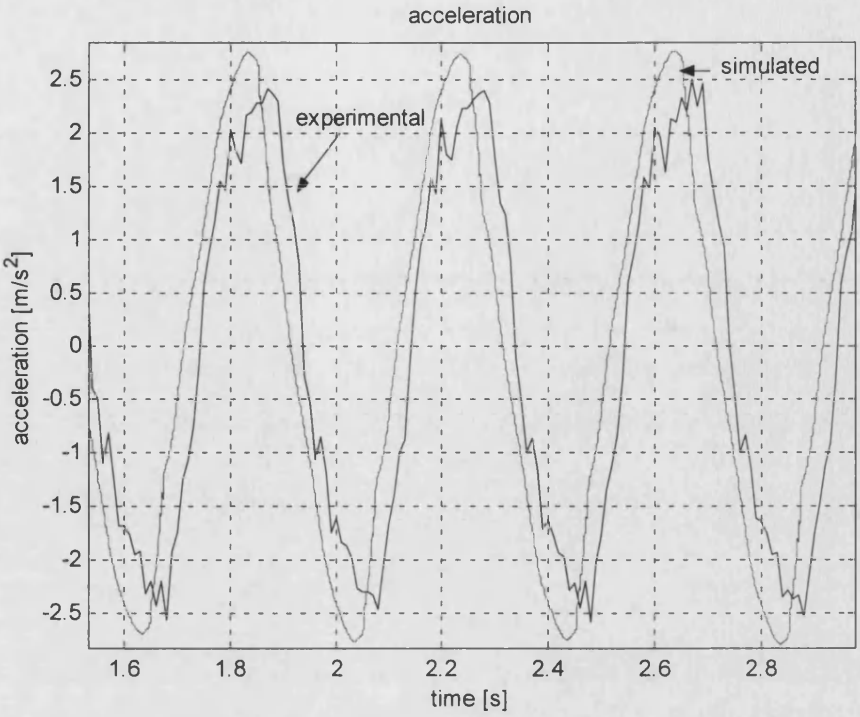

Figure 6.41 Rear-right semi-active acceleration; sinusoidal input to one wheel; amplitude: 7 mm; frequency 2.5 Hz.

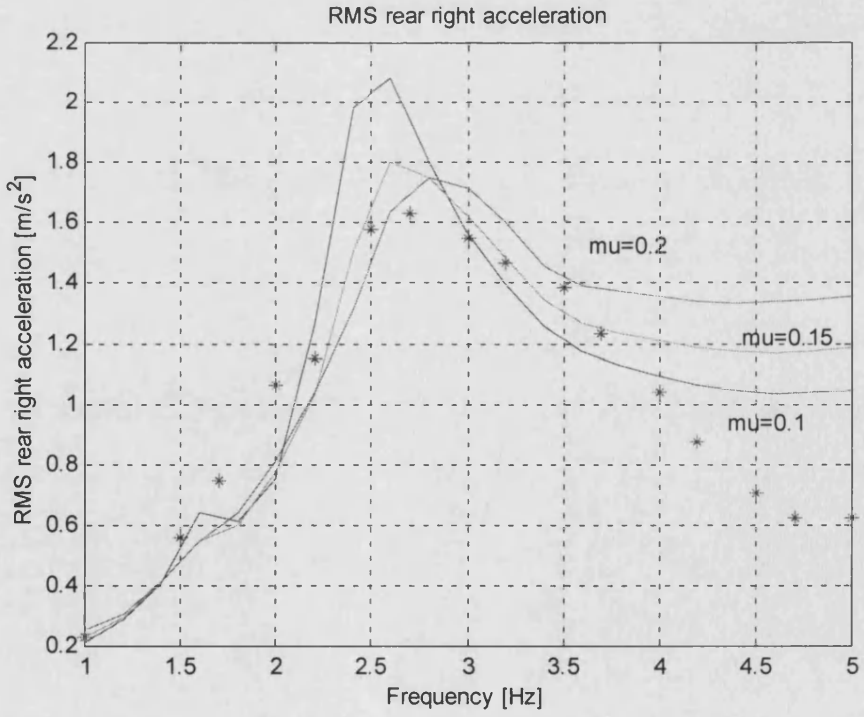

Figure 6.42 Rear-right semi-active acceleration frequency response varying friction coefficient; sinusoidal input to one wheel; amplitude: 7 mm.

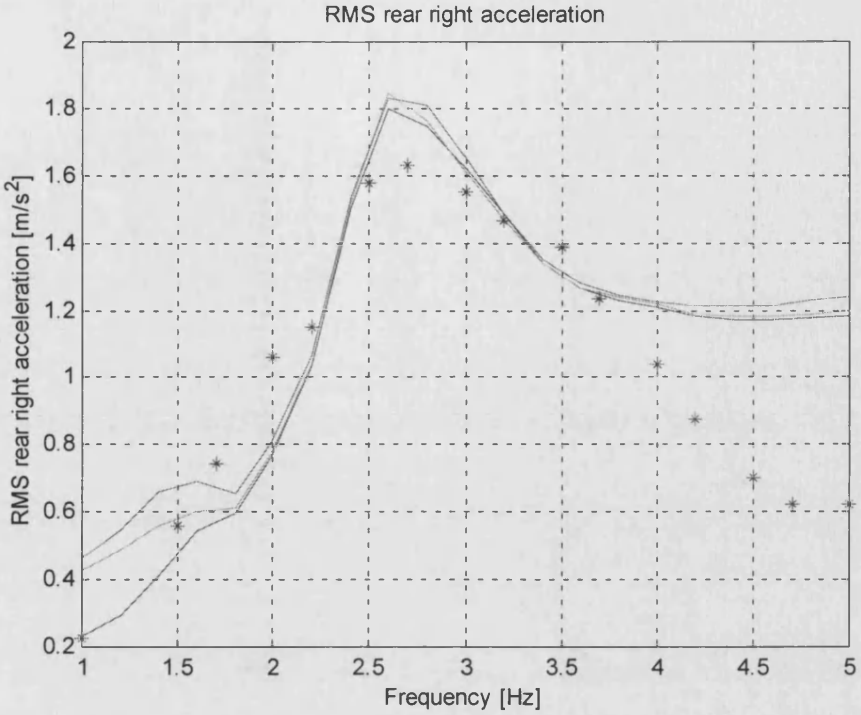

Figure 6.43 Rear-right semi-active acceleration frequency response varying "frictional memory"; sinusoidal input to one wheel; amplitude: 7 mm.

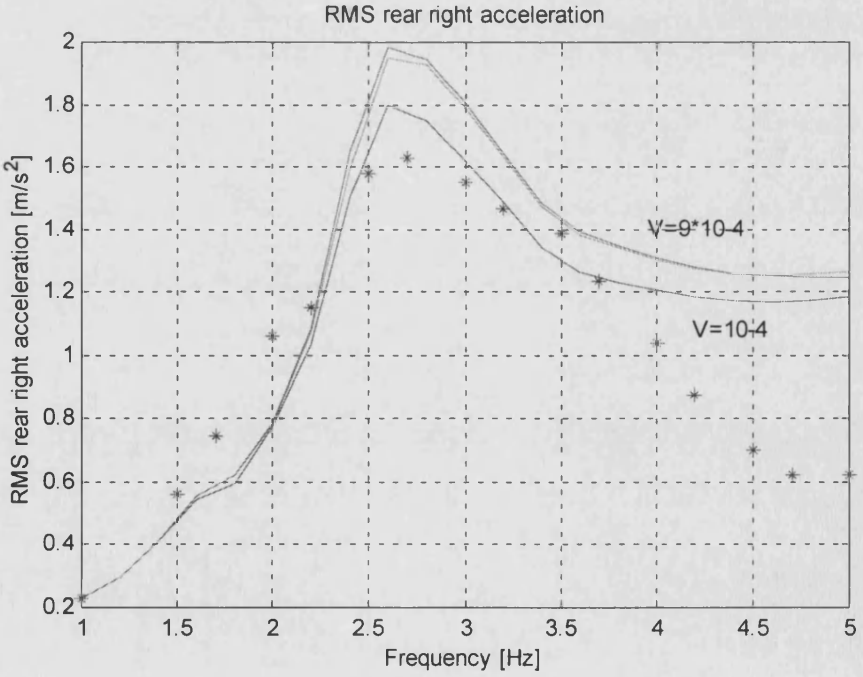

Figure 6.44 Rear-right semi-active acceleration frequency response varying volume; sinusoidal input to one wheel; amplitude: 7 mm.

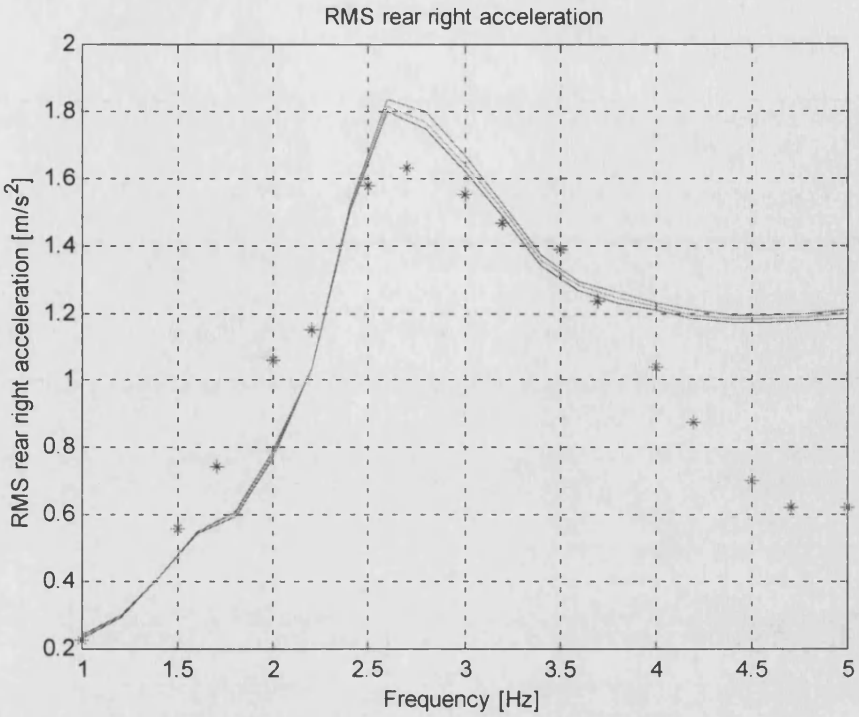

Figure 6.45 Rear-right semi-active acceleration; frequency response varying back-pressure; sinusoidal input to one wheel; amplitude: 7 mm.

7 MULTIVARIABLE CONTROLLER DESIGN AND SIMULATION

7.1 INTRODUCTION

So far the work has addressed modelling, designing and prototyping a single controlled friction damper unit. The physics and the performance of the novel damper, together with its hydraulic drive, have been extensively investigated, both numerically and experimentally. A comprehensive model of the system has been developed. The prototype damper has been experimentally tested and the experimental data obtained have been used to validate the mathematical model.

Following on from the single friction damper unit work, the subsequent step is the development of a controller for up to four friction dampers, constituting a semi-active car suspension. This implies an extension of the hydraulic drive and the design of a multivariable control law.

The behaviour of four dampers has been investigated only via computer simulation, assuming that the model, validated in the case of a single friction damper and a 7 DOF car model, would be sufficiently realistic for a preliminary study of a complete suspension system.

7.2 SOME GENERAL ISSUES ON THE MULTIVARIABLE CONTROLLER

Before proceeding to the design of the multivariable controller some general remarks on the characteristics, requirements and inherent limitations of a semi-active controller developed for a suspension system must be made. With regard to the hydraulic drive, one of the major issues is low-cost and this must be pursued with a design employing the minimum number of (ideally cheap) components. The minimal circuit configuration requires four proportional valves, supplied by a single pump in parallel with its relief

valve which sets the system pressure. Figure 1.5 shows a schematic of the hydraulic drive. As pointed out in chapter 1, other circuit configurations exist that provide pressure control; however some designs (employing pressure control relief valves for instance) would require a number of pumps equivalent to the number of control valves, thus increasing the overall cost.

As far as the control logic is concerned, some general properties of the multivariable controller must be outlined. The main vibrating modes in a car, which must be reduced, are heave (or bounce), roll and pitch. These modes are induced by road profile as well as by accelerating, braking (squat and dive, i.e. pitch) and cornering (roll).

1) According to a particular design, a controller can be more effective in controlling one or more modes, but it cannot perform equally well in response to all three modes and to their combinations (at most a controller can be designed which minimises some performance index of the weighted sum of the three modes).

2) Because the friction damper is not an active device, it cannot produce an anti-roll (or anti-pitch) moment, like for instance an active anti-roll bar.

3) For cost purposes and higher reliability, the number of transducers ought to be minimised. The minimal set of transducers in the current design is four displacement transducers, which measure working spaces at each corner; all the other quantities necessary for implementing the control law ought to be inferred from their measurements (preferably with small computational load).

4) The control law, generalising the previous control laws developed for the quarter car, is always of the variable structure, switched state feedback type. Such a control law can provide the required robustness in the control sense as well as to reduce the jerk content compared to a pure sliding mode law (Choi et al (2000)) and it can be implemented on a cheap processor board (not necessary a DSP). Furthermore different control laws can be readily obtained through tuning of the control gains.

7.3 MULTIVARIABLE CONTROLLER DESIGN

In section 7.2 it was stated that, depending on the design, different control schemes will be more effective in reducing different vibration modes. This is analogous to the 2 DOF quarter car model controllers, where the controlled responses have larger or smaller body acceleration or displacement (i.e. suspension working space), according to the degree of position or velocity feedback. Consider the 7 DOF model described by equation (3.3).

For each actuator the ith component of the control vector $\boldsymbol{u_2}$ is expressed by:

$$u_{2i}(\cdot) = F_{di}(\cdot) = -\mu F_{nij}(\cdot) sgn(\dot{z}_j - \dot{z}_{j+4}) \qquad (j=1...4) \tag{7.1}$$

$F_{nij}(\cdot)$ being the normal force diagonal matrix.

The natural extension of the scalar controller to the multivariable case is a control law, which performs force tracking on each corner of the car:

$$F_{nij} = a_{ij}(|\, z_j - z_{j+4} \,|) + b_{ij}(|\, \dot{z}_j - \dot{z}_{j+4} \,|) \quad \text{if } (z_j - z_{j+4})(\dot{z}_j - \dot{z}_{j+4}) \le 0 \tag{7.2a}$$

$$F_{nij} = g_{ij}(|\, \dot{z}_j - \dot{z}_{j+4} \,|) \quad \text{if } (z_j - z_{j+4})(\dot{z}_j - \dot{z}_{j+4}) > 0 \tag{7.2b}$$

$(j=1...4)$

$a_{ij}(\cdot)$, $b_{ij}(\cdot)$, $g_{ij}(\cdot)$ being state-dependent diagonal matrices.

The control law can be rewritten in more compact form, by defining the relative sprung-unsprung mass displacement vector $\boldsymbol{x}_{ws} \in \Re^4$ as:

$$\boldsymbol{x}_{ws} = [x_1, x_2, x_3, x_4]^T \tag{7.3}$$

where $x_j = z_j - z_{j+4} \quad (j=1...4)$

The control vector $\boldsymbol{u_2}$ can be written as:

$$u_2 = -\mu F_n \, sgn(\dot{x}_{ws}) \tag{7.4}$$

and equation (7.2) as:

$$F_{nij} = a_{ij}(|x_j|) + b_{ij}(|\dot{x}_j|) \quad \text{if} \quad x_j \dot{x}_j \leq 0 \tag{7.5a}$$

$$F_{nij} = g_{ij}(|\dot{x}_j|) \quad \text{if} \quad x_j \dot{x}_j > 0 \tag{7.5b}$$

Equation (7.5) hence becomes the natural multivariable extension of the scalar control law. This controller is aimed to control bounce motion. Nevertheless it affects pitch and roll as well; in fact pitch and roll angles are related to vertical displacements by:

$$\alpha = \frac{(z_3 + z_4) - (z_1 + z_2)}{2(a+b)} \tag{7.6}$$

$$\beta = \frac{z_1 - z_2}{2d'} \tag{7.7}$$

or equivalently

$$\beta = \frac{z_3 - z_4}{2d''} \tag{7.8}$$

The controlled variables, whose values must be reduced, are now the CG acceleration, roll and pitch angles, working spaces and dynamic tyre forces at each corner.

7.4 MULTIVARIABLE CONTROLLER SIMULATION

After having developed the controller for a single friction damper and having experimentally validated it (the validation was carried out against the 7 DOF car model for more precision), the simulation of a full semi-active system constituted of four independent friction dampers is presented, employing the multivariable control logic described previously.

The analysis of the results follows the approach adopted in the 2 DOF quarter car study. At first the response to sinusoidal inputs and subsequently the pseudo-random and the bump responses are investigated. Different types of sinusoidal disturbances can be applied to the 7 DOF car model: either pure heave, roll or pitch or any combination of these modes. A choice was made for an input resembling that applied to the tyres when the vehicle is driven on a straight road at a constant forward velocity V. This input excites both bounce and pitch modes. A pure roll input disturbance was subsequently applied, in order to test roll response.

The first input can be described by the following equations:

$$z_{01}(t) = A\sin(2\pi ft) \tag{7.9a}$$

$$z_{02}(t) = A\sin(2\pi ft) \tag{7.9b}$$

$$z_{03}(t-T) = A\sin[2\pi f(t-T)] \tag{7.9c}$$

$$z_{04}(t-T) = A\sin[2\pi f(t-T)] \tag{7.9d}$$

where the delay time between front and rear wheels is $T = \frac{a+b}{V}$.

Defining λ as the road wavelength, it follows that the spatial frequency Ω is its reciprocal i.e. $\Omega = 1/\lambda$, while the temporal frequency f is expressed by $f = \Omega V = V/\lambda$. Hence equations (7.9a-b-c-d) can be written as:

$$z_{01}(t) = A\sin(\frac{2\pi V}{\lambda} t) \tag{7.10a}$$

$$z_{02}(t) = A\sin(\frac{2\pi V}{\lambda} t) \tag{7.10b}$$

$$z_{03}(t-T) = A\sin[\frac{2\pi V}{\lambda} t - \frac{2\pi(a+b)}{\lambda}] \tag{7.10c}$$

$$z_{04}(t-T) = A\sin[\frac{2\pi V}{\lambda} t - \frac{2\pi(a+b)}{\lambda}] \tag{7.10d}$$

The multivariable controller is expressed by (7.4). In this preliminary simulation study for ease only the case $a_{ij} = diag(k_1|x_1|, k_1|x_2|, k_2|x_3|, k_2|x_4|)$, $b_{ij} = 0$ and $g_{ij} = 0$ is

considered. This is the vector equivalent of the "balance logic" (pure position-damping) in the scalar case. The sinusoidal road input has an amplitude of 2 cm.

Figure 7.1 depicts the Centre of Gravity (CG) chassis acceleration: a RMS reduction is obtained close to the first two resonances (at about 1.2 Hz and 2.6 Hz) and a worsening for frequencies higher than 3.5 Hz. This is slightly different from the scalar case (figure 5.4), where the controlled response was always better than the passive. The CG chassis displacement is reduced over the whole range of frequencies investigated, as portrayed in figure 7.2. As far as the pitch angle response is concerned (figure 7.3), the car equipped with the semi-active suspension presents a RMS pitch angle smaller than the passive one, over all the frequency range of interest. Figure 7.4 depicts dynamic tyre force for the rear-right wheel and shows a reduction of the force up to 4.3 Hz. At higher frequencies instead the passive system behaves better. This latter result shows that the force tracking controller produces a reduction of both acceleration and displacement.

It is not possible to evaluate the roll performance with this input since roll is negligible (ideally zero in the passive system). Therefore a simulation with a 2-cm sinusoidal pure roll input has been performed. In this case the CG vertical displacement is negligible as well as the pitch. Roll angle response is depicted in figure 7.5: roll is slightly larger up to 1.4 Hz, but for higher frequencies is reduced with respect to the passive case. Analogous conclusions can be drawn for rear-right acceleration (figure 7.6). Therefore an overall roll reduction in the highest frequency range has been obtained even though the controller was not designed according to any roll minimisation criterion. However working space and dynamic tyre force (figures 7.7 and 7.8) show an increase when a roll input is applied.

Consider now the time trends. Figure 7.9 depicts the CG acceleration at a frequency of 1.5 Hz. The trend is relatively smooth, despite the controller switching action, thus resulting in a reasonably comfortable ride. The cross-coupled dynamics of the car act as a sort of filter. The CG displacement (figure 7.10) is fairly smooth as well. The local accelerations at each corner are by far much jerkier (see figure 7.12 for instance) than the CG acceleration.

Figures 7.11 and 7.12 show the time histories of roll angle and of the rear-right acceleration in response to a roll input. Roll angle trend is fairly smooth whereas acceleration is somewhat spiky.

The next input test is the random input. Front wheel input is expressed by equation (7.10) and rear input is given by the delayed front input. Figures 7.13 and 7.14 depict CG acceleration time trends for passive and semi-active systems. Table 7.1 summarises the main results. It shows the RMS and peak values at a speed of 50 km/h.

Table 7.1: RMS and peak value acceleration and displacement for random input

CONTROLLER	RMS CG acceleration [m/s^2]	Max and min PEAK acceleration [m/s^2]
Passive	0.78	2.38/-1.55
Semi-active	0.87	2.49/-1.80
CONTROLLER	RMS CG displacement [cm]	Max and min PEAK displacement [cm]
Input	0.71	1.27/-1.63
Passive	0.96	1.62/-1.72
Semi-active	0.73	1.12/-1.38

Controlled response is better in terms of CG displacement but not of CG acceleration.

Finally the bump input test has been carried out. The peak value is 5 cm and the car is taken to pass over the bump with only rear-right wheel at the constant speed of 20 km/h as in the quarter car case. Figure 7.15 shows the rear-right and rear-left corner accelerations in the passive case and figure 7.16 in the semi-active case; peak values are reported in table 7.2.

Table 7.2: Peak value acceleration for bump input

CONTROLLER	Max PEAK acceleration [m/s^2]	Min PEAK acceleration [m/s^2]
Passive (right)	14.36	-15.61
Semi-active (right)	14.40	-15.75
Passive (left)	10.87	-15.18
Semi-active (left)	13.94	-17.96

The overall controlled bump response is not actually improved with respect to the passive response: the overshoot is only slightly smaller than the passive one and the undershoot higher and furthermore the number of oscillations is the same. In the quarter car case a net improvement was obtained. The cross-coupled car dynamics are the main reason; however as previously said the bump test must be judged with particular care.

The scheme simulated was a generalisation of the "balance logic". Such a logic aims to reduce bounce. The addition of some pseudo-viscous damping would have led to more or less similar results.

Other logic can be designed with the purpose of reducing roll or pitch. The semi-active system cannot create an anti-roll or anti-pitch moment. However schemes based on the measurement of roll angle or pitch angle (either via displacement transducers or accelerometers) and the consequent stiffening of the appropriate suspension units would be possible.

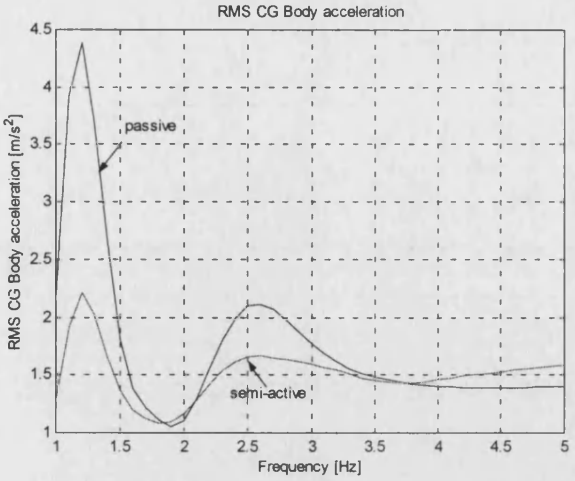

Figure 7.1 RMS CG chassis acceleration transmissibility curves. Controller defined by equation (7.5); sinusoidal input; amplitude: 2 cm.

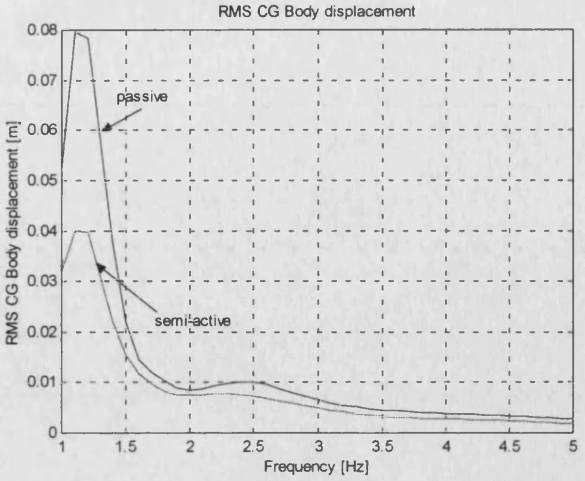

Figure 7.2 RMS CG chassis displacement transmissibility curves. Controller defined by equation (7.5); sinusoidal input; amplitude: 2 cm.

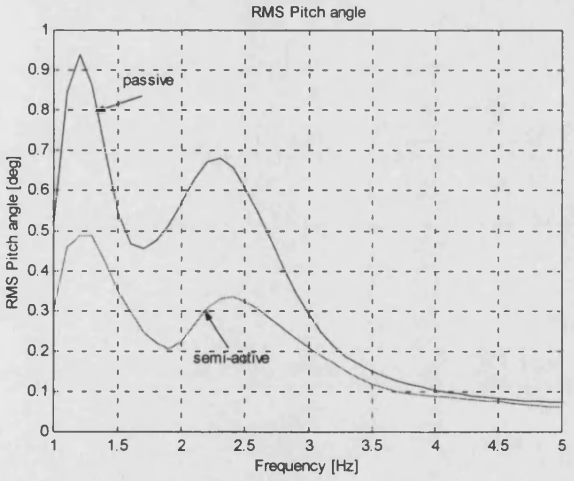

Figure 7.3 RMS pitch angle transmissibility curves. Controller defined by equation (7.5); sinusoidal input; amplitude: 2 cm.

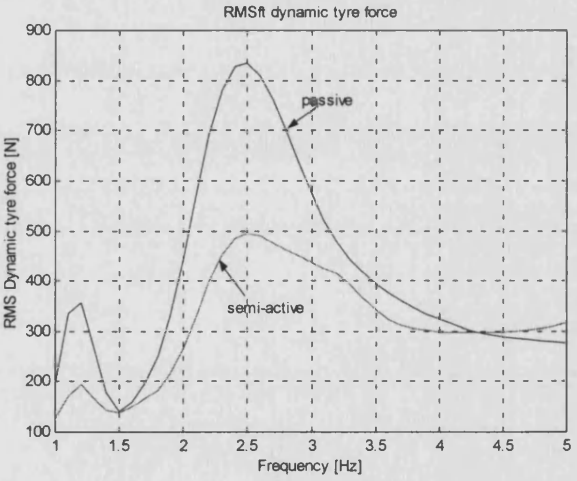

Figure 7.4 RMS dynamic tyre force transmissibility curves. Controller defined by equation (7.5); sinusoidal input; amplitude: 2 cm.

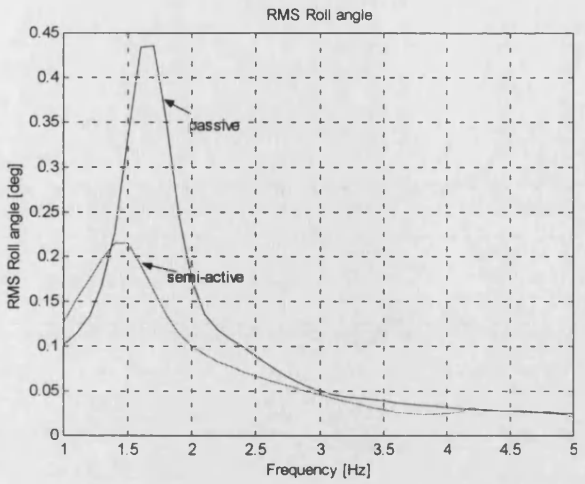

Figure 7.5 RMS roll angle transmissibility curves for a pure roll input. Controller defined by equation (7.5); sinusoidal input; amplitude: 2 cm.

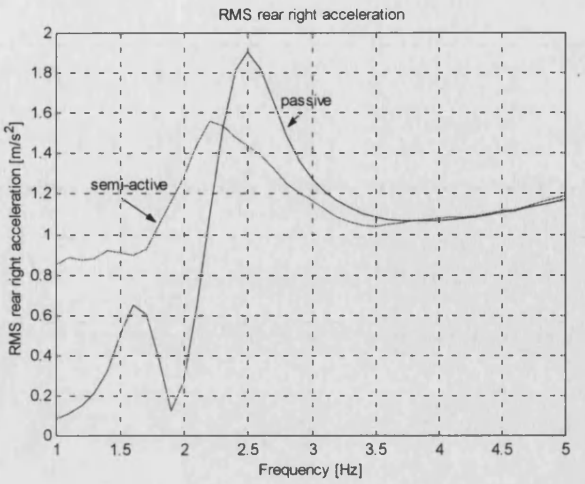

Figure 7.6 RMS rear right body acceleration transmissibility curves for a pure roll input. Controller defined by equation (7.5); sinusoidal input; amplitude: 2 cm.

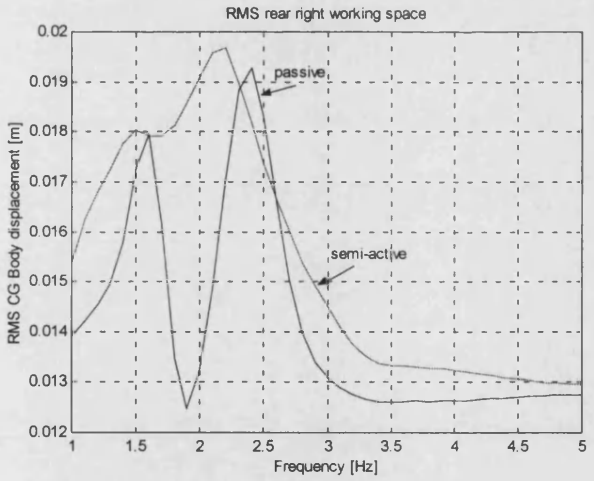

Figure 7.7 RMS rear-right working space transmissibility curves for a pure roll input. Controller defined by equation (7.5); sinusoidal input; amplitude: 2 cm.

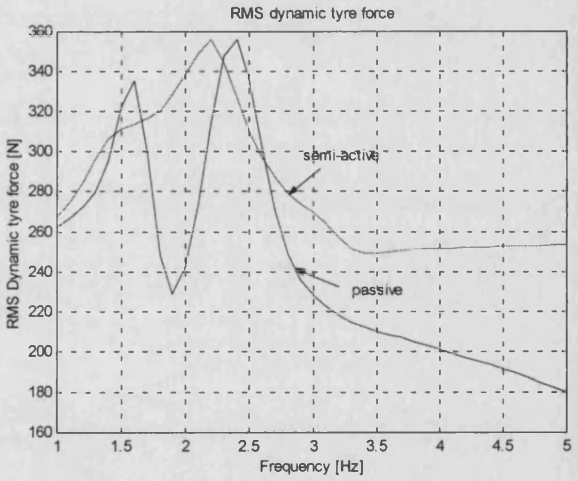

Figure 7.8 RMS dynamic tyre force transmissibility curves for a pure roll input. Controller defined by equation (7.5); sinusoidal input; amplitude: 2 cm.

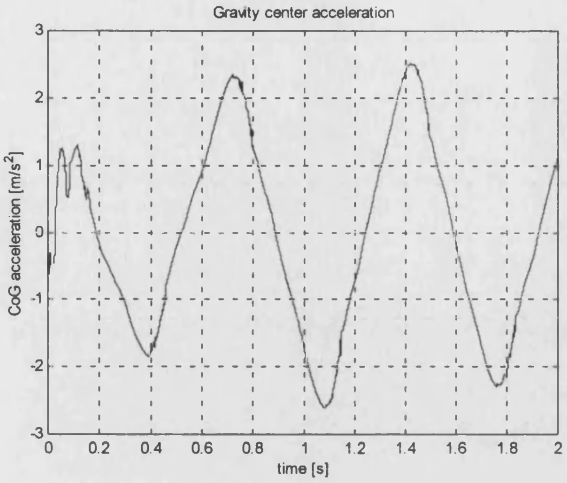

Figure 7.9 Time history of CG acceleration. Controller defined by equation (7.5); sinusoidal input; amplitude: 2 cm.

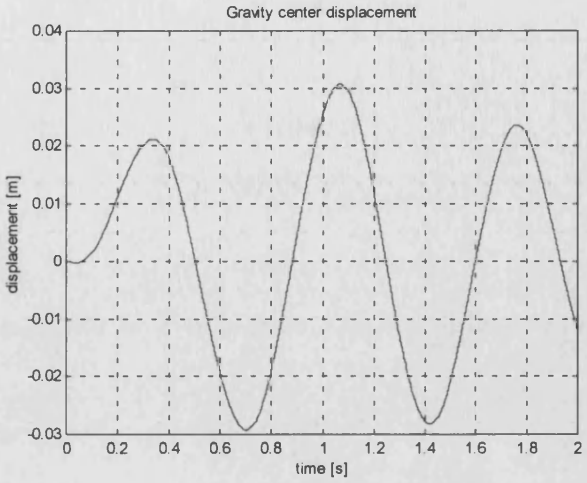

Figure 7.10 Time history of CG displacement. Controller defined by equation (7.5) sinusoidal input; amplitude: 2 cm.

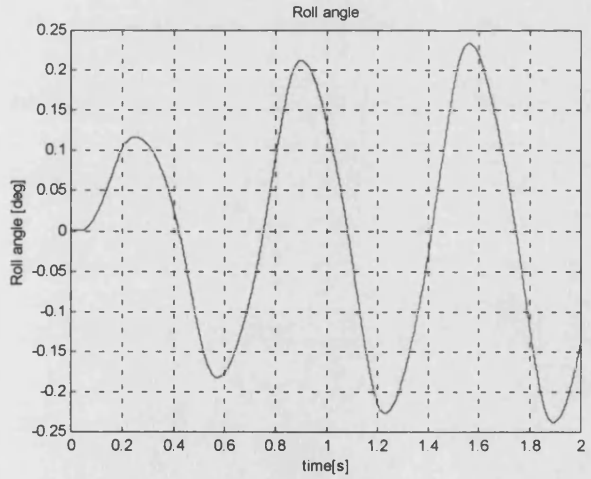

Figure 7.11 Time history of CG roll angle. Controller defined by equation (7.5). Sinusoidal roll input; amplitude: 2 cm.

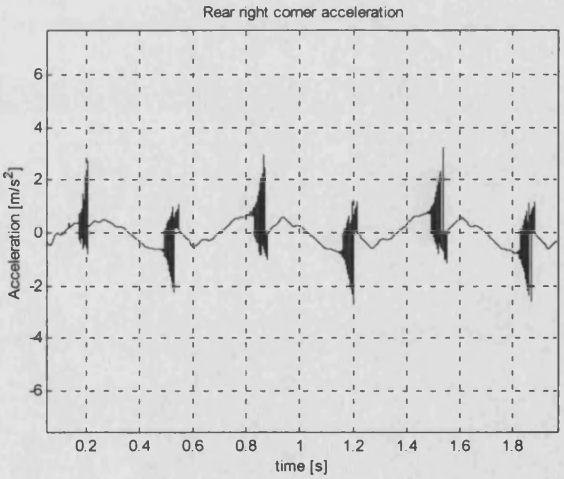

Figure 7.12 Time history of rear-right body acceleration. Controller defined by equation (7.5). Sinusoidal roll input; amplitude: 2 cm.

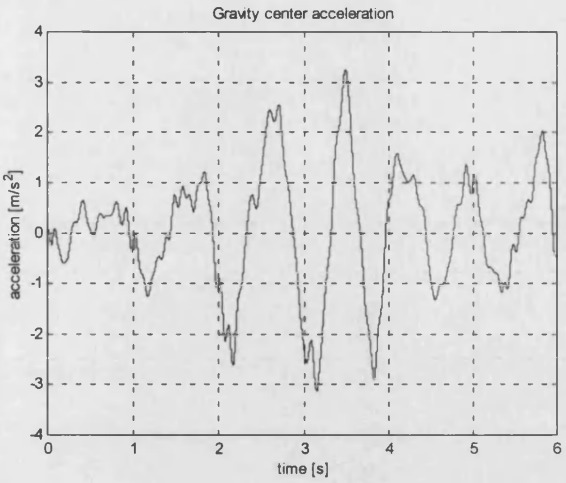

Figure 7.13 CG acceleration time history for random input; passive system.

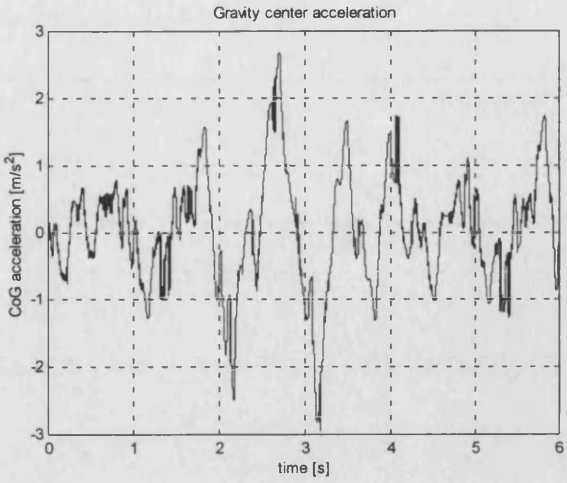

Figure 7.14 CG acceleration time history for random input; semi-active system. Controller defined by equation (7.5).

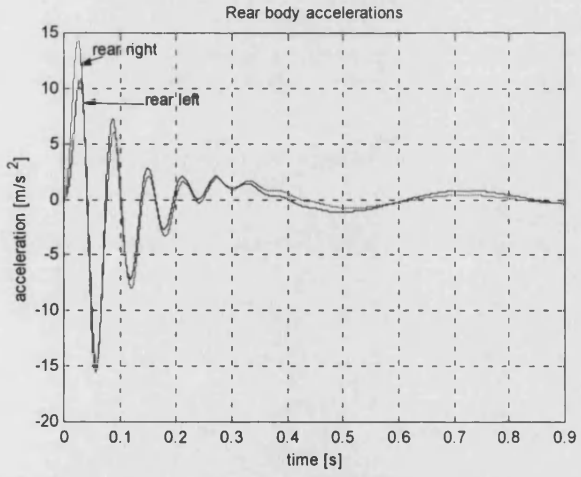

Figure 7.15 Rear acceleration time histories for bump input; amplitude 5 cm; passive system.

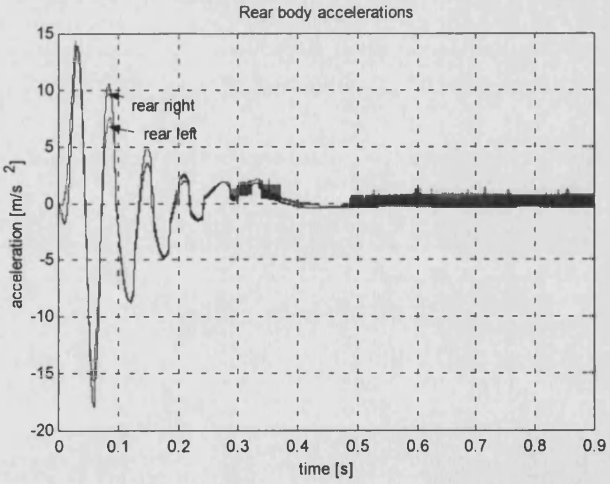

Figure 7.16 Rear acceleration time histories for bump input; amplitude 5 cm. Controller defined by equation (7.5).

8 CONCLUSIONS

8.1 INTRODUCTION

The objective of the project has been to prove the effectiveness of a controlled friction damper as an alternative to a viscous damper in a vehicle suspension application. This final chapter summarises and analyses critically the main results obtained together with the main problems encountered in the course of this work and how they have been tackled. Finally some hints for a possible development of the research are given.

8.2 GENERAL CONCLUSIONS

8.2.1 Conclusions on modelling and simulation

Models of the hydraulically actuated friction damper and of the vehicle have been developed and performance simulated numerically. An experimental validation of the simulation study has been undertaken on the various subsystems and on the whole system. The model of the hydraulic drive describes the measured behaviour very well. The leakage model employed is effective in predicting the actual pressure gain. The issue of potential air trapped in the oil, which created a dependency of the frequency response with pressure was tackled by reducing the value for bulk modulus in the simulation.

The model of the car is approximate in various aspects; particularly so as far as the modelling of the real characteristics of viscous dampers are concerned. On the other side, the linear model permits the use of the state space matrix representation and this was helpful for the multivariable controller design.

Handling behaviour (e.g. steering input and tyre lateral forces) has not been modelled, because the purpose of the investigation was not to assess the handling performance of the car (which could not be experimentally tested on the four-poster shaker).

The semi-active system model works reasonably well in terms of time domain response. The time responses, particularly chassis acceleration, are very accurate.

The frequency response matches the experimental data well up to the chassis resonance; at higher frequencies the results are overestimated because of the poor modelling of the residual viscous damping as well as of the linear model for the other three viscous dampers.

The main aim of the validation is to ascertain whether the model is reliable in the frequency range of interest and whether it can be reliably used for further investigations. At the conclusion of the validation process, it can be stated that the hydraulic model is accurate enough and can be readily extended, increasing the number of control valves, to represent a drive for two or four independently controlled friction dampers. Although the vehicle model grasps the principal modes of the car, it would need some further refinements such as the inclusion of the nonlinear characteristics of dampers and of the tyres and in a further stage also handling dynamics.

8.2.2 Conclusions on the control logic

With regard to the control logic, the simulation work has shown that a pure switching sliding mode controller is not appropriate for controlling the friction damper, the main reason being the high chattering that spoils the performance of the controller. The inherent limitation of the friction damper does not permit full advantage to be taken of the sliding mode control.

Switched state feedback has found to be more appropriate for the application. The controller performed a force tracking control. The controller has been not designed to achieve perfect tracking (in the intervals when it is on). In order to do so, a more complicated logic would be necessary which uses for instance an inverse model of the hydraulic drive, but this would make the logic extremely complicated and probably the overall benefit would be small. In fact in the suspension application it is not so crucial to have a good instantaneous tracking, as for instance it is typically required in pointing applications or in robotics. The non-perfect tracking does not affect RMS values very much. In control terms it could be said that it is necessary to reduce the integral of the absolute value of the error (assuming that zero error means perfect tracking) rather than its instantaneous value.

Reduction in chassis acceleration and working space has been obtained; on the other side dynamic tyre force was generally higher.

The uncertainty of the friction coefficient revealed to be a less important problem than expected. Tests carried out in dry and lubricated regime produced positive results in both cases.

The major problem that arose in the course of the experimental work (and unpredictable on the basis of only a simulation study) was the limited valve bandwidth at low pressure. This required an increase of the supply pressure with a subsequent increase of the power dissipated. The trade-off between power consumption and bandwidth is a serious problem. The problem can be addressed firstly by minimising the volumes which were shown to deeply affect the bandwidth by mounting the valve as close as possible to the damper (ideally inside it). The problem of the air trapped inside is more critical. The physical layout of the system must be opportunely designed so as to prevent the formation of air pockets within the system.

These unexpected difficulties on the valve have allowed some insights to be gained on the low-pressure behaviour of hydraulic systems. Hydraulic systems usually have higher working pressure and the behaviour at lower pressure in not usually investigated.

Passing to the multivariable control of four dampers, only a simulation study has been undertaken. The simulation has shown that the switched state feedback as implemented in the quarter car case does not produce as much improvement as in that case. Other control logic should be developed, namely anti-roll or anti-pitch strategies, based on the reduction of roll and pitch angles (possibly using these quantities in the feedback loop).

8.3 GUIDELINES FOR FUTURE WORK

The natural extension of what has been done so far is the control extended to the whole suspension system of the car. The natural extension is the installation of the second rear friction damper. The use of two dampers will allow anti-roll control strategies to be studied experimentally. The extension to the full suspension system is the final step.

After a thorough investigation of the ride performance of a full suspension system, it is necessary to investigate the handling behaviour of the car. This would involve the development of a handling model or better a model including both ride and handling variables and some road tests (steering, bends, U-turns etc).

The investigation has addressed a saloon car application. However it must be remarked that heavy vehicles (coaches, trains, lorries) or off-road vehicles, rather than saloon cars, are probably the most suitable for this kind of controlled suspensions, both in terms of feasibility and costs.

With regard to the control aspects, robust control techniques have been investigated thoroughly in the single damper system. It would be interesting to compare the performance with an adaptive controller.

As far as the multivariable controller is concerned, some work must be done on designing anti-roll or anti-pitch controllers.

A last word on the development of an integrated design approach for further improvements. Many car models are available (some of them extremely sophisticated), which have been developed with multibody techniques, and ad-hoc codes (such as ADAMS) exist. Not all the car simulation packages easily allow non-conventional elements such as controlled dampers to be introduced in the model. The incorporation of one or more hydraulically actuated friction damper models in one of these, would produce a realistic model which, integrated in an automotive software environment, would produce an effective and flexible tool for more refined analysis and further improvements.

After having fully ascertained the benefits offered by this type of suspension, a complementary line of research is concerned with the mechanical design of the friction damper itself; its design can be optimised through an opportune choice of materials and a more refined structural design, using computer aided tools that can help sizing the device more economically. The damping properties of rubber bushes and all the other joints must be considered as well, since finally the overall static friction characteristics of the system depends also on them.

A completely different field of investigation for friction damper is in structural applications. The problem is similar in principle although specification of the control is

very different. A small-scale model of a building should be designed as well in order to carry out some experimental work.

APPENDIX A

THE 7 DOF CAR MODEL

Equation (3.3), modelling the 7 DOF ride car model, is obtained here using the Lagrangian approach (Sireteanu et al (1990), Rao (1995)).

Let $\boldsymbol{q}$ be the vector of generalised co-ordinates:

$$\boldsymbol{q} = [q_1, q_2, q_3, q_4, q_5, q_6, q_7]^T \tag{A.1}$$

with the following choice of co-ordinates (figure 3.2):

$$q_1 = z\,;\ q_2 = z_5\,;\ q_3 = z_6\,;\ q_4 = z''\,;\ q_5 = \alpha\,;\ q_6 = \beta\,;\ q_7 = \beta'' \tag{A.2}$$

Defining the vertical displacement vector (the vertical displacements are not all independent):

$$\boldsymbol{z} = [z_1, z_2, z_3, z_4, z_5, z_6, z_7, z_8]^T \tag{A.3}$$

it is possible to write:

$$\boldsymbol{z} = \boldsymbol{P}\boldsymbol{q} \tag{A.4}$$

with $\boldsymbol{P}$ being defined as:

$$\boldsymbol{P} = \begin{bmatrix} 1 & 0 & 0 & 0 & -a & d' & 0 \\ 1 & 0 & 0 & 0 & -a & -d' & 0 \\ 1 & 0 & 0 & 0 & b & d'' & 0 \\ 1 & 0 & 0 & 0 & b & -d'' & 0 \\ 0 & 1 & 0 & 0 & 0 & 0 & 0 \\ 0 & 0 & 1 & 0 & 0 & 0 & 0 \\ 0 & 0 & 0 & 1 & 0 & 0 & \frac{E}{2} \\ 0 & 0 & 0 & 1 & 0 & 0 & -\frac{E}{2} \end{bmatrix} \tag{A.5}$$

The disturbance vector z_0 is then defined:

$$z_0 = [z_{01}, z_{02}, z_{03}, z_{04}]^T \tag{A.6}$$

The Lagrange equations, expressed as function of the kinetic energy (not of the Lagrangian function) are:

$$\frac{d}{dt}\frac{\partial T}{\partial \dot{q}_k} - \frac{\partial T}{\partial q_k} = g_k \quad (k=1...7) \tag{A.7}$$

where T is the total kinetic energy of the system, defined by the quadratic form:

$$T = \frac{1}{2}\dot{\boldsymbol{q}}^T \boldsymbol{M}\dot{\boldsymbol{q}} \tag{A.8}$$

$\boldsymbol{M}$ being the mass matrix:

$$\boldsymbol{M} = diag(m, m_1, m_1, m_2, J_\alpha, J_\beta, J_{\beta'}) \tag{A.9}$$

The right-hand side of equation (A.7) is defined as:

$$g_k = \sum_{i=1}^{8} f_i \frac{\partial x_i}{\partial q_k} \qquad (k=1...7) \tag{A.10}$$

Defining the vector $\boldsymbol{f}$ of the forces applied to sprung and unsprung mass:

$$\boldsymbol{f} = [f_1, f_2, f_3, f_4, f_5, f_6, f_7, f_8]^T \tag{A.11}$$

The forces applied to sprung and unsprung mass are:

$$\boldsymbol{f} = -[\boldsymbol{K}z + \boldsymbol{C}\dot{z} + \boldsymbol{K}_0 z_0 + \boldsymbol{C}_0 \dot{z}_0] \tag{A.12}$$

where $\boldsymbol{K}$ is the stiffness matrix:

$$\boldsymbol{K} = \begin{bmatrix} k_1 & 0 & 0 & 0 & -k_1 & 0 & 0 & 0 \\ 0 & k_1 & 0 & 0 & 0 & -k_1 & 0 & 0 \\ 0 & 0 & k_2 & 0 & 0 & 0 & -k_2 & 0 \\ 0 & 0 & 0 & k_2 & 0 & 0 & 0 & -k_2 \\ -k_1 & 0 & 0 & 0 & k_1+k_{01} & 0 & 0 & 0 \\ 0 & -k_1 & 0 & 0 & 0 & k_1+k_{01} & 0 & 0 \\ 0 & 0 & -k_2 & 0 & 0 & 0 & k_2+k_{02} & 0 \\ 0 & 0 & 0 & -k_2 & 0 & 0 & 0 & k_2+k_{02} \end{bmatrix} \tag{A.13}$$

and $\boldsymbol{K_0}$ is the unsprung mass stiffness matrix:

$$\boldsymbol{K_0} = \begin{bmatrix} 0 & 0 & 0 & 0 \\ 0 & 0 & 0 & 0 \\ 0 & 0 & 0 & 0 \\ 0 & 0 & 0 & 0 \\ -k_{01} & 0 & 0 & 0 \\ 0 & -k_{01} & 0 & 0 \\ 0 & 0 & -k_{02} & 0 \\ 0 & 0 & 0 & -k_{02} \end{bmatrix} \tag{A.14}$$

(analogously for matrices follow for $\boldsymbol{C}$ and $\boldsymbol{C_0}$)

Combining (A.4) and (A.8) yields:

$$x_k = \sum_{i=1}^{7} p_{ik} q_k \quad (k=1...8) \tag{A.15}$$

$$T = \frac{1}{2} \sum_{i=1}^{7} m_{kk} \dot{q}_k^2 \tag{A.16}$$

Developing (A.7) yields:

$$g_k = \sum_{i=1}^{8} p_{ik} q_k = (\boldsymbol{P}^T \boldsymbol{f})_k \quad (k=1...7) \tag{A.17}$$

$$\frac{d}{dt}\frac{\partial T}{\partial \dot{q}_k} = (\boldsymbol{M}\ddot{\boldsymbol{q}})_k \qquad (k=1...7) \tag{A.18}$$

hence:

$$\boldsymbol{M\ddot{q} = P^T f} \tag{A.19}$$

Taking into account (A.12), the governing equation (3.3) in matrix form is obtained:

$$\boldsymbol{M\ddot{q} + P^T CP\dot{q} + P^T KPq = -P^T K_0 z_0 - P^T C_0 \dot{z}_0} \tag{A.20}$$

APPENDIX B

CONTROLLER STABILITY

This appendix reports a formal proof of the stability of system (2.1) with the controller defined by (5.1). The proof, given in the 1 DOF case, is generalised to a more general class of damping forces than those given by (5.1).

Consider the system described by:

$$M\ddot{x} + c\dot{x} + kx + F_d = 0 \tag{B.1}$$

F_d is supposed to be a generic nonlinear controlled damping force of the type:

$F_d = f(x)g(\dot{x})$, with the constraints $f(x) \geq 0$ and $g(0) = 0$.

Subject to the following switching law:

$$F_d = f(x)g(\dot{x}) \quad \text{if} \quad x\dot{x} \leq 0 \tag{B.2}$$

$$F_d = 0 \quad \text{if} \quad x\dot{x} > 0$$

That can be written as:

$$F_d = f(x)g(\dot{x})\frac{1 - sgn(x\dot{x})}{2} \tag{B.3}$$

The switched state feedback (5.1) is a particular case with[1]:

$$f(x) = \mu b k |x| \tag{B.4a}$$

$$g(\dot{x}) = sgn(\dot{x}) \tag{B.4b}$$

---

[1]The function $y=sgn(x)$ is defined as $+1$ if $x>0$, -1 if $x<0$, 0 if $x=0$.

Hence equation (B.1) can be written as:

$$M\ddot{x} + c\dot{x} + kx + f(x)g(\dot{x})\frac{1-sgn(x\dot{x})}{2} = 0 \qquad \text{(B.5)}$$

which in canonical companion form is described by the following first order equations:

$$\dot{x}_1 = x_2$$

$$\dot{x}_2 = -\frac{k}{M}x_1 - \frac{c}{M}x_2 - \frac{f(x_1)g(x_2)}{2M}[1 - sgn(x_1 x_2)] \qquad \text{(B.6)}$$

A Lyapounov function is chosen as:

$$V(x_1, x_2) = \frac{1}{2}(x_1^2 + x_2^2) \qquad \text{(B.7)}$$

It is a Lyapounov function since it meets the requirement that it is a continuous and definite positive function of the system states. The following stability theorem (*Barbashin-Krasowsky*) will be employed:

If $\dot{V} \leq 0$ (semidefinite negative) and if the set of the points of the state space for which $\dot{V} = 0$ does not include any complete trajectory (except the origin), then the system is asymptotically stable.

The first derivative of V is:

$$\dot{V} = \frac{\partial V}{\partial x_1}\frac{dx_1}{dt} + \frac{\partial V}{\partial x_2}\frac{dx_2}{dt} = x_1 x_2 \left(1 - \frac{k}{M}\right) - \frac{c}{M}x_2^2 - \frac{x_2}{2M}f(x_1)g(x_2)[1 - sgn(x_1 x_2)] \qquad \text{(B.8)}$$

the set of points for which $\dot{V} = 0$ is:

$$\{x_2 = 0 \ \cup \ x_1\left(1 - \frac{k}{M}\right) - \frac{c}{M}x_2 - \frac{f(x_1)g(x_2)}{2M}[1 - sgn(x_1 x_2)] = 0\} \qquad \text{(B.9)}$$

Hence the set of points in the phase space where $\dot{V} = 0$ comprises the abscissa axis ($x_2=0$) and another curve which cannot be put in explicit form. However, according to

the previous theorem in order to prove the stability it is necessary only to show that the trajectories of (B.5) are not contained within the abscissa axis (which is a subset of $\dot{V}=0$). This would mean that the set $\dot{V}=0$ is unable to have system trajectories contained in itself and this proves the asymptotic stability of the system. This can be readily verified considering the tangent vectors to the trajectory when x_2=0. Their components are $(0,-\frac{k}{M}x_1)$, hence they are orthogonal to the abscissa axis. **Q.E.D.**

The switched position feedback (5.1) is a particular case with:

$f(x)=\mu bk|x|$ and $g(\dot{x})=sgn(\dot{x})$.

Equation (B.5) becomes:

$$M\ddot{x}+c\dot{x}+kx+\mu\frac{bk}{2}|x|[1-sgn(x\dot{x})]\,sgn(\dot{x})=0 \qquad \text{(B.10)}$$

which can be written as:

$$\dot{x}_1=x_2$$

$$\dot{x}_2=-\frac{k}{M}x_1-\frac{c}{M}x_2-\mu\frac{bk}{2M}|x_1|\,[1-sgn(x_1x_2)]\,sgn(x_2) \qquad \text{(B.11)}$$

The first derivative of the Lyapounov function is:

$$\dot{V}=x_1x_2(1-\frac{k}{M})-\frac{c}{M}x_2^2-\mu\frac{bk}{2M}|x_1|x_2[sgn(x_2)-sgn(x_1x_2^2)] \qquad \text{(B.12)}$$

the set of points for which $\dot{V}=0$ is:

$$\{x_2=0 \;\cup\; x_1(1-\frac{k}{M})-\frac{c}{M}x_2-\mu\frac{bk}{2M}|x_1|\,[sgn(x_2)-sgn(x_1x_2^2)]=0\} \qquad \text{(B.13)}$$

leading to analogous results.

In the case of a multidegree of freedom system, scalar quantities are replaced by matrices and vectors. The proof of stability is obtained with the same method. It is not presented here, as it is more difficult to visualise than the scalar case.

APPENDIX C

THE INSTRUMENTATION

A description of the characteristics of the instrumentation chosen is given here. The focus of this appendix is on the electronic hardware and software. The characteristics of the transducers utilised in the course of the experimentation in each rig have been described in the appropriate chapters.

Data were acquired via an 80486 PC; the data acquisition and control card used was the Data Translation DT 2812. Other signals, not relevant to the control algorithm (i.e. accelerations) were monitored off-line and processed on a digital oscilloscope. The A/D converter of the card is able to receive up to 16 single-ended channels with 12 bit resolution. The number of channels is more than sufficient to control independently all four actuators. Data are transferred to memory via DMA operation. The analogue inputs have an unipolar range of 0-10 V.

The D/A converter is 12 bit. It has a bipolar analogue output range of ± 5 V. This implies that the mean value of the quantisation error is 0.025 V, which is negligible with respect to the range of the converter[1]: in the suspension application this does not produce any appreciable deterioration of the tracking performance.

The card operates in clocked D/A mode; in this mode its clock is set up to produce the required frequency. The sampling frequency for most tests was set to 100 Hz, since the highest frequency in the plant was around 20 Hz. The delay introduced by the sample & hold block is negligible: the total delay in the sampling, holding and

---

[1] The resolution V_0 of the converter can be readily calculated with the following expression that links range of the converter, resolution and number of bits:

$$[K]\ Log_{10}\ 2 = Log_{10}\{(V_{max}-V_{min})/V_0 + 1\}$$

where $[K]$ is an integer that represents the number of bits and $V_{max}-V_{min}$ is the range of the converter.

multiplexing phases is 1 μs (the delay between corresponding samples for each channel, hence when all channels are used is 16 μs).

In some open-loop tests data were captured by the Hewlett-Packard DT-VEE data acquisition software and by FRADOS, a frequency response analyser software developed internally at the University of Bath.

The control is software driven: a C++ DOS-based code (more efficient in real-time applications) is used to manage the I/O and to implement the closed-loop control algorithm. The program has a user interface that allows the entry of the sampling frequency, the control parameters and the acquisition time; data are eventually saved to file.

Signals, before entering the card, are properly conditioned (amplified and filtered) by an analogue conditioning circuitry; the calibration constants of the transducers are introduced via software, by means of an appropriate routine. However the conditioning is unable to properly remove offsets that may arise from the transducers, particularly from linear inductive displacement transducers (LVDT) which inherently produce variable amplitude offsets.

In order to remove the offset problem, a further subroutine has been added: before starting the control, data acquisition is performed off-line and the results averaged over the time; this average value is then subtracted to the actual measured value.

APPENDIX D

SIMULATION PARAMETERS

Friction damper and hydraulic drive parameters

PARAMETER	VALUE
Valve underlap (u)	10^{-4} [m]
Actuator area (A)	6.28×10^{-4} [m^2]
Valve bore diameter (D)	10^{-2} [m]
Pump flow (Q_p)	9×10^{-5} [m^3/s]
Cracking pressure (P_c)	60 [bar]
Relief valve override (k_{rv})	10^4 [$bar/(m^3 s^{-1})$]
Actuator volume (V_t)	10^{-4} [m^3]
Connecting hose volume (V_{hose})	10^{-3} [m^3]
Bulk modulus (B)	5×10^2 [bar]
Discharge coefficient (C_q)	0.62 [N/m]
Valve leakage coefficient (k_{ls})	1.5 [-]
Valve spool damping ratio (ξ)	0.6 [-]
Valve spool resonance frequency (ξ_v)	105 [Hz]
Hydraulic oil density (ρ)	870 [kg/m^3]
Friction coefficient (μ)	0.4 [-]
Frictional memory (T_L)	4×10^{-2} [s]

Quarter car model parameters

PARAMETER	VALUE
Sprung mass (M_1)	165 [kg]

Unsprung mass (M_2)	20 [kg]
Spring rate (k_s)	12000 [N/m]
Damping ratio (ξ)	0.25 [-]
Tyre stiffness (k_t)	148000 [N/m]

7 DOF vehicle model parameters

PARAMETER	VALUE
Sprung mass (m)	1020 [kg]
Wheel mass (m_1)	14.17 [kg]
Axle mass (m_2)	50 [kg]
Pitch moment of inertia (J_α)	1859 [kgm^2]
Roll moment of inertia (J_β)	471 [kgm^2]
Axle moment of inertia ($J_{\beta''}$)	5.343 [kgm^2]
Front spring rate (k_1)	22000 [N/m]
Rear spring rate (k_2)	19000 [N/m]
Tyre stiffness (k_0)	148000 [N/m]
Viscous damper coefficient (c)	400 [N/ms^{-1}]
Tyre damping (c_0)	20 [N/ms^{-1}]
Centre of gravity (CG) distance from the front of the car (a)	1.025 [m]
CG distance from rear axle (b)	3.204 [m]
Axle length (E)	1.462 [m]

APPENDIX E

LIST OF PUBLICATIONS

Stammers C W, Guglielmino E and Sireteanu T. (1999)

A semi-active friction system to reduce machine vibration, *Tenth World Congress on The Theory of Machines and Mechanisms*, Oulu, Finland, June 1999.

Guglielmino E, Stammers C W and Edge K A. (2000)

Robust force control in electrohydraulic friction damper systems using a variable structure scheme with non linear state feedback, *2nd IFK (Internationales Fluidtechnisches Kolloquium)*, Dresden, Germany, March 2000.

Guglielmino E and Edge K A (2000)

Robust control of electrohydraulically actuated friction damper, *ASME-IMECE 2000*, Orlando, USA, November 2000.

Guglielmino E and Edge K A. (2001)

Modelling of an electrohydraulically-activated friction damper in a vehicle application, *ASME-IMECE 2001*, New York, USA, November 2001 (paper accepted for publication).

REFERENCES

Ahmadian M. and Marjoram R H. (1989)

Effects of passive and semi-active suspension on body and wheel-hop control, *SAE Paper N. 892487.*

Al-Houlu N, Weaver J, Lahdhiri T and Joo D S. (1999)

Sliding mode-based fuzzy logic controller for a vehicle suspension system, *Proc. of the American Control Conference*, San Diego, USA, pp. 4188-4192.

Alleyne A, Neuhaus P E and Hedrick J K. (1993)

Application of non-linear control theory to electronically controlled suspensions, *Vehicle System Dynamics*, Vol. 22, pp. 309-320.

Anderson J and Ferri A A. (1990)

Behavior of a single-degree-of-freedom system with a generalized friction law, *Journal of Sound and Vibration*, Vol. 140 (2), pp. 287-304.

Anon (2000)

Professional Engineer, June 2000, p. 63.

Anon (2001)

http://www.edisport.it/edisport/automobilismo/listino.nsf/main?OpenFrameset

Armstrong-Helouvry B. (1990)

Stick-slip arising from Stribeck friction, *Proc. of the International IEEE Conference on Robotics and Automation*, Cincinnati, USA, pp. 1377-1382.

Armstrong-Helouvry B, Dupont P and Canudas de Wit C. (1994)

A survey of models, analysis tools and compensation methods for the control of machines with friction, *Automatica,* Vol. 30 (7), pp. 1083-1138.

Åström K J. (1998)

Control of systems with friction, *MOVIC '98,* Zurich, Switzerland, Vol.1, pp. 25-32.

Åström K J, Hägglund T, Hang C C and Ho W K. (1993)

Automatic tuning and adaptation for PID controllers - a survey, *Control Engineering Practice*, Vol. 1 (4), pp. 699-714.

Baker A. (1984)

Lotus active suspension, *Automotive Engineer*, Feb/Mar 1984, pp. 56-57.

Barak P and Hrovat H. (1988)

Application of the LQG approach to the design of an automotive suspension for three-dimensional vehicle model, *Proc. IMechE Advanced Suspensions Conference*, London, UK, pp. 11-26.

Bastow D. (1993)

Car suspension and handling, Pentech Press.

Bellizzi S and Bouc R. (1989)

Adaptive control for semi-active isolators, *Proc. ASME-DED Conf. on Machinery Dynamics - Applications and Vibration Control Problems*, Montreal, Canada, Vol. 18 (2), pp. 317-323.

Bendat J S and Piersol A G. (1971)

Random data: analysis and measurement procedures, Wiley-Interscience.

Besinger F H, Cebon D and Cole D J. (1991)

An experimental investigation into the use of semi-active dampers on heavy lorries, *Proc. 12th IAVSD Symposium on Dynamics of Vehicles on Roads and on Railways Tracks*, pp. 26-30.

Bliman P-A and Sorine M. (1995)

Easy-to-use realistic dry friction models for automatic control, *Proc. of the 3rd European Control Conference*, Rome, Italy, pp. 3788-3794.

Bose B K. (1985)

Sliding mode control of an induction motor, *IEEE Trans. on Industrial Applications,* Vol. 21 (2), pp. 479-486.

Brun X, Sesmat S, Scavarda S and Thomasset D. (1999)

Simulation and experimental study of the partial equilibrium of an electropneumatic positioning system, cause of the sticking and restarting phenomenon, *Fourth JHPS, Japan Hydraulics and Pneumatics Society International Symposium on Fluid Power*, Tokyo, Japan, pp. 125-130.

Canudas de Wit C H, Olsson H J, Åström K J and Lischinsky P. (1993)

Dynamic friction models and control design, *Proc. of the American Control Conference*, San Francisco, USA, pp. 1920-1926.

Chalasani R M. (1987)

Ride performance potential of active suspension systems-part II: comprehensive analysis based on a full-car model, *ASME Symposium on Simulation and Control of Ground Vehicles and Transportation Systems*, Vol. 80, pp. 205-234.

Chang S-L and Wu C-H. (1997)

Design of an active suspension system based on a biological model, *Proc. of the American Control Conference*, Albuquerque, USA, pp. 2915-2919.

Chantranuwathana S and Peng H. (1999)

Adaptive robust control for active suspensions, *Proc. of the American Control Conference*, San Diego, USA, pp. 1702-1706.

Chapra S C and Canale R P. (1988)

Numerical methods for engineers, McGraw-Hill.

Chin Y, Lin W C, Sidlosky D M and Rule D S. (1992)

Sliding-mode ABS wheel-slip control, *Proceedings of the American Control Conference,* Chicago, USA, pp. 1-5.

Choi S B, Choi Y T and Park D W. (2000)

A sliding mode control of a full-car electrorheological suspension via hardware-in-the-loop simulation, *Journal of Dynamic Systems, Measurement and Control*, Vol. 122, pp. 114-121.

Cohen G H and Coon G A. (1953)

Theoretical consideration of retarded control, *Trans. ASME*, Vol. 75, pp. 827-834.

Coomber I. (1992)

Ford Escort & Orion owners workshop manual, Haynes.

Coulomb C A. (1785)

Theorie des machines simples, en ayant egard au frottement de leurs parties, et a la roideur des cordages, *Mem. Math. Phys.*, pp. 161-342 (in French).

Crolla D A. (1995)

Vehicle dynamics - theory into practice, *Proc. IMechE, Journal of Automobile Engineering,* Vol. 209, pp. 1-12.

Crolla D A and Abdel Hady M B A. (1988a)

Semi-active suspension control for a full vehicle model, *SAE Paper N. 911904.*

Crolla D A and Aboul Nour A M A. (1988b)

Theoretical comparisons of various active suspension systems in terms of performance and power requirements, *Proc. IMechE Advanced Suspensions Conference*, London, UK, pp. 1-9.

Crolla D A, Horton D N L, Pitcher R H and Lines J A. (1987)

Active suspension control for an off-road vehicle, *Proc. IMechE*, Vol. 201 (D1), pp. 1-10.

Crosby M J and Karnopp D C. (1973)

The active damper - a new concept for shock and vibration control, *The Shock and Vibration Bulletin*, Vol. 43 (4), pp. 119-133.

Cross J. (1999)

Farewell to rock and roll, *Automotive Engineer*, August 1999.

Curtis A. (1991)

Ride revolution, *Car Design and Technology*, USA, June/July 1991.

Dahl P. (1968)

A solid friction model, *Technical Report TOR-0158(3107-18)-1, The Aerospace Corporation*, El Segundo, USA.

Dahlin E G. (1968)

Designing and tuning digital controllers, *Instrum. Control Syst.*, Vol. 41 (6).

Da Vinci L. (1519)

The notebooks, Dover, New York.

De Carlo R A, Zak S H and Matthews G S. (1988)

Variable structure control of nonlinear multivariable systems: a tutorial, *Proc. IEEE*, Vol. 76 (3), pp. 212-232.

Decker H, Schramm W and Kallenbach R. (1988)

A practical approach towards advanced semi-active suspension systems, *Proc. IMechE Advanced Suspensions Conference*, London, UK, pp. 93-99.

Demic M. (1984)

Assessment of random vertical vibration on human body fatigue, using a physiological approach, *Proc. IMechE Conf. on Vehicle Noise and Vibration,* London, UK, pp. 91-95.

Dieckmann D. (1958)

A study of the influence of vibration in man, *Ergonomics*, Vol. 4, p. 347.

Dorf R C and Bishop R H. (1995)

Modern control systems, Addison-Wesley.

Dote Y, Takebe S and Ito T. (1982)

Variable structure with sliding mode for DC drive speed regulations, *Proc. IEEE, Power Electronics Specialist Conference, Pesc '82,* Cambridge, Massachusetts, USA, pp. 123-127.

Drazenovic B. (1969)

The invariance conditions in variable structure systems, *Automatica*, Vol. 5, pp. 287-295.

Dupont P, Kasturi P and Stokes A. (1997)

Semi-active control of friction dampers, *Journal of Sound and Vibration,* Vol. 202 (2), pp. 203-218.

Dyke S J and Spencer Jr B F. (1997)

A comparison of semi-active control strategies for the MR damper, *Proc. of the IASTED International Conference, Intelligent Information Systems*, The Bahamas.

Eryilmaz B and Wilson B H. (2000)

Modeling the internal leakage of hydraulic servovalves, *Journal of Dynamic Systems, Measurement, and Control,* Vol. 122 (3), pp. 576-579.

Federspiel-Labrosse G M. (1954)

Contribution a l' etude et au perfectionement de la suspension des vehicules, *J. de la SIA, FISITA*, pp. 427-436 (in French).

Ferri A A and Heck B S. (1998)

Vibration analysis of dry friction damped turbine blades using singular perturbation theory, *Journal of Vibration and Acoustics*, Vol. 120 (2), pp. 588-595.

Filippov A F. (1960)

Application of theory of differential equations with discontinuous righthand sides to nonlinear control problems, *Proc. 1st IFAC Congress,* URSS, pp. 923-927.

Filippov A F. (1988)

Differential equations with discontinuous righthand sides, Kluwer Academic Publishers.

Gamble J B. (1992)

Sliding mode control of a proportional solenoid valve, Ph.D. Thesis, University of Bath, UK.

Gao W and Hung J C. (1993)

Variable structure control of nonlinear systems: a new approach, *IEEE Trans. on Industrial Electronics*, Vol. 40 (1), pp. 45-55.

Gayed A, Benkhoris M F, Siala S and Le Doeuff R. (1995)

Time-domain simulation of discrete sliding control of permanent magnet synchronous motor, *Proc. of the 21st IEEE IECON International Conference on Industrial Electronics, Control, and Instrumentation,* Orlando, USA, Vol. 2, pp. 754-759.

Genta G. (1993)

Meccanica dell' autoveicolo, Ed. Levrotto & Bella (in Italian).

Genta G and Campanile P. (1989)

An approximate approach to the study of a motor vehicle suspensions with non-linear shock absorbers, *Meccanica,* Vol. 24, pp 47-57.

Gerdes J C and Hedrick J K. (1999)

Hysteresis control of nonlinear single-acting actuators as applied to brake/throttle switching, *Proc. of the American Control Conference,* San Diego, USA, pp. 1692-1696.

Goodall R M and Kortüm W. (1983)

Active control in ground transportation - a review of the state-of-the-art and future potential, *Vehicle System Dynamics*, Vol. 12, pp. 225-257.

Goodall R M, Williams R A, Lawton A and Harbrough P R. (1981)

Railway vehicle active suspensions in theory and practice, *Proc. 7th IAVSD Symposium on the Dynamics of the Vehicles on Roads and Railway Tracks*, pp. 301-306.

Griffin M. (1984)

Vibration dose values for whole body vibration: some examples, *Human Factor Research Unit, I.S.V.R.*, Southampton, UK.

Groenewald M L and Gouws J. (1996)

In-motion tyre pressure control system for vehicles, *Proc. IEEE Mediterranean Electrotechnical Conference - MELECON*, Vol. 3, pp.1465-1468.

Haalman A. (1965)

Adjusting controllers for deadtime process, *Control Eng.*, pp. 71-73.

Hac A. (1987)

Adaptive control of vehicle suspension, *Vehicle System Dynamics*, Vol. 16, pp. 57-74.

Hagedorn P. (1988)

Non-linear oscillations, Clarendon.

Handroos H and Liu Y. (1998)

Sliding mode control of a hydraulic position servo with different kinds of loads, *Power Transmission and Motion Control, PTMC '98*, Bath, UK, pp. 379-392.

Hashimoto H, Yamamoto H, Yanagisawa S and Harashima F. (1988)

Brushless servo motor control using a variable structure approach, *IEEE Trans. on Industrial Applications,* Vol. 24 (1), pp. 160-170.

Hedrick J K and Wormely D N. (1975)

Active suspension for ground support vehicles - a state-of-the-art review, *ASME-AMD,* Vol. 15, pp. 21-40.

Hertz H. (1881)

On the contact of elastic solids, *J. Reine und Anges. Math,* Vol. 92, pp. 156-171.

Hess D P and Soom A. (1990)

Friction at a lubricated line contact operating at a oscillating sliding velocities, *Journal of Tribology,* Vol. 112 (1), pp. 147-152.

Hickson L R. (1996)

Design and development of an active roll control suspension, Ph.D. Thesis, University of Bath, UK.

Hillebrecht P, Konik D, Pfeil D, Wallentowitz F and Zieglmeier F. (1992)

The active suspension between customer benefit and technological competition, *Proc. IMechE,* pp. 221-230.

Horrocks B S, Stammers C W and Gartner M. (1997)

The performance of a hydraulically activated semi-active friction damper, *Fifth Scandinavian International Conference on Fluid Power,* Linköping, Sweden, Vol. 3, pp. 47-55.

Hrovat D and Hubbard M. (1987)

A comparison between jerk optimal and acceleration optimal vibration isolation, *Journal of Sound and Vibration*, Vol. 112 (2), pp. 201-210.

Hung Y J, Gao W and Hung J C. (1993)

Variable structure control: a survey, *IEEE Trans. on Industrial Electronics,* Vol. 40 (1), pp.1-22.

ISO, International Standard Organisation. (1978)

International Standard 2631-1978 (E), guide for the evaluation of human exposure to whole-body vibration, 2nd Ed.

Itkis Y. (1976)

Control systems of variable structure, Wiley.

Jolly A. (1983)

Study of ride comfort using a non-linear mathematical model of a vehicle suspension, *International Journal of Vehicle Design*, Vol. 43 (3), pp. 233-244.

Johnson K L. (1987)

Contact mechanics, Cambridge University Press.

Karadayi R and Hasada G Y. (1986)

A non-linear shock absorber model, *Proc. of the ASME-AMD Symposium on Simulation and Control of Ground Vehicles and Transportation Systems*. Anaheim, USA, Vol. 80, pp. 149-165.

Karnopp D C, Crosby M J and Harwood R A. (1974)

Vibration control using semi-active force generators, *Journal of Engineering for Industry*, Vol. 97, pp. 619-626.

Kato S, Sato N and Matsubayashi T. (1972)

Some considerations of characteristics of static friction of machine tool slideway, *Journal of Lubrication Technology*, Vol. 94 (3), pp. 234-237.

Kim C and Ro P I. (1998)

A sliding mode controller for vehicle active suspension systems with non-linearities, *Proc. IMechE, Journal of Automobile Engineering*, Vol. 212 (2), pp.79-92.

Lambert J D. (1973)

Computational methods in ordinary differential equations, Wiley.

Lane J, Ferri A and Heck B. (1992)

Vibration control using semi-active frictional damping, *Proc. of the ASME-DED Winter Annual Meeting, Friction-Induced Vibration, Chatter, Squeal and Chaos,* New York, USA, Vol. 49, pp. 165-171.

Lantto B, Krus P and Palmberg J-O. (1993)

Robust control of an electrohydraulic pump using sliding mode planes, *The Third Scandinavian Conference on Fluid Power*, Linköping, Sweden, Vol, 3, pp. 3-24.

Leatherwood J, Dempsey T and Clevenson S. (1980)

A design tool for estimating passenger ride discomfort within complex ride environments, *Human Factors*, Vol. 22 (3), pp. 291-312.

Lee R and Pradko F. (1969)

Analytical analysis of human vibration, *SAE paper N. 680091.*

Lizell M. (1988)

Semi-active damping, *Proc. IMechE Advanced Suspensions Conference*, London, UK, pp. 83-91.

Lopez O, Garcia de Vicuna L, Castilla M, Matas J and Lopez M. (1999)

Sliding mode control design of a high power factor buck-boost rectifier, *IEEE Trans. on Industrial Electronics,* Vol. 46 (3), pp. 604-612.

Lord Corporation. (2001)

http://www.lord.com

Lucifredi A. (1978)

Meccanica delle vibrazioni, Ed. CLU (in Italian).

Margolis D L. (1982)

The response of active and semi-active suspensions to realistic feedback signals, *Vehicle System Dynamics*, Vol. 11 (5-6), pp. 267-282.

Majjad R. (1997)

Estimation of suspension parameters, *Proc. IEEE International Conference on Control Applications*, Hartford, USA, pp. 522-527.

Martins I, Esteves J, Da Silva F P and Verdelho P. (1999)

Electromagnetic hybrid active-passive vehicle suspension system, *Proc. of the IEEE 49th Vehicular Technology Conference*, Houston, USA, Vol. 3, pp. 2273-2277.

Mastinu G. (1988)

Passive automobile suspension parameter adaptation, *Proc. IMechE Advanced Suspensions Conference*, London, UK, pp 51-58.

McCloy D and Martin H R. (1980)

Control of fluid power: analysis and design, Wiley.

Miller L R. (1988)

The effects of hardware limitations on an "on/off" semi-active suspension, *Proc. IMechE Advanced Suspensions Conference*, London, UK, pp. 199-206.

Miller L R and Nobes C M. (1988)

The design and development of a semi-active suspension for a military tank, *SAE Paper N. 881133.*

Milliken Jr W F. (1987)

Lotus active suspension system, *Proc 11th Int. EVS Conference.*

Mohan B and Phadke S B. (1996)

Variable structure active suspension system, *Proc. of the IEEE 22nd International Conference on Industrial Electronics, Control, and Instrumentation, IECON*, Taipei, Taiwan, pp.1945-1948.

Mohan N, Undeland T M and Robbins W P. (1995)

Power electronics: converters, applications and design, Wiley.

Morin A J. (1833)

New friction experiments carried out at Metz in 1831-1833. *Proc. of the French Academy of Sciences*, Vol. 4, pp. 1-128.

Nishitani A, Nitta Y, Ishibashi Y and Itoh A. (1999)

Semi-active structural control with variable friction dampers, *Proc. of the American Control Conference*, San Diego, USA, pp. 1017-1021.

Ogawa Y, Kawasaki H, Arai J and Nakazato M. (1999)

Application of semi-active suspension system to railway vehicles, *Fourth JHPS, Japan Hydraulics and Pneumatics Society International Symposium on Fluid Power*, Tokyo, Japan, pp. 267-272.

O'Neill H and Wale G D. (1994)

Semi-active suspension improves rail vehicles ride, *Computing & Control Engineering Journal*, Vol. 5 (4), pp. 183-188.

Pall dynamics Ltd. (1999)

http://www.encs.concordia.ca/bce/deq.htm

Pandian S R, Leda K, Kamoyama Y, Kamawura S and Hayakawa Y. (1998)

Modelling and control of a pneumatic rotary actuator, *Power Transmission and Motion Control, PTMC '98*, Bath, UK, pp. 363-376.

Park J H and Kim Y S. (1998)

Decentralized variable structure control for active suspensions based on a full-car model, *Proc. of the 1998 IEEE International Conference on Control Applications*, Trieste, Italy, pp. 383-387.

Peel D J, Stanway R, Bullough W A. (1996)

Dynamic modelling of an ER vibration damper for vehicle suspension applications, *Smart Materials and Structures*, Vol. 5, pp. 591-606.

Petzold L. (1983)

Automatic selection of methods for solving stiff and non-stiff systems of ODE's, *SIAM J. Sci. Stat. Comput.*, Vol. 4, pp. 136-148.

Pollock A J and Craighead I A. (1986)

The selection of a criterion to evaluate ride-discomfort in off-road vehicles, *Proc. of Polymodel 9,* Newcastle upon Tyne, UK, pp. 21-31.

Pontryagin L S, Boltyanskii V G, Gamkrelidze D and Mishchenko A. (1962)

The mathematical theory of optimal processes, Interscience.

Rabinowicz E. (1958)

The intrinsic variables affecting the stick-slip process, *Proc. Physical Society of London*, Vol. 74 (4), pp. 668-675.

Rabinowicz E. (1965)

Friction and wear of materials, Wiley.

Ramallo J C, Johnson E A, Spencer Jr B F and Sain M K. (1999)

Semiactive building base isolation, *Proc. of the American Control Conference*, San Diego, USA, pp. 515-519.

Ramsbottom M, Crolla D A and Plummer A R. (1999)

Robust adaptive control of an active vehicle suspension system, *Proc. IMechE*, Vol. 213 (D), pp. 1-5.

Rao S S. (1995)

Mechanical vibrations, Addison-Wesley.

Reynolds O. (1886)

On the theory of lubrication and its application to Mr. Beauchamp tower's experiments, including experimental determination of the viscosity of olive oil, *Phil. Trans. Royal Soc.*, Vol. 177, pp. 157-234.

Rice J R and Ruina A L. (1983)

Stability of steady frictional slipping, *Journal of Applied Mechanics*, Vol. 50, pp. 343-349.

Richards C W. (1993)

Bath*fp* Manual, Vol. 1-2, University of Bath, UK.

Richards C W, Tilley D G, Tomlinson S P and Burrows C R. (1990)

Type-insensitive integration codes for the simulation of fluid power systems, *Proc. of the ASME Winter Annual Meeting*, Dallas, USA.

Ross-Martin T. (1994)

Low bandwidth active roll and warp control suspension, Ph.D. Thesis, University of Bath, UK.

Roxin E. (1965)

On generalized dynamical systems defined by contingent equations, *Journal of Differential Equations,* Vol. 1, pp. 188-205.

Sadeghi F and Sui P C. (1989)

Compressible elastohydrodynamic lubrication of rough surfaces, *Journal of Tribology*, Vol. 111 (1), pp. 56-62.

SAE, Society of Automotive Engineers. (1965)

Ride and vibration data manual, J6a.

Sammier D, Sename O and Dugard L. (2000)

H_∞ control of active vehicle suspensions, *Proc. of the 2000 IEEE International Conference on Control Applications,* Anchorage, USA, pp. 976-981.

Sanliturk K Y, Stanbridge A B and Ewins D J. (1995)

Friction dampers: measurement, modelling and application to blade vibration control, *Proc. of the 1995 ASME Design Engineering Technical Conference,* Boston, USA, Vol. 84 (3), pp. 1377-1382.

Sarpturk S Z, Istefanopoulos Y and Kaynak O. (1987)

On the stability of discrete-time sliding mode control systems, *IEEE Trans. on Automatic Control*, Vol. 32 (10), pp. 930-32.

Satoh M, Fukushima N, Akatsu Y, Fujimura I and Fukuyama K. (1990)

An active suspension employing an electrohydraulic pressure control system, *Proc. of the 29th Conference on Decision and Control*, Honolulu, USA,Vol. 4, pp. 2226-2231.

Sebesan I and Hanganu D. (1993)

Proiectarea suspensiilor pentru vehicule pe sine, Editura Tehnică, Bucarest (in Romanian).

Sharp R S and Crolla D A. (1987)

Road vehicle suspension system design-a review, *Vehicle System Dynamics*, Vol. 16, pp. 167-192.

Shaw M. (1999)

Application of hydro-elastomer technology to vehicle suspensions, Ph.D. Thesis, University of Bath, UK.

Silva J F. (1999)

Sliding-mode control of boost-type unity power-factor PWM rectifiers, *IEEE Trans. on Industrial Electronics*, Vol. 46, pp. 594-603.

Singh M P, Matheu E E and Suarez L E. (1997)

Active and semi-active control of structures under seismic excitation, *Earthquake Engineering and Structural Dynamics*, Vol. 26, pp. 193-213.

Sireteanu T, Gündisch O and Părăian S. (1981)

Vibraţile aleatoare ale automobilelor. Confort şi aderenţă, Editura Tehnică, Bucarest (in Romanian).

Sireteanu T, Stammers C W and Ursu I. (1997)

Analysis of a sequential dry friction type semi-active suspension system, *Active 97,* Budapest, Hungary, pp. 565-571.

Slotine J-J E. (1984)

Sliding controller design for nonlinear systems, *International Journal of Control*, Vol. 40 (2), pp.421-434.

Slotine J-J E and Li W. (1992)

Applied nonlinear control, Prentice-Hall.

Smith O J M. (1957)

Closer control of loops with dead time, *Chem. Eng. Progress*, Vol. 53, pp. 217-219.

Stammers C W and Sireteanu T. (1997)

Vibration control of machines by using semi-active dry friction damping, *Journal of Sound and Vibration,* Vol. 209 (4), pp. 671-684.

Stayner R M. (1988)

Suspensions for agricultural vehicles, *Proc. IMechE Conference on Advanced Suspensions*, London, UK, pp.133-140.

Steffens R J. (1966)

Some aspects of structural vibration, Vibration in Civil Engineering, Butterworth.

Stribeck R. (1902)

Die Wesentlichen Eigenschaften der Gleit und Rollenlager (The key qualities of sliding and roller bearings). *Zeitschrift des Vereines Seutscher Ingenieure*, Vol. 46 (38), pp. 1342-1348, Vol. 46 (39), pp. 1432-1437 (in German).

Tan H-S and Bradshaw T. (1997)

Model identification of an automotive hydraulic active suspension system, *Proc. of the American Control Conference*, Albuquerque, USA, Vol. 5, pp. 2920-2924.

The MathWorks Inc. (1992)

MATLAB user's guide, The MathWorks Inc., USA.

Thompson A G. (1973)

Quadratic performance indices and optimum suspension design, *Proc. IMechE*, Vol.187 (9), pp.129-139.

Thompson A G. (1976)

An active suspension with optimal linear state feedback, *Vehicle System Dynamics*, Vol. 5, pp. 187-203.

Tiliback L R and Brood S. (1989)

Active suspension - the Volvo experience, *SAE Paper N. 890083.*

Titli A, Roukieh S, Dayre E. (1993)

Three control approaches for the design of car semi-active suspension (optimal control, variable structure control, fuzzy control), *Proc. of the IEEE Conference on Decision and Control,* Vol. 3, pp. 2962-2963.

Tseng H E and Hedrick J K. (1994)

Semi-active control laws - optimal and sub-optimal, *Vehicle System Dynamics*, Vol. 23, pp. 545-569.

Tsypkin Y Z. (1974)

Relay control systems, Cambridge University Press.

Tunay I, Amin M and Beck A. (1998)

Robust control of a hydraulic valve for aircraft anti-skid operation, *Proc. of the 1998 IEEE International Conference on Control Applications*, Trieste, Italy, pp. 689-693.

Uebing M. (1999)

Simulation and control of a multi-axes pneumatically actuated animated figure, Ph.D. Thesis, University of Bath, UK.

Utkin V I. (1972)

Equations of sliding mode in discontinuous systems, vols. 1, 2, *Automation and Remote Control*, n. 1, pp. 1897-1907 (1971), n. 2, pp. 211-219 (1972).

Utkin V I. (1977)

Variable structure systems with sliding modes, *IEEE Trans. on Automatic Control,* Vol. 22, pp. 212-222.

Utkin V I. (1992)

Sliding modes in control optimization, Springer Verlag.

Utkin V I and Young K K D. (1978)

Methods for constructing discontinuity planes in multidimensional variable structure systems, *Automation and Remote Control*, Vol. 39 (10), pp. 1466-1470.

Vaughan N D and Gamble J. (1991)

Sliding mode control of a proportional solenoid valve, *Fourth Bath International Fluid Power Workshop*, Bath, UK, pp. 95-108.

Wang X, Noah S and Vahabzadeh H. (1996)

Analysis of a coulomb friction damper for suppressing oscillations of drive shafts of vehicles, *Proc. of ASME-IMECE*, Atlanta, USA, Vol. 91, pp. 51-58.

Williams R A, Burnham K J and Webb A C. (1996)

Developments for an oleo-pneumatic active suspension, *Proc. of the IEEE International Symposium on Computer-Aided Control System Design,* Dearborn, USA, pp. 44-49.

Wills G J. (1980)

Lubrication fundamentals, Marcel Dekker.

Wong J Y. (1993)

Theory of ground vehicles, Wiley.

Wonham W M and Johnson S. (1963)

Optimal bang-bang control with quadratic performance index, *4th Joint Automatic Control Conference,* Minneapolis, USA.

Yagtz N, Özbulur V, Inanc N and Derdiyok A. (1997)

Sliding modes control of active suspensions, *Proc. of the 12th IEEE International Symposium on Intelligent Control*, Istanbul, Turkey, pp. 349-353.

Yang J N, Li Z, Wu J C and Young K K D. (1993)

A discontinuous control method for civil engineering structures, *Proc. 9th VPI & SU Symposium on Dynamics and Control of Large Structures,* Blacksburg, USA, pp. 167-180.

Yi K and Song B S. (1999)

A new adaptive sky-hook control of vehicle semi-active suspensions, *Proc. IMechE, Automobile Engineering*, Vol. 213 (D), pp. 293-303.

Yokoya Y, Kizu R, Kawaguchi H, Ohashi K and Ohno H. (1990)

Integrated control system between active control suspension and four-wheel steering for the 1989 CELICA, *SAE Transactions*, Vol. 99, pp. 1546-1561.

Young K D and Özgüner Ü. (1999)

Sliding mode: control engineering in practice, *Proc. of the American Control Conference*, San Diego, USA, pp. 150-162.

Zeid A and Chang D. (1991)

Simulation of multibody systems for the computer-aided design of vehicle dynamic controls, *SAE Paper N. 910236.*

Zeller W. (1949)

Units of measurement for strength and sensitivity of vibrations, *ATZ*, Vol. 51, p. 95.

Ziegler J B and Nichols N B. (1942)

Optimum setting for automatic controllers, *Trans. ASME*, Vol. 65, pp. 433-444.

Zinober A S I. (1990)

Deterministic control of uncertain systems, Peregrinus.